VISCOELASTIC BEHAVIOUR OF THE CANINE CRANIAL CRUCIATE LIGAMENT COMPLEX

Thesis submitted in accordance with the requirements of the University of Liverpool for the degree of Doctor in Philosophy by

Rosti Abdulqader Hama Rashid

August 2017

Table of Contents

Acknowledgements

The following work was produced with the help of a number of people to whom I am forever grateful. First and foremost, I wish to take this opportunity to acknowledge and express my sincere gratitude to my primary supervisor Eithne Comerford, Professor in Small Animal Surgery at the University of Liverpool, and my secondary supervisor, Ahmed Elsheikh, Professor of Biomaterial Mechanics. Eithne has supported me with her profound expertise, continued guidance and by giving me the opportunity to advance my career in research. Despite being extremely busy with other professorial duties, Eithne and Ahmed have always made time for me whenever I needed them, whether the issue was personal or work-related.

I would like to thank Dr. Brendan Geraghty for helping me get onto my feet at the beginning of my PhD through abundant advice relating to possible experimental and numerical works. A very special gratitude goes out to Dong Zhou for providing me with the Particle Swarm Optimisation code written in MATLAB which I used in the current study.

Within the Institute of Aging and Chronic Disease, I would like to acknowledge the work of Dr. Yalda Ashraf Kharaz and Dr. Sumaya Allaith for preparing the buffer solutions and undertaking the biochemical assessment on my samples.

I would like to thank my friend Juliet Coria, an English language teacher, for grammatical proof reading my thesis. I feel so blessed to have friends like her who supported me to get this PhD completed to a high standard.

I want to take this opportunity to thank my parents, Warda and Qadir, my sister, Dwen, and my husband, Lonnie, for their continuous support, emotionally and financially. I simply could not have done this work without their constant encouragement. They were the people who never doubted my ability and always gave me the impression that I can overcome challenges without any hesitations. From an early age, my mum and dad have always encouraged me to aim high

and lifted me up whenever I was discouraged. There is no way I can repay them for all they have done for me; therefore, I would like to dedicate this thesis to my parents.

Viscoelastic behaviour of the canine cranial cruciate ligament complex

Rosti Abdulqader Hama Rashid

Abstract

The canine stifle joint is one of the most vulnerable joints within the musculoskeletal system and the cranial cruciate ligament (CCL) is the most susceptible ligament to rupture within the joint. When this ligament is damaged, the stifle joint becomes mechanically unstable leading to abnormal load distribution within the joint. This physiological change is associated with osteophyte formation at the joint margins, thickening of the medial aspect of the joint capsule and the medial collateral ligament, softening of the articular cartilage resulting in osteoarthritis (OA). Ligament injury can be either purely traumatic or a degenerative non-contact form. The aetiopathogenesis of non-contact cranial cruciate ligament rupture (CCLR) is unclear, however alterations in the composition of the extracellular matrix (ECM) has been implicated as one of its causes.

This thesis aimed to advance the current understanding of the biomechanical behaviour of the canine CCL and investigated the contribution of proteoglycans (PGs) to the viscoelastic behaviour of the CCL. The objectives comprise of experimental and numerical studies, including the development and utilisation of a novel full-field three-dimensional digital image correlation method (3D DIC) and a representative FEM of the whole canine stifle joint.

Experimental Study I on the canine CCLs was the first to focus on characterising slow strain rate sensitivity and hysteresis behaviour of the ligament at the toe-region of stress-strain behaviour. This study showed that arranging mechanical tests in different orders of strain rates resulted in different tissue response, such that tensile responses of the CCL during the ascending (increasing order of strain rates from 0.1 to 1%/min, and 1 to 10%/min) tests were significantly different from the descending tests (decreasing order of strain rates from 10 to 1%/min, and 1 to 0.1%/min). Only during ascending tests were the CCLs strain rate sensitive and hysteresis was strain rate dependent. The different tensile responses of the CCLs during the ascending and descending order of strain rate may be associated with strain history of the tissue.

In Experimental Study II, two groups of the CCLs (control and treatment (PG depletion)) were tested under tensile load at slow strain rates (0.1, 1 and 10%/min). PG content in the treatment group was depleted by 21.11 ± 14.51% ($p=0.45$). Water content in the treatment group reduced by approximately 5.2% ($p=0.048$). Although there were no statistically significant values; stress-strain, tangent modulus, hysteresis and creep behaviour in the treatment was different from the control groups. Stress relaxation rate was significantly higher in the control than the treatment group ($p=0.039$). The lower relaxation rate in the treatment group could be associated with sGAGs which provides cross-links between collagen molecules. Hence, it is possible that an efficient depletion of PGs in canine CCLs could result in significant mechanical changes in the tissue.

A full-field 3D DIC method was developed to generate five CCL-specific FEM and provide load-deformation behaviour across the middle region of the CCLs. This information was utilised to predict stress-strain behaviour of the CCLs through inverse analysis. In addition, an anatomically representative FEM of the canine stifle joint was developed and employed to investigate the joint when PGs in the CCL were depleted. Results showed reduction in joint stability in joints with depleted CCLs ($p=0.56$). Hence, PG content in the CCL could be one of the ECM components contributing to the mechanical behaviour of the ligament, and affecting the stability in canine stifle joints.

This research leads to a better understanding of the biomechanical behaviour of canine CCL, and it is useful for researchers in the field of biomechanics and biomedical science who are seeking advanced experimental and numerical works in tissue mechanics.

List of Publications

Journal publications have been prepared from the content in this present study:

1. **R. Hama Rashid**, A. Elsheikh, B. Geraghty and E. Comerford. The contribution of proteoglycans to the non-linear viscoelastic behaviour of the canine cranial cruciate ligament. Targeted journal: Osteoarthritis and Cartilage. 2017. *(Currently under review).*

2. **R. Hama Rashid**, E. Comerford and A. Elsheikh. Development of a full-field three-dimensional digital image correlation technique for local surface strain measurements in cranial cruciate ligaments. Targeted journal: International Journal for Numerical Methods in Engineering. 2017. *(Currently under review).*

3. **R. Hama Rashid**, A. Elsheikh and E. Comerford. Anatomically representative finite element modelling of the canine stifle joint. Targeted journal: Journal of Biomechanics. 2017. *(Currently under review).*

4. **R. Hama Rashid**, A. Elsheikh and E. Comerford. Regional stiffness variations across the surface of the canine stifle ligaments. Targeted journal: International Journal for Numerical Methods in Engineering. 2017. *(Currently under review).*

In addition, the works in this thesis have been presented in a number of conferences:

1. **R. Hama Rashid**, B. Geraghty, A. Elsheikh and E. Comerford. Development of a Finite Element Model of the Canine Stifle (Knee) Joint. PGBiomed: the 9th IEEE EMBS UK & Republic of Ireland Postgraduate Conference on Biomedical Engineering and Medical Physics. July 14th -16th 2015. Liverpool, UK.

2. **R. Hama Rashid**, B. Geraghty, A. Elsheikh and E. Comerford. The effect of Ascending and Descending Strain Rate on the Mechanical Properties of Canine Cranial Cruciate Ligaments. ESB2014: the 26th Annual Conference of the European Society for Biomaterials. August 31st – September 3rd 2014. Liverpool, UK.

3. E. Comerford, B. Geraghty, **R. Hama Rashid** and A. Elsheikh. The Contributions of Proteoglycans to the Viscoelasticity of the Canine Anterior Cruciate Ligament. Osteoarthritis and Cartilage. Vol. 22, April 2014.

List of Abbreviations

ANOVA	Analysis of variance
ACL	Anterior cruciate ligament
AMB	Anteromedial band
BSA	Bovine serum albumin
CaCL	Caudal cruciate ligament
ChABC	Chondroitinase ABC
CT	Computed tomography
CCL	Cranial cruciate ligament
CCLD	Cranial cruciate ligament disease
CCLR	Cranial cruciate ligament rupture
CLB	Caudolateral band
CMB	Craniomedial band
CV	Coefficient of variation
DS	Dermatan sulphate
DIC	Digital image correlation
ECM	Extracellular matrix
FE	Finite element
FEA	Finite element analysis
FEM	Finite element model
GAG	Glycosaminoglycan
HSPG	Heparan sulphate proteoglycans
ICP	Iterative closest point
IU	International unit
LCL	Lateral collateral ligament
MRI	Magnetic resonance imaging
MCL	Medial collateral ligament
µl	Microliter
mg	Milligram
ml	Millilitre
mM	Millimole
mm	Millimetre
N	Newton
OA	Osteoarthritis
%/min	Percent per minute
PBS	Phosphate buffer saline
pH	Potentia hydrogenii
PMMA	Polymethyle-methacrylate
PCL	Posterior cruciate ligament
PLB	Posterolateral band
PG	Proteoglycan
RMS	Root mean square
s	Second

SLRP	Small leucine rich proteoglycan
SD	Standard deviation
sGAG	Sulphated glycosaminoglycan
3D	Three-dimensional
2D	Two-dimensional

List of Figures

List of Tables

1. Introduction

1.1. Background

The living body is the only machine for which there are no spare parts.

-Adapted from Hermann M. Biggs-

Early researchers who studied the mechanics of biological structures described the living body as a machine and the whole machine as an assembly of smaller ones (Pope, 2005; Boschiero, 2007). Living bodies, such as humans and dogs, are constructed of bone, cartilage, ligament, tendon, muscle and other connective tissues. These muscular and skeletal arrangements produce an active system commonly known as the musculoskeletal system. These biological structures function on their own as well as together in the joints (Amis and Dawkins, 1991; Carpenter and Cooper, 2000). For example, the knee joint in the human body (known as the stifle joint in quadrupeds) is part of the musculoskeletal system and it plays an important role in allowing relative movement between bones whilst connecting individual bones and transferring forces from one bone to the next. These joints also facilitate biochemical and physiological interaction between neighbouring biological materials (Thornton *et al.*, 2007). There are several studies looking at the biomechanics of various biological tissues, and this study will focus on the biomechanics of canine stifle ligaments. This field is an area of clinical importance, as stifle ligaments provide structural stability to the joint by acting as strong fibrous connective tissues preventing hyperextension and anterior translation of the femur in relation to the tibia within the joint (Levangie and Norkin, 2005; Budras, 2007).

The stifle joint is a compound joint in which three long bones (the distal femur, proximal tibia, and proximal fibula) and four sesamoid bones articulate (Carpenter and Cooper, 2000; Budras, 2007) (Figure 1.1). The major bones in the canine stifle joint are the femur, tibia and fibula

(Carpenter and Cooper, 2000). The femur is the heaviest bone in the skeleton of the canine and it articulates with the acetabulum proximally and with the tibia distally creating femorotibial articulations (Adams, 2004; Evans *et al.*, 2012). The long bone of the tibia, which lies in the medial part of the pelvic limb, articulates with the tarsus proximally and the fibula both proximally and distally. The fibula is a long and thin bone located in the lateral part of the pelvic limb; its main function is to facilitate muscle attachment, as it can only support a small amount of weight (Adams, 2004; Evans *et al.*, 2012). The basic anatomy of these bones plays a major role in the overall motion of the stifle joint and these articulations are responsible for improving the mechanical efficiency of the joint (Carpenter and Cooper, 2000; Vasseur, 2002). As mentioned above, ligaments provide structural stability in the stifle joint. These ligaments are strong fibrous connective tissues allowing motion in three planes (Carpenter and Cooper, 2000; Levangie and Norkin, 2005; Budras, 2007). Fifteen ligaments are found in the canine stifle joint with the primary ligamentous support of the joint being provided by the femorotibial ligaments, which are identified by their relationship to a joint, e.g. lateral (LCL) and medial (MCL) collateral ligaments, and their relationship to each other, e.g. cranial (CCL) and caudal (CaCL) cruciate ligaments (Carpenter and Cooper, 2000; Vasseur, 2002) (Figure 1.1). Cruciate ligaments lie between the condyle of the femur and the proximal tibia. Their location within the joint is in the cranial-caudal and medial-lateral planes (Saunders, 1933). The LCL is attached to the joint capsule by loose connective tissue and is not attached to the lateral meniscus, whereas, the MCL is attached to the medial meniscus (Vasseur and Arnoczky, 1981).

The CCL consists of two bands; a caudolateral band which is taut in extension but loose in flexion and a craniomedial band which is taut in flexion and extension (Carpenter and Cooper, 2000). The CaCL has also two bands; the cranial band in the CaCL is loose in extension and taut in flexion while the caudal band is taut in extension and loose in flexion (Arnoczky and Marshall, 1977). The collateral ligaments (MCL and LCL) control varus and valgus angulation,

such that the LCL is taut in extension and loose in flexion (Vasseur and Arnoczky, 1981). However, the cranial part of the MCL is stretched in both flexion and extension, while its caudal part is stretched in extension only (Vasseur and Arnoczky, 1981). All four ligaments function together to provide translation and rotational stability. When these ligaments are damaged, the stifle joint becomes mechanically unstable and results in an abnormal load distribution within the joint (Nagelli *et al.*, 2017). Consequently, this instability leads to changes associated with osteoarthritis (OA) such as osteophyte formation at the joint margins, thickening of the medial aspect of the joint capsule and the medial collateral ligament, and increased water content and softness of the articular cartilage (Bray *et al.*, 1992; Herzog *et al.*, 1993; Herzog *et al.*, 1998). Research on the long-term effect of canine CCL rupture (CCLR) shows that this injury results in OA as demonstrated by thickness loss of articular cartilage in some load bearing areas of the joint leading to an increase in joint friction, decrease in motion, pain and loss of muscle mass and strength in muscles crossing the stifle (Brandt *et al.*, 1991a; Brandt *et al.*, 1991b).

Unfortunately, the human knee joint is also one of the most vulnerable joints within the musculoskeletal system, and amongst the four major ligaments, anterior cruciate ligament (ACL) is the most susceptible ligament to rupture (Gianotti *et al.*, 2009). In the United States, approximately a quarter of a million people experience ACL injuries annually costing over 2 billion dollars per year in medical expenses (Novak *et al.*, 1996; Gottlob *et al.*, 1999; Griffin *et al.*, 2000; Gianotti *et al.*, 2009). Injuries occur due to non-contact and contact (traumatic) mechanisms (Hewett *et al.*, 2010; Smith *et al.*, 2012b; Smith *et al.*, 2012a). Contact injuries can be a result of direct contact with a force to the limb, whereas the non-contact mechanism does not result from such interaction (Hewett *et al.*, 2010; Smith *et al.*, 2012b; Smith *et al.*, 2012a). Non-contact injury mechanisms are typically associated with evasive manoeuvres such as sudden deceleration prior to a change of direction or motion (Boden *et al.*, 2000). It was estimated that over a five-year period, more than 58% of ACL ruptures occurred because of

non-contact injuries, where no overt joint trauma has occurred when the ligament ruptures (Boden *et al.*, 2000; Gianotti *et al.*, 2009). In addition, some researchers have identified that there is a greater risk of non-contact rupture in athletes, such as ligament mid-substance and bony avulsion injuries, reporting the ratio of non-contact to contact ACL injuries as 7:3 (Noyes and Grood, 1976; McNair *et al.*, 1990; Boden *et al.*, 2000). Similarly, the most common pathogenesis of canine CCLR is a gradual degenerative process (cranial cruciate ligament disease (CCLD)) generally resulting in a non-contact injury. Canine CCLD has a major financial impact; for example, in 2003 the management of CCLR was estimated to cost more than $1 billion (Bennett *et al.*, 1988; Wilke *et al.*, 2005). The cause of non-contact injury is controversial but factors such as joint conformation (i.e. femoral condyle width and height) (Comerford *et al.*, 2006; Ragetly *et al.*, 2011), altered ligament extracellular matrix (ECM) composition (Comerford *et al.*, 2005; Hasegawa *et al.*, 2013), genetics (Wilke *et al.*, 2004; Baird *et al.*, 2014) and obesity (Duval *et al.*, 1999) have been implicated in its aetiopathogenesis. The detailed literature review in Section 2.3 identified a knowledge gap in our understanding of the role of proteoglycans (PGs) to the viscoelastic behaviour of the canine CCLs. Therefore, it is the hypothesis of this study that PGs in the canine CCLs contributes to the structural integrity of the ligaments whilst altering PG content will result in a microstructural change in the tissue. This change may contribute to the decreased structural support in the CCL, resulting in ligament laxity and CCLR which is believed to be a leading cause of joint degeneration and OA (Comerford *et al.*, 2006).

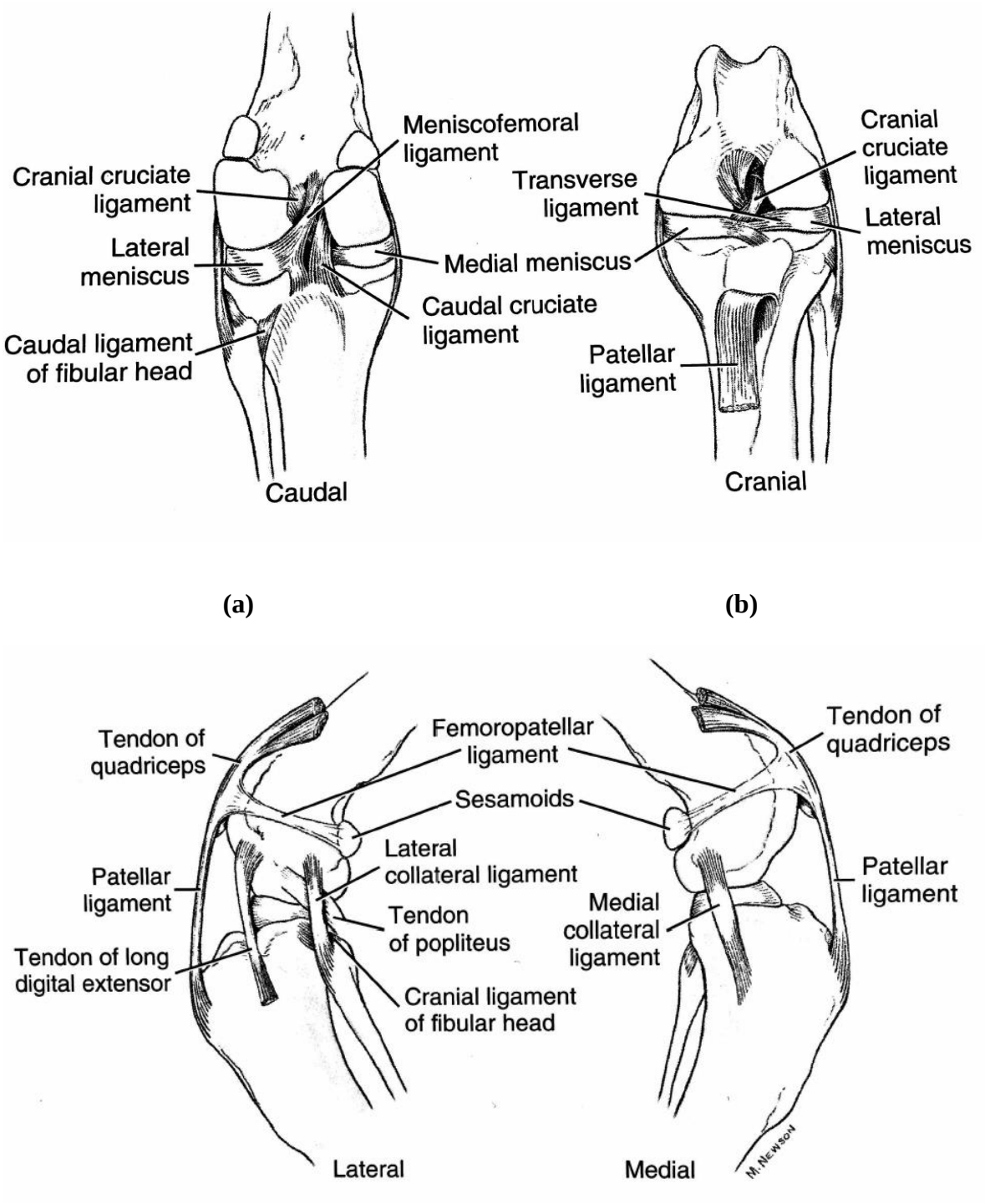

Figure 1.1: Line drawings of the canine stifle joint showing the major anatomical components in caudal (a), cranial (b), lateral (c) and medial (d) views. Taken from Miller's Anatomy of the Dog (Evans *et al.*, 2012).

1.2. Scope of Research

As reviewed in Section 1.1, the CCL is different to the other canine stifle ligaments in its function, structure and complexity (Arnoczky and Marshall, 1977). The current study recognised these differences; therefore, experimental tests were carried out to specifically characterise material properties of the CCL.

Non-contact joint degeneration due to CCLD is believed to be a leading cause of progressive OA in the stifle joints (Comerford *et al.*, 2006). As rupture of the canine CCL is thought to be averted by its viscoelastic material properties (Cook, 2010), the current study is focused on characterising these properties. The microstructural origins of the viscoelastic behaviour of CCLs are unknown, and there are no previous investigations to identify the role of proteoglycans (PGs) to the mechanobiology of this ligament. Therefore, this study examined the contribution of PGs to the material properties of CCLs because it has been hypothesised that PGs could affect the viscoelastic behaviour of the human MCL by forming molecular bridges between neighbouring collagen fibrils (Lujan *et al.*, 2009). To address the effect of PGs to the mechanical behaviour of the CCLs, experimental methods, such as tensile tests, and numerical methods, such as finite element analysis (FEA), comparing material characteristics of healthy and microstructurally altered CCLs were employed (Chapter 3).

FEA has been used as an effective method to manage injury and plan surgery in clinical practice (Wismans *et al.*, 1980). To be successful in a clinical setting, advanced imaging systems such as ultrasound, computerised tomography (CT) and magnetic resonance imaging (MRI) have been used to generate representative numerical models of the biological body (Baird *et al.*, 1998; Elsheikh, 2010; Stylianou *et al.*, 2014). This study used 3-tesla MRI to generate an anatomically representative three-dimensional (3D) FEM of the canine stifle joint that was a true representation of the joint *in vivo*. Previously, one study developed a 3D FEM for the stifle

joint from CT scans, however multiple assumptions were made to simplify the numerical model, for example excluding the geometries of major components like the ligaments or articular cartilage (Brown *et al.*, 2013). However, the current study developed and employed a 3D FEM of a canine stifle joint to include geometries of the major components in the joints, including the cruciate and collateral ligaments, the femur, tibia, fibula, articular cartilage and menisci. The material properties of these components were defined for the canine stifle joint, and the material parameters of the CCLs were described experimentally with the aid of digital image correlations and inverse analysis.

1.3. Thesis Structure

This thesis provides a clear description of the doctoral research including its aim and objectives, methodology, major results and main conclusions. The thesis is organised as follows:

Chapter 1 provides a background introduction to the knee joint and the scope of the study.

Chapter 2 reviews previous research on the morphology and functional anatomy of the canine CCL; methods applied to mechanically testing ligaments for their tensile and viscoelastic behaviour; the application of the DIC method on biological tissues and generating numerical models to represent the knee and stifle joints. Hypothesis, aim and objectives are outlined in this chapter.

Chapter 3 describes the experimental methods adopted for Experimental Study I, II and III including sample preparation, experimental setup, 3D DIC methods and analysis, FEM and inverse analysis of the CCLs, development and employment of the FEM of the whole stifle joint and statistical analysis.

Chapter 4 outlines the experimental findings for Experimental Study I, II and III. The numerical results, including the FEM of the CCL and the stifle joint are also presented in this Chapter.

Chapter 5 provides an overall discussion of the study and its main conclusions, as well as recommendations for future research.

2. Literature Review

2.1. Introduction

As far back as the golden age of Greek science (4th Century B.C.), pioneering work has been done to further our understanding of musculoskeletal tissues in terms of mathematical and physical principles (Braun, 1941; Ascenzi, 1993). In this Chapter, the anatomical structure and biomechanical properties of ligaments, with emphasis on the canine CCL, were reviewed. In addition, this Chapter looked at the main components present in the microstructure of CCLs and their contribution to the joint mechanics. It also reviewed previous publications on different experimental test methods and previous findings on the viscoelastic behaviour of ligaments and other soft biological tissues. Subsequently, studies on the application of DIC and inverse analysis on ligaments and other soft biological tissues were evaluated. In the last part of this Chapter, previous research on the development of numerical models for the canine stifle joint were appraised, and limitations of and gaps in some of the existing numerical stifle model data were identified. In this Chapter and throughout the thesis, canine joints and cranial cruciate ligaments were referred to as stifle joints and CCLs, respectively. Any joints and ligaments belonging to species other than canine were referred to by the human nomenclature (knee joint and the ACL).

2.2. Morphology of Canine CCLs

The late Middle English word *ligament* is derived from the Latin word *ligare*, which means “to bind”. According to Frank *et al.* (1985) the gross appearance of a ligament is white, firm, homogenous and fibrous. Their study categorised ligaments into two subgroups: those connecting other soft tissues, for example the suspensory ligaments in the abdomen, and those connecting the components of the skeleton. The major functions of skeletal ligaments are to

attach bones to form a joint, guide joint movement, sustain joint harmony and act as positional bend and strain sensors for the joint (Thornton *et al.*, 2007). The location and microstructure of ligaments dominate their functionality in the living body, hence a review on the macroanatomy, microanatomy and functional anatomy of the ligaments, in particular the CCL of the canine stifle joint, is presented in the following subsections.

2.2.1. Macroanatomy

The CCL originates from the caudomedial part of the lateral femoral condyle and runs diagonally across the intercondyloid fossa (joint cavity) to attach at the cranial intercondyloid area of the tibia (Arnoczky and Marshall, 1977; De Rooster *et al.*, 2006). The tibial attachment site is caudal to the attachment of the cranial tibial ligament of the medial meniscus and cranial to the attachment of the cranial tibial ligament of the lateral meniscus, while the intermeniscal ligament crosses over the insertion proximally (Figure 2.1). The CCL is narrowest in its mid-region and spreads out proximally and distally (Heffron and Campbell, 1978). The entheses (origin and insertion) of the CCL are directly inserted into the tibia and femur bones. Direct insertions (fibrocartilaginous entheses) contain four different transition zones: ligament mid-substance (fibrous tissue), fibrocartilage, mineralised (calcified) fibrocartilage and bone (Benjamin and Ralphs, 1998; Doschak and Zernicke, 2005) (Figure 2.2). This zonal transition from ligament to bone is of great importance because the mechanical properties of the two tissues are vastly different. Without a gradual transition in the mechanical characteristics of the ligament, abnormal stress concentrations may form in areas where the two tissues with significantly different behaviour meet (Moffat *et al.*, 2008).

Arnoczky and Marshall (1977) described the CCL as two parts which functioned independently from one another in flexion and extension (Figure 2.3). The two parts of the cranial cruciate ligaments (caudolateral (CLB) and craniomedial bands (CMB)) were named based on their

relative sites to the tibial plateau. The craniomedial band is found to be the most twisted and the longest, and it originates more proximally from the femur and attaches more cranially on the tibial attachment region. The caudolateral band originates from the most lateral and distal part of the lateral femoral condyle and attaches on the most caudal region of the tibial attachment area (Arnoczky and Marshall, 1977; De Rooster *et al.*, 2006). Despite the complex anatomical structure of the CCL, previous studies successfully obtained the length and cross-sectional area (CSA) of this tissue in different breeds of canine. CCL length and CSA in different canine breeds, such as rottweilers and greyhounds, were reported to vary between 17-19 mm and 19-29 mm^2, respectively (Wingfield *et al.*, 2000; Comerford *et al.*, 2006). Even with the differences between the two breeds, no statistical differences were found in the length and mid-CSA of the CCLs (Wingfield *et al.*, 2000; Comerford *et al.*, 2006).

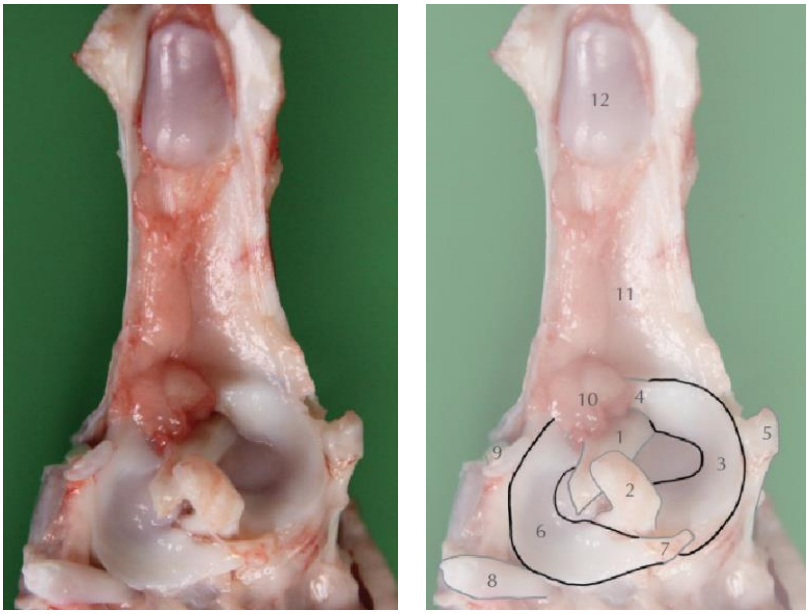

(a) **(b)**

Figure 2.1: Cranial cross-sectional view of a left stifle joint of a canine including the patella and patellar ligament (a) and line drawing of the same view (b) showing cranial (1) and caudal (2) cruciate ligaments; medial (3) and lateral (6) meniscus; intermeniscal ligament (4); medial collateral ligament (5); meniscofemoral ligament (7); popliteal tendon (8); tendon of the long digital extensor (9); infrapatellar fat pad (10); patellar tendon (11) and patella (12). Taken from De Rooster *et al.* (2010).

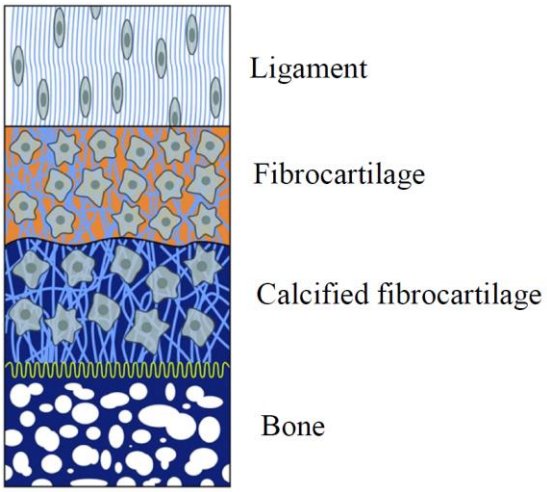

Figure 2.2: Schematic diagram of a zonal ligament insertion into bone. Fibroblasts are embedded throughout the aligned collagen fibrils (collagen type I) in the ligament, whereas larger and less parallel collagen bundles (collagen types I and II) and oval shaped cells are seen in the uncalcified fibrocartilage. The mineralised fibrocartilage is separated from the uncalcified fibrocartilage by the wavy tidemark between them. The calcified fibrocartilage shows mineralised tissue, circular chondrocytes and collagen type I, II and X. Taken from Yang and Temenoff (2009).

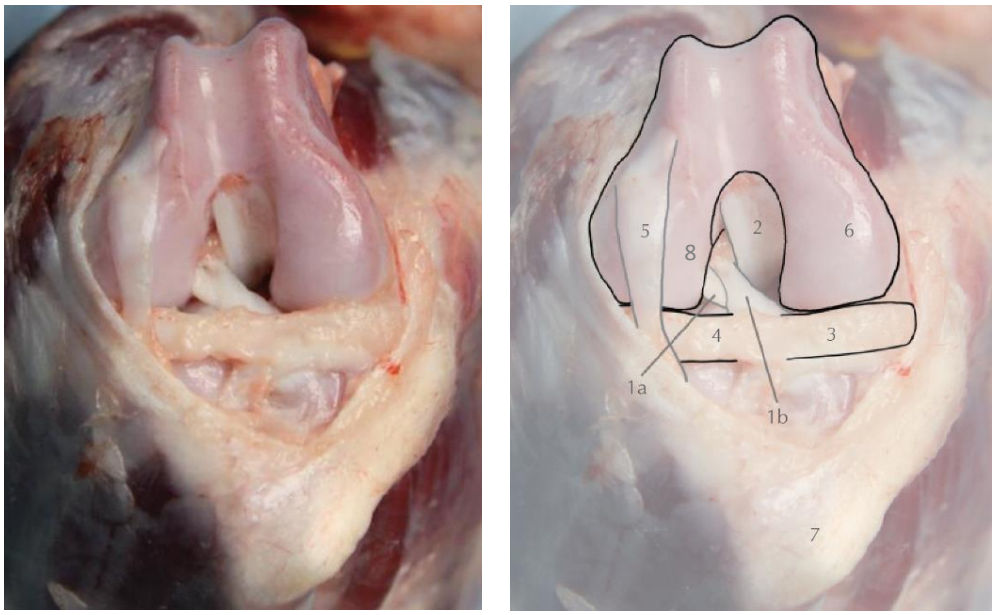

(a) **(b)**

Figure 2.3: Cranial view of a flexed right stifle joint of a canine (a) and line drawing of the same view (b) showing the caudolateral band (1a) and craniomedial (1b) band of the cranial cruciate ligament; caudal cruciate ligament (2); medial (3) and lateral (4) meniscus; tendon of the long digital extensor (5); medial (6) and lateral (8) femoral condyle; and tibial tuberosity (7). Taken from De Rooster *et al.* (2010).

2.2.2. Functional Anatomy

The CCL is a dynamic structure and it is one of the four most important anatomical structures involved in the stability of the stifle joint (Arnoczky and Marshall, 1977). The main function of canine CCLs is mechanical as they provide joint stability. The CCLs control cranial translation of the tibia (primarily) and internal tibial rotation (secondarily). However, they do not provide any restraint to the caudal translation of the tibia (Thornton *et al.*, 2007). In addition, Arnoczky and Marshall (1977) studied the role of CCLs in joint stability using selective cutting techniques. They suggested the use of the CMB of the CCLs as the primary check for cranial drawer motion because the CMB is taut in both flexion and extension, while using the CLB of the CCLs as the secondary check for this because the CLB is taut in extension and loose in flexion. During hyperextension, when the CCL is highly susceptible to rupture, CMB could be used as the primary check against hyperextension of the joint (Arnoczky and Marshall, 1977).

2.2.3. Microanatomy

The hierarchical structure of soft connective tissues, such as tendons and ligaments, is complex and consists of mainly collagen (70-80% of ligament dry weight) (Frank *et al.*, 1983; Amiel *et al.*, 1984). The hierarchical structure was firstly described in tendon by Kastelic *et al.* (1978) who reported that the tropocollagen molecules are synthesised by tendocytes (ligamentocytes in ligaments (Lo *et al.*, 2002a)) then self-assembled and grouped together in a highly ordered way to create fibrils. Fibrils have a periodicity (spacing) of 64nm and they are under maximum crimp at the fascicular periphery, whereas internal ones are nearly straight (Alm and Stromberg, 1974; Kastelic *et al.*, 1978). These wavy fascicular fibrils tend to arrange themselves non-uniformly in a parallel and helical fashion to the longitudinal axis to allow for multiaxial loading patterns (Yahia and Drouin, 1989; Amis, 1998). The combination of fibrils form fibres

which have an undulating crimp and the crimp period can vary significantly between different locations within ligaments (Frank *et al.*, 1999). The length of a single fibre changes by straightening its crimp as it is loaded under tension and this change has been reported by many authors by using a histologic assessment (Yahia and Drouin, 1989; Amis and Dawkins, 1991). The fibres were found to be denser and arranged tangentially to the ligament surface when the tissue is in contact with another surface (Vasseur *et al.*, 1985). This fibre arrangement is maintained even when the ligaments are twisted around each other, as seen in cruciate ligaments (Vasseur *et al.*, 1985). It is important to note that fibres and fibre bundles may or may not aggregate into fascicles. For example fascicles are not as obvious in MCL as they are in the ACL (Thornton *et al.*, 2007). As illustrated in Figure 2.4, the grouped fascicles form the entire ligament and each fascicle is separated by endoligament (Arnoczky, 1983; Yahia and Drouin, 1989). In addition, the morphological study by Arnoczky and Marshall (1977) and De Rooster *et al.* (2006) showed that the canine CCLs are not in a single-strand configuration of longitudinally aligned collagen fibres, but are made up of twisted collagenous fascicles and fibre bundles. The crimp in the CCL is believed to diminish under progressively larger mechanical loads, and disruption of the ligament fascicles is caused by further tensile loading (Hayashi *et al.*, 2003a; Hayashi *et al.*, 2003b).

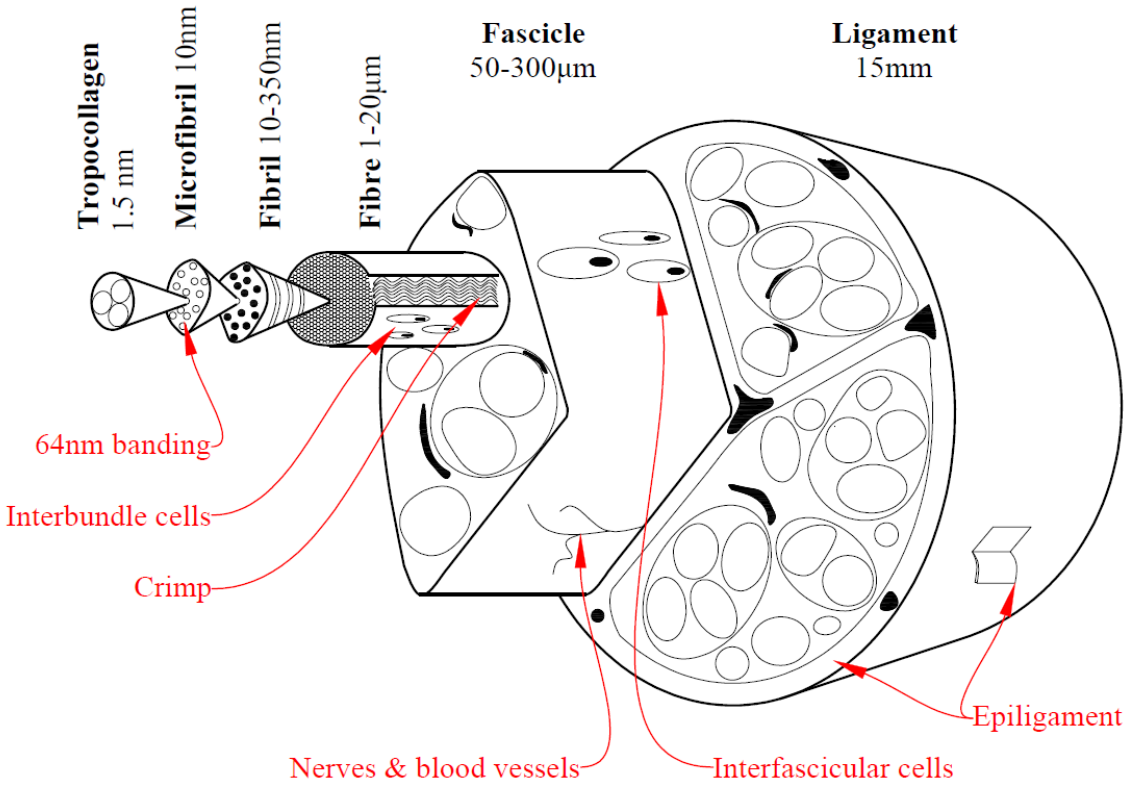

Figure 2.4: A simplified hierarchical structure of tendon and ligament. Image redrawn based on previous studies (Kastelic *et al.*, 1978; Kannus, 2000; Thornton *et al.*, 2007). This image illustrates the organisation of ligament/tendon microstructure and it does not illustrate shape of the connective tissues. For example, the overall complex shape of the CCL changes during physiological loads by acting as two bundles (CMB and CLB) to accommodate joint stability. However, the two bundles are not distinguished in the microstructural organisation. It is important to note that this illustration, similar to previous literature, is simplified by assuming that the connective tissues have a cylindrical shape whereas in reality the ligament cross section is irregular and complex (Carpenter and Cooper, 2000).

2.3. Major Structural Components of Canine CCLs

Ligaments are strong fibrous tissues which consist of cellular and extracellular components. This Section will outline the major components in canine CCL and their contribution to ligament mechanics.

2.3.1. Cellular Matrix

Most cells in soft connective tissues, such as tendons and ligaments, are fibroblasts and in ligaments they are referred to as ligamentoblast or ligamentocytes (Amiel *et al.*, 1984). The cells are present in long parallel columns between the collagen fibres (Amiel *et al.*, 1984). Their arrangement in normal ligaments creates a complex 3-dimensional network which consists of a series of parallel rows. Within each row, the spindle shaped cells have long cytoplasmic projections connected by gap junctions and the adjacent rows are interconnected by long projections and gap junctions (Figure 2.5) (Lo *et al.*, 2002b). Ligamentocytes in the canine CCL are not homogenous and vary in size, shape, orientation and number (Smith *et al.*, 2012c). The cell types, shapes and density were found to change along the length of CCLs (Vasseur *et al.*, 1985; Smith *et al.*, 2012c). Smith *et al.* (2012c) observed an increase in cellularity of the epiligament in the region where the CCL is in contact with CaCL (the mid-substance of the CCL). However, no change in epiligament cellularity was observed regionally on the surface of the CaCL (Smith *et al.*, 2012c). Unlike healthy canine CCLs where the cell density is high and many spindle shaped cells were found, ruptured CCLs have low cell density and both spindle and round shaped cells were observed (Ichinohe *et al.*, 2015). The role of these cells (i.e. fibroblasts) in soft connective tissues is to synthesis and assemble ECM molecules, such as fibrous proteins (i.e. collagen and elastin) and adhesive molecules (i.e. fibronectin and laminin) (Yamada *et al.*, 1985; Hardingham and Fosang, 1992; Yang *et al.*, 1999; Tozer and Duprez, 2005). In addition, there are other cell populations including fibrocartilage at attachment sites, myofibroblasts at sites of ligament healing and various stages of chondrocyte-like cells which are generally aligned within the matrix (Vasseur *et al.*, 1985). The cells in connective tissues, such as ligaments, organise themselves in a three-dimensional cellular matrix and the matrix senses the mechanical environment through cell-to-cell and cell-to-matrix interactions (Lo *et al.*, 2002a). Lo *et al.* (2002a) suggested that direct cell-to-cell

communication was responsible for coordinating cellular behaviour mainly in response to mechanical load within ligaments.

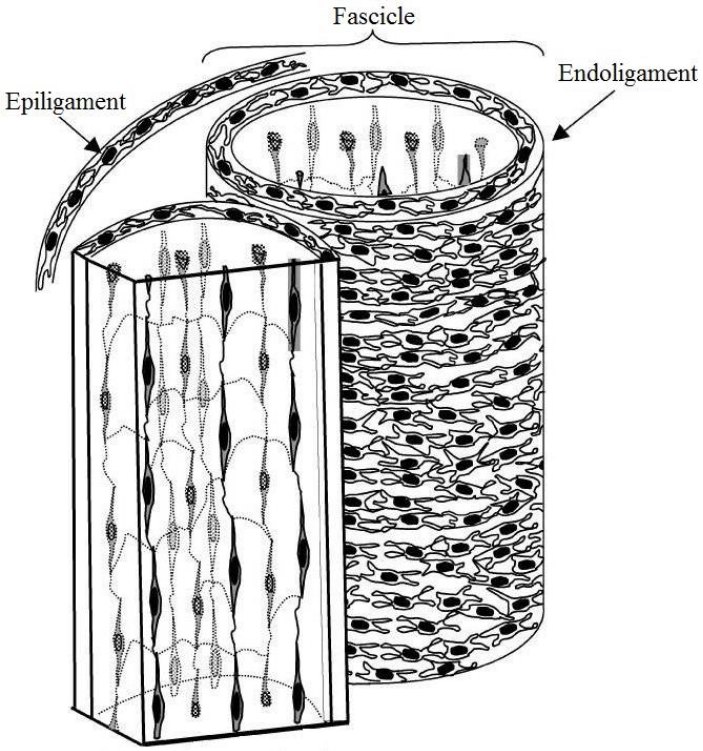

Figure 2.5: Schematic representation of the three-dimensional array of cells in a normal ligament. Epiligament refers to the surface layer associated with ligaments and endoligament refers to the tissue dividing ligament collagen fibres into separate fascicles. Taken from Lo *et al.* (2002b).

2.3.2. Extracellular Matrix

The ECM is the non-cellular structural system that is formed by cells and provides physical scaffolding for the cellular matrix (Frantz *et al.*, 2010). The ECM is also responsible for initiating biochemical and biomechanical signals that are required for tissue morphogenesis, differentiation and homeostasis (Benjamin and Ralphs, 1997; Frantz *et al.*, 2010). The ECM in ligaments consists of water, collagen, proteoglycans, fibronectin, elastin, actin and a few other

glycoproteins, which are described below (Benjamin and Ralphs, 1997; Frank, 2004; Thornton *et al.*, 2007).

2.3.2.1. Water

Water comprises 60-80% of the total wet weight of ligaments, and the water content is likely to contribute to cellular functions and viscoelastic behaviour (Khatod and Amiel, 2003; Frank, 2004). Within ligaments, water can be freely bound or be structurally bound to other ECM components and it can be bound to polar side chains, known as transitional water (loosely bound) (Thornton *et al.*, 2007). It is believed that a significant part of the water in ligaments is associated with the PGs, and together they interact with each other and define the viscoelastic characteristics of ligaments (Frank, 2004; Bray *et al.*, 2005). It is also presumed that water with PGs provides lubrication and facilitates sliding between the fascicles, hence affecting the gliding function of a ligaments (Woo *et al.*, 1999; Bray *et al.*, 2005). In addition, water is responsible for carrying nutrients to the fibroblasts and removing waste substances (Thornton *et al.*, 2007).

2.3.2.2. Dry matter of canine CCLs

The dry matter of a ligament (approximately one third total wet weight) includes fibrous protein (i.e. collagen, elastin, and other proteins such as fibronectin and laminin) and polysaccharides (i.e proteoglycans and glycosaminoglycans) (Frank, 2004).

2.3.2.2.1. Collagen

Collagen is a triple helix protein and comprises approximately 70-80% of the dry weight of ligaments (Frank *et al.*, 1983; Amiel *et al.*, 1984). Up to 90% of the ligamentous collagen is fibrillar type I, with the second and third most common type being fibrillar III and beaded filament VI respectively (Amiel *et al.*, 1984; Frank, 2004). A very small amount of collagen

types V, XI, and XIV have also been reported in ligaments (Amiel *et al.*, 1984; Frank, 2004). Collagen is important for ligament scaffolding, maintaining the tissue structure, cell adhesion, morphogenesis and tissue repair (Kadler *et al.*, 2007). Collagen type I, in particular, is the major protein that provides mechanical stability, elasticity and strength to ligaments (Kadler *et al.*, 2007). Collagen molecules are covalently cross-linked, transferring loads from one molecule to another (Gautieri *et al.*, 2012). As illustrated in Figure 2.6, the collagen molecules are assembled in a parallel fashion forming fibrils and the fibrils are cross-linked with macromolecules, such as PGs when forming collagen fibres (Gautieri *et al.*, 2012).

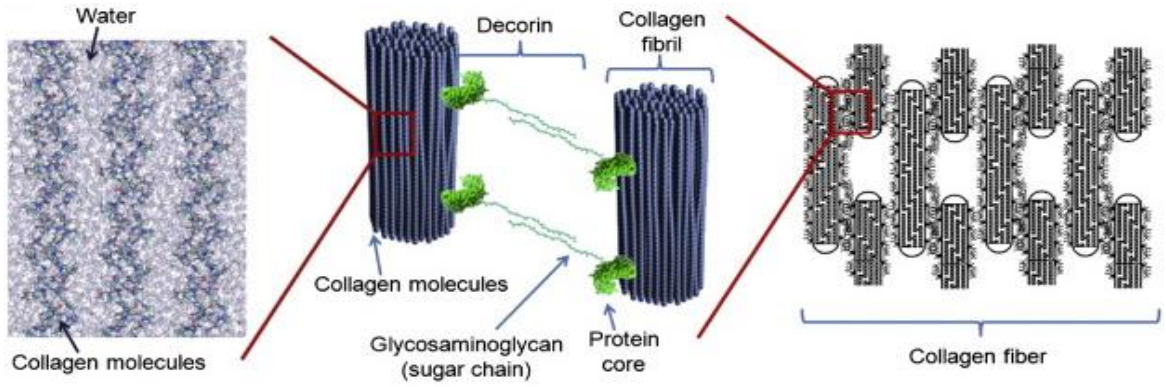

Figure 2.6: Schematic illustration of collagen fibre relationship with other ECM molecules. Taken from Gautieri *et al.* (2012).

2.3.2.2.2. Elastin

Elastin and microfibrils form elastic fibres which are one of the major assemblies in the ECM of connective tissues (Wise and Weiss, 2009). Elastic fibres are reported to account for about 1-2% of the dry weight of ligaments (Thornton *et al.*, 2007), however this quantity can vary significantly between different species. For instance, the ACL in human was found to contain <5% elastin (Dodds and Arnoczky, 1994), whereas in canine CCLs, elastin comprised approximately 10% and 4.6% of its dry weight in greyhounds and Staffordshire bull terriers, respectively (Smith *et al.*, 2014; Kharaz, 2015). The tropoelastin molecules (the precursor of

elastin) assemble into fibres and become highly cross-linked to one another via their lysine residue when unstressed (Frantz *et al.*, 2010). However, elastin stretches into a more ordered configuration under stress and reverts into a coiled arrangement when the stress is removed again (Frantz *et al.*, 2010). Importantly elastin stretch is crucially limited by tight association with collagen fibrils (Frantz *et al.*, 2010). The role of elastin in a ligament is related to the tensile response of the tissue to applied loads, recovery of ligament length after removing stress and protecting collagen at low strains (Thornton *et al.*, 2007).

2.3.2.2.3. Glycoproteins

Glycoproteins such as laminin and fibronectin are found in small quantities in the ligament ECM (Frank, 2004; Thornton *et al.*, 2007). Fibronectin facilitates a wide range of cellular interactions with the ECM and plays an important role in the matrix-cell feedback mechanism (Pankov and Yamada, 2002). Laminin plays a role in cell adhesion, migration, growth and differentiation (Kreis and Vale, 1993).

2.3.2.2.4. Glycosaminoglycans

Glycosaminoglycans (GAGs) occur in many vertebrate connective tissues and GAG content can be up to approximately 5% of normal ligament dry weight (Amiel, 1990). GAGs consist of large linear (unbranched) polysaccharides formed by repeating disaccharide units containing uronic acid (glucuronic or iduronic) or hexose (galactose) and hexosamine (galactosamine or glucosamine) (Ruoslahti, 1988; Schagemann *et al.*, 2004). GAGs contain negatively charged carboxylate or sulphate groups, hence they play an important role in controlling electrolytes and water in the extracellular fluid (Chakrabarti and Park, 1980). The polyanionic nature of GAGs is thought to provide electrostatic interaction with polycationic molecules or the positively charged region of a macromolecule (Chakrabarti and Park, 1980; Hardingham and Bayliss, 1990). Hence, the main role of GAGs is thought to be structural, rather than chemical,

as they occupy a large amount of space and provide toughness and flexibility in the connective tissues (Chakrabarti and Park, 1980). It has been reported that disturbance in the normal distribution of these polysaccharides can lead to serious clinical abnormalities that are characteristic of various diseases such as rheumatoid arthritis (Wang and Roehrl, 2002). There are different types of GAG in mammalian tissue and they are distinguished by their saccharides (sugar), the type of linkage between saccharides, and the number and location of sulphate groups. They are: hyaluronic acid or hyaluronan, chondroitin sulphate-4 and -6, dermatan sulphate, keratan sulphate, and heparin/heparan sulphate (Hardingham, 1981; Schagemann *et al.*, 2004).

2.3.2.2.5. Proteoglycans

A PG is a composite molecule consisting of a protein core that is attached to one or more GAG chains (Figure 2.7). The number of GAG chains on the core protein varies from 1 to 100 and their lengths vary from a few disaccharide units to hundreds (Vogel, 1994; Schagemann *et al.*, 2004). Proteoglycans are categorised into three types depending on the types of GAG chain: those with chondroitin or dermatan sulphate chains, those with heparan sulphate chains and those substituted with keratan sulphate (Vogel, 1994). PGs with a long protein core and many GAG chains are referred to as large aggregating PGs such as aggrecans and versican, whereas PGs with a shorter protein core and fewer GAG chains are called small leucine rich proteoglycans (SLRPs) such as decorin and biglycan (Vogel, 1994; Schagemann *et al.*, 2004). PGs comprise less than 3% of ligament dry weight and approximately 20% of the total PG content is large chondroitin and keratan sulphate containing PGs (Hey *et al.*, 1990). Ilic *et al.* (2005) stated that versican is the predominant large PG in ligament and the major type of PG in ligaments is decorin (~90%).

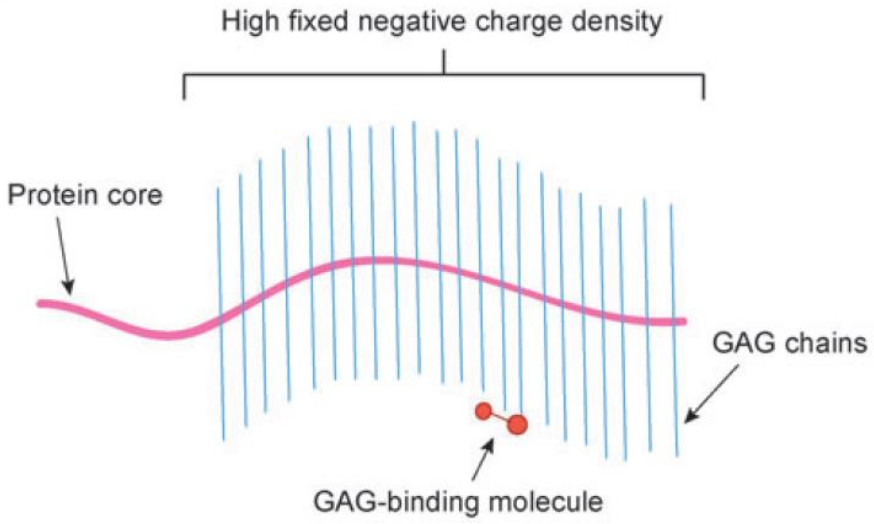

Figure 2.7: Schematic illustration of a proteoglycan showing glycosaminoglycan chains covalently bonded to a protein core. Taken from Swartz and Fleury (2007).

It is reported that PGs are responsible for organising and orienting the collagen fibres within ligament ECM, in which individual collagen fibrils are linked together by PGs (Figure 2.6) (Gautieri *et al.*, 2012). Rumian *et al.* (2007) hypothesised that increasing PG content may allow for more slippage between fibrils and fascicles allowing more deformation, thus preventing strain-damage during sport activities such as running. In an attempt to describe the contribution of GAG chains to the mechanical and viscoelastic behaviour of ligaments, some researchers investigated the effect of dermatan sulphate (DS) on the tensile and resistance properties of the human MCL under quasi-static loading conditions (Lujan *et al.*, 2009). Consequently, they determined the contribution of GAGs to the viscoelastic behaviour of the MCL, reporting that the interactions between GAGs and collagen fibrils had no impact on the viscoelastic properties (Lujan *et al.*, 2009). Similar findings were observed in studying the contribution of GAGs to viscoelastic properties of aortic valve tissue (Eckert *et al.*, 2013). It was reported that the GAG content in porcine aortic heart valve leaflets under tensile forces have no direct role in the time-dependent properties of the tissue (Eckert *et al.*, 2013). However, the researchers strongly associate the role of GAGs with fibre-fibre and fibre-matrix interaction at low stress levels,

such that they hypothesised that GAGs could provide a damping mechanism reducing aortic valve leaflet flutter when the leaflet is not under high tensile stress (Eckert *et al.*, 2013). Similarly, Eshel and Lanir (2001), in a study using rat dorsal skin, showed that PGs control the tissue's response at low strain level where the collagen fibres are crimped (toe region of stress-strain behaviour). Associating GAGs with fibre-fibre and fibre-matrix interactions has also been suggested by a number of authors, as they reported that the interaction between PGs and collagen fibrils organises the ECM, and transmits and resists tensile stresses in the tissue, hence contributing to the strength and material behaviour (Cribb and Scott, 1995; Eshel and Lanir, 2001; Schagemann *et al.*, 2004).

Furthermore, another study focused on the effect of sulphated glycosaminoglycans (sGAGs) on the permeability of porcine MCL, with the hypothesis that depleting sGAGs would decrease compressive stress and increase MCL transverse permeability (Henninger *et al.*, 2010). Their results showed that sGAG depletion significantly increased permeability and reduced peak stress during confined compressive loading. They studied transverse compressive loading because ligaments frequently undergo lateral contraction during axial tensile loading. When a ligament experiences dynamic compressive loading, the pressure from interstitial fluid within the tissue contributes to the compressive modulus (Swartz and Fleury, 2007). However, this mechanism was found to be greatest at low volumetric strain because permeability was dependent on strain (Henninger *et al.*, 2010). Therefore, at low strain levels sGAGs were found to have an important role in providing compressive support by controlling permeability within ligaments (Henninger *et al.*, 2010). The process of sGAG depletion showed an increase in water content in the ligaments (Henninger *et al.*, 2010). For example, the increase in water content was only notable when researchers compared chondroitinase ABC (ChABC) buffer treated with untreated ligaments, but the water content was not statistically different in ChABC buffer and enzyme treated ligaments ($p>0.05$) (Henninger *et al.*, 2010). Increase in tissue hydration

with sGAG depletion was also observed in the study by Murienne *et al.* (2015) when they depleted sGAGs from porcine sclera. They explained the increase in hydration after sGAG removal by distinguishing "bound" and "free" water in the matrix composed of charged GAG chains. When the GAG chains are abundant and long, which is the case of chondroitin sulphate (Schagemann *et al.*, 2004), they tend to interact with each other and create a tight matrix. This matrix has a large number of polar sites to which water binds but little space for free water (Murienne *et al.*, 2015). However, when a large majority of the GAG chains are removed, the matrix losses water-binding sites, hence increasing its capacity for free water absorption (Murienne *et al.*, 2015). They also reported that an increase in hydration resulted in minimal increase in volume which means that the water molecules occupied less volume than the GAGs, and lowered interfibrillar friction which decreased high-pressure stiffness in the tissue. Consequently, they concluded that sGAGs may affect the viscoelastic and tensile behaviour of sclera in the opposite way to an increase in hydration (Murienne *et al.*, 2015). This suggestion is similar to the hypothesis of this thesis, that altering PG content in canine CCLs changes the ECM composition which may in turn alter the viscoelastic properties of the tissue, resulting in ligament laxity CCLD and CCLR which is the leading cause of joint degeneration and progressive OA (Comerford *et al.*, 2006).

2.4. Experimental Testing Methods

To determine the mechanical properties of a given tissue, one must initially choose an appropriate experimental method. The most desirable method to determine ligament behaviour which is representative of that observed *in vivo* is uniaxial testing of bone-ligament-bone complex (Butler *et al.*, 1978a; Danto and Woo, 1993). Uniaxial tests involve subjecting the tissue to a one-dimensional tensile force at a prescribed strain rate. Subsequently, the load-deformation measurements are used together with the tissue's geometrical measurements

(length and CSA) to determine stress-strain characteristic, and hence the stiffness of the material (Fung, 1993). The CCL has a complex anatomical structure and broad insertion regions; therefore, it is difficult to obtain the CCL length and CSA with a high level of accuracy (Carpenter and Cooper, 2000).

Vasseur *et al.* (1991) determined the average length of canine CCLs from the craniomedial and caudolateral portions of the ligament before mounting the intact bone-CCL-bone to the tensile testing machine. CCL lengths were found to vary between canine breeds, for example CCL length in mature mongrel canines (20.5mm) was greater than in rottweilers (18.7mm), greyhounds (17.3mm) and Labrador Retrievers (17.2mm) (Vasseur *et al.*, 1991; Wingfield *et al.*, 2000; Comerford *et al.*, 2005).

Researchers have used several methods to measure the CSA of soft tissues such as tendons and ligaments (Gillis *et al.*, 1995; Noguchi *et al.*, 2002; Liu *et al.*, 2008; Vergari *et al.*, 2010). The two most common methods employed by previous investigators include contact (i.e. destructive or non-destructive) and non-contact (i.e. non-destructive) methods. Of the contact methods, the constant pressure area micrometre and the strain gauge micrometre technique have been identified as producing more accurate CSA measurements than non-contact CSA measurements (Woo *et al.*, 1990a; Goodship and Birch, 2005). However, both methods resulted in sample destruction; therefore, different tissues were used for mechanical tests, making the results non-comparable. For this reason, non-contact techniques to measure the CSA of ligaments have been employed by researchers, including computerised tomography, ultrasonography and laser scanning (Gillis *et al.*, 1995; Noguchi *et al.*, 2002; Liu *et al.*, 2008; Vergari *et al.*, 2010). However, the method used by Goodship and Birch (2005) produced a more accurate CSA measurement than those reported by Noguchi *et al.* (2002) using ultrasonography determination. This was a non-destructive replica method for determining the

CSA of soft connective tissues (Goodship and Birch, 2005). There are many advantages to using the replica technique: it is quick, simple, can be done at a low cost and can be used on samples with an irregular shape such as CCLs (Race and Amis, 1996; Wingfield *et al.*, 2000; Goodship and Birch, 2005). Also, it produces comparatively better results than other non-contact methods (Noguchi *et al.*, 2002; Goodship and Birch, 2005).

The experimental apparatus employed to determine the material characteristics of knee ligaments contributes to the accuracy of the results. Several researchers have used a custom-built clamp to test the knee bone-ligament-bone complex under tensile loads (Haut and Little, 1969; Noyes and Grood, 1976; Woo *et al.*, 1987; Woo *et al.*, 1990c; Danto and Woo, 1993). The illustration in Figure 2.8 shows an example of a specially designed clamp employed to hold the ACL and perform tensile tests (Woo *et al.*, 1987; Danto and Woo, 1993). The clamp holds the femoral and tibial bones in place with two ¼-inch steel bars secured at the top of the bones. In addition, orthodontic cement was used to help further secure the bones whilst allowing ligaments to be free from obstruction. The clamping system was designed to orientate the ACL so that the longitudinal axis of the ACL was in line with the loading axis (Woo *et al.*, 1987; Danto and Woo, 1993). Using this type of clamping arrangement allowed for determination of ligament behaviour which was representative of that observed *in vivo*. In addition, other researchers have extracted strip-like shaped ligaments for tensile tests and they excluded the use of femur and tibia bones to assist with gripping (Lujan *et al.*, 2009). This approach was seen in the studies by Lujan *et al.* (2009) as they used a hardened steel punch to extract four tensile samples from different locations in the MCL at different regions between the tibia and femur attachments. The shape of the steel punch included bevelled ends for gripping and was oriented so that its long axis was aligned with visible fibre bundles (Figure 2.9). However, extracting tensile specimens from the MCLs using a steel punch inevitably cuts

the collagen fibres and breaks the fibre-matrix bonds. Hence, the mechanical response of the tissue to the applied load may be affected (Quapp and Weiss, 1998).

Another important aspect of obtaining a reliable experimental result is the testing environment. Haut and Little (1969) investigated three different types of testing environments, including a slightly moistened environment during mechanical tests with a saline solution, immersion in a saline solution at room temperature and immersion in a saline solution at 38.3°C (canine body temperature). Their results showed that the moistened CCLs behaved in a similar fashion to those immersed in saline at room temperature, whereas the stress-strain curve for ligaments immersed in saline at canine body temperature was significantly different. They suggested that elevated temperature may drastically change the material response of tissue to tensile loads, however, they could not give conclusive proof about the effect of temperature during tests because of the limited number of varying temperature tests which resulted in the irregularities in their results (Haut and Little, 1969). Similarly, Haut and Powlison (1990) highlighted the importance of an appropriate test environment for investigating material parameters of soft connective tissues. They found a significantly higher modulus and strength for the patella tendon when it was tested in a temperature-controlled saline bath compared to testing the tendon in a drip (moistened) environment suggesting that soft tissues such as ligaments tested in air may be subject to dehydration.

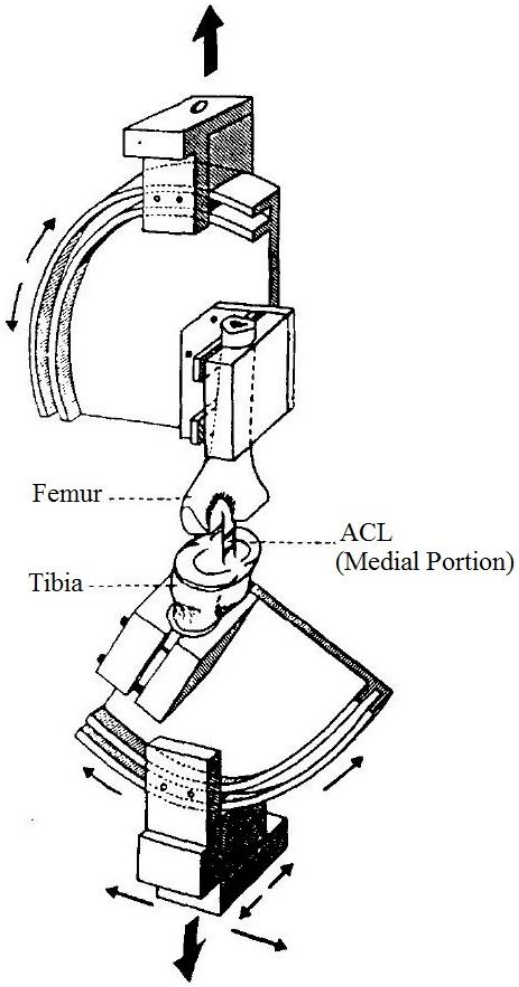

Figure 2.8: Schematic diagram of the anterior cruciate ligament (ACL) in a specially designed clamp. The clamp was employed in previous studies to perform tensile tests on the ACLs. Taken from Danto and Woo (1993).

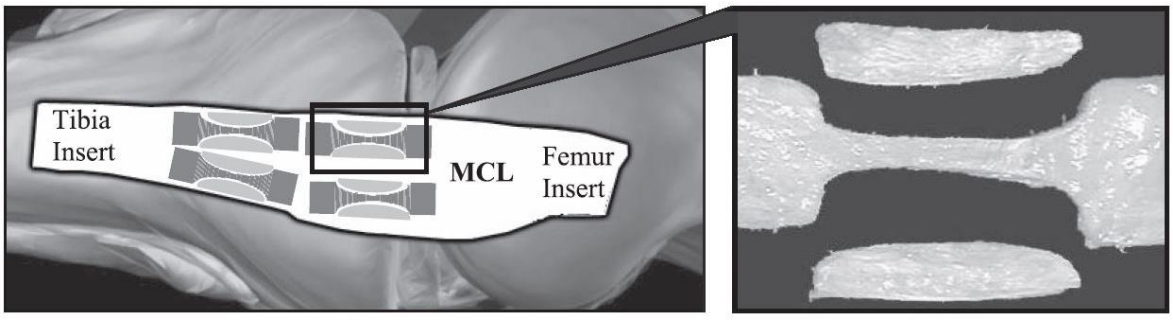

Figure 2.9: Illustration of specimen acquisition from different regions of an MCL using a steel punch. As shown, the punch shaped specimen is cut from the MCL leaving bevelled ends for gripping. The two adjacent half-elliptical strips were used for tissue hydration monitoring. The magnified image on the right shows a photograph of the specimen set obtained from the MCLs. Taken from Lujan *et al.* (2009).

2.5. Material Properties

The mechanical properties of ligaments vary depending on their location in the body, their function, age and gender (Woo *et al.*, 1990b; Woo *et al.*, 1992). As shown in Figure 2.10, the stiffness of ligaments (rate of change of load with deformation) varies non-linearly with load (Woo, 1982). The initial part of the load-deformation diagram, zone I, is the toe region where ligament fibres tighten and the crimp is removed. In this zone, there is a relatively large deformation of the tissue with little increase in load and this permits initial joint deformations with minimal tissue resistance (Dale and Baer, 1974; Fratzl *et al.*, 1998; Wingfield *et al.*, 2000). With the disappearance of crimp, the linear part (elastic phase) of the load-deformation curve (zone II) starts where the collagen fibres are all recruited to resist applied load (Dale and Baer, 1974; Fratzl *et al.*, 1998; Wingfield *et al.*, 2000). Together with other ligaments, and major components of the knee joint, ligaments work within their low-force level to guide normal joint movements (Dale and Baer, 1974; Fratzl *et al.*, 1998; Wingfield *et al.*, 2000). Zone III is the plastic phase where ligament stretching is irreversible. At higher loads, ligaments become stiffer, providing more resistance to tissue deformation. Increasing the applied load to further deform the ligament and overcome stage III resistance will lead to tissue rupture (zone IV) (Dale and Baer, 1974; Fratzl *et al.*, 1998; Wingfield *et al.*, 2000; Thornton *et al.*, 2007). It is the toe region and the lower strain portion of the elastic phase that is addressed in the current study.

The mechanical behaviour of most biological tissues is non-linear viscoelastic rather than elastic (Haslach, 2005). Viscoelastic materials exhibit both elastic and viscos behaviour including history- and time-dependent characteristics (Fung, 1993). To understand the material behaviour of knee and stifle ligaments, researchers have investigated different forms of viscoelastic characteristics including preconditioning, strain rate sensitivity, hysteresis, creep

and stress relaxation (Haut and Little, 1969; Fung, 1993; Hingorani *et al.*, 2004; Solomonow, 2004; Quinn and Winkelstein, 2011; Miller *et al.*, 2012). These properties which are the focus in the current study are reviewed in the following Sections.

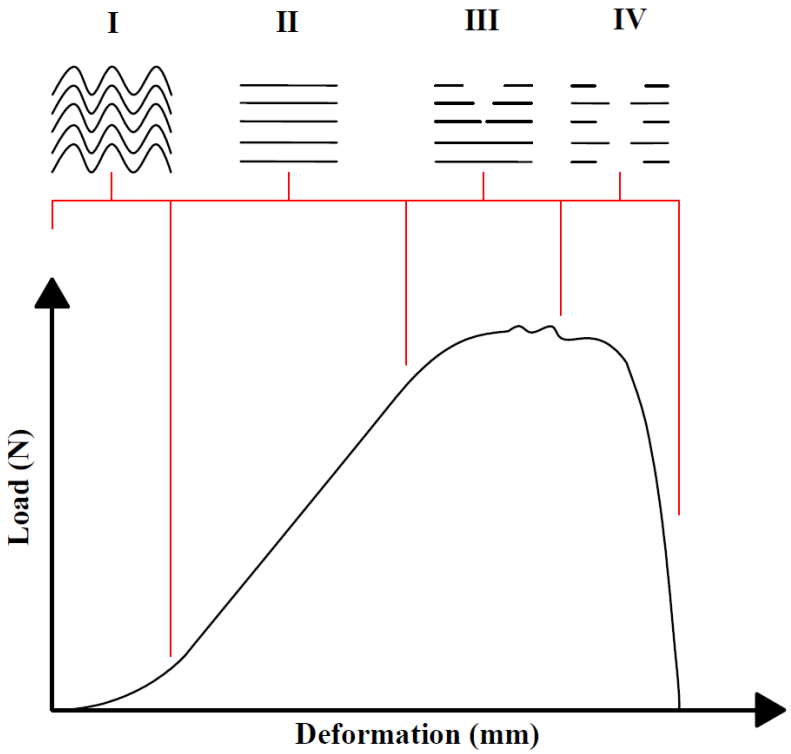

Figure 2.10: A typical load-deformation curve of a healthy ligament loaded under tensile force to failure. The top part of the diagram shows schematic representations of ligament fibres going through stages of crimp (I) through recruitment (II) to progressive failure (III and IV). Redrawn based on Thornton *et al.* (2007) and Wingfield *et al.* (2000).

2.5.1. Preconditioning

Fung (1993) described the preconditioning of soft biological tissues as a process of repeated cyclic loading of a sample whereby a gradual adaptation of the tissue to its loading is achieved. The preconditioning process is used prior to mechanical tests to eliminate the effects of tissue handling and establish a steady state condition for the tissue (Fung, 1993). Although this is a widely used process, its effects are not thoroughly understood (Conza, 2005). Typically,

preconditioning results in a stiffening of the tissue with the progressive increase of loading cycles, although Eshel and Lanir (2001) reported a decrease in stiffness when they preconditioned rodent dermal tissue. However, it should be noted that they preconditioned their samples under cyclic stretch at a fast rate to a high strain of approximately 20% (Eshel and Lanir, 2001). Consequently, the decrease in stiffness could be a result of microstructural failure or plastic deformation of some ECM components (Quinn and Winkelstein, 2011). There are no standard preconditioning procedures because preconditioning is highly dependent on the mechanical test profile such as the amount of load or elongation (Conza, 2005). One way to establish a common baseline for testing material properties of soft tissues is to perform a series of preliminary experiments, such as subjecting the tissue to several loading and unloading cycles until consistent behaviour is observed (Fung, 1993). It has been reported that applying low loads (below 30-50% of ultimate failure) allows the tissue to reach its preconditioning state with a lower number of loading and unloading cycles (Conza, 2005).

During preconditioning cycles, the stress associated with a given strain decreases within the first few cycles, until consistent stress-strain behaviour is established (Figure 2.11). The specific microstructural mechanisms that drive this change in the mechanical properties are associated with the realignment of the collagen fibres within the tissue in the direction of the applied load (Quinn and Winkelstein, 2011). Similarly, prior to the study by Quinn and Winkelstein (2011), other authors suspected that the process of preconditioning involved a large viscous energy loss which may be associated with rearrangement of the interfibrillar matrix including water and PGs (Yahia and Drouin, 1990). During cyclic loading and unloading, it is important to provide adequate rest time to allow tissue recovery, including a combination of water influx, returning collagen crimps, elastin tensile force, and decreasing collagenous organisation under unloaded conditions (Thornton *et al.*, 2007).

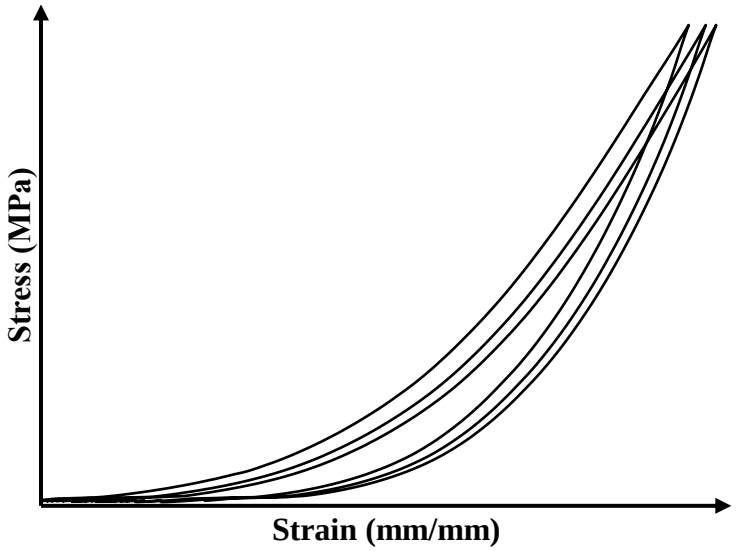

Figure 2.11: Typical stress-strain behaviour of a ligament tissue during preconditioning demonstrating the shifting behaviour with progressive cycles. Redrawn based on Schatzmann *et al.* (1998).

2.5.2. Strain Rate Sensitivity

Strain rate sensitivity is a time-dependent characteristic of certain materials in which the stress-strain behaviour alters depending on the rate at which strain is applied (Fung, 1993). Typically, higher strain rates will produce stiffer behaviour, producing a higher modulus. This phenomenon of viscoelastic characteristics has been observed in soft biological tissues such as the sclera (Elsheikh *et al.*, 2010), cornea (Elsheikh *et al.*, 2011), tendon (Robinson *et al.*, 2004) and ligaments (Bonner *et al.*, 2015). The tension which develops in a ligament is dependent on strain rate. For example, slow strain rates result in the development of low tension, whereas high strain rates cause high tension (Woo *et al.*, 1990c). Several researchers focused on the effect of loading to failure using high strain rates. This is when ligament failure occurrence is likely due to contact and non-contact sport injuries (Crowninshield and Pope, 1976; Lydon *et al.*, 1995; Crisco *et al.*, 2002). Haut and Little (1969) investigated lower strain rates between

approximately 2 and 54%/min. In their study on the mechanical properties of the canine CCL, they reported that the tissue stiffness (measured by tangent modulus) increased with strain rate, the overall shape of the stress-strain curve did not undergo major changes, but the transition from the toe region appeared at lower strain levels in tests with higher strain rates. In the same tests, rapid change in the tangent modulus was found with the slow strain rates (between 1.7 and 10.8 %/min) but the change became progressively smaller with higher strain rates (above 10.8 %/min). Moreover, they reported that stress-strain behaviour at the toe region was dependent on strain rates up to 6% strain (Haut and Little, 1969). Similarly, Pioletti *et al.* (1999) showed that for a given strain level the stress increases with augmentation of the strain rate. For example, when they tested bovine ACL at 2400%/s they reported that 70% of stress was due to the effect of strain rate. However, some authors studied the mechanical properties of the rabbit MCL between the strain rates of 0.66 and 9300%/min and found that the MCL complex was only minimally strain rate sensitive (Woo *et al.*, 1981; Woo *et al.*, 1990c). Similarly, others have reported that the strain rate sensitivity decreases with the increase of deformation rate (Crisco *et al.*, 2002; Bonner *et al.*, 2015). Bonner *et al.* (2015) undertook macroscale experiments at strain rates ranging from (~6-300%/min) on the porcine stifle LCL. They observed a typical stress-strain behaviour showing a toe region up to 3-4% strain followed by a linear region. As described in Section 2.5, previous literature showed the toe region to be associated with the uncrimping of the collagen fibrils followed by a sequence of molecular twists within the gap regions of collagen fibrils (Misof *et al.*, 1997; Thornton *et al.*, 2007). As presented in Figure 2.12, Bonner *et al.* (2015) believed that at slow strain rate (~6%/min) the unloaded fibrils (Figure 2.12 (i)) go through the toe region (Figure 2.12(ii)) before presenting intra-fibrillar gliding (Figure 2.12(iii)). However, at fast strain rates (~300%/min) fibrils start from an unloaded state (Figure 2.12 (i)) then move directly to intra-fibrillar gliding (Figure 2.12 (iv)). PGs are believed to greatly contribute to the organisation and cross-linking of fibrils

in connective tissues (Gautieri *et al.*, 2012), and are also believed to affect the strain rate sensitivity (Robinson *et al.*, 2004). These authors believe that decorin significantly affects the strain rate sensitivity of tendons in mice and they observed that tendon fascicles without decorin had similar elastic properties to normal fascicles, but reduced strain rate sensitivity (Robinson *et al.*, 2004). In addition, they found that collagen fibre content had little effect on viscoelasticity of the tendon. Their study suggested that the strain rate sensitivity in a tendon is more associated with ECM components, such as PGs, rather than collagen. Since decorin is also a major PG in the ligaments (Ilic *et al.*, 2005), these findings could also provide an insight into the viscoelastic behaviour of the canine CCL.

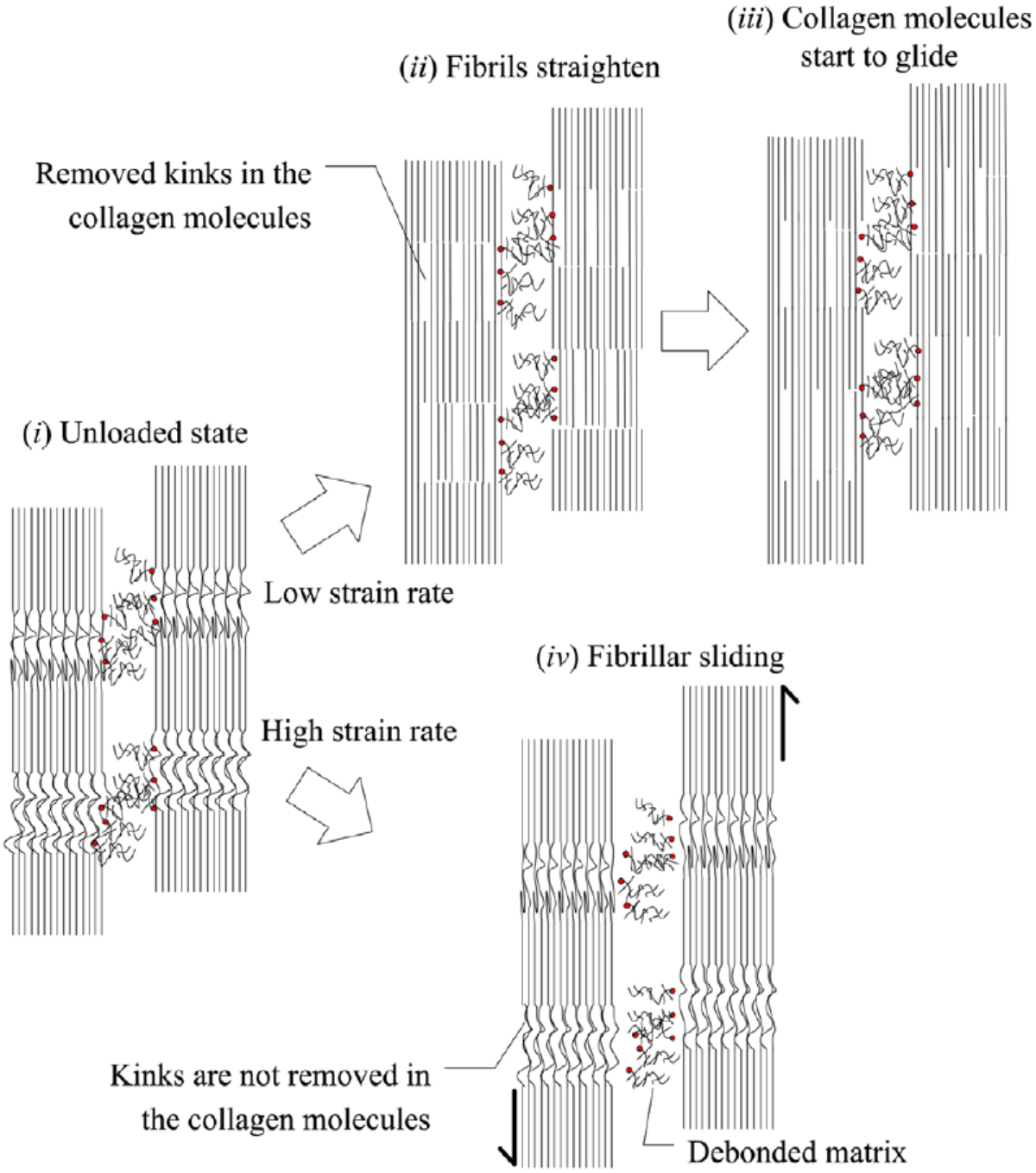

Figure 2.12: Deformation mechanisms proposed by Bonner *et al.* (2015) of the actions of intra- and inter-fibrillar structures in ligament during low (top) and high (bottom) strain rates.

2.5.3. Hysteresis

Hysteresis is characterised during cyclic loading of soft biological tissues and it can be measured by finding the difference between the loading and unloading stress-strain curves

(Fung, 1993) (Figure 2.13). Hysteresis represents the loss of energy (energy dissipated) within the material. This phenomenon is only weakly dependent on strain rates within soft biological tissues (Fung, 1993). However, Haslach (2005) pointed out that Fung's belief in this phenomenon was based on a small number of experiments on rabbit papillary muscle using only three different strain rates. Hence, Fung's findings only approximately support the independence of hysteresis from strain rates. Boyce (2007) studied on the viscoelastic tensile response of bovine cornea and supported Haslach's suggestion and they found an increase in hysteresis with decreasing strain rates. Hysteresis is associated with cyclic deformations and load at a constant peak magnitude (Solomonow, 2004) (Figure 2.14). Increasing the number of cyclic deformations at a constant peak stretch results in a decrease in tension which reflects the development of load-relaxation (Figure 2.14 (a)). However, increasing the number of load cycles at a constant peak load results in an increase in ligament length showing the development of creep (Figure 2.14 (b)). In summary, Solomonow (2004) observed that the impact of hysteresis gradually decreases tension in the ligament, develops joint laxity, reduces joint stability and hence increases the risk of ligament injuries. Therefore, it is important to allow a sufficient rest period between test cycles to facilitate recovery of the ligament function (Solomonow, 2004).

Decorin accounts for 90% of the PGs within ligaments (Ilic *et al.*, 2005) and it is believed to contribute to the material properties of ligaments (such as permeability) (Henninger *et al.*, 2010). However, a reduction in decorin content as determined by depletion with chondroitinase B (ChB) in human MCL was found to have no effect on hysteresis of the tissue (Lujan *et al.*, 2007).

During *in vitro* mechanical tests of soft biological tissues, it is important to employ careful sample handling and storage (Section 2.5.1). To minimise the effect of tissue handling, a

precondition process is used prior to mechanical tests (Fung, 1993). During preconditioning cycles, hysteresis was found to decrease significantly (Woo *et al.*, 1986; Fung, 1993). The effect of tissue storage, such as freezing-thawing, on hysteresis has been studied in connective tissues such as ligaments and tendons (Woo *et al.*, 1986; Giannini *et al.*, 2008; Chen *et al.*, 2011). Chen *et al.* (2011) found no significant differences in stiffness, maximum strain, elastic modulus and energy density of rabbit Achilles tendon after repeated freezing-thawing at -80°C. However, histological changes were observed as the number of freezing-thawing increased from three to ten times (Chen *et al.*, 2011). For example, the arrangement of tendon bundles and collagen fibrils were disordered and apparent gaps appeared between the tendon bundles because of the formation of ice crystals (Chen *et al.*, 2011). This change in the tendon histology only affected certain biomechanical measurements such as the values of maximum load and stress and energy at maximum load (Giannini *et al.*, 2008; Chen *et al.*, 2011). Woo *et al.* (1986) studied biomechanical properties of fresh and frozen rabbit MCLs at -20°C for three months. They reported significant differences in hysteresis area between fresh and frozen MCLs during the first few load-unload test cycles. However, with exception to the hysteresis area, prolonged freezing and storage did not significantly affect the stress-strain, tensile strength and ultimate strain of ligaments (Woo *et al.*, 1986). This is similar to the findings by Moon *et al.* (2006) who studied stress relaxation behaviour of fresh and frozen (two times at -20°C for four weeks) rabbit MCL and found no statistical differences between the two groups. Therefore, careful storage and refreezing of the CCL is suggested to have little or no effect on the biomechanical properties (Woo *et al.*, 1986; Moon *et al.*, 2006).

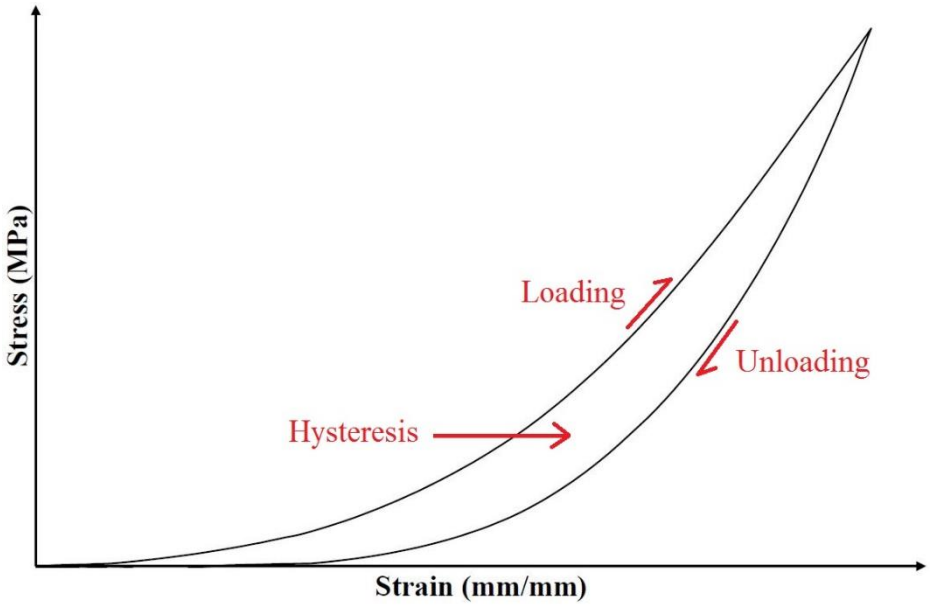

Figure 2.13: Hysteresis area between a loading and unloading stress-strain curve. Redrawn based on Elsheikh *et al.* (2008).

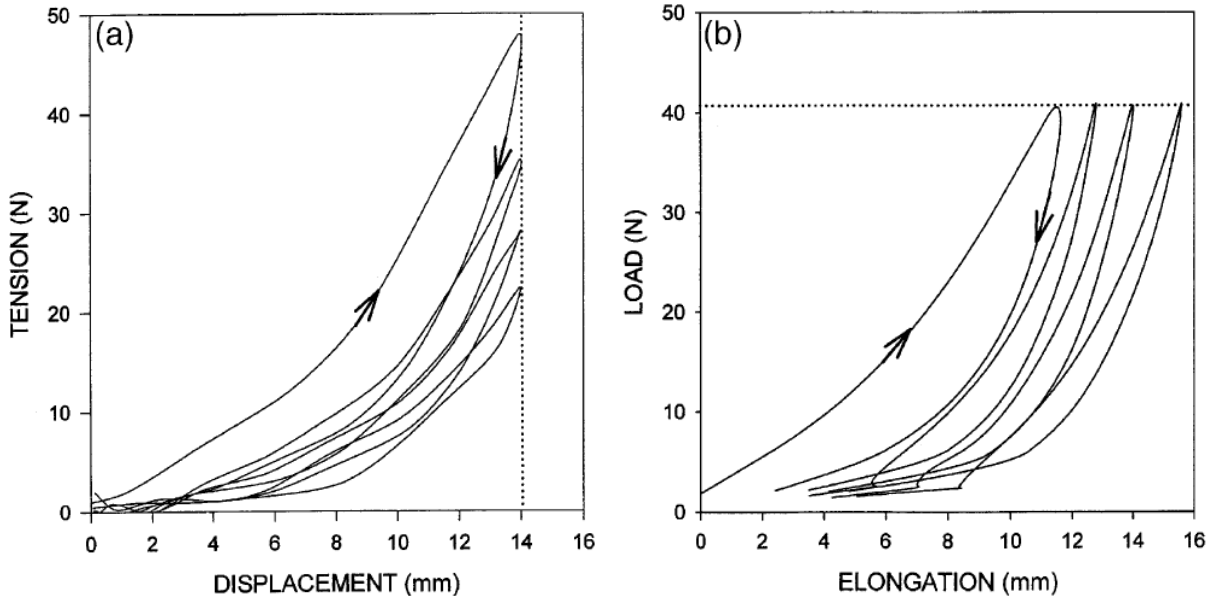

(a) **(b)**

Figure 2.14: Hysteresis associated with cyclic displacement (a) and load (b) at the same peak magnitude. Taken from Solomonow (2004).

2.5.4. Creep

Ligaments creep when subjected to a constant load (Figure 2.15), and it is observed that creep behaviour in ligaments results in extension over time until the point of unloading or failure (Frank, 2004; Robinson *et al.*, 2004).

One of the studies on quantifying creep behaviour of knee ligaments was by Thornton *et al.* (2002), and they used rabbit MCLs to examine creep over a range of stresses, including toe-region, transition between toe- and linear-regions and linear-region of the stress-strain curves. Their concurrent crimp analysis showed that fibre recruitments helped minimise the creep of ligaments at low, toe-region stresses hence preventing joint instability (by minimising ligament elongation) and ligament fibre rupture (by progressively reducing the stress on the initially loaded fibres) during normal knee joint movements. At this physiologically relevant region (toe and linear regions) of ligament behaviour, the rate of creep was reported to be stress dependent in the rabbit MCL, with the rate of creep decreasing with increasing stress (Hingorani *et al.*, 2004). However, they found resistance to creep by fibre recruitments to be limited at higher stresses (linear-elastic).

As described in Section 2.3.2.2.5, at a low strain level, the sGAGs of PGs were found to characterise permeability in ligaments, hence digesting sGAGs was reported to increase hydration in ligaments leading to an increase in ligament capacity of free water absorption (Henninger *et al.*, 2010; Murienne *et al.*, 2015). Moreover, a change in water content in ligaments was reported to be directly proportional to change in creep behaviour (Thornton *et al.*, 2001). They reported that increasing ligament hydration led to an increase in ligament creep (Thornton *et al.*, 2001). However, previous literature did not indicate the direct relationship between creep behaviour and PG content in the canine CCL. Hence, this study further

investigates creep behaviour with changing PG content in the canine CCLs which may in turn lead to CCLD and CCLR.

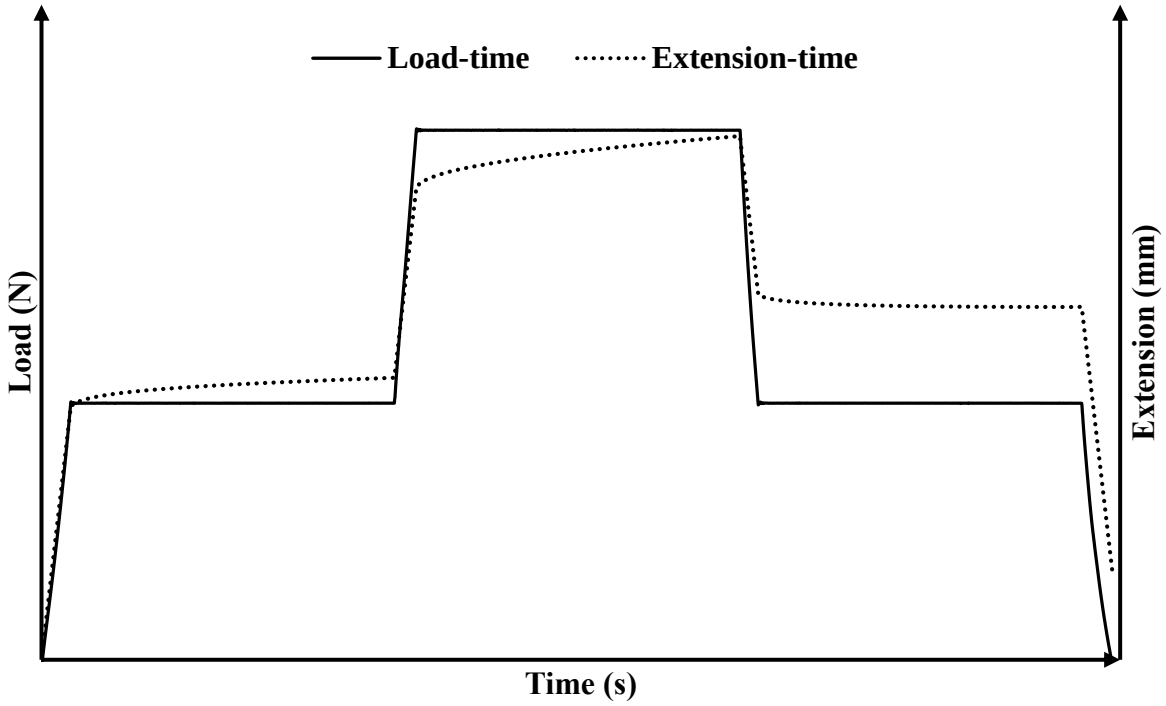

Figure 2.15: A typical load-time (input) and extension-time (response) profile during a loading and unloading test to study the creep behaviour of ligaments at a low stress level. Redrawn based on Thornton *et al.* (2001).

2.5.5. Stress Relaxation

Stress relaxation is a characteristic similar to creep, however, rather than a constant load being held, a constant deformation is applied (Figure 2.16). Stress relaxation is a characteristic of ligaments and it decreases stress over time as the microstructures of the tissue reorganise themselves to reduce the applied load (Frank, 2004). Stress relaxation is a result of the viscous component of the ligament's response to load. The faster a load is applied, the less time there is for the viscous component to dissipate (Thornton *et al.*, 2007). Also, a study on human MCL showed that the stress relaxation of ligaments tested at lower strain levels was significantly

greater than that at higher strain levels (Lujan *et al.*, 2009). Similarly, Hingorani *et al.* (2004) also showed that within the physiologically relevant region of ligament behaviour, the rate of stress relaxation is strain dependent in the rabbit MCL, with the rate of relaxation decreasing with increasing tissue strain. Unlike the preconditioning phenomenon, where a large collagen fibre realignment was observed, no significant changes were seen during stress relaxation in the rat supraspinatus tendon (Miller *et al.*, 2012). The microstructural mechanism of stress relaxation is also different from creep (Fung, 1993), as found by crimp analysis in rabbit MCL where no changes in collagen fibre crimp behaviour was found before and after stress relaxation tests, whereas fibres were engaged during creep tests (Thornton *et al.*, 2002). This finding, together with the results from Miller *et al.* (2012) on tendons showing the lack of collagen fibre realignment during stress relaxation, suggests that a shift in the structural organisation of collagen fibres may not be responsible for this phenomenon. Other than collagenous fibres, other ECM components in connective tissues, such as PGs, are believed to affect the viscoelasticity of the tissue (Robinson *et al.*, 2004). A quantitative study on the effect of PGs on the viscoelastic behaviour of tendons in rat tails illustrated faster and larger stress relaxation in decorin-deficient tissues compared to the tendons in the control group (Elliott *et al.*, 2003). Similarly, a study on human MCL showed a small increase (approximately 2.1%) in stress relaxation after treating the ligaments with chondroitinase ABC (ChABC) to remove the sGAGs which contribute to a large proportion of decorin, the predominant PG in ligaments (Lujan *et al.*, 2009). The rabbit MCL, which has been reported to have a high water content, has been shown to undergo greater stress relaxation during cyclic loading than those ligaments with lower water content (Chimich *et al.*, 1992). Consequently, removing a large majority of the sGAG chains in PGs is expected to result in the ligament ECM losing water-binding sites and increasing its capacity of free water absorption (Murienne *et al.*, 2015) and this may increase stress relaxation values. Other factors such as strain rate and post-mortem effects on

the stress relaxation of ligaments have been studied by previous researchers (Woo *et al.*, 1986; Weiss *et al.*, 2002). The effect of strain rates on the stress relaxation behaviour of human MCL were found to be unaffected by the different magnitudes of strain rates (Weiss *et al.*, 2002). Similarly, as explained in Section 2.5.3, no significant differences were reported between the fresh and the frozen ligaments although after relaxation the former showed a slightly lower stress value than the latter (Woo *et al.*, 1986).

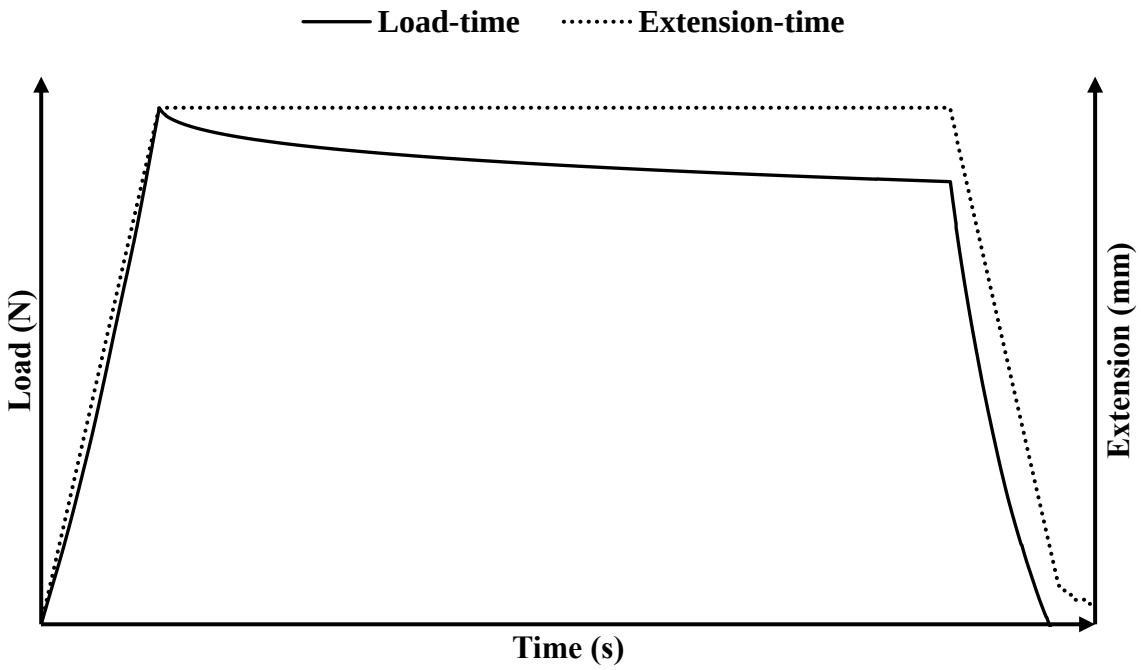

Figure 2.16: A typical extension-time (input) and load-time (response) profile during a loading and unloading test to study the stress relaxation behaviour of ligaments at low stress levels. Redrawn based on Miller *et al.* (2012).

2.6. Digital Image Correlation (DIC)

Digital Image Correlation (DIC) is a non-contact method for optically measuring local strain on the surface of an object without any contact between the object and the loading equipment (Peters and Ranson, 1982). This method obtains results with greater accuracy because there are

no fixing points between the optical measurement equipment (i.e. digital cameras) and the sample during mechanical tests. These fixing points have the potential to create boundary conditions and, as such, alter the results (Yamaguchi, 1981; Peters and Ranson, 1982). Different arrangements of DIC have been used by multiple researchers (Yamaguchi, 1981; Peters and Ranson, 1982; Helfrick *et al.*, 2011). For example, a two-dimensional (2D) DIC technique was first developed and used by several researchers in the 1980s (Yamaguchi, 1981; Peters and Ranson, 1982). This method utilises a single fixed camera which results in a limited measurement of the in-plane deformation of the object. Any out-of-plane deformation will change the magnification and can lead to errors in the measurements obtained. To overcome this limitation, a method of three-dimensional (3D) DIC was developed. This method is based on the principle of stereoscopic vision and is well known for its simple experimental set-up and preparation, whilst giving accurate results (Helfrick *et al.*, 2011). Errors due to oblique angle observations, present in the 2D setup, are compensated for in the 3D method (Hu *et al.*, 2010; Hu *et al.*, 2011). However, Chen *et al.* (2013) stated that the 3D DIC method also has its own limitations when used during mechanical tests. One of the limitations identified was that when the size of the object is beyond the field of view of the cameras, the distance between the cameras and the object or camera lenses needs to be adjusted and these adjustments could lead to a reduction in the number of effective pixels. Another limitation is associated with the object shape. For example, an object with complex curvature may produce visual blind spots that the camera cannot resolve properly into an accurate 3D image. To overcome these, Chen *et al.* (2013) proposed a multi-camera (for example 4, 5, 6, or more cameras) system. In their study, they used four synchronised charge-coupled device (CCD) cameras and grouped any two random cameras into a pair, with each pair measuring a plane of the object. They calibrated their system to account for the real world and image coordinate systems, using a calibration target with precisely manufactured patterns of fixed sized black and white squares. The main

advantage of this system is that no special marks are required to allow the computer to combine the resultant images. The system also reduces calculation errors because there is no translation or rotation required in any areas which overlap between images (Figure 2.17).

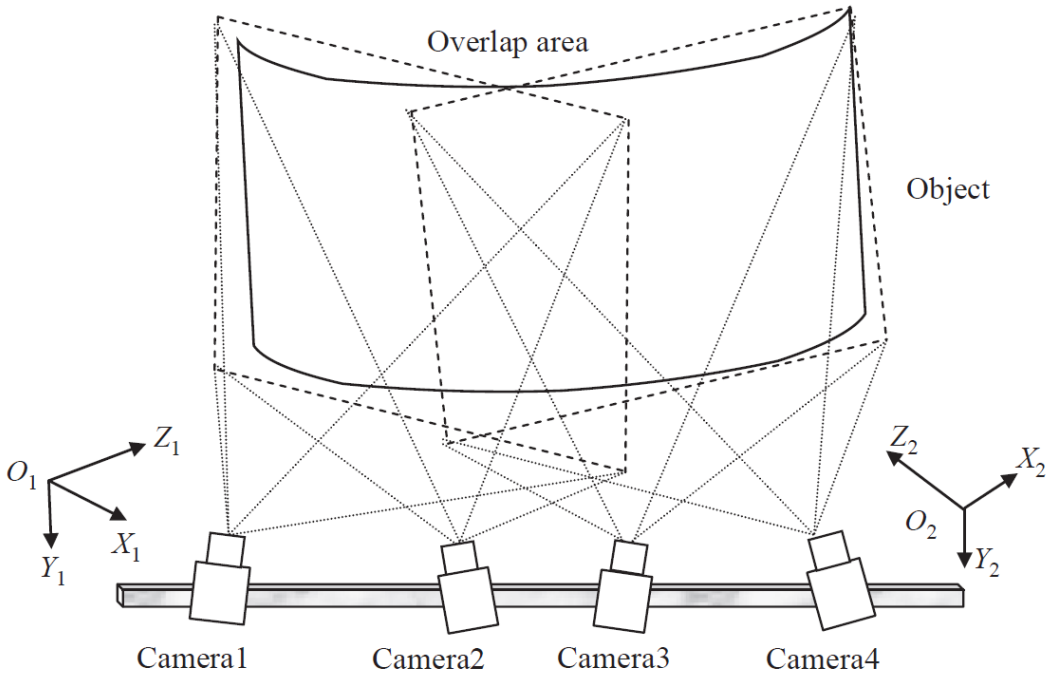

Figure 2.17: A four camera digital image correlation (DIC) system to determine surface deformation of a test sample. Taken from Chen *et al.* (2013).

In order to apply this system to biological tissues, such as sclera, ligament and others with little to no texture, a speckle pattern needs to be applied to the area under observation (Sutton *et al.*, 2009). Some authors hypothesised that different speckle patterns, such as rigid and deformable particles, might affect the results obtained from a DIC system, however their findings showed no significant difference in results between the two approaches (Barranger *et al.*, 2012). Creating an effective speckle pattern on biological soft tissue which would be suitable for DIC measurements is challenging. This is because the creation of the speckle pattern should adhere to the tissue surface and withstand large deformation, but not cause sample dehydration, nor

change the tissue's mechanical properties. Several approaches have been used by previous researchers to create speckle patterns on biological tissues. One was using a two-step procedure to create a highly-contrasted pattern which required staining of the tissue with methylene blue solution to obtain a dark background and airbrushing the surface with paint to create white speckles (Lionello *et al.*, 2014). This method showed small but non-significant changes in the stiffness behaviour of the tissue. Whitford *et al.* (2016) did not stain the whole biological tissue and instead created discrete speckles using cellulose-based paints chosen for their stability, rapid solvent evaporation and organic nature. These authors applied this method to corneal tissue and optimised the DIC output, and similar to Lionello *et al.* (2014) they found no significant differences in material behaviour before and after the application of paints (Whitford *et al.*, 2016).

One study used 3D DIC to examine the strain distribution in the human Achilles tendon and showed that measurements obtained from the 3D DIC method were more accurate in the centre of the tendon where scatter values around 0.03% strain were attained (Luyckx *et al.*, 2014). Similarly, Mallett and Arruda (2017) used the mid-substance of the anterior medial bundle of ovine ACL to characterise the mechanical properties of the ligament because the axial response of this region was found to be relatively homogenous. Several authors have proved 3D DIC to be a very accurate and reproducible tool for strain measurements in soft biological tissues because DIC measures the tissue-level strain and it is not affected by the mechanical testing system (i.e. test clamps) (Lionello *et al.*, 2014; Luyckx *et al.*, 2014; Luyckx *et al.*, 2016; Whitford *et al.*, 2016; Mallett and Arruda, 2017). For example, Mallett and Arruda (2017) showed lower strain values in the anterior medial bundle of ovine ACLs than that of traditional grip-to-grip method. This difference could be due to similar reasons to those reported by Rigozzi *et al.* (2009) which states that a combination of relative movement between the internal tissue substructure or slippage of the tissue within the grip system could affect the machine-

based strains. Some studies compared the DIC data with machine-based results (Mallett and Arruda, 2017), whereas other authors used DIC information to perform inverse analysis (Whitford *et al.*, 2016). In the case of the latter study, inverse analysis used to derive the representative material properties of the porcine eye globe (Whitford *et al.*, 2016). To achieve this, they created an FEM of the eye globe. The geometry of the models was defined based on the topographical information extracted using a 2D DIC method. Several studies used either a 2D or a 3D DIC methods to study the surface strain of biological tissue. However, to date, this is the first complex tissue study using a full-field multi-camera 3D DIC method to derive representative material parameters of ligaments such as the canine CCL through inverse analysis in conjunction with CCL-specific FEM.

2.7. Numerical Simulations of the Stifle Joint

Numerical methods have been used over the last four decades for the simulation of the biomechanical behaviour of the knee joint (Wismans *et al.*, 1980). A numerical knee model can be used as a powerful tool to support medical decisions in ligament surgery and physical therapy (Donahue *et al.*, 2002; Donahue *et al.*, 2003) as it has allowed scientists to examine the mechanical response of knee joints under different loading conditions without the need for dissection (Li *et al.*, 1999; Stylianou *et al.*, 2014). Numerical modelling also allows multiple variables to be tested easily with limited input requirements (Pena *et al.*, 2006). To create a numerical model of the knee joint, it is important to use anatomically accurate geometric measurements. Several methods have been used to obtain such data, most commonly laser, magnetic resonance imaging (MRI) and computed tomography (CT) scans (Li *et al.*, 1999; Weiss *et al.*, 2005; Pena *et al.*, 2006). The main drawback of using laser scanning is that it cannot differentiate ligaments from the surrounding bone structure (Weiss *et al.*, 2005). Peng *et al.* (2010) developed a 2D numerical model of the human knee joint using ABAQUS/CAE

software. The geometry of the FEM was based on the anatomical structure of the sagittal view of a human knee joint derived from Gray (2000). The FEM included the femur, tibia, patella, quadriceps, patellar tendon, and cartilages (Figure 2.18). The numerical model was then employed to investigate stress distribution in the tibia and contact area during contact in knees with and without articular cartilage. Other authors used MRI and CT scans to establish ligament geometry (Weiss *et al.*, 2005). They have used two different software packages, Surfdriver (www.surdriver.com) and Amira (www.amiravis.com), to perform segmentation of ligaments from 3D images subsequently generate a 3D finite element (FE) mesh of the ligament with the aid of TrueGrid (XYZ Scientific Application, Livermore, CA) software. Weiss *et al.* (2005) produced 3D FEMs of the human knee joint using two different methods. The first method was to produce a model of the entire knee joint and include all the soft tissues. However, due to the complexity of the model, it was found to be difficult to validate the model without detailed experimental studies. As a result, they modified their approach and produced a model of a single ligament to predict stress-strain behaviour and load transfer to the bones (Weiss *et al.*, 2005).

In addition to human knee FEM developments, other authors have also developed 3D FEMs of canine stifle joints (Brown *et al.*, 2013; Stylianou *et al.*, 2014). Brown *et al.* (2013) generated a 3D computer model of a quasi-static rigid body canine pelvic limb to simulate the CCL intact and the CCL deficient joints during walking stance in order to describe stifle biomechanics. The skeletal geometry of the canine pelvic limb (CPL) and the ligament anatomy were determined from CT images of a five-year-old healthy Golden Retriever. These CT images were used to generate the 3D geometry of the CPL through medical image segmentation software (Mimics, V.14.0, Materialise, Ann Arbor, MI). Subsequently, they exported the 3D geometry as point clouds and reconstructed the CPL as a solid model. The numerical model included the pelvis, femur, patella, medial and lateral menisci, tibia, fibula, tarsus, and

metatarsus (Figure 2.19). The stifle ligaments, including the CCL, CaCL, MCL, LCL, patellar ligament, lateral and medial femoropatellar ligament, were modelled as tension-only and non-linear springs and they were treated as a single line element that was directed along the vector from the ligament origin to insertion. This model was verified based on previously reported *in vivo, in vitro* and mathematical modelling studies (Holden *et al.*, 1994; Warzee *et al.*, 2001; Shahar and Banks-Sills, 2004). However, it has a number of limitations; for example, the ligaments were approximated as single elements, the effect of ligaments wrapping around bone geometry or ligaments twisting were overlooked, and more importantly ligaments were modelled as time-independent non-linear springs with material properties based upon ligament CSA at mid-substance. Moreover, other researchers have developed an anatomically representative canine stifle joint model (Stylianou *et al.*, 2014). However, unlike the study by Brown *et al.* (2013), Stylianou *et al.* (2014) divided the four major ligaments (CCL, CaCL, MCL and LCL) into two bundles (anterior and posterior bundles), while both studies modelled the ligaments as non-linear springs using a piecewise function. Modelling ligaments in stifle joints as a single element or bundles rather than their complex anatomical structure will simplify the numerical model. To develop a representative stifle joint and study the effect of altering ligament microstructure on the joint biomechanics, it is important to generate an anatomically accurate stifle and its major components as well as assigning representative (time and history dependent) material behaviour to the soft tissues within the joint.

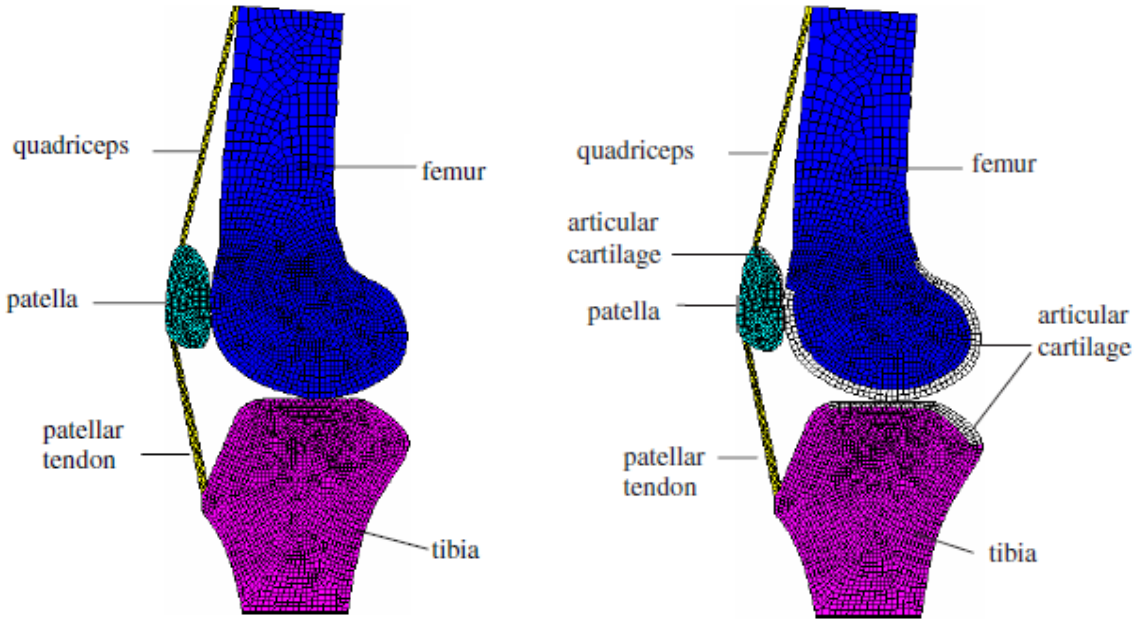

Figure 2.18: FEM of a sagittal human knee joint without cartilage (a) and with cartilage (b). Taken from Peng *et al.* (2010).

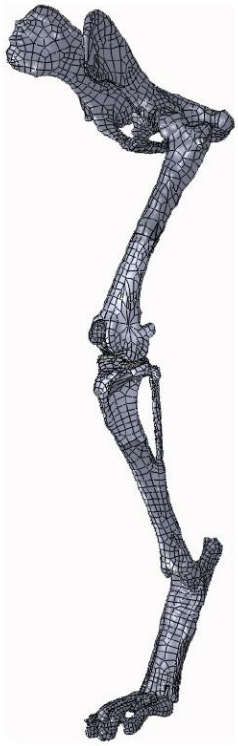

Figure 2.19: A 3D numerical model of the canine pelvic limb. Taken from Brown *et al.* (2013).

2.8. Summary

The CCL is one of the most important anatomical structures involved in stabilising the canine stifle joint and the microstructure of this ligament dominates its functionality (Arnoczky and Marshall, 1977). The hierarchical structure of ligaments such as the canine CCL is complex consisting of cellular and extracellular matrices which are comprised of collagen fibres, elastin, PGs and some other proteins (Amiel *et al.*, 1984; Benjamin and Ralphs, 1997; Frank, 2004). The structure of ligaments mainly consists of twisted collagenous fascicles and collagen fibres (Frank *et al.*, 1983). The combination of fibrils form fibres and the fibres are non-uniformly orientated to allow for multiaxial loading patterns and their crimp tends to diminish under progressive mechanical loads (Yahia and Drouin, 1989). Apart from collagen, the dry matters in ligaments are believed to contribute to the mechanical properties of the tissue (Frank, 2004). For example, the GAGs of PGs are believed to affect biological tissues in their responses to mechanical loads (Chakrabarti and Park, 1980; Rumian *et al.*, 2007; Gautieri *et al.*, 2012). To date, there are contradicting opinions about the contribution of GAGs to the viscoelastic behaviour of stifle ligaments. One study showed that GAGs have no effect on the interaction of collagen fibres to resist tensile or shear deformation under loading conditions in the human MCL (Lujan *et al.*, 2007), whereas other authors strongly associate the role of GAGs with fibre-fibre and fibre-matrix interaction at low stress levels in rat tail tendons, swine aortic valves and rat dorsal skin (Cribb and Scott, 1995; Eshel and Lanir, 2001; Eckert *et al.*, 2013). Many of these researchers have noted that PGs dominate tissue response at low strain level (the toe region) when the collagen fibres are crimped. This is because at higher strain levels the collagen fibres become dominant and active. Several studies have observed an increase in water content after PG depletion within soft biological tissues and this change has given an impression that altering PG content affects the permeability of the tissue (Henninger *et al.*,

2010; Murienne *et al.*, 2015). The microstructure and behaviour of biological tissues change based on their location and function; hence using previous studies on tendons and other tissues as comparable tissues to understand the biomechanical behaviour of the intact canine CCL is not a realistic approach and will introduce limitations. In the quest to understand the influence of PGs on the viscoelastic behaviour of the canine CCL, this thesis will further investigate strain rate, hysteresis, stress relaxation and creep behaviour of CCLs before and after PG digestion. Because of the similarity with *in vivo* behaviour, the most desirable method to test the material properties of the CCL is to extract the bone-ligament-bone complex from the stifle joint. The bone parts of this complex will facilitate the gripping during clamping and minimise errors due to tissue slippage as well as providing a mechanism to measure bone-to-bone deformation. Due to the variability in ligament micro and macrostructure, the most appropriate test analysis method for the CCL is inverse analysis in combination with FEM. To the author's knowledge there are no studies which have represented the complex anatomical structure of the canine CCL as an FEM of the CCL and combined it with its viscoelastic behaviour before and after PGs depletion.

FEMs can reflect the material properties of biological tissue. However, there are very few studies which attempt to generate a representative canine stifle joint in conjunction with the significant viscoelastic behaviour of the soft tissues, and no studies were found to include all the major stifle components important to the stability of joints. Based on this evidence, the current study will develop and utilise an anatomically representative FEM of the whole stifle joint, including the femur, tibia, fibula, the four major ligaments, menisci and articular cartilage combining this with the ligament viscoelastic behaviour.

Reviewing previous literature led to the establishment of the hypothesis and aim of this doctorate research which is to gain a greater understanding of the biomechanical behaviour of the canine CCLs at the toe-region of the stress-strain behaviour. This is to be accomplished by

investigating the contribution of proteoglycans to the viscoelastic behaviour of the CCLs and the effect of PGs in the CCLs on the stability of the whole stifle joint. It is the hypothesis of this study that decreasing PG content in the CCLs would lead to a decrease in water binding molecules, hence less interfibrillar lubrication, thereby increasing interfibrillar friction and resulting in a stiffer behaviour of the ligaments.

The aim of this research required the following objectives to be accomplished:

- Investigating the tensile response of CCLs from healthy stifle joints at three strain rates (0.1, 1 and 10%/min) and identifying a test protocol to determine the viscoelastic characteristics of the ligaments.
- Developing a full-field three-dimensional digital image correlation (3D DIC) method to capture the non-deformed surface of the CCLs and optically measure the load-deformation behaviour across the surface of the ligament.
- Generating 3D CCL-specific FEMs using the non-deformed surface of the CCLs from the DIC results so that the FEMs were employed during an inverse analysis study to predict material parameters for the ligaments.
- Investigating the non-linear viscoelastic behaviour of the canine CCLs with and without chondroitinase ABC (ChABC) enzyme treatments using a combination of uniaxial tensile tests, a 3D DIC and inverse analysis. This is to understand the effect of PG depletion on material hysteresis, tangent modulus, strain rate sensitivity, creep and stress relaxation at three strain rates (0.1, 1 and 10%/min).
- Developing an FEM of the canine stifle joint to represent the geometry and function of a realistic joint. Subsequently, utilising the FEM to investigate stability in the canine stifle joint when PG content in the CCL was altered.

3. Experimental Methods

3.1. Introduction

This Chapter outlines the methodology used to determine the tensile and viscoelastic behaviour of the CCL and the contribution of PGs to the viscoelastic behaviour. Initially, the collection and preparation of samples for three studies are described, with the studies fulfilling the objectives outlined in Section 2.8:

- Experimental Study I investigated the tensile behaviour of the CCL at slow strain rates and studied the best test protocol to determine the viscoelastic characteristics of the ligaments.
- Experimental Study II explored the viscoelastic characteristics of CCLs before and after PGs depletion. For this study, a full-field 3D DIC method was developed to optically measure load-deformation and create 3D FEMs of the CCLs. The FEMs were employed to perform inverse analysis.
- Experimental Study III determined the geometry of a whole canine stifle joint from MRI scans using a manual segmentation process and direct modelling. Subsequently, an FEM of the whole canine stifle joint was generated. In conjunction with the results obtained from Experimental Study II, the FEM was utilised to investigate the effect of PGs in the CCLs on the stability of the whole canine joint.

The experimental setup in this Chapter outlines different methods used to measure the geometry of the CCL, including length and CSA. This Chapter also includes a description of the methods used to measure the water content and sGAGs in the CCLs before and after PG depletion. Furthermore, a detailed description of the mechanical test procedure for all studies is given. This Chapter provides detailed information about the custom-built full-field 3D DIC

setup and analysis, followed by a full description of the development of FEMs of the CCLs and inverse analysis. In addition, methods used to develop and analyse FEM of the canine stifle joint are also reported. Finally, the procedures employed to perform statistical analysis of all data for each study are detailed.

3.2. Sample Preparation

In total for all three studies, eleven pairs of canine cadaveric stifle joints (from right and left pelvic limbs) were collected. The cadaveric samples of the same breed (Staffordshire Bull Terrier) were distributed between the prearranged experimental studies, so that n=5, n=5 and one pair of stifle joints were used in Experimental Study I, II and III respectively. The inclusion criteria for all studies required that the stifle joints were disease free, from canines of a similar breed, had an age of >18 months (skeletally mature), a body-weight of >20kg and body condition between 3 to 5 (ideal body condition score). Full ethical permission to use these donated canine stifle joints in clinical research was granted by the School of Veterinary Science Research Ethics Committee (RETH000553 and VREC65). Cadaveric canine stifle joints wrapped in their surrounding tissues were stored at -20^{0}C prior to the dissection of the ligaments.

To perform uniaxial tensile tests, an Instron 3366 testing machine (Instron, Part No. 2530-428) with a 10N load-cell capacity was used (Figure 3.1 (a)). The CCLs were firstly dissected carefully to avoid damage to the ligament insertion site and so that approximately 10mm of bone was left on each side of the ligament (Figure 3.1 (b and c)). The femur and tibia bone sections that were left connected to the ligament formed a femoral-CCL-tibial complex and allowed for the measurement of end-to-end ligament deformation as well as helping to facilitate the clamping of the sample. In the current study, the femoral-CCL-tibial complex is referred to as the CCL.

These dissected CCLs were wrapped in paper soaked with phosphate buffered saline (PBS) and frozen at -20^0C to preserve them until they were required for testing. Before any tests took place, the CCLs were thawed to room temperature (20°C) and two 1.1mm arthrodesis wires (Veterinary Instrumentation, Sheffield, UK) were drilled through the tibia and femur bone ends. These wires were placed in positions to replicate the ligament's normal physiological position (Figure 3.1 (d)) and the CCL had a proximal-to-distal outward spiral of about 90 degrees (Arnoczky and Marshall, 1977).

Prior to mechanical tests, the CCLs were secured inside the Instron testing machine in a custom-built stainless-steel clamp and rig. This steel clamp was built by creating a 3D model of the required clamp (Figure 3.2 (a)) using Pro/Engineer software (Pro/Engineer Wildfire 4.0, Parametric Technology Corporation, USA, 2008) and then the clamps were manufactured based on this customised design (Figure 3.2 (b)). During the experiment, these custom-built clamps gripped the tibial and femoral bones attached to the CCL (Figure 3.2 (c)). Two benefits of using these custom-built clamps were that it provided a mechanism through which the grip on the tibial and femoral bones could be increased by the application of screws and that it left the ligament free and unobstructed throughout the experiment.

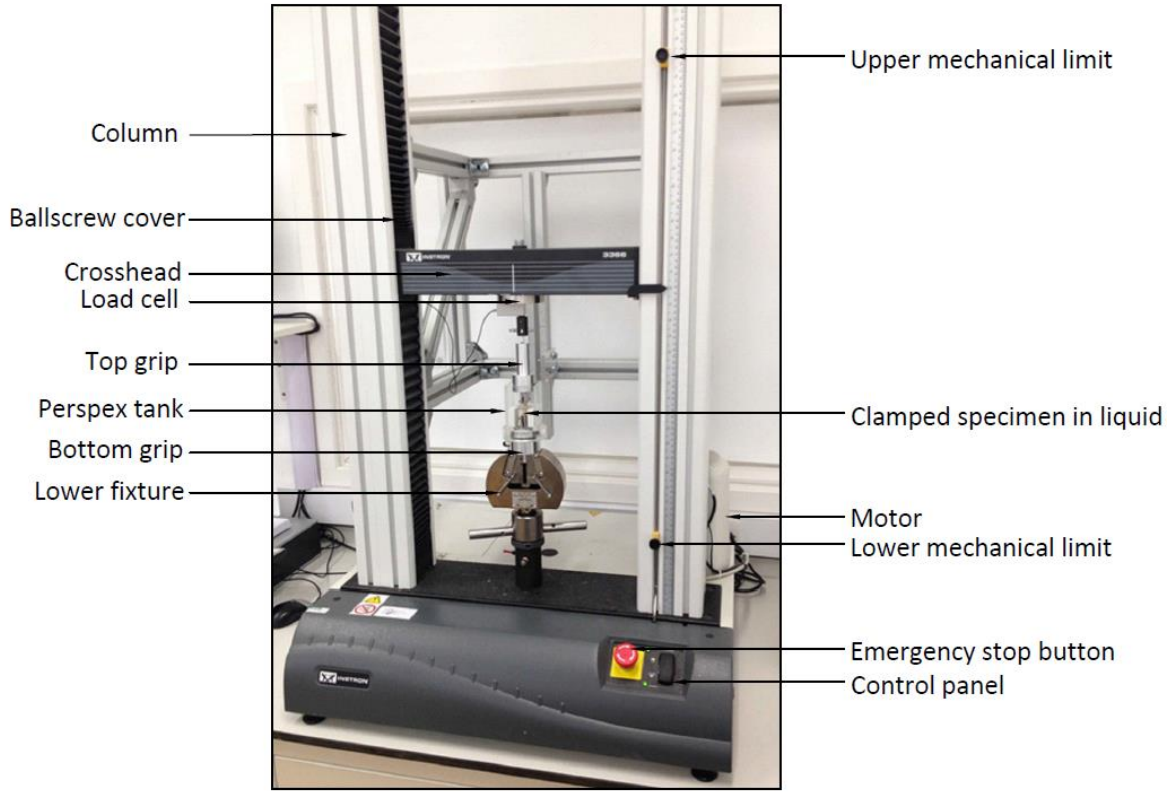

(a)

(b) **(c)** **(d)**

Figure 3.1: An Instron 3366 testing machine used to study mechanical behaviour of the canine CCLs (a). Cranial (b) and caudal (c) views of a canine CCL. The CCL was pinned with 1.1mm arthrodesis wires in the femoral and tibial bones (d) to facilitate clamping of the sample.

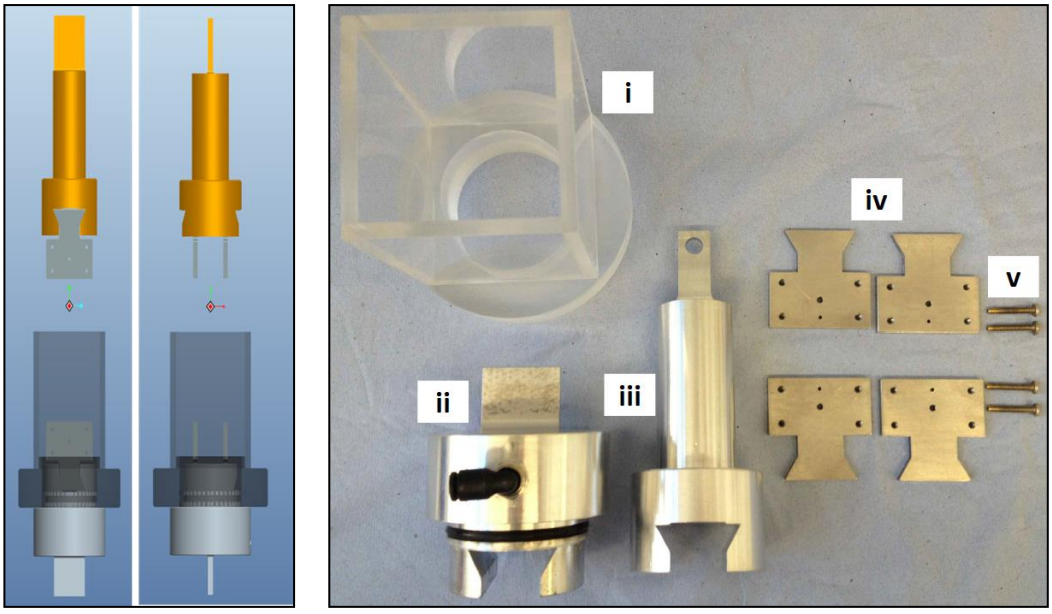

(a) **(b)**

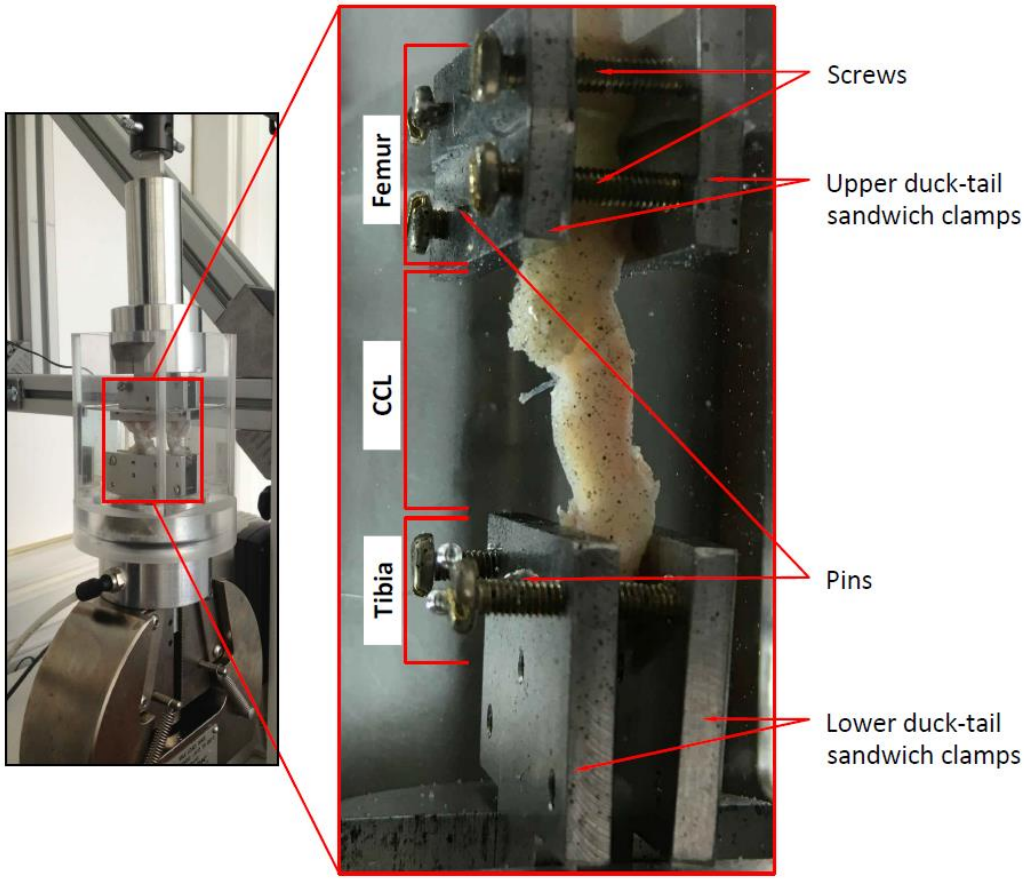

(c)

Figure 3.2: The clamps were custom designed (a) and manufactured (b) to provide tight clamping. The custom-built clamps included a cylindrical prespex tank (b (i)), bottom (b (ii)) and top (b (iii)) grips, duck-tail sandwich clamps (b (iv)) and screws (b (v)). An example of a CCL which is clamped and placed in the perspex tank (c).

3.2.1. Experimental Study I: Tensile behaviour of CCLs at slow strain rates

In the first experimental study, five pairs of canine CCLs were used to study stress-strain and hysteresis behaviour, as well as studying the effect of different strain rate arrangements during loading-unloading tests. Canine CCLs from the left pelvic limbs were used in the ascending (increasing value of strain rate) test protocol, while CCLs from the right pelvic limb of the same canine were used in the descending (decreasing value of strain rate) tests (Section 3.3.4). During the uniaxial tensile tests, the CCLs were protected against dehydration by keeping them in a custom-built tank filled with PBS at room temperature (20°C) (Figure 3.2).

3.2.2. Experimental Study II: Contribution of PGs to the viscoelastic behaviour of CCLs

This experimental study was set up to investigate viscoelastic behaviour of CCLs before and after PG depletion. In this study, CCLs were tested under tensile forces and surface deformation of these ligaments was monitored using a full-field 3D DIC method. The DIC method was also used to construct the surface geometry of the CCLs before deformation.

Five pairs of canine cadaveric stifle joints (right and left pelvic limbs) were collected. The four major ligaments, including cranial (CCL) and caudal (CaCL) cruciate ligaments, and lateral (LCL) and medial (MCL) collateral ligaments were extracted from the stifle joint in the same way as described in Section 3.2 to produce bone-ligament-bone complexes. In addition to the ligaments, lateral (LM) and medial (MM) menisci, and patellar tendons (PT) were collected. This study focused on the viscoelastic behaviour of the CCLs, therefore the other major parts of the stifle joints, named above, were collected for future study purposes (Section 5.4). CCLs from the right pelvic limbs were kept as a control group where PGs were not depleted (control group) while the CCLs from the left pelvic limbs were treated with chondroitinase ABC (ChABC) (SIGMA-ALDRICH, USA) to achieve PG depletion (treatment group). ChABC degrades chondroitin sulphate (types A and C, or chondroitin-4-sulphate and chondroitin-6-

sulphate) and dermatan sulphate without affecting other PG macromolecules (Hascall *et al.*, 1972) and has been reported to remove at least 88% of sGAGs (Lujan *et al.*, 2007).

As shown in Figure 3.3, both left and right CCLs were first bathed for one hour at room temperature (20°C) in 20ml buffer solution (15ml of 20mM Tris pH 7.5, 150mM NaCl, 5mM $CaCl_2$) with protease inhibitors (1 tablet of mini-cOmplete per 10ml of buffer, SIGMA-ALDRICH/Roche, USA) (Lujan *et al.*, 2009). The CCLs from the control group were sprayed with fast drying matt black colour paint (RS 764-3039) to create distinct speckle patterns, (Figure 3.4 (a and b)). Mechanical tests (Section 3.3.5) were then performed once the speckle pattern had dried. In addition, the CCLs in the treatment group were incubated for three hours in ChABC 0.25IU/ml enzyme which was dissolved in 0.01% bovine serum albumin (BSA) (Figure 3.4 (c)). The method was similar to that described by other authors (Lujan *et al.*, 2009). However, the incubation time and enzyme concentration was based on a preliminary study by Comerford *et al.* (unpublished, 2012) which showed that approximately 82.3% of PGs in CCLs were digested within 3 hours of incubation using the enzyme concentration described above (Appendix (1): Table 1 and Figure 1). Subsequently CCLs in the treatment group were also sprayed with matt black colour paint to create speckle patterns on their surface prior to mechanical tests. Both control and treatment groups were hydrated during the mechanical tests in a custom-built tank (Figure 3.4 (d and e)) filled with 600ml of the ChABC buffer solution and protease inhibitors at room temperature (20°C) (1 tablet of cOmplete Protease Inhibitor Cocktail per 50ml of buffer, SIGMA-ALDRICH/Roche, USA). Following completion of the mechanical tests, CCLs were stored at -80°C before they were prepared for hydration tests (Section 3.3.2.1) as well as biochemical assays (Section 3.3.2.2) to determine the level of sGAG contents (Farndale *et al.*, 1986) in the control and the treatment groups.

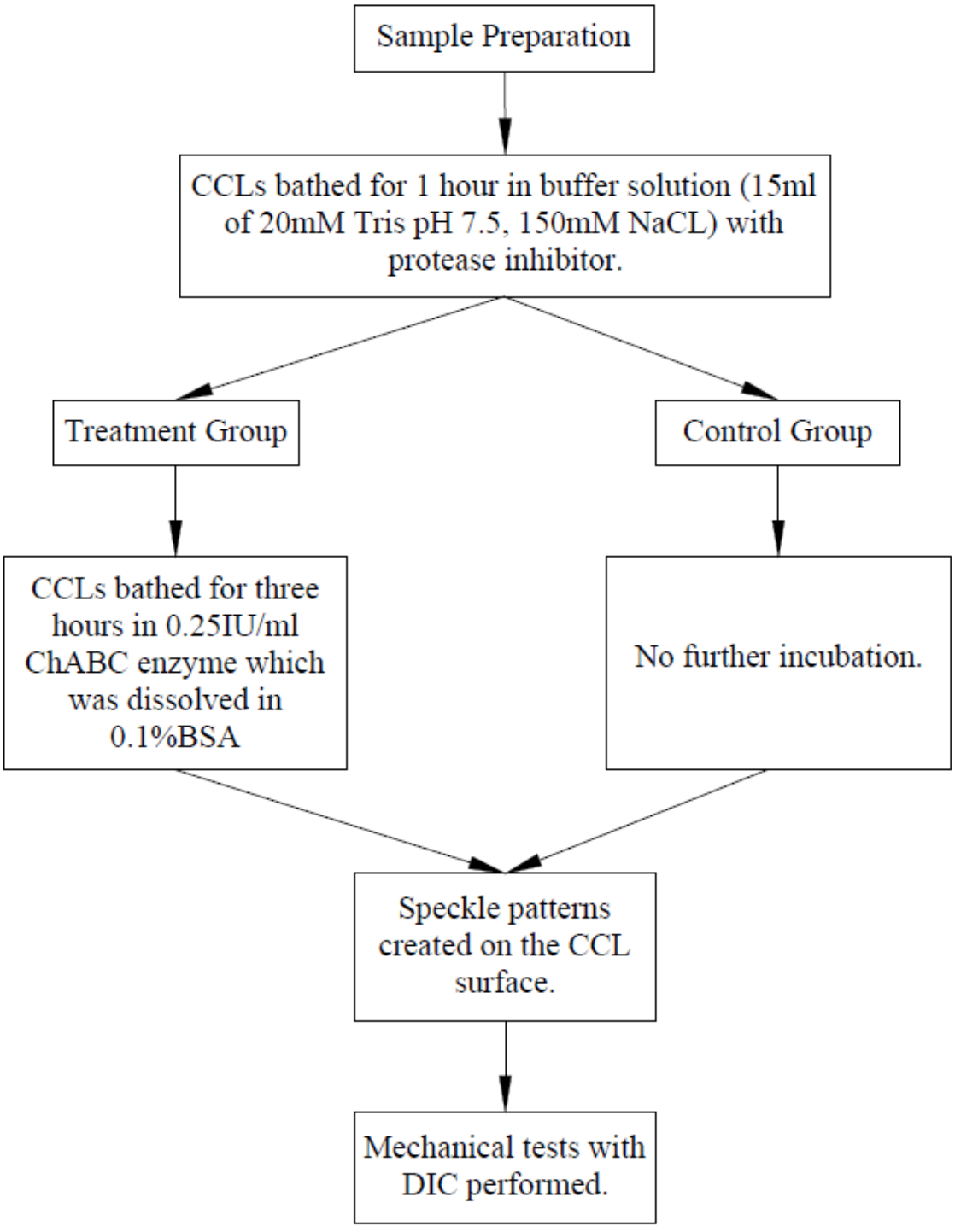

Figure 3.3: An illustration presenting CCL preparation for Experimental Study II.

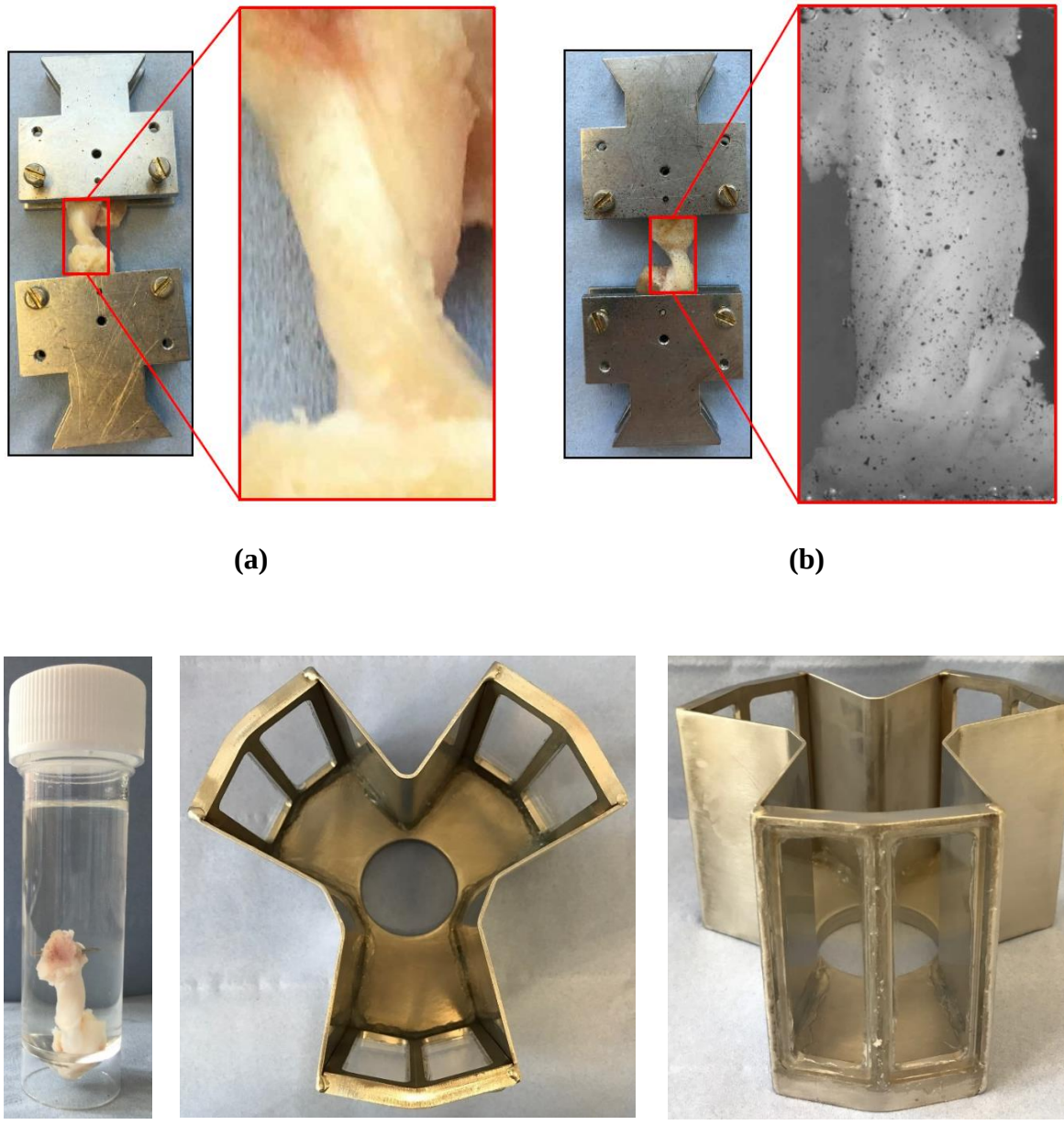

Figure 3.4: The CCLs without speckle patterns (a) and with speckle patterns (b). The CCLs were first incubated in a test tube (c) before being fixed to the duck-tail sandwich clamps and creating the speckle patterns with matt black colour paint. Top (d) and front (e) view of the custom-built tank which allowed viewing from six windows for the application of the DIC method.

3.2.3. Experimental Study III: Canine stifle joint finite element model development

One pair of canine stifle joints was collected for the third experimental study. The sample was separated into left and right pelvic limbs. The right pelvic limb was used for MRI scanning to develop an FEM of the whole stifle joint, whilst the left pelvic limb was retained for future experimental study (Section 5.4).

3.3. Experimental Setup

3.3.1. Geometrical Measurements of CCLs

Geometry of the CCLs was determined before undertaking mechanical tests using the methods detailed in Section 3.3.1.1 and 3.3.1.2. These measurements were essential in determining the material properties (stress and strain) of the ligament.

3.3.1.1. Length

The CCL has a complex anatomical structure and broad insertion sites; therefore, it was difficult to measure the CCL length with a high level of accuracy. The length measurement protocol adopted in this study was based on a method described by other authors (Vasseur *et al.*, 1991; Comerford *et al.*, 2005) which determined the average length of CCL from the craniomedial and caudolateral portions of a ligament. However, this was improved in the current study by taking measurements from the cranial and caudal faces of the CCL, as well as the lateral and medial faces (Figure 3.5).

The mean values of these four length measurements were recorded for the experimental studies to give an accurate record of the length of the CCL before deformation (Figure 3.5). CCL length was measured between the femoral and tibial attachments with Vernier callipers (±10μm).

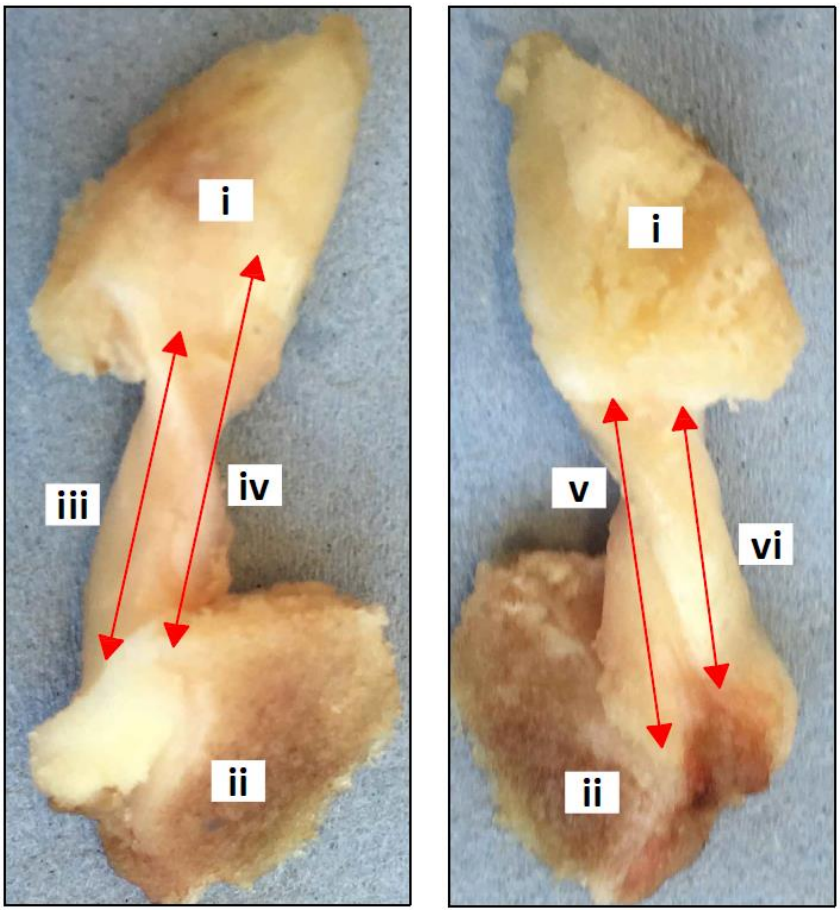

(a) **(b)**

Figure 3.5: CCL from a right canine stifle joint from the cranial (a), and caudal (b) views of the ligament. The length of the CCL, attached to the femur (i) and tibia (ii) was measured at four different points: lateral (iii), cranial (iv), medial (v) and caudal (vi) sides.

3.3.1.2. Cross-sectional area (CSA)

The CSA of the CCL was measured following the replica technique described in the study by Goodship and Birch (2005) with some adaptations.

In this study alginate dental impression paste (UnoDent, UnoDent Ltd., UK) was used to make a mould around the ligament. Two different approaches were used to create the CCL replicas using a hanged and non-hanged method to check for any differences when the replicas were prepared in and out of the materials testing machine. In the non-hanged method (Figure 3.6 (a))

the CCL was positioned flat on a bench without a clamp, while in the hanged method (Figure 3.6 (b)) the CCL was clamped and mounted on an Instron 3366 testing machine.

3.3.1.2.1. Method 1: The non-hanged method

A small amount of alginate paste was placed on a flat surface (i.e. cutting board) with the CCL positioned horizontally on top of the paste (Figure 3.6 (a)). The remainder of the paste was then used to cover the top of the CCL. After 2 minutes and 30 seconds (as recommended in the manufacturer's instructions), the mould had set and a cut was made in the side of the mould with a scalpel blade. The CCL contained within the mould was then carefully removed from the casing. The CSA of the CCLs used in studies in Experimental Study I and II, were measured using the non-hanged method because of its simple procedure.

3.3.1.2.2. Method 2: The hanged method

The CCL was firstly clamped and mounted in the Instron testing machine (Figure 3.6 (b)). The CCL was then covered with the alginate paste and left to set as detailed in Section 3.3.1.2.1. Once the paste had set, the CCL was dismounted from the machine and a cut made in the side of the mould through which the ligament was carefully removed. The CCLs in Experimental Study I were measured using this method in addition to the non-hanged method.

3.3.1.2.3. CCL cast preparation

Once the moulds had been created with either the non-hanged or hanged method and the CCLs removed, the moulds were used to cast a set of polymethyl-methacrylate (PMMA) (Teknovit 6091, Heraeus Kulzer GmbH, Wehrheim, Germany) models of the CCLs. To create these models, PMMA paste was injected into the hardened alginate moulds and left for 2 minutes to set (as recommended in the manufacturer's instructions) (Figure 3.6 (c)). Next, the PMMA replicas were removed from the mould by hand and cut into two in the middle using a junior

hacksaw. The end surface of each half of the PMMA models was then coloured black with a permanent marker to prepare the PMMA models for image analysis (Figure 3.6 (c)). The surface colouring of the PMMA models helped to distinguish the PMMA surface of the model from its background colour and thus simplified the image analysis. Pictures of the two ends of the sectioned replicas were taken using a Canon EOS 600D camera with a ruler placed in the field of view (Figure 3.6 (c)). The black surface areas of the replicas were then measured using ImageJ (a public domain Java image processing program) and, to ensure accuracy, the mean value of the two ends were taken as the CSA for each ligament.

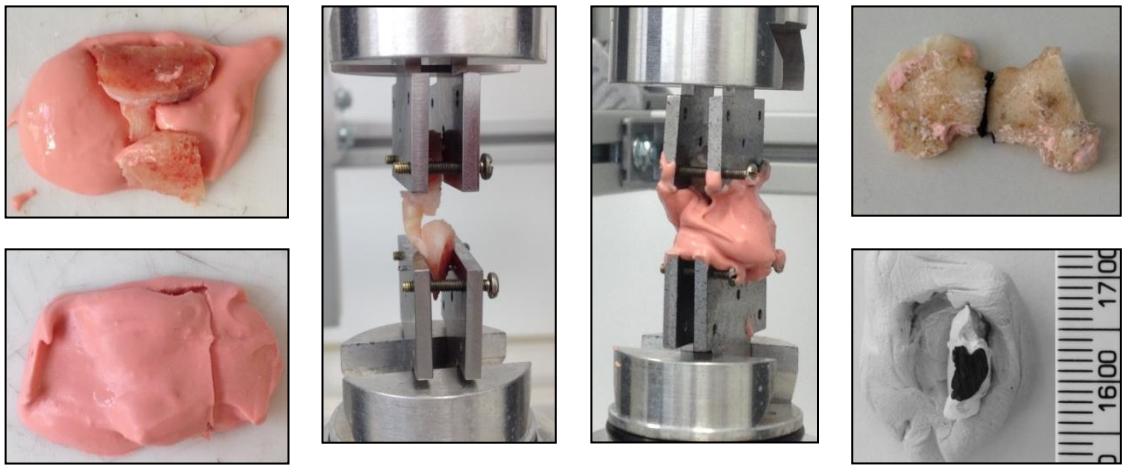

(a) **(b)** **(c)**

Figure 3.6: CSA of the CCL was measured by firstly creating an alginate paste mould. The mould was created using the non-hanged (a) and hanged (b) methods. Subsequently, PMMA replica model of the CCL was cast within the alginate mould. The replica was cut into two in the middle and the surface of the replica showing mid-CSA was marked in black coloured paint (c).

3.3.1.3. Statistical Analysis

CCL lengths measured at different planes (Section 3.3.1.1) were categorised into cranial, caudal, medial and lateral groups. Statistical tests were performed using one-way analysis of variance (ANOVA) followed by a Bonferroni post-hoc test for multiple comparisons. Analyses were performed in Microsoft Office Excel (Microsoft Office, Version 2016, US) and in SPSS 20.0 (SPSS Inc., Illionois) and $p<0.05$ was an indication of statistical significance.

CSA measurements obtained from the two methods (Section 3.3.1.2) were categorised into hanged and non-hanged cohorts. Statistical tests were performed using a two-tailed t-Test in Microsoft Office Excel (Microsoft Office, Version 2016, US) to analyse differences between CSA measurements from the two methods and $p<0.05$ was an indication of statistical significance.

For Experimental Study II, CSA measurements for the CCLs in the control and treatment groups were statistically analysed to investigate change in geometry due to the PGs depletion process. The CSA measurements were categorised into CSA control (right pelvic limb) and treatment (left pelvic limb) groups. Statistical tests were performed using a two-tailed t-Test in Microsoft Office Excel (Microsoft Office, Version 2016, US) to analyse differences between the two groups and $p<0.05$ was an indication of statistical significance.

3.3.2. Biochemical Assays on Experimental Study II

The mid substance of the CCLs from the control and the treatment groups in Experimental Study II were used to quantify water and sGAGs contents as previously described by Farndale *et al.* (1986) and in canine CCLs by Kharaz (2015) and Comerford *et al.* (2005)

3.3.2.1. Water content

CCLs from the control and the treatment groups in Experimental Study II were tested for their water content (Allaith, 2016). The water content in percentile was expressed in terms of the mass of water per unit mass of the moist ligament (Equation 3.1). Initially, the CCLs were left to thaw at room temperature (20°C) and wet mass was measured. Subsequently, these CCLs were freeze dried overnight and then the dry mass of the CCLs was measured.

$$Water\ Content\ (\%) = \frac{Wet\ mass - Dry\ mass}{Wet\ mass} \times 100 \qquad \text{Equation 3.1}$$

3.3.2.2. Sulphated glycosaminoglycan assay

CCLs from the control and the treatment groups in Experimental Study II were digested for 48hours with 10unit/ml papain in 100mM sodium acetate, 2.4mM Ethylenediaminetetraacetic acid (EDTA) and 5mM cysteine hydrochloric acid (HCL) at 60°C. Dimethylmethylene blue (DMMB) dye binding assay (1, 9-dimethylmethylene blue) was used to determine the sGAG content of the CCLs (Farndale *et al.*, 1986). 250µl of DMMB dye was added to 40µl duplicates of papain-digested CCLs, and this was immediately analysed at 570nm wavelength. Shark chondroitin sulphate over a concentration range of 0-75µg/ml was used as a standard (Figure 3.7) and sGAG content was calculated by comparison with the standard line.

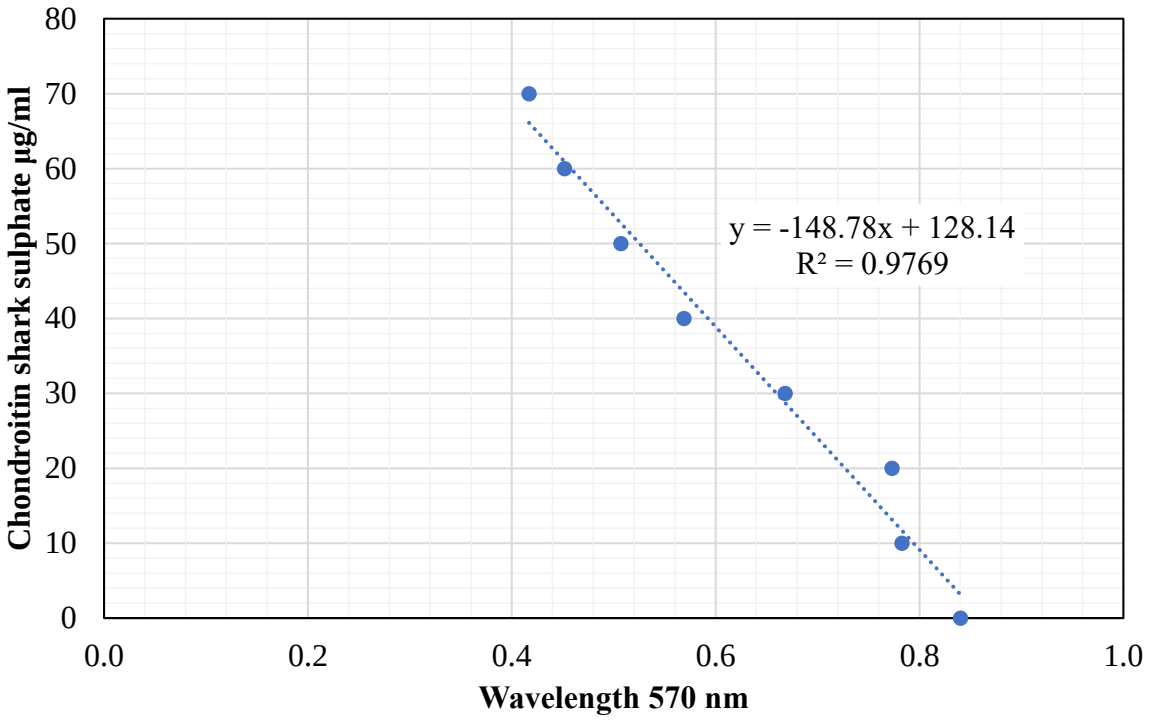

Figure 3.7: An example of the linear line used as a standard line to quantify sGAG content.

3.3.3. Uniaxial Tensile Tests

Once the CCL was mounted on the testing machine, a preload of 0.1N was applied to remove laxity within the CCL (Provenzano *et al.*, 2002). The CCLs were then tested to determine their tensile and viscoelastic behaviour. Similar to Dorlot *et al.* (1980) load-elongation data was collected to study the mechanical properties of the canine CCLs. In the current study, uniaxial testing machine was used to collect load-elongation data which was then analysed using Excel spreadsheets (Microsoft Office Excel 2010, US) and MATLAB (MATLAB2015a, The MathWorks, Natick, 2015). Similar to other studies on canine CCLs (Haut and Little, 1969; Woo *et al.*, 1981), approximate stress was calculated by dividing the applied load by the CSA of the CCLs at the mid region (Equation 3.2) and the corresponding deflection data was used to calculate strain in the tissue (Equation 3.3). Subsequently, exponential curves were fitted onto the calculated stress and strain data using the least squares method (Equation 3.4). Fitting an exponential curve to the stress-strain behaviour of soft biological tissue such as the mesentery of rabbits was firstly proposed by Fung (1967) and the exponential equation was further utilised on canine CCLs by Haut and Little (1969). The transition strain at the start of strain stiffening was calculated to characterise the stiffness and non-linearity of the tensile response during loading (Murienne *et al.*, 2015). The transition point was evaluated by fitting straight lines to the initial and final 30% of data points to define the lower and higher stress slopes, respectively (Figure 3.8 (a)). Similar to Elsheikh *et al.* (2008), numerical integration (trapezoidal rule) was used to calculate hysteresis, defined as the area between loading-unloading stress-strain curves (Figure 3.8 (a)). Similar to the studies by Geraghty et al. (2012), the tangent modulus of the CCLs was calculated by applying Equation 3.5 and the polynomial curve fit, using the least squares method, was employed to produce tangent modulus-stress curves (Equation 3.6).

$$\sigma = \frac{F}{CSA}$$ Equation 3.2

where σ is stress in MPa, F is applied load in N and CSA is cross-sectional area in mm^2.

$$\varepsilon = \frac{\Delta L}{L_0}$$ Equation 3.3

where ε is strain, ΔL is change in length in mm ($\Delta L = L_0 - L_1$), and L_0 is initial length of the ligament in mm.

$$\sigma = a(e^{b\varepsilon} - 1)$$ Equation 3.4

where a and b are coefficients.

$$E_{tan} = \frac{\sigma}{\varepsilon}$$ Equation 3.5

where E_{tan} is tangent modulus in MPa.

$$E_{tan} = ax^3 + bx^2 + cx + d$$ Equation 3.6

where $a, b, c,$ and d are coefficients.

In Experimental Study II, the load-hold creep rate from strain-time curves and stress relaxation from stress-time curves were determined to characterise the viscoelastic response of the CCLs. Exponential curves were fitted onto strain-time data using the least squares method (Equation 3.4). Subsequently, the initial and final creep rates were defined by slopes of the linear fit of strain-time response. The first 20s defined the initial creep rate and the last 500s determined

the final creep rate from strain-time curves (Figure 3.8 (b)). Similar to the tangent modulus-stress curves, polynomial curves (Equation 3.6) were fitted on normalised stress-time data to illustrate stress relaxation response. The stress was normalised by the peak stress at t=0 to obtain reduced relaxation curves (Fung, 1993). The current study illustrated average viscoelastic behaviour of the CCLs such as stress-strain, tangent modulus-stress, hysteresis for Experimental Study I. In addition to these, the average creep and stress relaxation behaviour for Experimental Study II.

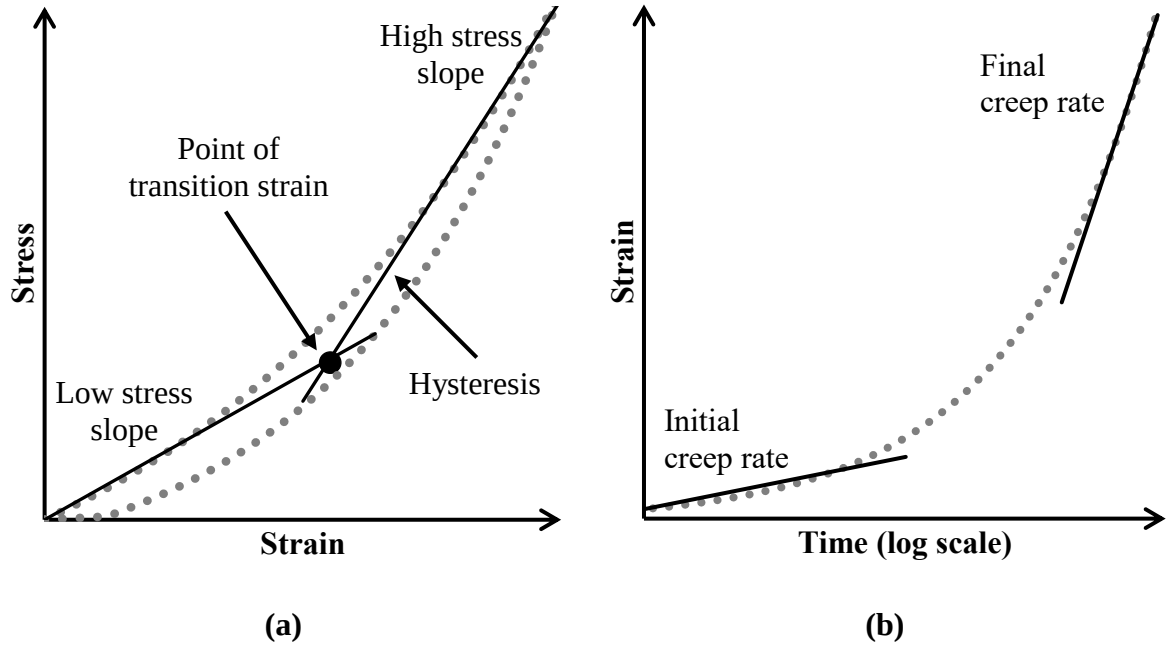

Figure 3.8: Line drawing of the mechanical properties determined from the loading-unloading stress-strain, with low stress slope fitted into the initial 30% and the high stress slope fitted into the last 30% of stress-strain behaviour (a) and load-hold strain-time (b) curves of a canine CCL. Redrawn based on Murienne *et al.* (2015).

3.3.4. Experimental Study I: Tensile behaviour of CCLs at slow strain rates

In this study, mechanical tests were carried out on the first set of CCLs (n=5 pairs) to investigate the mechanical properties of healthy canine CCLs at slow strain rates. As detailed in Section 2.5.2, there are greater chances to observe strain rate sensitivity of ligaments at slow strain rates

(Bonner *et al.,* 2015). Therefore, slow strain rates (<10%/min) were utilised when testing mechanical responses of the CCLs. To compare the tensile and viscoelastic behaviour of the CCLs three mechanical outcomes were defined, namely strain rate sensitivity, hysteresis and the effect of test protocols.

The first part of the test involved preconditioning the CCLs to ensure that they were in a steady state and would produce comparable and reproducible load-elongation curves (Butler *et al.*, 1978b; Fung, 1993; Savelberg *et al.*, 1993). Preconditioning involved performing ten loading-unloading cycles (Woo *et al.,* 1991) to a maximum load of 9.9N at strain rate of 10%/min. The low load had been determined to be well within the elastic limit for the CCLs. Preconditioning the CCLs after five cycles showed reproducible behaviour (Woo *et al.*, 1991). Following the preconditioning procedure (Woo *et al.,* 1990c), the CCL was then subjected to cyclic tensile loading-unloading tests. To investigate the toe-region of the stress-strain behaviour of the CCL, a maximum load of 9.9N at sequential strain rates of 0.1, 1 and 10 %/min was applied to the CCL. Each strain rate consisted of three loading-unloading cycles which allowed for reproducible results. Between each loading-unloading cycle, including the preconditioning procedure, a period of six minutes recovery time was given (Viidik, 1968). This time had been identified by analysing the load-deflection curve data and was observed to be sufficient for the CCL to closely reach its original state (Viidik, 1968). Left CCLs were exposed to an ascending strain rate test in which the rate of strain was increased from 0.1 to 10%/min (Figure 3.9 (a)) and right CCLs were exposed to a descending strain rate in which the CCL was tested for its tensile behaviour under a decreasing strain rate from 10 to 0.1%/min (Figure 3.9 (b)) (Pioletti *et al.*, 1999; Pioletti and Rakotomanana, 2000).

3.3.4.1. Statistical Analysis

CCLs collected for the ascending and descending tests (Section 3.2.1) were statistically compared for their significant differences in hysteresis, area under stress-strain, transition strain and tangent modulus-stress curves using a two-tailed t-Test in Microsoft Office Excel (Microsoft Office, Version 2016, US) and $p<0.05$ was an indication of statistical significance.

One-way ANOVA followed by a Bonferroni post-hoc test for multiple comparisons were performed in Microsoft Office Excel (Microsoft Office, Version 2016, US) and in SPSS 20.0 (SPSS Inc., Illionois) to analyse differences between area under the curves at the three strain rates (0.1, 1 and 10%/min). The curves included stress-strain, tangent modulus-stress, transition strain and hysteresis. The statistical significant value was set at $p<0.05$. This statistical test was performed twice and independently, once to test CCL behaviour during the ascending test and another time to test the CCLs during the descending test.

In an additional analysis, hysteresis and strain rates were also tested as a continuous variable, using Pearson's correlation coefficient (r) to detect linear correlations between CCL hysteresis and changing strain rates. Coefficient of correlations between hysteresis and strain rates, such as strong and positive (r=+1) and strong and negative (r=-1), were determined for CCL behaviour during the ascending and descending tests.

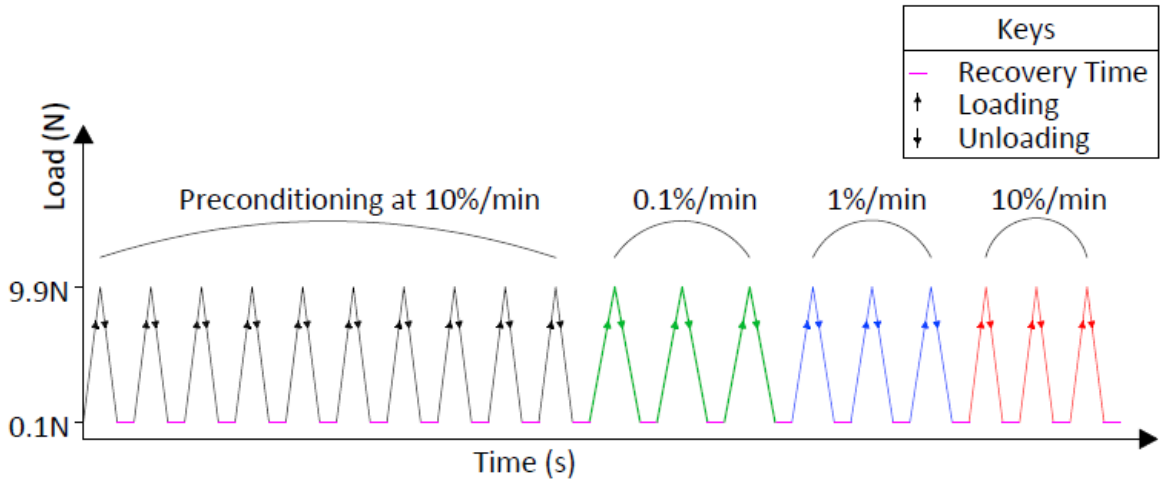

(a)

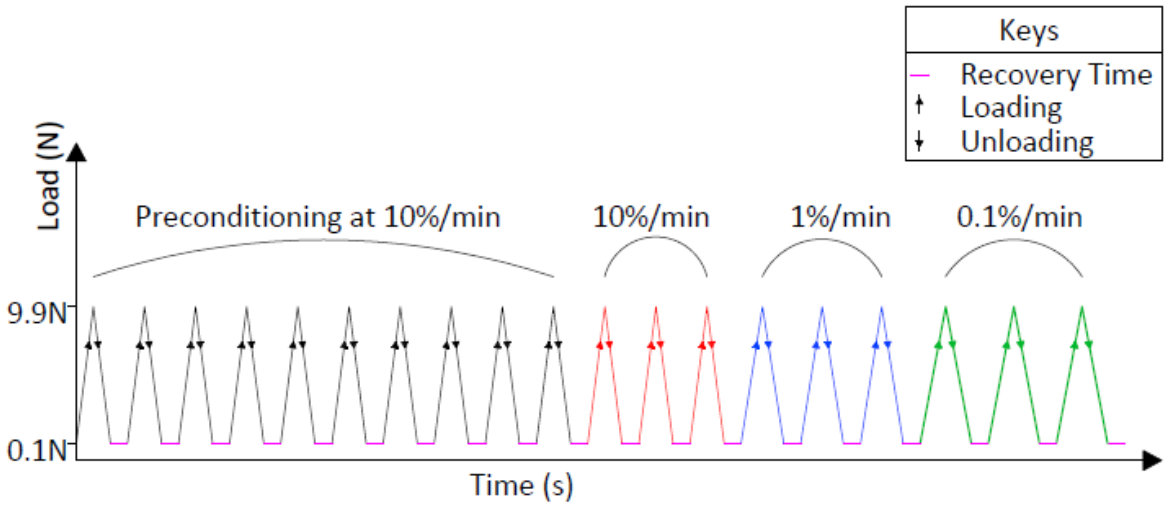

(b)

Figure 3.9: Experimental Study I test protocol; commencing with preconditioning at 10%/min strain rate which was then followed by 3 loading-unloading cycles at 0.1%/min, 1%/min and 10%/min for ascending tests (a) or 10%/min, 1%/min, and 0.1%/min for descending tests (b).

3.3.5. Experimental Study II: Contribution of PGs to the viscoelastic behaviour of CCLs

In Experimental Study II, the contribution of PG depletion to the viscoelastic behaviour of the CCL, namely strain rate sensitivity, hysteresis, creep and stress relaxation, was investigated. The CCLs (n=5 pairs) in the control and treatment groups were tested under cyclic loading-unloading conditions (Lujan *et al.*, 2009). Prior to mechanical tests, images of the CCL were

taken from different angles using the DIC setup. The DIC setup is further explained in Section 3.3.6.

As illustrated in Figure 3.10, the CCLs were preconditioned by performing five loading-unloading cycles to a maximum load of 9.9N at a maximum strain rate of 10%/min. Preconditioning was followed by cyclic loading-unloading at strain rates 0.1, 1 and 10%/min successively. Robinson *et al.* (2004) believed that PGs affect the strain rate sensitivity and it was reported that strain rate sensitivity is more distinguished at slow strain rates (<10%/min) (Bonner *et al.*, 2015). Therefore, the current study investigates the role of PGs in the canine CCLs at slow strain rates. Two cycles of loading and unloading tests were performed at 0.1 and 10%/min strain rate and three cycles at 1%/min strain rate. At each strain rates, multiple loading-unloading cycles were utilised to ensure the CCL behaviour was reproducible (Fung, 1993). At the last two loading-unloading cycles of 1%/min strain rate, pictures of the CCL were taken at 0.1, 1.1, 2.2, 3.3, 4.4, 5.5, 6.6, 7.7, 8.8, and 9.9N during loading and unloading to obtain the stress-strain target curves (Section 3.4.2.2). The last four cycles consisted of two cycles of creep and two cycles of stress relaxation tests (Hingorani *et al.*, 2004; Lujan *et al.*, 2009). The creep behaviour of the CCL was determined by subjecting the CCL to constant tension loads of 4.9N and 9.9N for 15min each during loading and unloading tests (Hingorani *et al.*, 2004). For the stress relaxation test, the CCL was deformed by applying a 9.9N load and monitoring the decrease in stress over 15min whilst the extension of the CCL was held. Loading and unloading during creep and stress relaxation tests were performed at 1%/min strain rate. Similar to Experimental Study I (Section 3.3.4), the recovery period of 6min was applied between each loading-unloading cycle to allow tissue recovery.

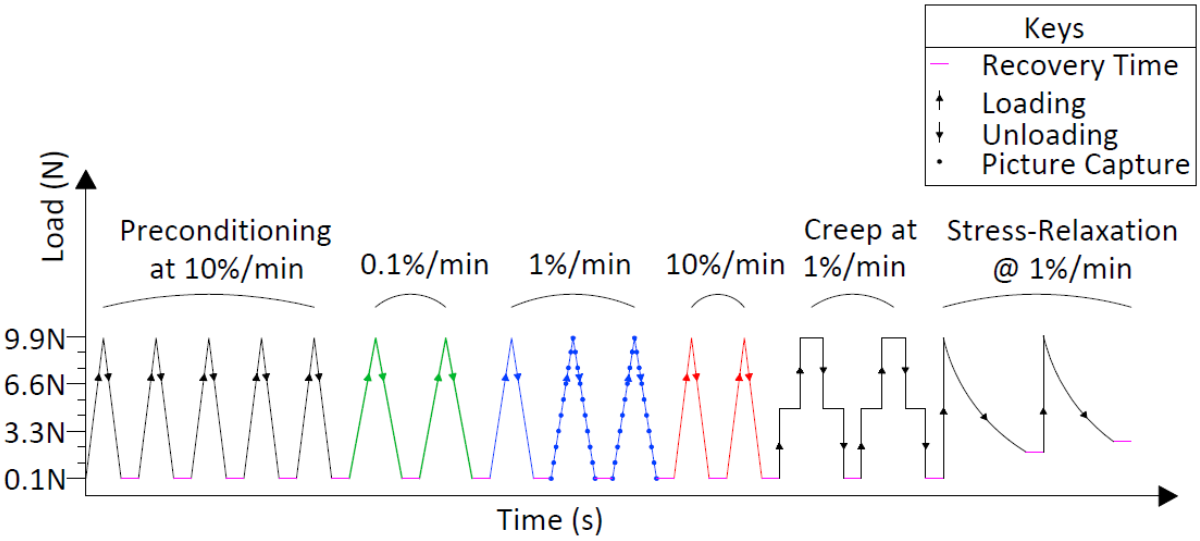

Figure 3.10: Experimental Study II test protocol investigating complete viscoelastic characteristics of the CCLs by applying tensile loads. The CCLs were preconditioned at 10%/min strain rate which was then followed by 2 loading-unloading cycles at 0.1%/min, 3 loading-unloading cycles at 1%/min, 2 loading-unloading cycles at 10%/min, 2 cycles of two-step creeps and 2 cycles of stress relaxations. During the last two loading-unloading cycles of the 1%/min strain rate, pictures of the deformed CCLs were taken from different load points.

3.3.5.1. Statistical Analysis

CCLs from the control and treatment groups were statistically compared and tested for their significant differences in content of water and PG, area under stress-strain, tangent modulus-stress, stress-time (stress relaxation) and strain-time (creep) curves, hysteresis, and transition strain using a two-tailed t-Test in Microsoft Office Excel (Microsoft Office, Version 2016, US) and $p<0.05$ was an indication of statistical significance.

One-way ANOVA followed by a Bonferroni post-hoc test for multiple comparisons were performed in Microsoft Office Excel (Microsoft Office, Version 2016, US) and in SPSS 20.0 (SPSS Inc., Illionois) to analyse differences between area under the curves at the three strain rates (0.1, 1 and 10%/min). The curves included stress-strain, transition strain, tangent modulus-stress, stress-time (stress relaxation) and strain-time (creep) and hysteresis. The

statistical significant value was set at $p<0.05$. This statistical test was performed twice and independently, once to test the CCLs in the control group and another time to test the CCLs in the treatment group.

In an additional analysis, hysteresis and strain rates were also tested as a continuous variable, using Pearson's correlation coefficient (r) to detect linear correlations between CCL hysteresis and changing strain rates. Coefficient of correlations between hysteresis and strain rates, such as strong and positive (r=+1) and strong and negative (r=-1), were determined for CCLs in the control and treatment groups.

One-way ANOVA in Microsoft Office Excel (Microsoft Office, Version 2016, US) was performed to analyse differences between hysteresis at the five precondition cycles. No post-hoc test was performed as no statistical significant values were found (Section 4.3.3.1.3).

Statistical analyses were performed using a two-tailed t-Test in Microsoft Office Excel (Microsoft Office, Version 2016, US) to analyse differences in creep and stress relaxation rates between the initial 20s and the last 500s and $p<0.05$ was an indication of statistical significance. In addition, CCLs from the control and treatment groups were statistically compared for their significant differences in creep and stress relaxation rate at the initial 20s and then at the last 500s, using a two-tailed t-Test in Microsoft Office Excel (Microsoft Office, Version 2016, US). The statistical significant value was set at $p<0.05$.

3.3.6. DIC Setup

In this study, a novel full-field three-dimensional digital image correlation (3D DIC) method was developed to capture the non-deformed surface of the CCLs and optically measure the load-deformation behaviour across the surface of the ligament.

In addition to recording the load-deformation of CCLs subjected to tensile tests from the materials testing machine, successive images of the ligaments were recorded to obtain measurements of the deformation distribution across their surface (Sutton *et al.*, 2009; Chen *et al.*, 2013). With reference to Figure 3.11, the CCLs were monitored in all three directions (x, y, and z), using six digital SLR camera bodies with Canon EF 100mm f2.8 USM Macro lenses (Canon, Tokyo, Japan), obtaining 5184 x 3456 pixels per image. Adjacent cameras were paired generating three pairs in total (Figure 3.11). Each pair was positioned 25^0 to the adjacent one to obtain the desired stereovision output. The first pair consisted of cameras 1 and 2, the second pair cameras 3 and 4 and the third pair cameras 5 and 6. As shown in Figure 3.11 (a), front (detachable) and back (stationary) frames were custom designed around the materials tensile testing machine in order to hold the cameras in place around the CCL on the load cell.

The first camera pair was mounted on the detachable front frame, whereas the second and third pairs were placed on the back frame (Figure 3.11). The centreline of the first pair was positioned at 130^0 to both the second and third pairs whilst the centrelines of the second and third pairs were positioned at 100^0 to one another (Figure 3.11 (a)). This positioning of camera pairs facilitated a full-field (360^0 view) of the CCL.

During mechanical tests, the CCL was kept in a custom-made stainless-steel tank which was used to control the hydration and degradation of the tissue as well as accommodating the cameras around the tissue. This custom-made tank was built by creating a 3D model of the required tank (Figure 3.12) using AutoCAD 3D (AutoCAD 2014, Autodesk, US) and then the tank was manufactured based on this customised design. The body of the tank was made of stainless-steel to avoid any potential chemical reactions or contamination between the tank and its medium. Six windows were introduced into the steel tank to accommodate views of the CCL (Figure 3.12). These windows, made from 3mm thick borosilicate glass pieces

(Spectraglass Ltd, Perth, UK), were positioned orthogonally (90° ± 0.1°) to the cameras (Figure 3.11 (a)) minimising the distortion due to light refraction, especially when light passed between the different mediums (i.e. between the air and the glass windows and the glass windows and the buffer solution).

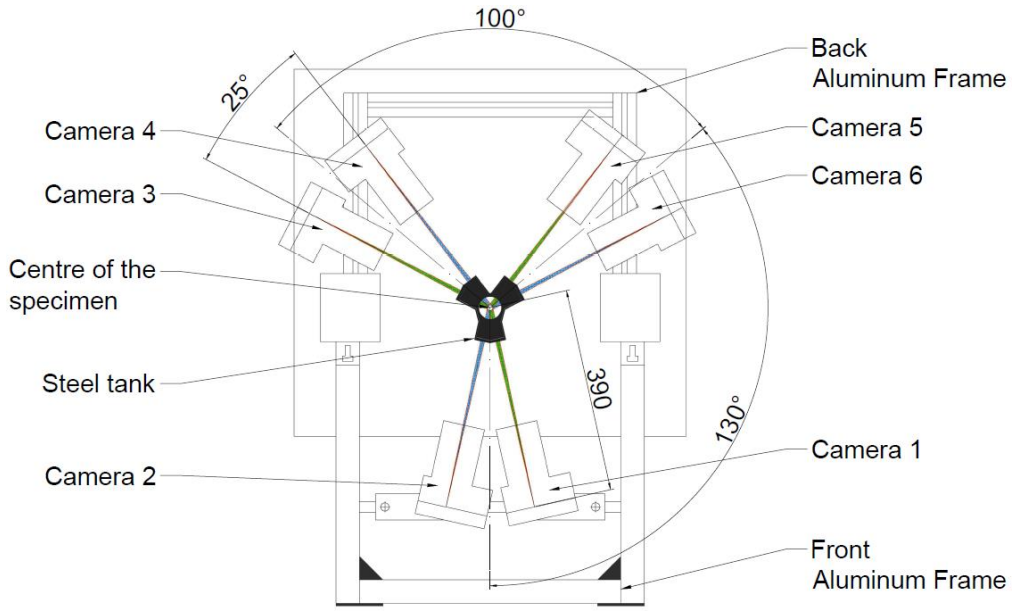

(a)

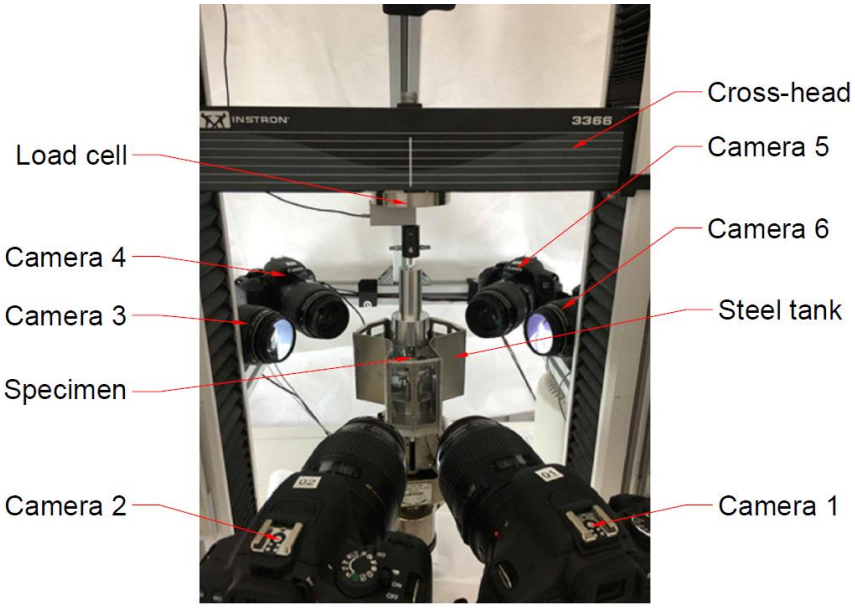

(b)

Figure 3.11: The DIC setup for testing CCLs. Schematic top view of the DIC test setup on the material testing machine (a). Photographic front view of the DIC setup showing all six cameras, stainless-steel tank and the CCL submerged in liquid (b).

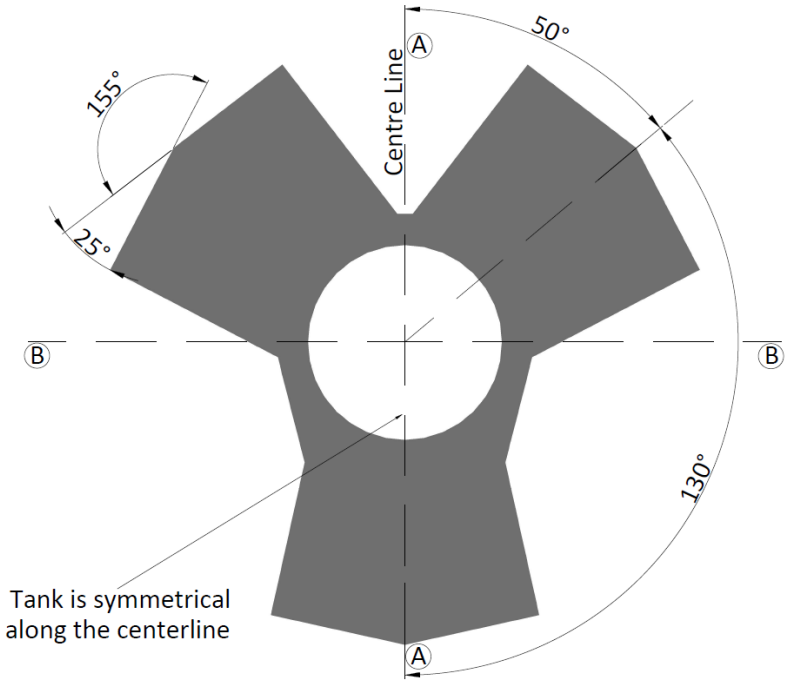

(a)

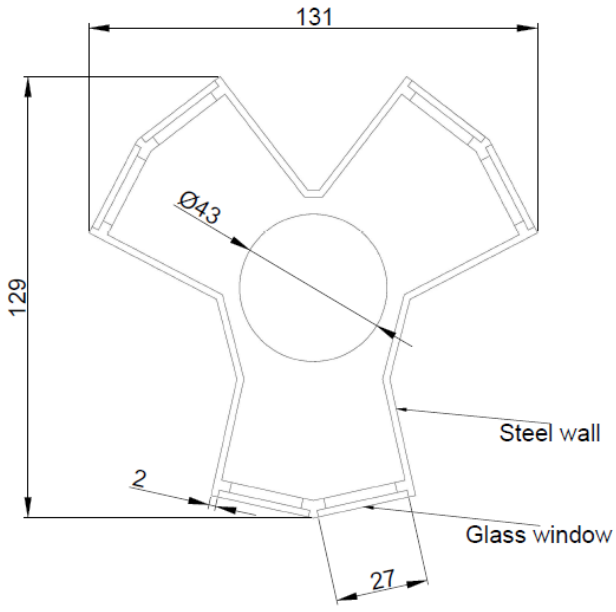

(b)

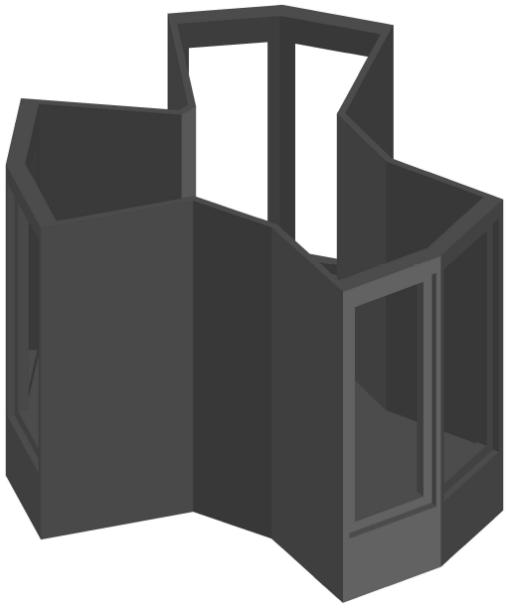

(c)

Figure 3.12: Solid (a) and wireframe (b) top view of the stainless-steel tank, length dimensions detailed on drawing are given in mm. 3D solid view of the tank (c) showing the six glass windows.

3.4. DIC Analysis

3.4.1. Calibration

The six camera DIC system was calibrated twice; firstly, for determining the image parameters (intrinsic and extrinsic parameters) between the adjacent cameras (for instance, calibrating camera 1 and 2) (Section 3.4.1.1), and secondly for the whole DIC setup between each camera pair (for instance, calibrating the position of camera pair 1 with pair 2 and pair 3) (Section 3.4.1.2) (Dantec Dynamics, 2014).

3.4.1.1. Calibration of the cameras

In the first calibration process, the intrinsic and extrinsic parameters between two adjacent cameras were obtained. The intrinsic parameters are internal and fixed to a particular camera and allow a mapping between camera coordinates and pixel coordinates in the image frame (Dantec Dynamics, 2014). The extrinsic camera parameters, the relative position and orientation of one camera to another, are external to the camera (Dantec Dynamics, 2014). These projection parameters were obtained by firstly taking pictures of a 1.5mm 9x9 marked white glass calibration plate (Dantec Dynamics Calibration Target, Dantec Dynamics, Denmark, 2014) (Figure 3.13). The calibration plate was immersed inside the test solution within the steel tank in order to calibrate the cameras to the environment where the CCL would be tested. Pictures of calibration plates were taken by one camera pair at a time and these pictures were analysed to extract the projection parameters for all three camera pairs.

Initially 70 Canon Raw Version 2 (.CR2) image files of the calibration plate at different angles and positions were collected for each camera pair. These images were analysed using DIC software (Istra4D, Dantec Dynamics, Denmark, 2014). The images needed to be converted from their original format, which was .CR2, into Tag Image File Format (.tiff) so that Istra 4D

could read and process the images. To do this a MATLAB script, shown in Figure 3.14, was used. In the MATLAB script, lines 1 and 2 cleared and deleted any previously stored data, lines 3 to 5 located the existing files, lines 6 to 18 changed the extension of the exiting files from .CR2 to .tiff, and finally lines 19-25 read the newly generated .tiff file and converted its true colour (RGB image) to grey scale intensity image then converted the grey scale image to 8 bit. The code sharpened the image, changed the contrast of the image and finally wrote the file. These image files were organised effectively to ease the process of image analysis and eliminate the potential for misplacing information. A folder named 'Calibration' was created with three subfolders named 'cam1_2', 'cam3_4', and 'cam5_6' each of which was divided into further subfolders, for example 'Cam1' and 'Cam2', etc. (Appendix (2): Figure 1 (a)).

Once all the images for the calibration target were converted and placed in their allocated folders, they were imported into Istra4D to calculate the projection parameters. To do this the following steps were undertaken:

1. Istra4D software started.
2. Within Istra4D a new projection calibration was created (Appendix (2): Figure 1 (b)).
3. The converted image files of a camera pair (i.e. camera pair 1 which included images from camera 1 and 2) were imported into Istra4D (Appendix (2): Figure 1 (c)).
4. Calibration target pane was set to 1.5mm 9x9 Marked White to match the target plate used (Appendix (2): Figure 1 (d (i))).
5. Within the calibration setting, the morphological mask was set to '5x5 Extended' and the rest of the settings were left on their default parameters (Appendix (2): Figure 1 (d (ii) and (e))).

6. The markers on the surface of the target plate were extracted, with 0 indicating that no markers and 64 indicating that all the square corners (markers) of the target plate were found (Appendix (2): Figure 1 (d (iii))).
7. The two sets of images from each camera were connected and calibrated (Appendix (2): Figure 1 (d (iv))). The software used an optimisation algorithm to calculate the calibration parameters (Appendix (2): Figure 1 (d (v))) and the Residuum. The Residuum value was calculated by taking an average uncertainty of the found markers in the unit of pixels (Appendix (2): Figure 1 (d (vi))). Residuum of less than 1 pixel was achieved to obtain a good calibration (Dantec Dynamics, 2014).
8. Finally, the intrinsic and extrinsic parameters for the camera pairs were exported in a file (Appendix (2): Figure 1 (f)).

The steps described above were repeated for the three camera pairs separately, generating three projection calibration reports for each camera pair. Changing the position of a camera or a camera image setting (i.e. focus) would have required a new projection parameter to be determined in order to accurately analyse the images. However, in this study this calibration process was performed only once because none of the settings were altered (the clamping system allowed each CCL to be placed in the same way in each test) until the completion of all the mechanical tests.

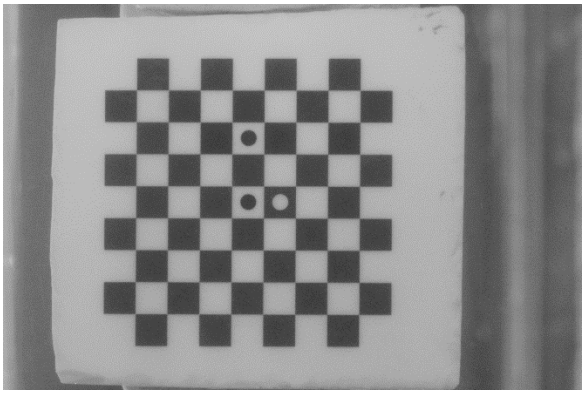

Figure 3.13: The calibration target used to calibrate the cameras and its centreline positioned at the centre of the system within the custom designed tanks with solution.

```
clear all,
clc,
for X = 3348:3367  %Change the numbers to match the minimum and maximum file
numbers.
A = num2str(X);
B = 'CR2';
if length(A) == 1
R = strcat('IMG_000',A,'.',B);
W = strcat('IMG_000',A,'.tiff');
elseif length(A) == 2
R = strcat('IMG_00',A,'.',B);
W = strcat('IMG_00',A,'.tiff');
elseif length(A) == 3
R = strcat('IMG_0',A,'.',B);
W = strcat('IMG_0',A,'.tiff');
elseif length(A) == 4
R = strcat('IMG_',A,'.',B);
W = strcat('IMG_',A,'.tiff');
end
C = imread(R);
D = rgb2gray(C);
E = im2uint8(D);
G = imsharpen(E,'Radius',6 ,'Amount',8 , 'Threshold', 0.9);  %Sharpness
H = imadjust(G,[0.3, 0.7],[]);  %Contrast
imwrite(H,W,'tiff','Compression','none');
end
```

Figure 3.14: MATLAB script used to convert .CR2 to .tiff image files to allow analysis of images obtained from the cameras.

3.4.1.2. Calibration of the DIC setup

The second calibration process was performed to ensure the three topographies created from each camera pair would successfully reproduce the full field of view of the CCLs. In order to achieve this correction, one image of a rotationally non-symmetric object with a known geometry (Figure 3.15) was taken by all three camera pairs. This custom-built reference object

was made of steel with a high resolution (±0.05mm). The surface of the reference object was spray painted matt white to give a distinct bright surface and then matt black spray paint was applied to create speckle patterns on the white surface. This object was placed in the same environment and position as the CCLs would be positioned during mechanical tests (Figure 3.15 (b)).

Subsequently this image was analysed using the DIC (Istra4D) software in order to obtain x, y and z coordinates of the three surfaces captured by the three camera pairs. Similar to the initial calibration, changing camera settings or the position of a camera would have required the object calibration to be repeated. However, in this study the calibration process was performed only once because nothing was altered with the sample testing until the completion of all the mechanical tests.

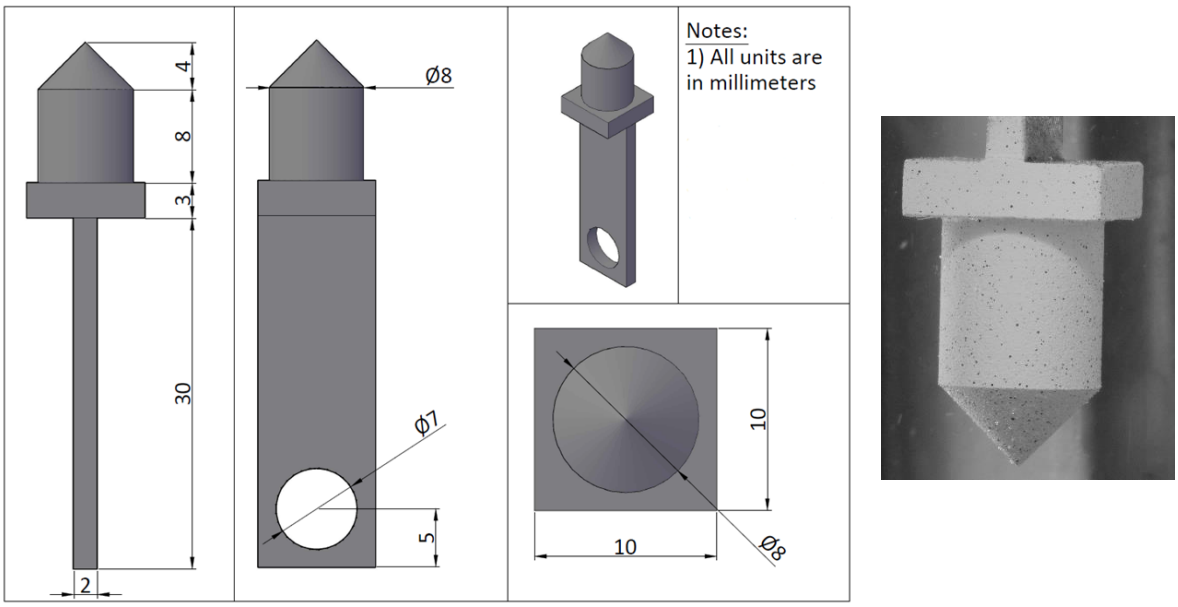

(a) **(b)**

Figure 3.15: Reference steel object with defined geometry (a) used in the initial process of image registrations and the same object placed in the environment and the position where the CCL was later clamped and tested (b).

3.4.2. DIC Image Analysis

For the DIC image analysis process Istra4D software was used to extract x, y and z coordinates of the CCL and the surface of the custom-built calibration object (Dantec Dynamics, 2014).

3.4.2.1. DIC image analysis of calibration object

One image of the calibration (reference) object was taken by all six cameras. As described in Section 3.4.1.1, the image was converted from a .CR2 file to a .tiff file so that it could be read by the DIC software. Each camera pair was used to create a 3D surface of the object, hence creating three surfaces of the object at different angles in 3D. The 3D surfaces were created using the following the steps:

1. Istra4D software started.
2. As shown in Appendix (3): Figure 1 (a), a new correlation series was created by importing the image files of camera pair in the same way as described in step 3 of Section 3.4.1.1.
3. A new evaluation was created (Appendix (3): Figure 1 (b)) then the calibration file generated previously from the calibration plate (Appendix (3): Figure 1 (c)) was inputted.
4. In the evaluation setting, facet size was defined based on the speckle pattern on the surfaces. To achieve optimal accuracy in DIC image analysis, a minimum of three speckles per facet was attained (Sutton *et al.*, 2009). In the setting for correlation parameters, the advanced full-user defined setting was selected, allowing facet size to be set to 79 pixels (Appendix (3): Figure 1 (d (i))). The grid size defining the distance between the centre of the facets was set at 53 pixels which was 2/3rd of the facet size (Appendix (3): Figure 1 (d (ii))). As illustrated in Appendix (3): Figure 1 (e), facet overlap was allowed in this study.

5. A polygon was drawn around the calibration object leaving space around it to provide acceptable surface coverage. In addition, a specific point on the object was selected so that the software could find the rest of the speckles on the surface (Appendix (3): Figure 1 (f)).
6. In the control pane, the evaluation for the images (steps) was performed (Appendix (3): Figure 1 (g (i))). Once the evaluation for the steps was completed the number of successfully solved facets was indicated (Appendix (3): Figure 1 (g (ii))).
7. Finally, the evaluated data was exported (Appendix (3): Figure 1 (h)) and saved as an ASCII (American Standard Code for Information Interchange) file (Appendix (3): Figure 1 (i)).

The steps described above were repeated for the three camera pairs separately, generating three surfaces in 3D, one for each camera pair.

3.4.2.2. DIC image analysis of CCLs

As stated in Section 3.3.5, one image of each CCL was taken from all six cameras prior to preloading and, subsequently, multiple images were taken at different load points. The 3D surface of the CCL was constructed from the image of the CCL prior to mechanical tests whilst the successive images of the CCL during mechanical tests were used for obtaining load-displacement target curves at the mid-substance of the CCL.

The three CCL surfaces in 3D were generated from the three camera pairs. Similar steps to those given in Section 3.4.2.1 were taken to generate the surfaces of the CCL. The process began with importing images of the CCL from a camera pair, masking the area around the CCL (Figure 3.16 (a)) and consequently obtaining the x, y, and z coordinates of the CCL (Figure 3.16 (b)). Due to the complex anatomical structure of the CCL, in particular the ligaments' complex curvature, there were some blind spots where the cameras could not identify the

speckle pattern. Hence, there were regions across the surface of the CCL with missing data points, in particular around the tibial and femoral insertion area of the ligaments (Figure 3.16 (b)).

During loading in the third cycle of the 1%/min strain rate test, ten CCL images were collected from each camera pair and these images were used to obtain load-displacement target curves. In this study, the images were used to monitor longitudinal deformation at the mid-substance of the CCL during loading. Hence, a mask around the mid-substance (valid grid points between 10-60) of the CCL was created (Appendix (4): Figure 1 (a)) for the image analysis. The masked area contained 10-60 valid grid points and these points were combined to produce an estimated average behaviour of the CCL at the mid region. This process was repeated for all three camera pairs (Appendix (4): Figure 1 (b-d)); hence three target curves were obtained for each CCL. Subsequently, these three curves were combined to calculate a mean target curve which was used for inverse analysis (Section 3.6).

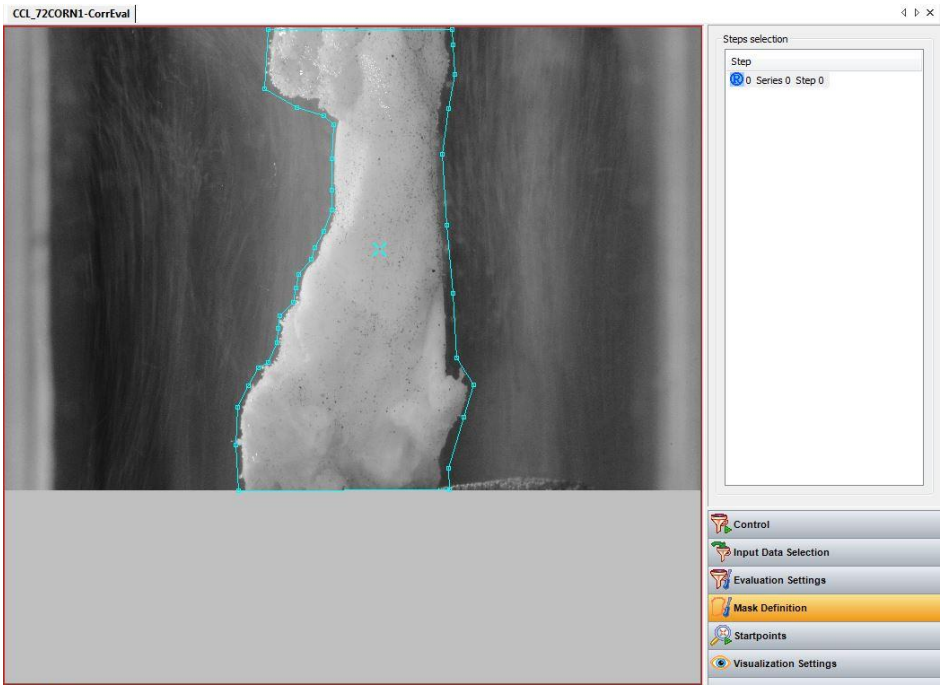

(a)

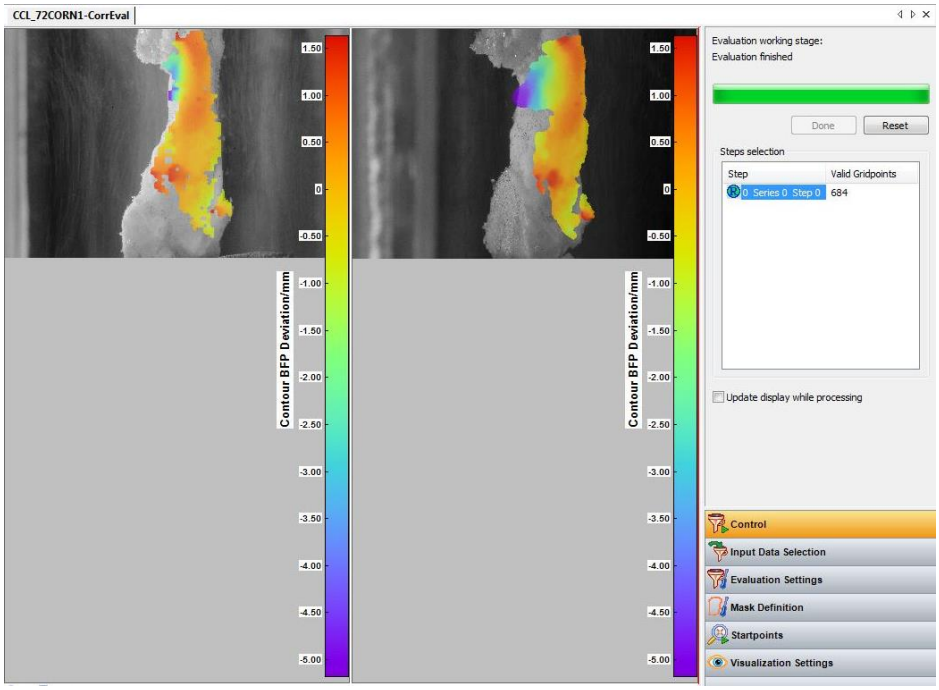

(b)

Figure 3.16: Image of a canine CCL from a reference camera with a mask around the desired area of the ligament (a). View of a CCL from a camera pair showing best fit plane contour to indicate the solved facets of the surface (b).

3.5. Finite Element Model of CCLs

3.5.1. CCL Topography Matching by Iterative Registrations

Images of the calibration (reference) object were evaluated to obtain three surfaces of the object in 3D (Section 3.4.2.1). These surfaces were aligned and combined using iterative registrations (Wang *et al.*, 2014).

Initially, the coordinate transformation (rotation (R), and translation (t)) that matched two surfaces of the reference object, static surface S and dynamic surface D, were found. Each surface was defined by discrete sets of data points ($s_i \, \epsilon \, S; i = 1, 2, 3, \dots, n$) and ($d_j \, \epsilon \, D; j = 1, 2, 3, \dots, m$). The static surface S was generated by inputting the exact dimensions of the calibration object using MATLAB as shown in Figure 3.17 (a), whilst the dynamic surface D was the data collected from the six cameras using DIC method. The dynamic surface D underwent an extrinsic rotation R and translation t about the origin of the fixed coordinate system of the static surface S. These translation (Equation 3.7) and rotation (Equation 3.8) corrections were necessary to perform the surface matching process.

$$\bar{d}_j = R d_j + t \qquad \text{Equation 3.7}$$

where the overbar represents the transformed data points in terms of x, y, and z coordinates, and all data points $j = 1, 2, 3, \dots, m$ are required to undergo the same transformation. The rotation matrix is given by

$$R = R_x R_y R_z \qquad \text{Equation 3.8}$$

where

$$R_x = \begin{bmatrix} 1 & 0 & 0 \\ 0 & cos\,\theta_x & -sin\,\theta_x \\ 0 & sin\,\theta_x & cos\,\theta_x \end{bmatrix},$$

$$R_y = \begin{bmatrix} cos\,\theta_y & 0 & sin\,\theta_y \\ 0 & 1 & 0 \\ -sin\,\theta_y & 0 & cos\,\theta_y \end{bmatrix},$$

$$R_z = \begin{bmatrix} cos\,\theta_z & -sin\,\theta_z & 0 \\ sin\,\theta_z & cos\,\theta_z & 0 \\ 0 & 0 & 1 \end{bmatrix} \qquad \text{Equation 3.9}$$

$\theta_z, \theta_y, and\ \theta_z$ are Euler angles

$$t = (t_x t_y t_z)^T \qquad \text{Equation 3.10}$$

where T denotes matrix transposition.

The process of registration focused on determining transformation (rotation and translation) parameters ($t_x, t_y, t_z, \theta_z, \theta_y, and\ \theta_z$). Once these parameters were found, the topography of the dynamic surface overlapped the topography of the static surface.

These transformation (correction) parameters were estimated using the point-to-point Iterative Closest Point (ICP) algorithm on both static and dynamic surfaces (Kjer and Wilm, 2010), (Figure 3.17 (b, c)). In this study 100 iterations were selected to calculate the optimal match between the two surfaces, and this iteration value was chosen based on the satisfactory value achieved for the root mean square (RMS). The accuracy of this matching process was examined by deriving RMS error as a percentage of the surface area of the reference object (Equation 3.11).

$$RMS = \frac{1}{L} \times \sum_{l=1}^{L} \frac{\sqrt{\left(\frac{1}{K}\right)\sum_{k=1}^{K}(S_k - D_k)^2}}{Surf.A_{\,ref.object}} \times 100 \qquad \text{Equation 3.11}$$

where L is the total number of dynamic surfaces obtained from the cameras (L=3), K is the number of surface points, S_k and D_k are $3 \times n$ matrices defining the static and dynamic surfaces, and $Surf.A_{\,ref.object} = 642.414 \pm 0.05\, mm^2$ is the exterior surface area of the reference object. The MATLAB code written to perform this optimisation is presented in Appendix (5).

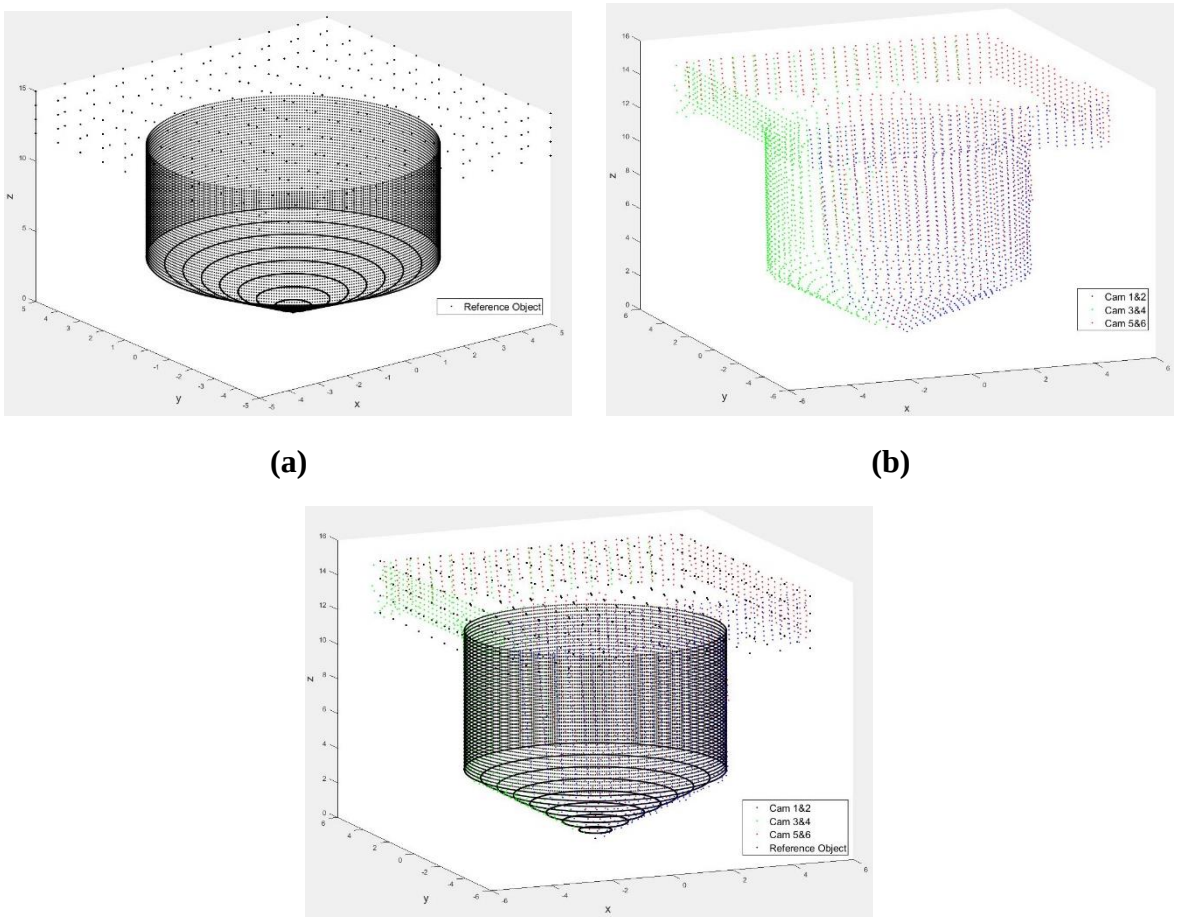

(a) **(b)**

(c)

Figure 3.17: The cloud points of the reference object as generated from a MATLAB script (a) and obtained from the DIC images, applying a point-to-point ICP algorithm (b). The match between these two surfaces is presented (c).

3.5.2. Finite Element Model Generation of CCLs

Coordinate geometry of the CCL was obtained at three different viewpoints to cover views around the whole ligament. The three surfaces of the CCL in 3D (3D point cloud) were combined to create a full-field 3D surface of the CCL.

It was indicated in Section 3.4.2.2 that the complex anatomical structure of the CCL limited the possibility of tracking all the speckles across the surface of the ligament. To overcome this limitation, the Poisson surface reconstruction algorithm was used to generate a hole-free surface (Kazhdan *et al.*, 2006). This reconstruction algorithm was employed in addition to other operations (i.e. computing normal for point sets, Poisson-disk sampling (Corsini *et al.*, 2012)) using MeshLab (MeshLab, Visual Computing Lab – Italian National Research Council - CNR, Italy) (Figure 3.18 (a and b)).

A numerical solid section (volumetric part) of the CCL was generated from the mesh surface described above. The creation of this solid part was achieved using MIMICS (Materialise, Leuven, Belgium) (Figure 3.18 (c)).

Subsequently, the volumetric CCL part was exported into FEM software Abaqus/Standard 6.13 (Dassault Systèmes Simulia Corp., Rhode Island, USA) to seed for a hybrid ten-node tetrahedral element (C3D10H) type of mesh with an approximate global size of <1mm (Elsheikh *et al.*, 2013) (Figure 3.19). The CCL FEM was partitioned into three regions, namely tibia bone, middle substance, and femur. This division of the CCL model in this way is important to investigate mechanical behaviour of the ligament. Each part was defined with specific material properties and the material properties of the femur and tibia bones were derived from previous studies and defined as being linear elastic with 11000MPa for elastic modulus and 0.3 for Poisson's ratio (Reilly *et al.*, 1974; Reilly and Burstein, 1975).

The middle region of the FEM of the CCL, however, included an isotropic Ogden material model (Ogden, 1984) to represent the incompressible and hyperelastic behaviour of the ligament. The Ogden form of the strain energy potential for incompressible models is expressed in terms of the principal stretches (Equation 3.12).

$$U = \sum_{i=1}^{N} \frac{2\mu_i}{\alpha_i^2}(\overline{\lambda}_1^{\alpha i} + \overline{\lambda}_2^{\alpha i} + \overline{\lambda}_3^{\alpha i} - 3) + \sum_{i=1}^{N} \frac{1}{D_i}(J_{el} - 1)^{2i} \qquad \text{Equation 3.12}$$

where U is the strain energy potential, $\overline{\lambda_\iota}$ is a product of the total volume strain J and the principal stretch λ_i, which is defined as $\overline{\lambda_\iota} = J^{-\frac{1}{3}}\lambda_i$. The μ_i and α_i are material constants, and the D_i defines the compressibility of the material. J_{el} is the elastic volume strain and is negligible in this study because zero was chosen as the value of D_i to account for the nearly incompressible nature of the CCLs (Fung, 1993). When biological samples subjected to biaxial tension, the principal stretches λ_2 and λ_3 are assumed to be equal ($\lambda_2 = \lambda_3 = \lambda_1^{-\frac{1}{2}}$), hence the strain energy equation could be rewritten as:

$$U = \sum_{i=1}^{N} \frac{2\mu}{\alpha_i^2}(\lambda_1^{\alpha i} + 2\lambda_1^{-\frac{1}{2}\alpha i} - 3) \qquad \text{Equation 3.13}$$

To write the equation in terms of stress in one direction, Equation 3.13 could be differentiated with respect to λ_1 and form the following equation:

$$U = \sum_{i=1}^{N} \frac{2\mu}{\alpha_i}(\lambda_1^{\alpha i-1} - \lambda_1^{-\frac{1}{2}\alpha i-1}) \qquad \text{Equation 3.14}$$

This process was repeated to create FEMs of all the canine CCLs (n=5 pairs) tested in Experimental Study II. These FEMs of the CCLs were used in the inverse analysis study,

explained in Section 3.6, to predict μ_i and α_i which are important parameters defining the hyperelastic behaviour of the ligaments.

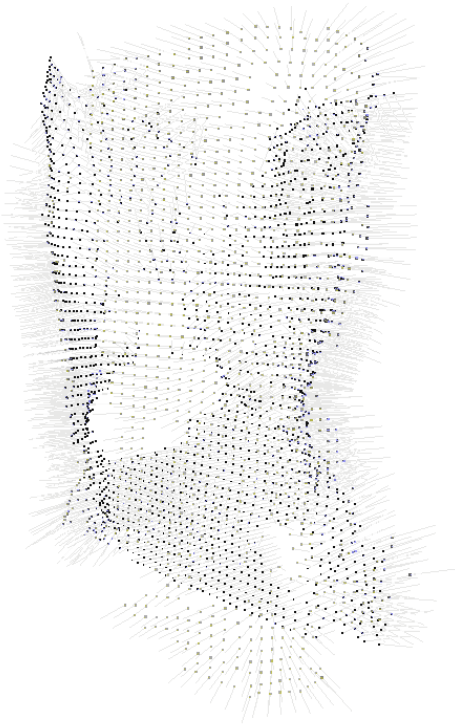

(a)

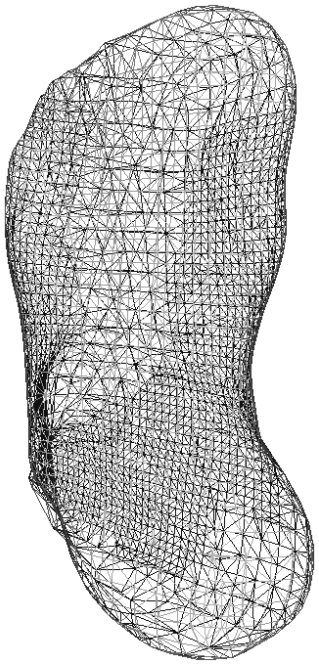

(b)

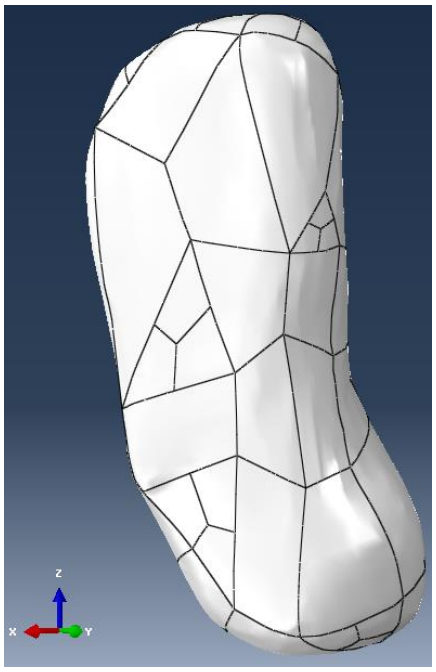

(c)

Figure 3.18: Point cloud of the CCL obtained from the DIC image analysis and the lines emerging from each point represent normal for the point sets (a). The point cloud used to construct the surface of the CCL using the Poisson surface reconstruction algorithm (b). Subsequently, a refined solid section of the CCL was generated using MIMICS (c).

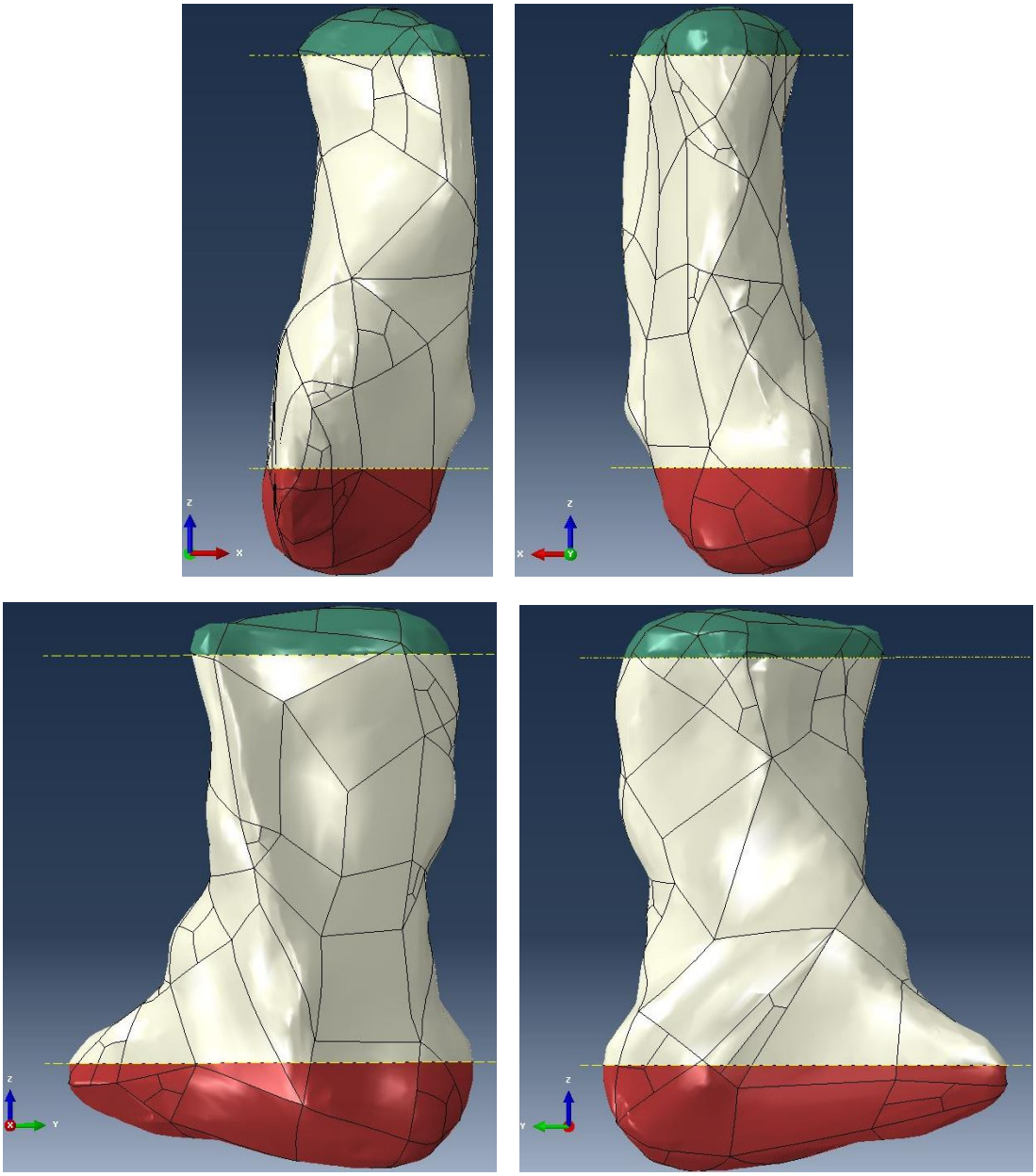

Figure 3.19: The solid section of the CCL was exported into Abaqus to generate an FEM of the CCL as well as partition the CCL model into the tibia (red), the mid-substance of the CCL (grey) and the femur (green).

3.6. Inverse Analysis

Particle swarm optimisation (PSO), written in MATLAB in combination with Abaqus, was used in the inverse analysis study (Freutel *et al.*, 2015). This study was designed to predict the

hyperelastic material parameters (μ_i and α_i) of the CCL based on the best possible match between applied load and displacement results as obtained experimentally and predicted numerically.

The optimisation objective was to minimise the RMS error between the experimental and numerical displacements at a targeted point on the mid-substance of the CCL and this limit was set at 0.1%. Similar to the studies by Whitford *et al.* (2016), the RMS was calculated as percentages of the final deformation at a particular point across the surface of the CCL (Equation 3.15).

$$RMS = \frac{\sqrt{((\frac{1}{N})\sum_{n=1}^{N}(\delta_n^{exp} - \delta_n^{num})^2)}}{\delta_{max,n}^{exp}} \times 100 \qquad \text{Equation 3.15}$$

where N = 10 is the number of load increments, and δ_n^{exp} and δ_n^{num} are the experimental (exp) and numerical (num) deformation for a given point across the surface of the CCL at a particular load point.

One node at the middle region was monitored and the optimisation software modified the material parameters until a satisfactory design between the experimental target curve and numerical results was produced.

3.7. Canine Stifle Joint Finite Element Model Development

A 3T MRI scanner using three-dimensional (3D) Dual Echo Steady State (DESS) sequence was used to scan the left canine pelvic limb collected for Experimental Study III. This magnitude scanner was used to accurately detect the soft tissues around the stifle joint with high resolution (Gold *et al.*, 2009; Naraghi and White, 2012).

The consecutive images from the MRI scans of the stifle joints were manually segmented in different planes (i.e. xy, xz, and yz planes) using SIMPLEWARE Scan IP (SIMPLEWARE LTD, EXETER, UK) software (Figure 3.20 (a, b and c)). The segmented components determined were the femur, tibia, fibula, cartilage, menisci, cranial ligament of fibular head, and the four major ligaments – cruciate ligaments (CCL and CaCL) and collateral ligaments (LCL and MCL).

Completing the manual segmentation led to the generation of a 3D model (Figure 3.20 (d)) which was then exported from the SIMPLEWARE Scan IP 5.0 (SIMPLEWARE LTD, Exeter, UK) software into the finite element software ABAQUS 6.13 (Dassault Systèmes Simulia Corp., Rhode Island, USA) to create an FEM. The solid sections of the stifle model were meshed appropriately with non-hybrid (C3D4) and hybrid (C3D4H) elements for the elastic and hyperelastic sections respectively enabling good representation of the variable surface and behaviour of the stifle (Elsheikh *et al.*, 2013). The elastic behaviour of bone, cartilage and meniscus were defined based on the literature relating to human (Reilly *et al.*, 1974; Reilly and Burstein, 1975; Oshkour *et al.*, 2011) (Table 3.1) and the non-linear material properties of the four major ligaments were defined based on the hyperelastic behaviour of CCLs obtained through inverse analysis in Experimental Study II. These material properties were taken from other samples and species and they were not directly pertinent to the specific model. However, place holder values were required to proceed with the development of the stifle joint FEM whilst the representative material parameters could be determined experimentally by future work (Section 5.4). Subsequently, the FEM of the whole stifle joint was tested to investigate the effect of PG depletion in CCLs on the joint stability (Section 3.8).

Table 3.1: Elastic material properties of bones, cartilage and meniscus were taken from previous literature relating to human (Reilly et al., 1974; Reilly and Burstein, 1975; Oshkour *et al.*, 2011) and used in the development of the FEM of the stifle joint.

	Bones	**Cartilage**	**Meniscus**
Young's Modulus (MPa)	11000	5	59
Poisson's Ratio	0.30	0.46	0.49

3.7.1. Statistical Analysis

Load-displacement behaviour obtained from the control and the treatment FEMs were compared for statistical differences. To perform this comparison, the areas under the load-displacement curves were calculated and they were statistically analysed using a two-tailed t-Test in Microsoft Office Excel (Microsoft Office, Version 2016, US) and $p<0.05$ was an indication of statistical significance.

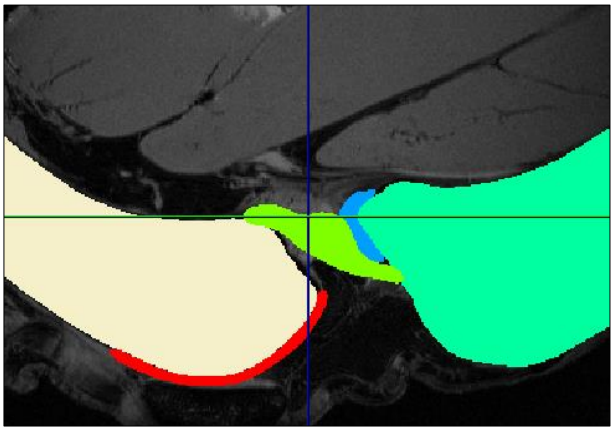

(a)

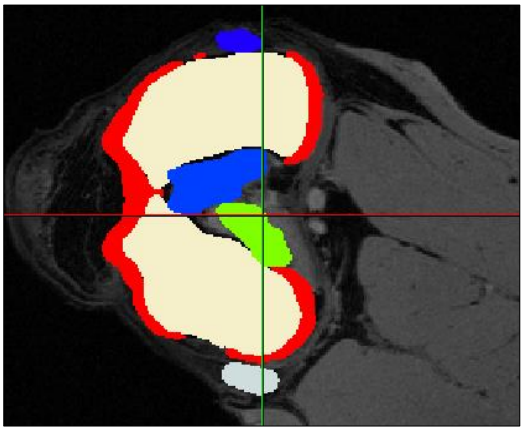

(b)

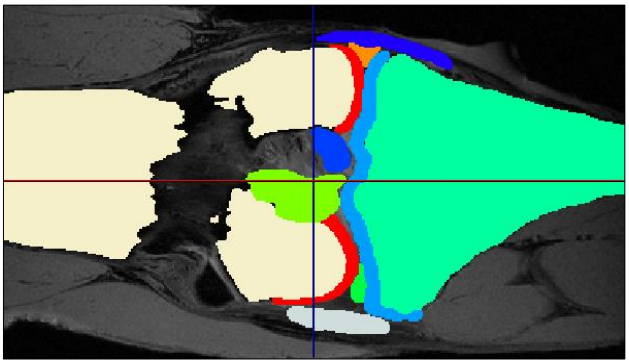

(c)

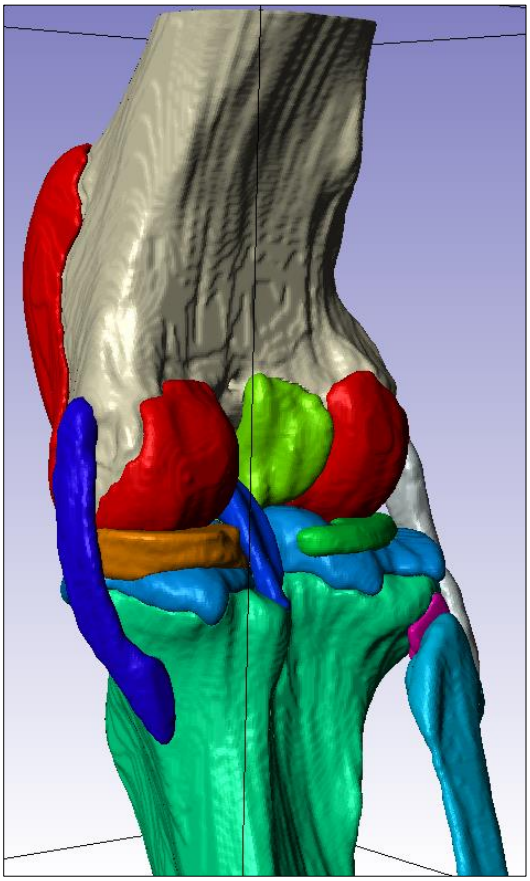

(d)

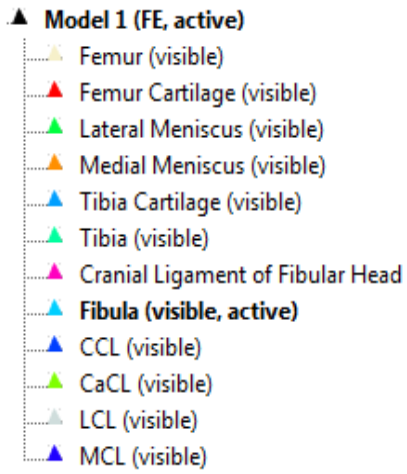

(e)

Figure 3.20: An MRI scan of a canine stifle joint (skeletally mature Staffordshire bull terrier) showing segmented components of the joint tissues presented in the sagittal (a), transverse (b), and coronal (c) planes. A 3D model of the same canine stifle joint after manual segmentation of the MRI scans (d) with keynotes (e).

3.8. Canine Stifle Joint Finite Element Model Stability Analysis

As illustrated in Figure 3.21, the movement of the femur relative to the tibia can be described by a set of three orthogonal axes (x, y and z) (Arnoczky, 1985). The x-axis passes through the femoral condyles parallel to the joint line in the medial-lateral directions (Arnoczky, 1985). The y-axis is parallel to the shaft of the tibia and passes through the medial tibial condyle, and the z-axis passes through the centre of the stifle space in a craniocaudal orientation (Arnoczky, 1985). There are six degrees of freedom resulting from translation (xx, yy, and zz) and rotation (xy, xz and yz) along and about each axis. As described in Section 2.2.2, in the healthy canine stifle joint, there are different motions including flexion-extension, varus-valgus angulation, axial rotation, cranial-caudal translation, and these movements are guided by various ligaments (Table 3.2) (Arnoczky and Marshall, 1977; Vasseur and Arnoczky, 1981; Arnoczky, 1983; Arnoczky, 1985). Abnormal motion along the z-axis of Figure 3.21, such as the cranial drawer motion, indicates joint instability due to the CCL damage. Diagnostic tests for stifle stability such as clinical examinations of CCLD and CCLR are commonly performed by means of cranial "drawer" test (Harasen, 2002; Millis and Mankin, 2014; Biskup *et al.*, 2017). The cranial drawer test is performed by placing a thumb on the head of the fibula and with the index finger on the tibial tuberosity (Harasen, 2002; Millis and Mankin, 2014; Biskup *et al.*, 2017). The ability to move the tibia cranially with respect to the fixed femur is an indication of a CCLD or CCLR (Harasen, 2002; Millis and Mankin, 2014; Biskup *et al.*, 2017) (Figure 3.22).

In the current study, an FEM of canine stifle joint (Section 3.7) was used to assess cranial drawer motion, hence investigating joint stability in conjunction with the contribution of the PGs to the mechanical behaviour of the CCLs. FEMs of the stifle joints were categorised into two cohorts, one being the control (n=5) and the other being the treatment (n=5) FEMs. The material parameters of the CCLs (control and treatment groups) obtained through inverse

analysis from Experimental Study II (Section 3.6). For the control FEMs the material parameters of CCL from the control group were used to define the CCL in the model, whereas for the treatment FEMs the material parameters of the CCLs from the treatment group were used to define the CCL in the model. Material parameters for the rest of the ligaments (CaCL, MCL and LCL) were based on the CCLs from the control group. To create cranial drawer motions in the FEMs, the femur was restrained from all translational and rotational displacements. The tibia and fibula were restrained from all motions except from the translational motions allowing the tibia and fibula to translate cranially in relation to the femur. The cranial translation of the tibia was achieved by applying a 10N load to the end of the tibia and fibula bones. Displacement of the tibia was monitored through a node (Node ID: 49362) at the end of the tibia while the load was applied incrementally (Section 4.7). Subsequently, load-displacement curves for the control (n=5) and treatment (n=5) FEMs obtained to compare the effect of PG depletion in the CCLs on the stability of the whole canine stifle joint. For the graphical presentation, displacements from the control and treatment FEMs were compared at their corresponding loads and the difference between the two groups was scaled up for graphical purposes using Equation 3.16.

$$U_{Treatment} = U_{Control} + (U_{Treatment} - U_{Control}) \times 100 \qquad \text{Equation 3.16}$$

where $U_{Treatment}$ is an average displacement at a given load obtained from the treatment FEMs and $U_{Control}$ is an average displacement at a given load obtained from the control FEMs.

Sensitivity analysis was carried out to determine how different values of independent variables such as the hyperelastic material parameters (alpha and mu) impact the dependent variable such as displacement under a given set of assumptions (Equation 3.14). In this study, the two material parameters were changed systematically to test the sensitivity of the FEM of the stifle

joint. It is expected that change in material parameters of the CCL would lead to change in FEM response which is studied through cranial drawer displacement, hence proving a numerical model sensitive to input parameters. A parametric study was developed to systematically alter the values of the material parameters as shown in Table 3.3. The values of μ and α of CCL1 (Table 4.4) was used as a benchmark for the sensitivity study. Subsequently, percentage differences in cranial drawer displacements were calculated and graphically presented between the benchmarked FEM and FEMs with changed material characteristics.

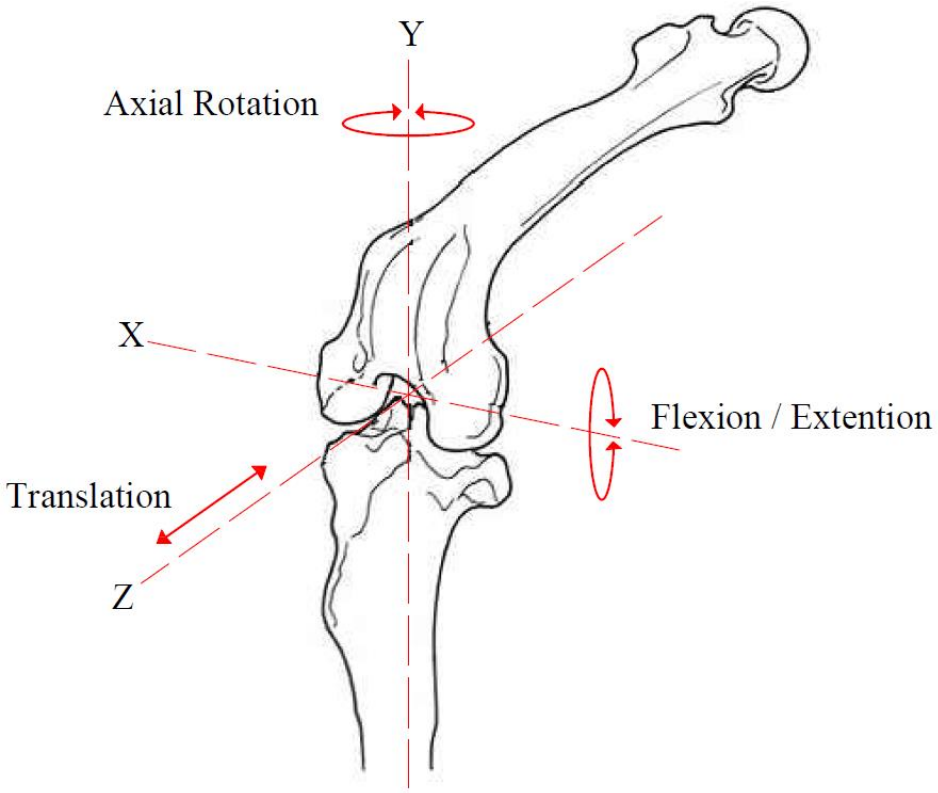

Figure 3.21: Schematic drawing of the canine stifle joint showing the axes of motion (x, y and z) and their directions. Redrawn from Arnoczky (1985).

Table 3.2: Individual motions on or about a specific axis present in the normal canine stifle which are guided by various ligamentous constraints (Arnoczky, 1985).

Stifle Motions	x-axis	y-axis	z-axis
Rotation	Normal flexion and extension of the stifle	Prohibited by the collateral ligaments and limited by the cruciate ligaments	Varus and valgus angulation prohibited by the collateral ligaments
Translation	Prohibited by cruciate and collateral ligaments	Prohibited by the cruciate and collateral ligaments in tension and articular cartilage and menisci in compression	Drawer movement prohibited by the cruciate ligaments

Figure 3.22: An image showing clinical assessment of a stifle laxity by palpation for cranial drawer motion. The red arrow indicates the cranial drawer motion. There should be small or no cranial drawer motion in healthy mature canines. Taken from Millis and Mankin (2014).

Table 3.3: Table showing the arrangement of the parametric study developed and carried out to investigate sensitivity of the stifle joint FEM.

	Benchmark	Study 1	Study 2	Study 3	Study 4	Study 5	Study 6	Study 7	Study 8
α		Increase by 10%	Increase by 50%	Decrease by 10%	Decrease by 50%	No change	No change	No change	No change
	20.3636	22.4000	30.5454	18.3272	10.1818	20.3636	20.3636	20.3636	20.3636
μ		No change	No change	No change	No change	Increase by 10%	Increase by 50%	Decrease by 10%	Decrease by 50%
	2.5756	2.5756	2.5756	2.5756	2.5756	2.8332	3.8634	2.3180	1.2878

3.8.1. Statistical Analysis

Statistical study on the sensitivity analysis was performed to identify the significant difference in the mechanical responses of the stifle joint FEM when the material properties of the model were altered. Cranial drawer displacements obtained from the sensitivity study compared for statistical differences using a two-tailed t-Test in Microsoft Office Excel (Microsoft Office, Version 2016, US) and $p<0.05$ was an indication of statistical significance.

4. Experimental Results

4.1. Introduction

This Chapter presents results obtained during the three previously listed experimental studies (Chapter 3) performed to test the hypothesis that PGs in the canine CCL contribute to the structural integrity of the ligament. Altering PG content could lead to a microstructural change in the tissue, predisposing the ligament to non-contact CCLD and eventual CCLR which will result in stifle joint OA (Comerford *et al.*, 2005). The first Section of this Chapter presents the results (age and bodyweight of the canine cadavers from which the CCLs were obtained). It also details the geometrical parameters, such as length and CSA, of the CCLs and their variations. Furthermore, results for statistical analysis on the variation of these geometrical measurements are detailed in this Section. This Chapter presents stress-strain, tangent modulus-stress and hysteresis graphs for Experimental Study I and II.

In Experimental Study II, where the CCLs were treated with ChABC enzyme to deplete PG content, quantification of water and sGAG contents were performed and the results for these measurements are presented within this Chapter. Experimental Study II also describes creep and stress relaxation behaviour for the CCLs with and without ChABC enzyme treatment. In this experimental study, CCLs treated with ChABC enzyme are referred to 'the treatment group' and CCLs without enzyme treatment are referred to 'the control group'. On the graphical presentations of the data with Experimental Study II, the word 'Depleted' is referring to CCLs in the treatment group whereas 'Control' is referring to CCLs in the control group.

This Chapter also presents results obtained from the numerical analysis of the CCLs with the aid of inverse analysis as well as numerical models of a whole canine stifle joint.

4.2. Sample Preparation

All the cadaveric samples collected in this research were disease canine free stifle joints from skeletally mature (2 to 3 years old) Staffordshire bull terriers. As mentioned in Section 3.2, full ethical permission to use these donated canine stifle joints in clinical research was granted by the School of Veterinary Science Research Ethics Committee (RETH000553 and VREC65).

4.2.1. Experimental Study I: Tensile behaviour of CCLs at slow strain rates

The first set of samples (n=5 paired stifle joints), used for tensile tests, were of mixed gender (female=3, male=2) and had a bodyweight of 21.46 ± 3.75kg with body condition scores of 3.5 ± 0.94.

4.2.2. Experimental Study II: Contribution of PGs to the viscoelastic behaviour of CCLs

The second set of samples (n=5 paired stifle joints), collected to investigate the contribution of PGs to the viscoelastic behaviour of the CCL as well as to develop the FEM of the CCLs using the DIC method (Section 3.3.6), were of mixed gender (female= 1, male=4) and had a bodyweight of 25.49 ± 1.80kg with body condition scores of 4.30 ± 1.92.

4.2.3. Experimental Study III: Canine stifle joint finite element model development

The paired canine stifle joint collected for this study was male and had a bodyweight of 25.96kg with body condition scores of 4.0. Resolution of scale was ± 0.01kg and accuracy in the body condition measurement was ± 0.5.

4.3. Experimental Setup

4.3.1. Geometrical Measurements of CCLs

4.3.1.1. Length

As detailed in Section 3.3.1.1, the lengths of CCLs in Experimental Study I and II were measured at the cranial, caudal, medial and lateral planes (Table 4.1 and Table 4.2) and the mean length values at these planes were used in the calculations of the material properties of the CCLs. The ANOVA test for all the studies showed statistically significant results ($p<0.05$) in measuring CCL length at different plane views. The post-hoc results showed significant differences ($p<0.05$) between cranial and caudal, cranial and lateral, and caudal and medial planes (Appendix (6): Table 1).

Table 4.1: Length of CCLs (mm) at different measurement planes for Experimental Study I.

CCL Number	**Cranial Plane**		**Caudal Plane**		**Medial Plane**		**Lateral Plane**		**Average**		**SD**	
	Right	**Left**	**Right**	**Left**	**Right**	**Left**	**Right**	**Left**	**Right**	**Left**	**Right**	**Left**
1	13.51	14.54	7.88	8.16	11.76	14.10	11.00	12.31	11.04	12.28	±2.35	±2.91
2	22.79	22.07	11.20	12.00	17.00	13.1	20.54	16.93	17.88	16.03	±5.05	±4.55
3	21.44	23.16	13.53	11.55	17.51	19.05	16.05	14.37	17.13	17.033	±3.31	±5.12
4	17.88	18.58	10.37	13.02	13.94	15.12	16.51	16.82	14.68	15.89	±3.30	±2.38
5	15.30	17.83	9.20	9.38	13.50	15.81	13.1	12.31	12.78	13.83	±2.57	±3.74
Mean ± SD	**18.71 ± 3.54**		**10.63 ± 1.96**		**15.09 ± 2.25**		**14.99 ± 2.90**		**14.86 ± 2.31**		-	

Table 4.2: Length of CCLs (mm) at different measurement planes for Experimental Study II.

CCL Number	Cranial Plane		Caudal Plane		Medial Plane		Lateral Plane		Average		SD	
	Right	**Left**	**Right**	**Left**	**Right**	**Left**	**Right**	**Left**	**Right**	**Left**	**Right**	**Left**
1	23.86	21.97	9.07	10.80	17.63	18.54	17.74	16.08	17.08	16.85	±6.08	±4.70
2	20.51	21.88	11.31	13.76	13.60	16.85	15.61	18.18	15.26	17.67	±3.92	±3.36
3	20.04	19.76	10.92	11.3	18.72	15.44	13.66	16.83	15.84	15.83	±4.28	±3.52
4	23.96	21.92	13.19	14.38	19.29	15.61	20.57	16.29	19.25	17.05	±4.50	±3.34
5	20.71	22.45	11.27	11.52	11.88	15.52	14.47	18.04	14.58	16.88	±4.31	±4.58
Mean ± SD	**21.71 ± 1.47**		**11.75 ± 1.58**		**16.31 ± 2.37**		**16.75 ± 2.00**		**16.63 ± 1.32**		**-**	

4.3.1.2. Cross-sectional area (CSA)

CSAs from the CCLs in Experimental Study I were measured using the hanged and non-hanged methods (Section 3.3.1.2.1 and 3.3.1.2.2). However, only the non-hanged method was used to measure CSA in Experimental Study II because the non-hanged method was easy to follow and no statistically significant differences were found between the two methods (Section 3.3.1.2.1). The mean CSA values of the CCLs for the two experimental studies are presented in Table 4.3. The CSA of each individual CCL can be found in Appendix (6): Tables 2 and 3.

CSA measurements in Experimental Study I showed a small difference in the measurements of the CCLs between the hanged and non-hanged methods. For example, the average CSA value obtained through the non-hanged method was 9.48% smaller than CSA value in the hanged method. However, statistical analysis confirmed that there was not any significant difference between the two methods ($p=0.42$).

Similarly, average CSA value for CCLs in the control group was 16.79% smaller than CSA value in the treatment group. However, there were no statistically significant differences between the two groups ($p=0.298$) (Appendix (6): Table 3).

Table 4.3: The mean CSA values (mm^2) of the CCLs obtained in Experimental Study I and II.

CSA measurement method (mm^2)	Experimental Study I	Experimental Study II
Non-hanged	15.30 ± 3.09	23.50 ± 5.23
Hanged	16.75 ± 4.58	-

4.3.2. Biochemical Assays on Experimental Study II

4.3.2.1. Water content

Water content for CCLs in the control and the treatment groups were calculated (Section 3.3.2.1) and it was found to be 73.85 ± 2.17% for the control and 70.03 ± 2.93% for the treatment groups. The range in water content in the control group was tighter (72-77%) when compared to the range for the treatment group (66-73%). The water content in the treatment group was approximately 5.2% less when compared to the control group and this was statistically significant ($p=0.048$) (Appendix (7): Table 1 and Figure 1).

4.3.2.2. Sulphated glycosaminoglycans assay

sGAG content of the CCLs in the treatment group measured as a percentage of dry weight (Section 3.3.2.2) which ranged from 1.71 to 4.70% (average 2.93 ± 1.19), whereas the range was 2.15 to 6.58% (average 3.71 ± 1.81) in the control group. Hence, approximately 21.11 ± 0.15% of the sGAGs was depleted in the treatment group. Despite the differences in the sGAG content between the control and the treatment groups no statistically significant differences were found ($p=0.45$) (Appendix (7): Table 1 and Figure 2).

4.3.3. Uniaxial Tensile Tests

4.3.3.1. Experimental Study I: Tensile behaviour of CCLs at slow strain rates

4.3.3.1.1. Stress-strain

The loading (Figure 4.1 (a and c)) and unloading (Figure 4.1 (b and d)) stress-strain curves at 0.1, 1 and 10%/min strain rates conformed to the typical J-shaped non-linear behaviour as expected in ligament tissue (Haut and Little, 1969), for all five CCLs and for both testing protocols (ascending and descending tests). The loading and unloading stress-strain curves illustrated an exponential growth with increasing strain level, and a more pronounced stiffness was observed with increasing strain rates.

During the ascending testing protocol, the stress resulting from a 0.03mm/mm strain (approximately where the transition region from non-linear to linear stress-strain curves occurred) increased by 26.5 ± 0.11% at 1%/min and 35 ± 0.12% at 10%/min when compared to stress generated by the same amount of strain at 0.1%/min. Similarly, the stress-strain curves at lower (<0.03mm/mm) and higher (>0.03mm/mm) strain levels showed a similar increase in stress with increasing strain rates (Figure 4.1 (a)).

During the descending testing protocol, the stress resulting from a 0.03mm/mm strain increased by 0.40 ± 0.35% at 1%/min and 3.80 ± 0.38% at 10%/min when compared to stress due to the same amount of strain at 0.1%/min. Similarly, the stress-strain curves at higher strain levels (>0.03mm/mm) produced a similar increase in stress with increasing strain rates. However, the lower strain levels (<0.03mm/mm) showed inconsistent results. For instance, at a 0.01mm/mm strain level the stress decreased by 4.7 ± 0.02% at 1%/min and 5.2 ± 0.03% at 10%/min when compared to stress at the same strain level at a 0.1%/min strain rate (Figure 4.1 (c)).

Stress-strain data collected from ascending and descending testing procedures demonstrated similar trend lines (Figure 4.2). The ascending stress-strain curves deviate from the descending curves at approximately 0.03mm/mm strain level. There were no significant differences between the two test protocols at 1%/min ($p=0.104$). However, stress-strain behaviour during the ascending tests was statistically different from the descending tests at 0.1%/min ($p=0.007$) and 10%/min ($p=0.020$).

The response of the CCLs to the tensile load at different strain rates presented statistically different behaviour in both ascending ($p=0.0001$) and descending tests ($p=0.0104$). The statistical tests showed statistically different stress-strain curves during ascending tests between 0.1 and 1%/min ($p=0.009$), 0.1 and 10%/min ($p=0.002$), 1 and 10%/min ($p=0.004$), whereas during descending tests the tensile response was statistically different only between 0.1 and 10%/min ($p=0.009$).

The transition strain indicating the non-linearity of the tensile behaviour increased with increasing strain rates (Figure 4.3). This increase in transition strain was observed in both the ascending and descending protocol with the change being more pronounced during ascending tests. The transition strain during ascending tests increased by 2.22 ± 0.06 % at 1%/min and 3.65 ± 0.06% at 10%/min when compared to transition strain at 0.1%/min, whereas the transition strain during descending tests only increased slightly by 0.94 ± 0.23% at 1%/min and 1.65 ± 0.23% at 10%/min when compared to transition strain at 0.1%/min. Statistical analysis showed no significant difference in the transitional strain between different strain rates, during ascending ($p=0.07$) and descending ($p=0.96$) tests. Similarly, values of the transitional strain were not statistically different between the ascending and descending tests ($p=0.48$).

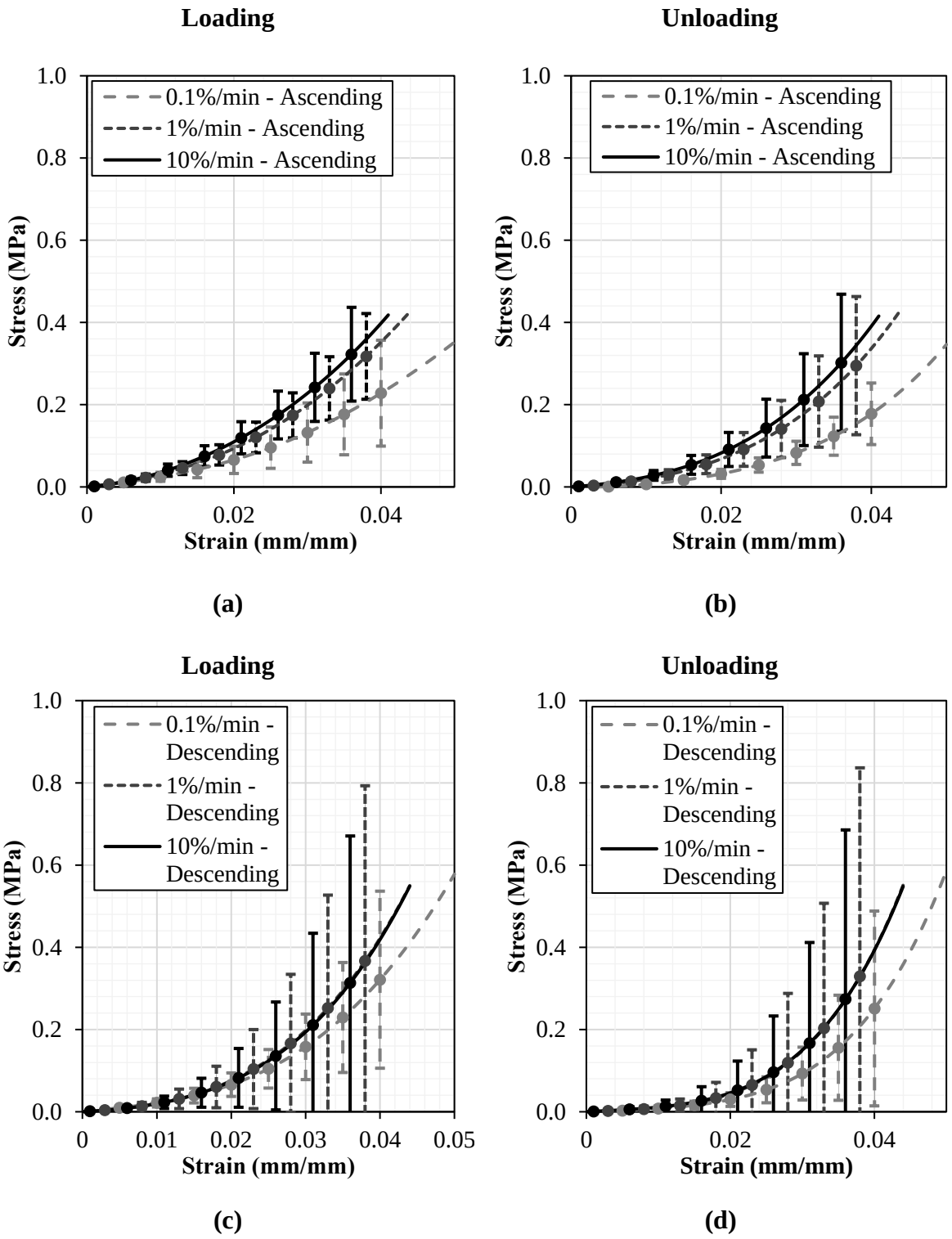

Figure 4.1: Average stress-strain curves for all the CCLs (n=5 pairs) during ascending (a and b) and descending tests (c and d). The stress-strain showed a stiffer behaviour during unloading (b and d) than during loading (a and c) which resulted in a considerable amount of hysteresis in the CCLs. Standard deviations represent sample variations.

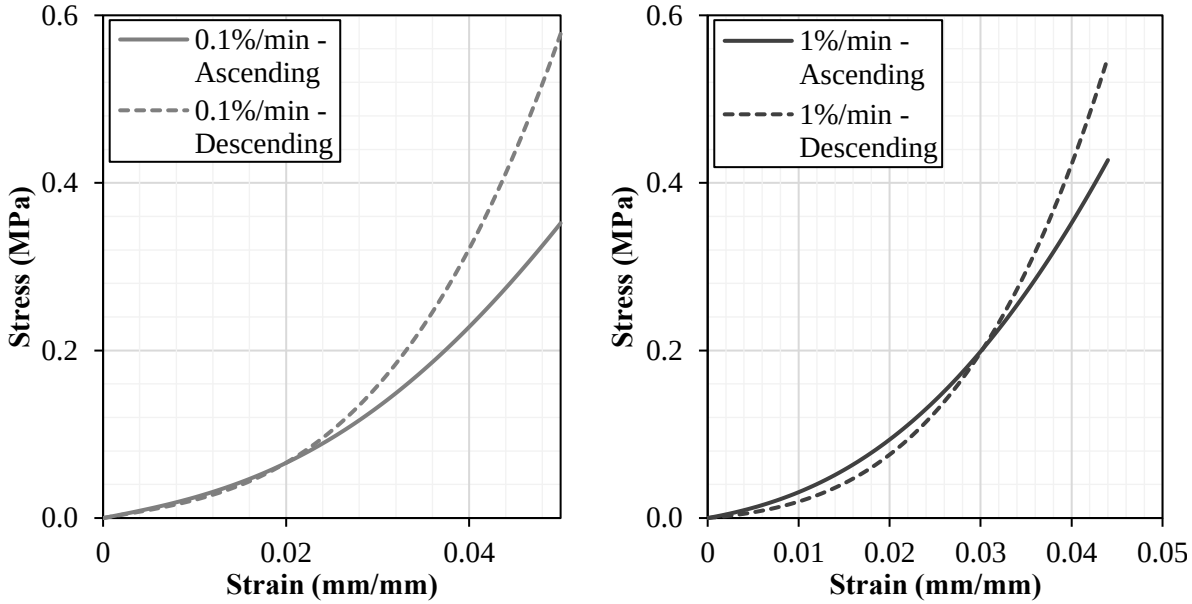

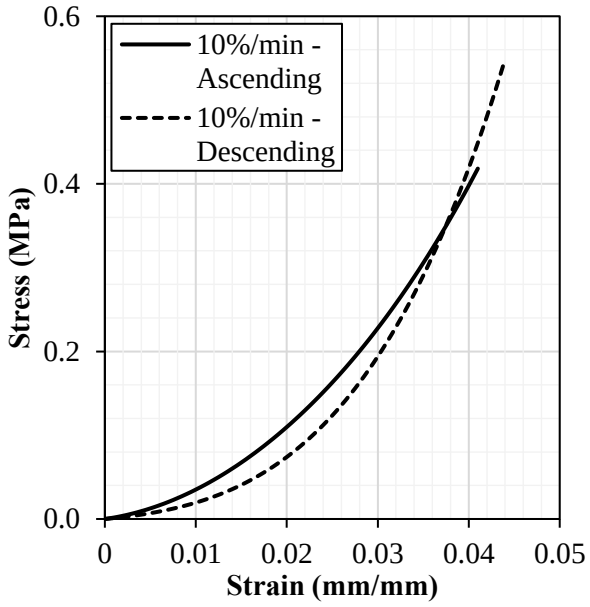

Figure 4.2: The comparison in average stress-strain behaviour upon loading of the CCLs (n=5 pairs) between the ascending and descending tests at 0.1%/min (a), 1%/min (b) and 10%/min (c) strain rates. Load-displacement behaviour for each individual specimen is presented in Appendix (8).

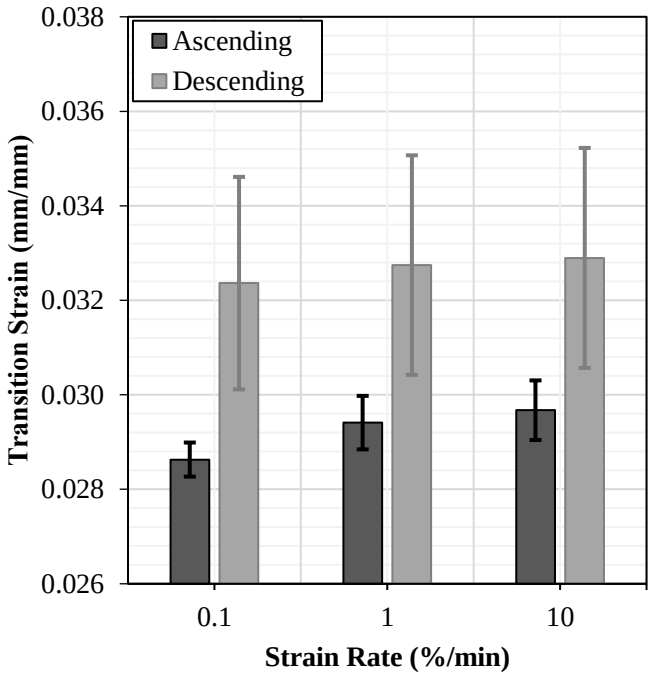

Figure 4.3: The transition strain values upon loading at different strain rates were used to compare the non-linear behaviour of the CCLs during the ascending and descending tests. Standard deviations represent sample variations.

4.3.3.1.2. Tangent modulus

Tangent modulus (E_t), indicating the stiffness behaviour of the CCLs, increased with increasing stress and strain rate (Figure 4.4 (a and b)) in both ascending and descending tests. This increase in tangent modulus with stress was evidenced during both loading and unloading. The increase in stiffness of the CCLs in ascending tests with increasing strain rates was different compared to the descending test, such that in descending tests there was inconsistency in tensile response below 0.15MPa. In addition, there were greater variations in the CCLs' responses to tensile loading during descending compared to ascending test protocols. However, statistical analysis showed no statistically significant difference in tangent modulus between the two protocols.

Tangent modulus-stress curves at 0.1, 1 and 10%/min strain rates were normalised by the tangent modulus-stress curve at 0.1%/min (Figure 4.4 (c and d)). The normalised tangent

modulus-stress curves (E_t / $E_{t\ (\dot{\varepsilon} = 0.1\%/min)}$) were plotted to describe the amount of increase in stiffness with increasing strain rates. The increase in stress from 0.2 to 0.5 MPa introduced stiffer behaviour by a factor of approximately 0.998 to 1.036 at 1%/min and 1.001 to 1.039 at 10%/min in ascending tests. However, the corresponding values in descending tests were a factor of approximately 1.001 to 1.039 at 1%/min and 1.005 to 1.066 at 10%/min (Figure 4.4 (c and d)). Stiffness behaviour of the CCLs during ascending and descending tests was statistically proven to be strain rate sensitive. The statistical difference was found between 0.1 and 1%/min strain rates ($p=0.021$ for ascending and $p=0.030$ for descending) and 0.1 and 10%/min ($p=0.005$ for ascending and $p=0.0002$ for descending). However, no statistically significant changes in tangent modulus curves were noted when comparing the stiffness curves at 1 and 10%/min ($p=0.667$ for ascending and $p=0.126$ for descending).

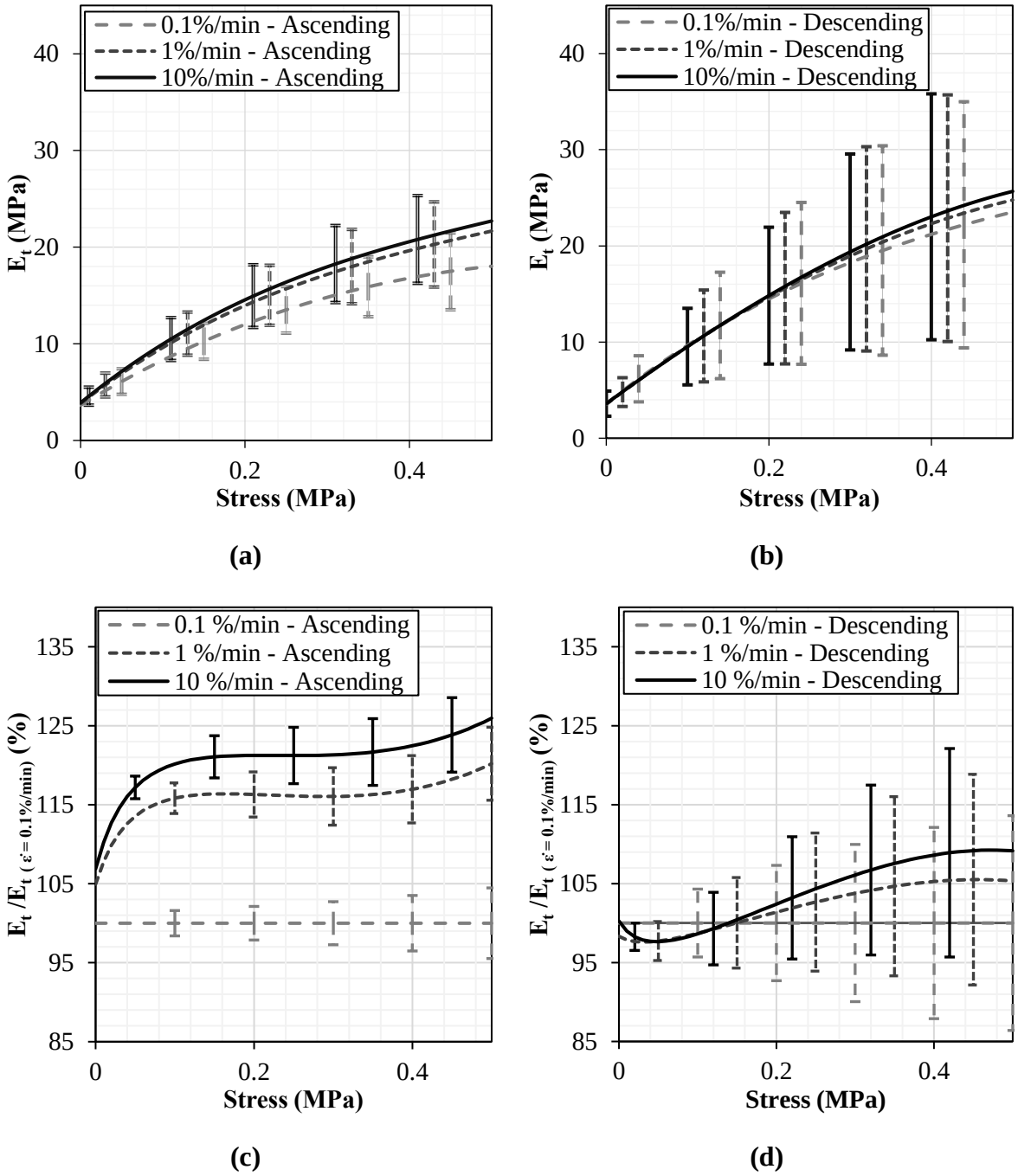

Figure 4.4: Average tangent modulus-stress behaviour of the CCLs during the ascending (a) and descending (b) uniaxial tests. Tangent modulus was normalised by the tangent modulus at 0.1%/min to indicate the percentile increase in stiffness during the ascending (c) and the descending (d) uniaxial testing protocols. Standard deviations represent sample variations.

4.3.3.1.3. Hysteresis

The viscoelastic effect of hysteresis was assessed during the ascending and descending test protocols (Figure 4.5). Increasing strain rate from 0.1 to 1 and then to 10%/min during the ascending test protocol and decreasing strain rates from 10 to 1 and then to 0.1%/min presented similar characteristics for hysteresis. The hysteresis, calculated from the area bounded between the loading and unloading stress-strain curves, was found to be smaller at higher strain rates compared to hysteresis at lower strain rates (Figure 4.5). This decrease in hysteresis with increasing strain rate was statistically significant between 0.1 and 1%/min ($p=0.030$), and 0.1 and 10%/min ($p=0.002$) in ascending tests, however, no statistically significant changes were found in hysteresis between 1 and 10%/min ($p=0.581$). In descending tests, hysteresis was not strain rate sensitive ($p=0.497$), and no statistical differences were found in hysteresis between ascending and descending tests ($p=0.077$). However, the correlation between hysteresis and strain rate in the descending tests was found to be higher with r=-0.99 for descending and r=-0.79 for ascending tests.

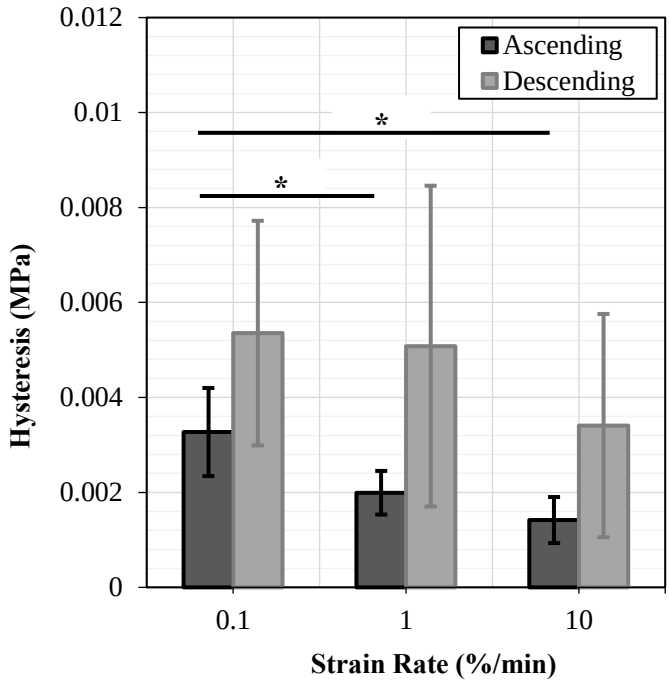

Figure 4.5: A bar chart showing the difference in hysteresis values of CCLs between ascending and descending uniaxial tests, at different strain rates, with * indicating statistically significant ($p<0.05$) differences in ligament behaviour. Standard deviations represent sample variations.

4.3.3.2. Experimental Study II: Contribution of PGs to the viscoelastic behaviour of CCLs

4.3.3.2.1. Stress-strain

The loading (Figure 4.6 (a and c)) and unloading (Figure 4.6 (b and d)) stress-strain curves in both the control and treatment groups followed similar patterns to each other and to the results in Experimental Study I, with an exponential growth in stress with increasing strain in the tissue. At an increasing strain rate, CCLs in both groups showed an increase in stress and this was indicative of greater stiffness in the CCLs under tensile loads at higher strain rates (Haut and Little, 1969).

The average stress-strain curves illustrated that the CCLs in the control group at 0.03 mm/mm strain (approximately where the transition region from non-linear to linear stress-strain curves

occurred) had higher stress values with a difference by approximately 49.8 ± 0.30% at 1%/min and 84.0 ± 0.42% at 10%/min compared to stress generated by the same amount of strain at 0.1%/min. Similarly, increasing stress behaviour was noted when the ligaments were strained by >0.03mm/mm (Figure 4.6 (a)).

An increase in strain from 0 to 0.03 mm/mm strain in the CCLs from the treatment group showed an increase in stress of approximately 11.8 ± 0.27% at 1%/min and 31.5 ± 0.35% at 10%/min when compared to stress at the same strain level during loading at 0.1%/min. Similar to the stress-strain curves in the control group, the stress was increased consistently with increasing strain up to 0.05mm/mm (Figure 4.6 (c)).

Despite some differences in the stress-strain behaviour, there were no statistically significant values in testing strain rate sensitivities for the CCLs in the control ($p= 0.359$) and the treatment ($p= 0.760$) groups (Figure 4.7). Similarly, no statistically significant difference was found between the control and the treatment groups in the stress-strain curves ($p= 0.725$). The spread of stress-strain curves of the CCLs, indicated by standard deviations (SD), was found to be greater in the treatment (maximum coefficient of variation (CV) = 0.96, 1.17, and 1.32 at 0.1, 1 and 10%/min respectively) when compared to the control (maximum CV= 0.68, 0.75, and 0.85 at 0.1, 1 and 10%/min respectively) groups (Figure 4.6).

The CCLs in both control and treatment groups showed an increase in the transition strain with increasing strain rates (Figure 4.8). The CCLs in the control group showed an increase in transition strain of approximately 3.36 ± 0.16% at 1%/min and 4.76 ± 0.17% at 10%/min compared to transition strain at 0.1%/min. Comparably, the increase in transition strain in the treatment group was approximately 6.46 ± 0.15% at 1%/min and 10.64 ± 0.15% at10%/min compared to transition strain at 0.1%/min. This increase of transition strain with strain rate was

not statistically significant ($p=0.366$ and $p=0.605$ for CCLs in the control and the treatment groups respectively).

In addition, some differences were noted between the control and the treatment groups in terms of the values of transition strain, for instance CCLs in the treatment group produced higher transition strain compared to CCLs in the control group. Despite the difference between the two groups, the statistical tests showed no statistically significant results ($p=0.576$).

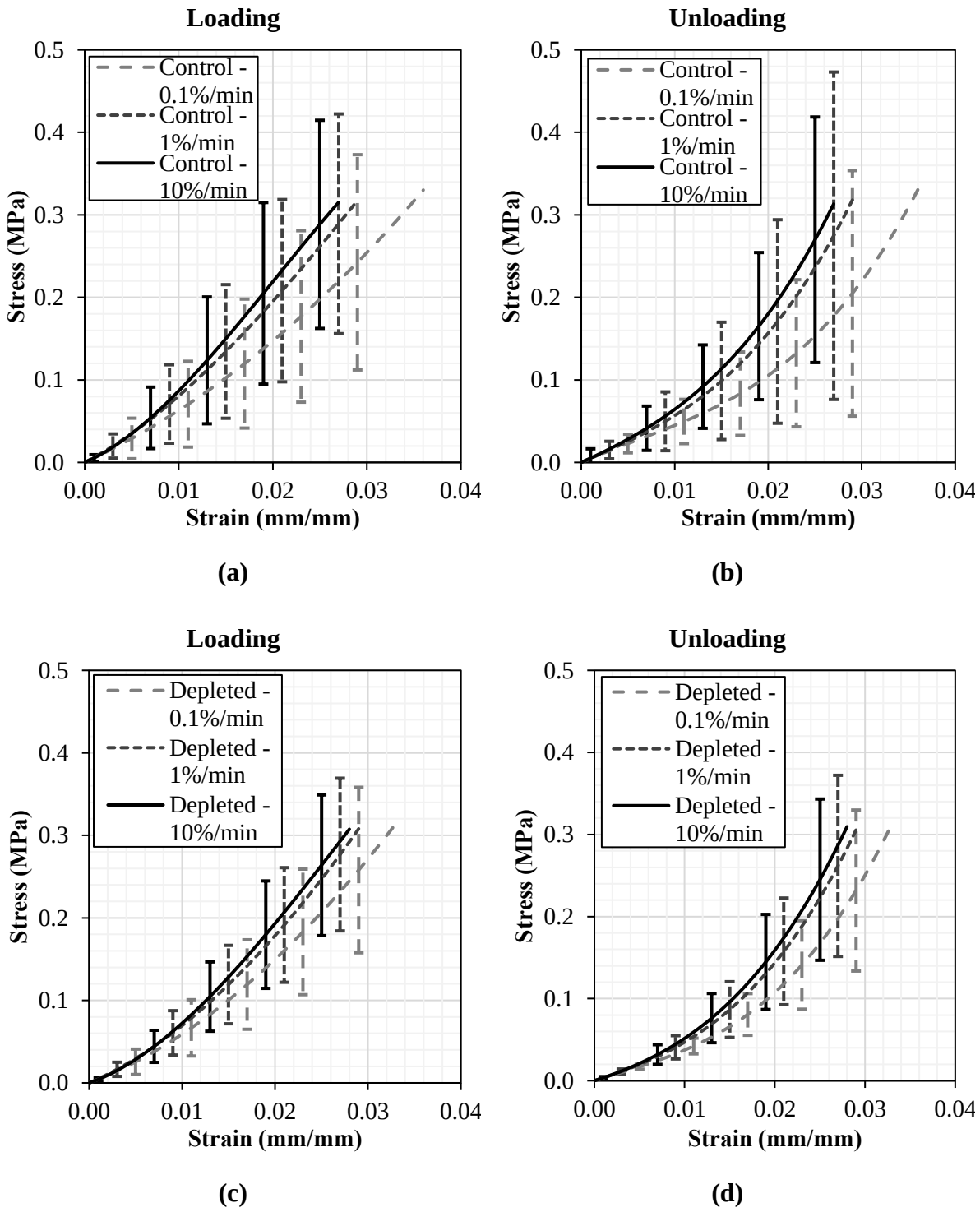

Figure 4.6: Average stress-strain values for the CCLs (n=5 pairs) in the control (a and b) and the treatment (c and d) groups. Similar to the results obtained from Experimental Study I, the stress-strain showed a stiffer behaviour during unloading (b and d) than during loading (a and c) which resulted in a considerable amount of hysteresis in the CCLs. Standard deviations represent sample variations.

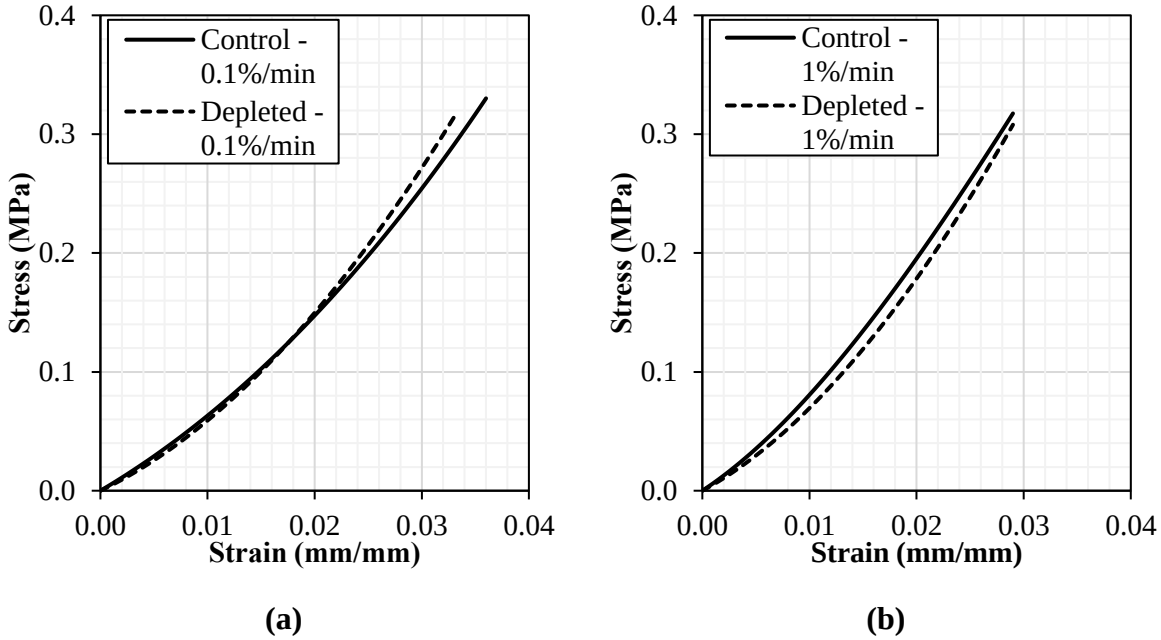

(a)

(b)

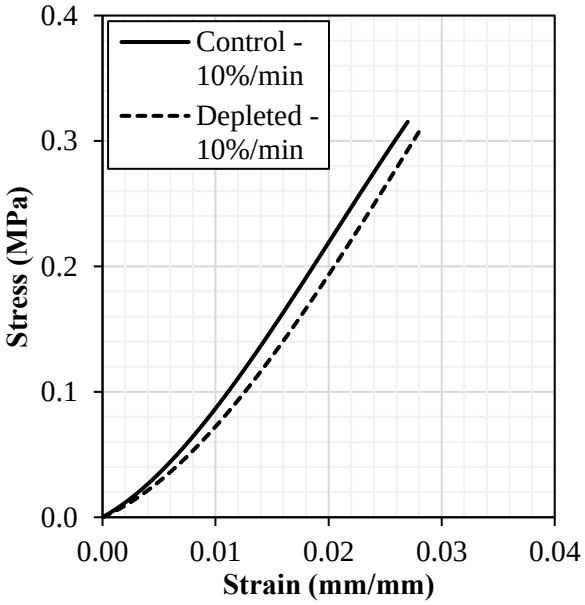

(c)

Figure 4.7: The comparison in average stress-strain behaviour upon loading between the CCLs (n=5 pairs) from the control and the treatment groups at 0.1%/min (a), 1%/min (b) and 10%/min (c) strain rates.

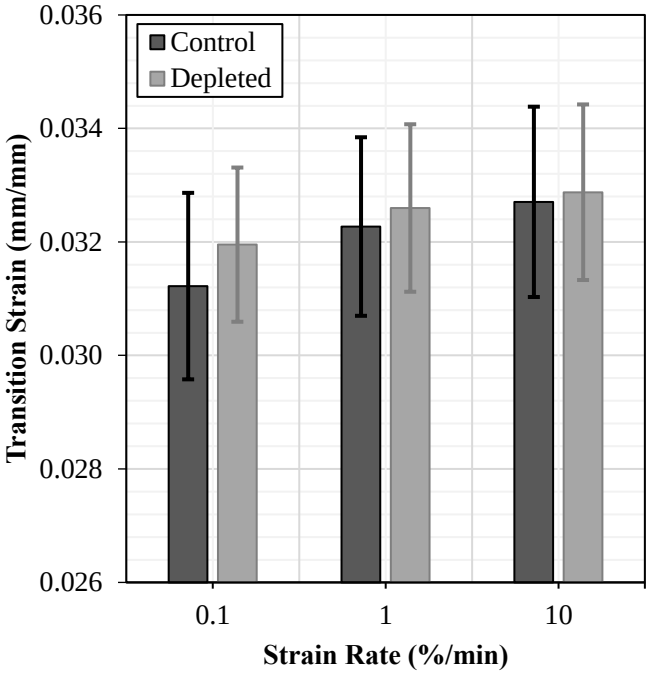

Figure 4.8: A chart showing different values of transition strain upon loading in the CCLs from the control and the treatment groups at different strain rates. Standard deviations represent sample variations.

4.3.3.2.2. Tangent modulus

Tangent modulus (E_t)-stress curves obtained for both groups (control and treatment) indicated an increase in stiffness with increasing stress and strain rates during loading and unloading tests (Figure 4.9 (a and b)). At 0.3MPa stress, the tangent modulus of the CCLs from the treatment group increased from approximately 21.3 to 23.5 and to 24.5MPa when strain rate increased from 0.1 to 1 and to 10%/min, and the corresponding tangent modulus from the control group increased by approximately 17.2 to 20.5 and to 22.0MPa. The study of sample variation for the stiffness curves showed a higher SD in the control CCLs by approximately 10%, with an average SD of 6.32 and 5.70MPa for CCLs in the control and the treatment groups respectively. However, the CV in stiffness behaviour for CCLs in the control (CV=0.34) and the treatment (CV=0.39) groups indicated an acceptable spread of data.

The normalised tangent modulus at 0.1, 1 and 10%/min strain rates provided a detailed description of change in stiffness in relation to that at the slowest strain rate (0.1%/min) for both control and treatment groups (Figure 4.9 (c and d)). The initial behaviour (stress<0.04MPa) of the normalised tangent modulus in the treatment group was not consistent, however the curves started to follow a consistent behaviour when the stress was gradually increased from 0.04 up to 0.5MPa. The normalised E_t at 0.3MPa increased by approximately 19.20 ± 5.76% at 1%/min and 27.83 ± 6.32% at 10%/min in the control group, whereas the corresponding values in the treatment group were approximately 10.34 ± 6.22% at 1%/min and 14.88 ± 6.44% at 10%/min (Figure 4.9 (c and d)). Despite the differences in normalised E_t curves, statistical analysis for E_t-stress curves showed no statistical differences with changing strain rates in the control (*p=0.48*) and the treatment (*p=0.72*) groups. Similarly, no statistical difference was observed in E_t-stress behaviours between CCLs in the control and the treatment groups (*p=0.74*).

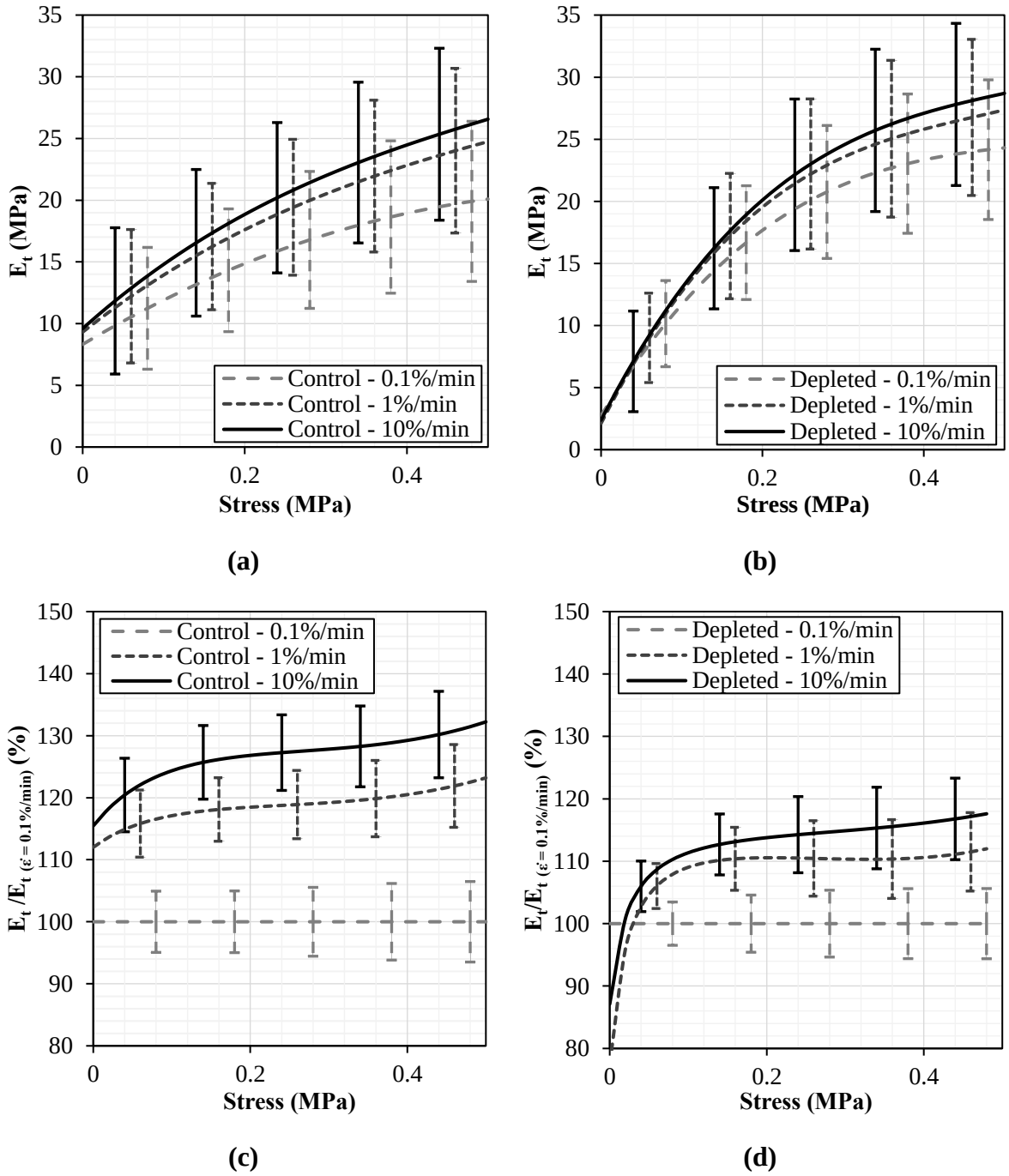

Figure 4.9: Average tangent modulus-stress behaviour of CCLs in the control (a) and the treatment (b) groups. Tangent modulus normalised by the tangent modulus (E_t/E_t) at 0.1%/min indicating change in stiffness in relation to stiffness at 0.1%/min of CCLs in the control (c) and the treatment (d) groups. Standard deviations represent sample variations.

4.3.3.2.3. Hysteresis

In this study, the effect of hysteresis was investigated during preconditioning as well as during the actual test on CCLs from the control and the treatment groups. CCLs in the control group showed a decrease in hysteresis with increasing preconditioning cycles (r=-0.85), but this decreasing behaviour was not observed in the treatment group (r=-0.04) (Figure 4.10 (a)). Despite the negative correlation in the control CCLs, the statistical study showed that hysteresis in the control and the treatment groups were not affected by the number of preconditioning cycles ($p=0.86$).

Both groups presented a decrease in the hysteresis value with increasing strain rate from 0.1 to 10%/min (Figure 4.10 (b)). Strong negative correlations between hysteresis and strain rate in the control (r=-0.976) and the treatment (r=-0.992) groups were observed. However, the change in hysteresis with strain rates was not significantly different in the control ($p=0.12$) and the treatment ($p=0.29$) groups. Moreover, no statistically different behaviours were observed in hysteresis between CCLs in the control and the treatment groups ($p=0.13$) (Figure 4.10 (b)).

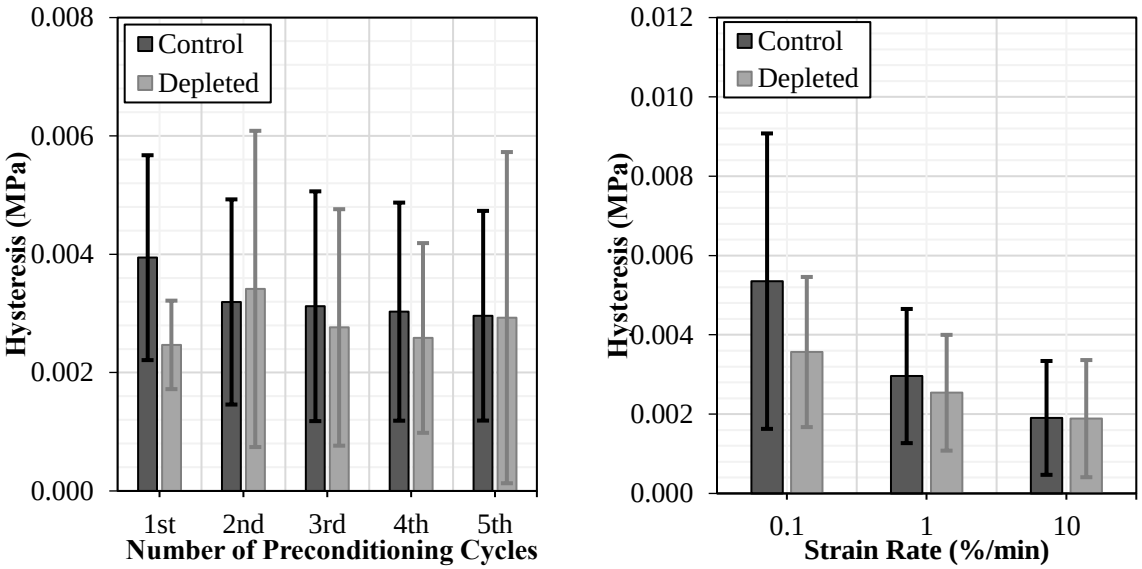

Figure 4.10: The graphs show the effect of hysteresis during preconditioning (a) and change in hysteresis with altering strain rates (b) in the control and the treatment groups. Standard deviations represent sample variations.

4.3.3.2.4. Creep

CCLs from the control and the treatment groups exposed to 9.9N during creep tests showed higher strain compared to when they were exposed to 4.9N for the same period of time (Figure 4.11 (a and b)). The strain-time curves, indicating creep rates, presented larger deformations in the control compared to the treatment groups, such that at approximately 316.2 s ($10^{2.5}$s) the CCL in the control group strained by 0.16 ± 0.09% at 4.9N and 0.22 ± 0.11% at 9.9N whereas the corresponding strain in the treatment group was approximately 0.10 ± 0.01% at 4.9N and 0.14 ± 0.01% at 9.9N. The overall behaviour of strain-time curves showed no significant difference in creep at 4.9 and 9.9N ($p=0.49$ for control and $p=0.17$ for treatment groups) and no statistically significant creep behaviour was found between the two groups ($p=0.34$). Further studies into the initial 20s and last 500s of creep rates presented statistically different outcomes in the control and the treatment groups (Figure 4.12 (a and b)). The difference between creep rate at the initial 20s and last 500s was greater in the treatment ($p=0.0007$) than

the control (*p=0.0047*) groups. The CV in creep behaviour for both groups showed a reliable spread of data (CV<1).

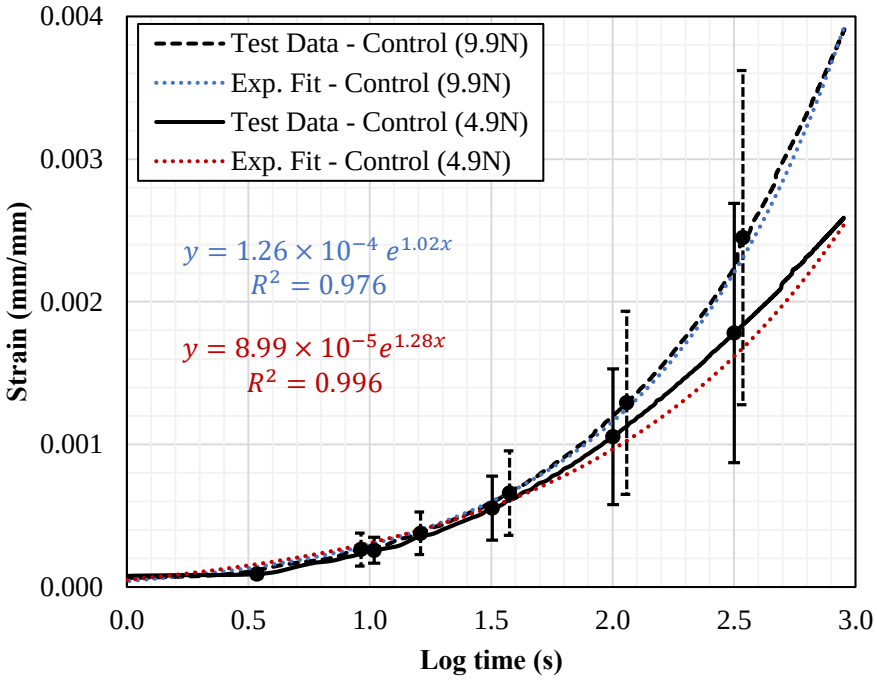

(a)

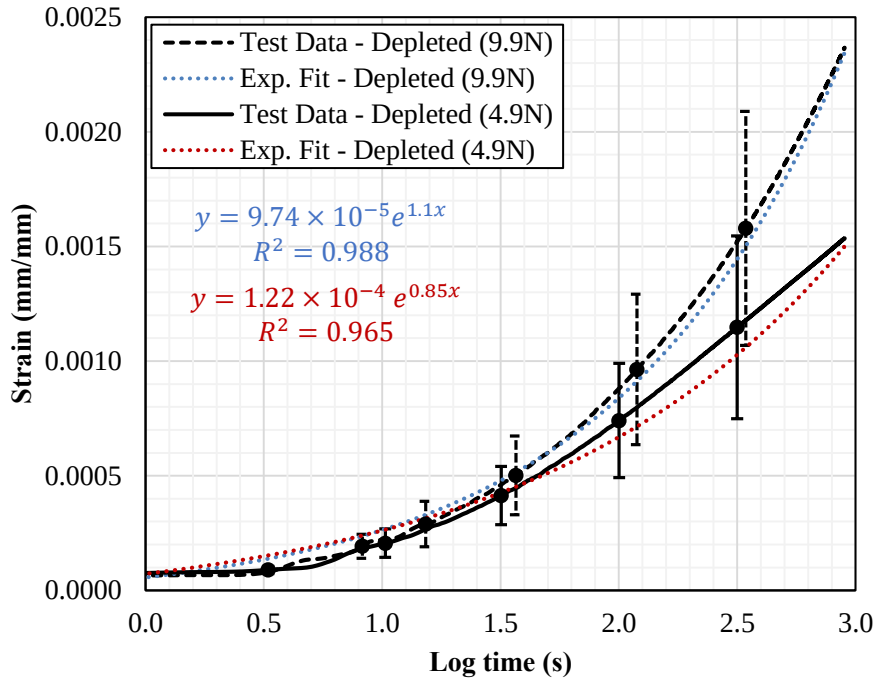

(b)

Figure 4.11: Exponential curves were fitted onto the average strain-time behaviour for the CCLs (n=5 pairs) in the control (a) and the treatment (b) groups. Standard deviations represent sample variations.

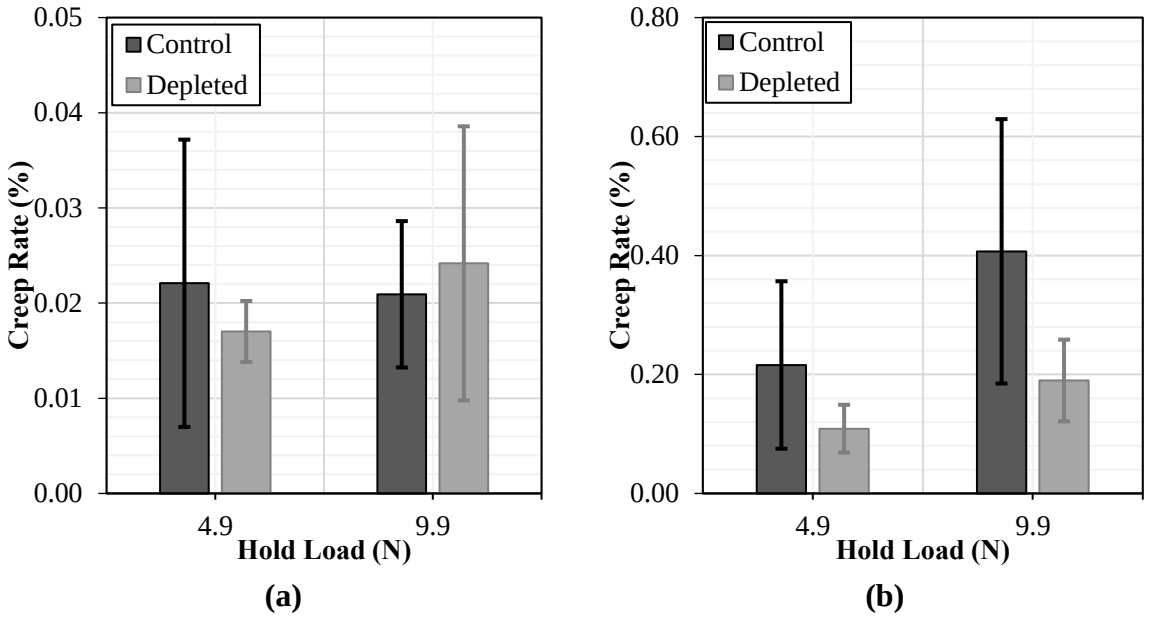

Figure 4.12: Creep rates were calculated at different loads during the initial 20s (a) and the last 500s (b) and found statistically significant differences between the initial and the last stages (*p=0.0047* in the control and *p=0.0007* in the treatment groups), however no statistically significant results were found between the control and the treatment groups. Standard deviations represent sample variations.

4.3.3.2.5. Stress relaxation

Reduced stress relaxation curves in the control and the treatment groups were very similar during the initial relaxation time; however, the curves started to behave differently after the initial 20s of relaxation (Figure 4.13 (a)). The overall shape of the relaxation-time curves for the control and the treatment groups were compared and no statistically significant differences were found within each group (*p=0.16*). Both groups, however, showed statistically different behaviour during the initial 20s and the last 500s. The difference in stress relaxation rate between the initial 20s and the last 500s was found to be more significant in the control (*p=0.00003*) than in the treatment (*p=0.00028*) groups. In the initial 20s the stress relaxation rate was higher in the control (1.14 ± 0.26%) than in the treatment (0.96 ± 0.14%) groups (*p=0.197*). In the last 500s, the stress relaxation rate was statistically higher by 2.52 ± 1.42% in the control compared to the treatment groups (*p=0.039*) (Figure 4.13 (b and c)).

Reduced relaxation data showed larger variation in the control (average CV=0.17 and SD=0.52) than in the treatment group (average CV=0.27 and SD=1.18), however this variation was found to be acceptable.

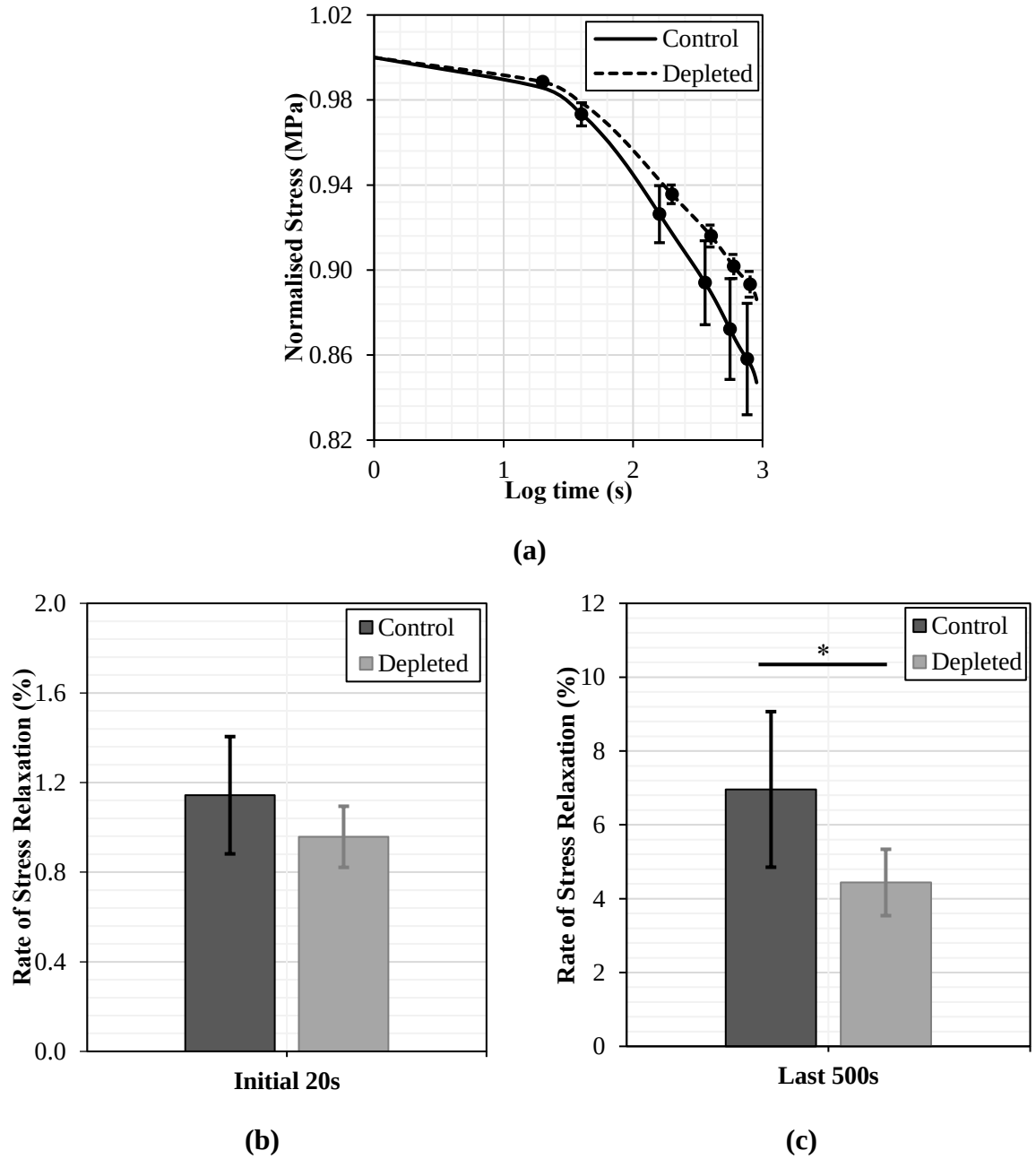

Figure 4.13: The graphs show the average stress relaxation curves for the CCLs (n=5 pairs) in the control and the treatment groups (a). The rate of stress relaxation in the initial 20s (b) and the last 500s (c) was found to be higher in the control than in the treatment groups. *Indicates statistically significant results ($p<0.05$). Standard deviations represent sample variations.

4.4. DIC Analysis

Load-deformation curves for the mid-substance of the CCLs from Experimental Study II, obtained digitally from the correlation of successive images during tensile tests (Section 3.4), presented similar non-linear behaviour obtained from the materials testing machine (Figure 4.14 (a and b)). As evidenced by the load-deformation target curves in Figure 4.14 (b), the CCLs in the control group showed greater stiffness than in the treatment group. For instance, the average deformations of all the CCLs in the control group were approximately 0.17 ± 0.08mm and 0.23 ± 0.10mm and the CCLs in the treatment group was approximately 0.19 ± 0.12mm and 0.25 ± 0.15mm at load of 3.3 and 5.5N respectively. However, the statistical analysis showed no significant differences between the two groups.

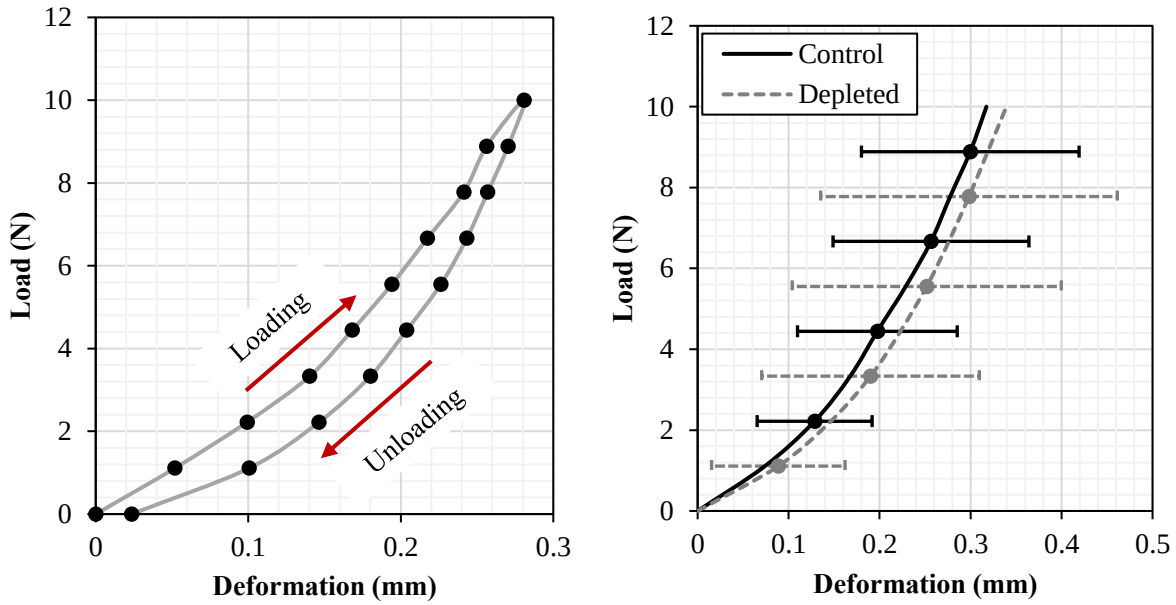

Figure 4.14: An example of a load–deformation curve for one CCL during loading and unloading generated from the three camera pairs (a). Average load-deformation curve of the CCLs (n=5 pairs) in the control and the treatment groups (b). Standard deviations represent sample variations. These curves are referred to as target curves because they are used as a convergence target in the FE inverse analysis.

4.5. Finite Element Model of CCLs

Development of FEMs of the canine CCLs were performed as described in Section 3.5.2. The transformation parameters, used during the surface matching processes (ICP method) to obtain a CCL-specific FEM, were improved by increasing the number of iterations. However, it was noted that after approximately 60 iterations the matching process could not reduce the RMS values any further (Figure 4.15). The overall accuracy of the transformation parameters was estimated as a percentage of the total surface area of the reference object and was found to be 0.039%. A total of ten FEM of the CCLs from Experimental Study II were generated (five of the CCLs from right for the control and five of the CCLs from left for the treatment groups) (Appendix (9)). These FEMs consisted of three parts, separating the middle region of the CCLs with tibia and femur bones at each end.

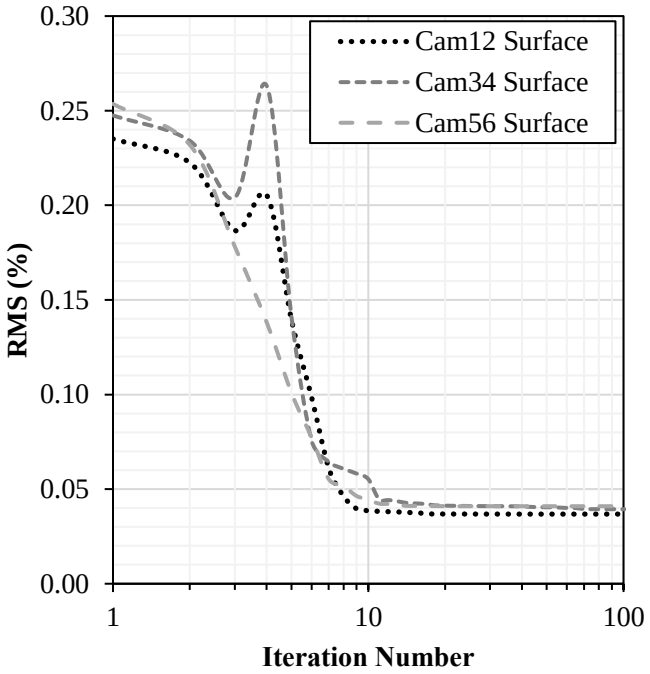

Figure 4.15: A graph illustrating the reduction in average RMS values with an increase in iteration numbers during the ICP optimisation process. SD showing sample variation was negligible ($<10^{-6}$).

4.6. Inverse Analysis

Parameters for the FEM presented in Section 4.5 were derived through inverse analysis (Section 3.6) to simultaneously represent characteristics of a hyperelastic material (**Error! Reference source not found.**). The error (RMS) for the inverse analysis simulation decreased when the number of iterations was increased (Figure 4.16 (a)) and all simulations reached an RMS of approximately <1.5% by the 50th iteration. Figure 4.16 (b) provides comparisons between characteristic experimental data and numerical simulations (predicted data). Similar to the experimental data, the characteristics of the numerical results for CCLs in the control group exhibited approximately 0.023 ± 0.088mm less deformation at 5.5N compared to the numerical behaviour of the CCLs in the treatment group. Moreover, the numerically obtained load-deformation data used to present CCL stress-strain behaviour, and the trends in the control group showed stiffer behaviour than in the treatment group which was in agreement with the experimental results from Experimental Study II (Figure 4.17).

Due to the specific and complex geometry of CCLs, hyperelastic parameters were derived individually through inverse analysis. Hence, the results illustrate a diverse map of von Mises stress between the CCLs (Appendix (10)).

Table 4.4: Numerical parameters derived from inverse analysis of the CCL-specific FEMs defining non-linear hyperelastic behaviour of the CCLs.

	Control group			**Treatment group**		
CCL No.	$\boldsymbol{\mu_1}$	$\boldsymbol{\alpha_1}$	**Error (%)**	$\boldsymbol{\mu_1}$	$\boldsymbol{\alpha_1}$	**Error (%)**
1	2.5756	20.3636	0. 64	0.9691	37.0120	0.72
2	0.2329	17.7154	1.11	0.7634	35.3546	0.89
3	0.8175	70.3163	0.53	1.4846	32.5953	1.30
4	0.6394	44.5159	0.67	0.3191	53.4824	0.31
5	0.0773	14.3079	0.76	0.0554	11.1211	0.75

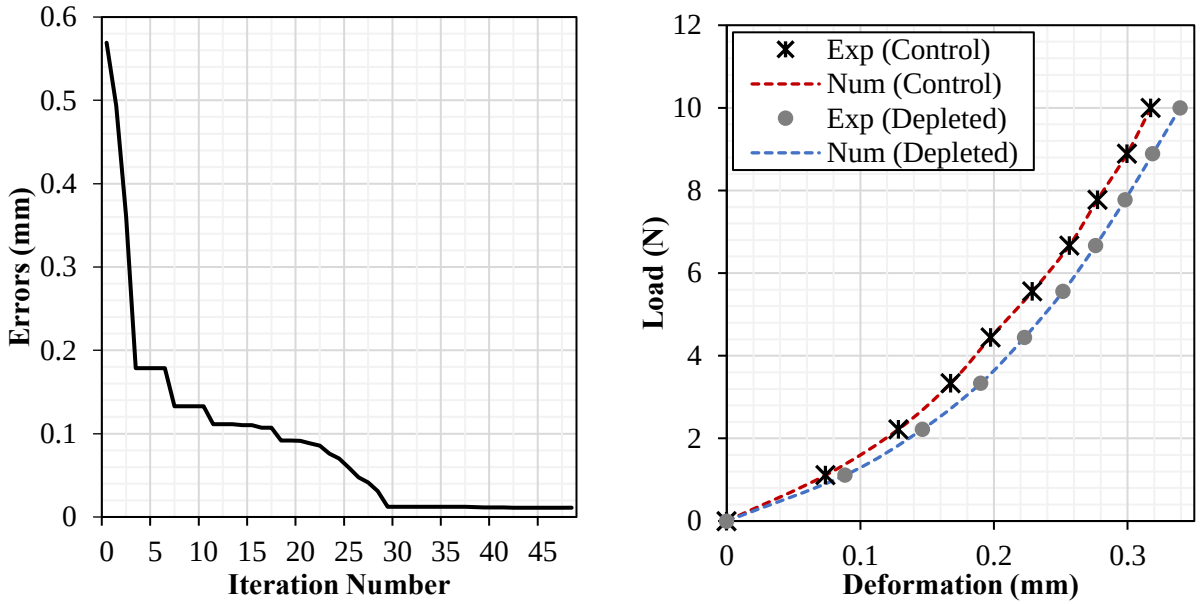

Figure 4.16 : A graph describing the reduction in errors with increasing iteration number (a). Average numerical (Num) and experimental (Exp) load-deformation curves for CCLs in the control and the treatment groups (b). For both experimental and numerical tests, SD showing sample variation was in the range of 0.04-0.11mm and 0.07-0.18mm in the control and the treatment groups respectively.

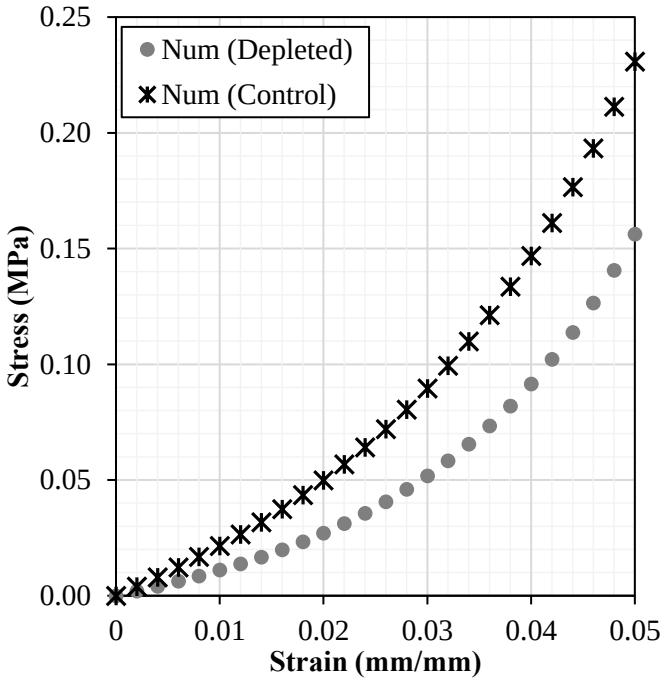

Figure 4.17: Stress-strain characteristics for CCLs in the control and the treatment groups calculated using the inverse FEM technique.

4.7. Canine Stifle Joint Finite Element Model Development

Following the method detailed in Section 3.7, a canine stifle joint FEM comprised of the femur, tibia, fibula, articular cartilage, menisci, and cranial ligament of the fibula head, MCL, LCL, CaCL and CCL was generated (Figure 4.18). The node and element numbers for the FEM were 90386 and 392089 respectively (Figure 4.19). The input file of the stifle FEM and its related analysis are presented in the attached DVDs.

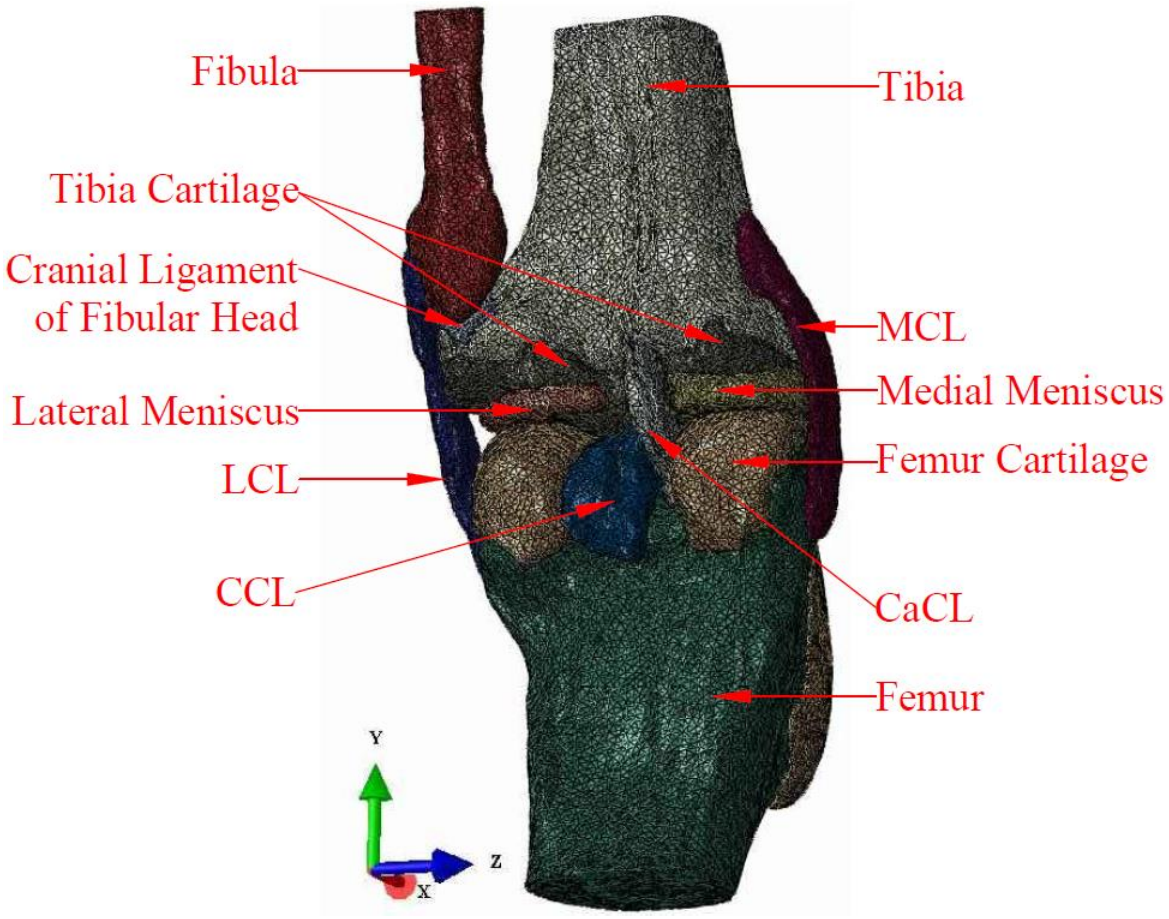

Figure 4.18: Finite element model of a canine stifle joint, indicating the major components of the joint.

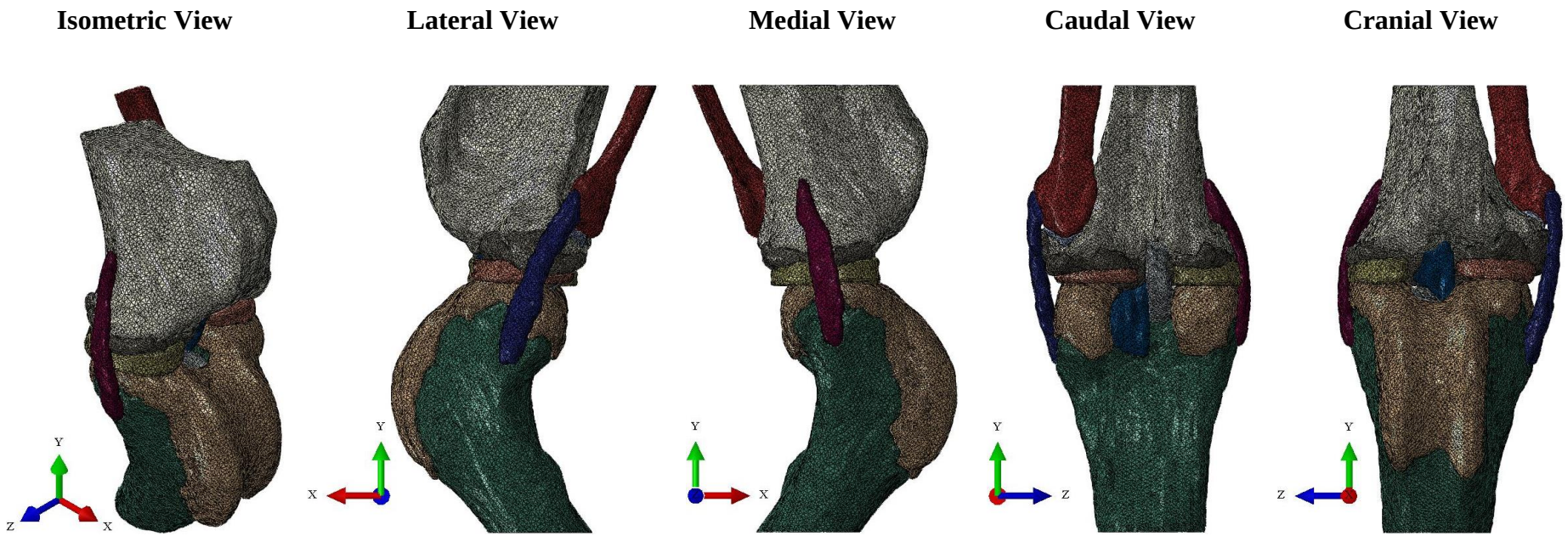

Figure 4.19: An FEM of the canine stifle joint including femur, tibia, fibula, articular cartilage, menisci, and cranial ligament of the fibula head, MCL, LCL, CaCL and CCL from different views.

4.8. Canine Stifle Joint Finite Element Model Stability Analysis

The FEM of the stifle joint (Figure 4.19) was used in numerical analysis (n=5 pairs of FEMs) to assess the joint stability by means of cranial drawer test (Section 3.8) (Attached DVDs). The displacements resulted from the cranial drawer tests in the numerical analysis were different for the control and the treatment FEMs. The control FEMs (FEMs with material parameters of the control CCLs (DVD – Control Group)) showed slightly lower displacement when compared to the treatment FEMs (FEMs with material parameters of the treatment CCLs (DVD – Treatment Group)) (Figure 4.20 (a and b)). However, this difference was small and not statistically significant ($p=0.56$) and therefore the graphical comparison was scaled up by a percentage difference between the two groups (Figure 4.20 (c)). For example, at 10N the corresponding average displacements were 0.1014 ± 0.0066mm and 0.1137 ± 0.0058mm in the control and the treatment FEMs respectively with the difference being 0.0123% (Figure 4.20 (c)).

Sensitivity analysis showed that the stifle joint FEM was responsive to altering material characteristics (μ and α) of the CCL, such that when the values of μ and α were changed statistically significant differences were observed in the cranial drawer displacement (Table 4.5). Cranial drawer displacement values obtained from the FEM with increased value of μ by 10% was statistically different from the displacement from the FEMs with increased value of μ by 50% ($p=4.25 \times 10^{-7}$), Figure 4.21 (a). Similarly, displacements from FEMs with decreased value of μ by 10% was statistically different from displacements from the FEMs with decreased value of μ by 50% ($p=5.27 \times 10^{-7}$), Figure 4.21 (b). However, no statistical difference was found when the value of α was changed from 10% to 50% (p=0.329), Figure 4.21 (c and d).

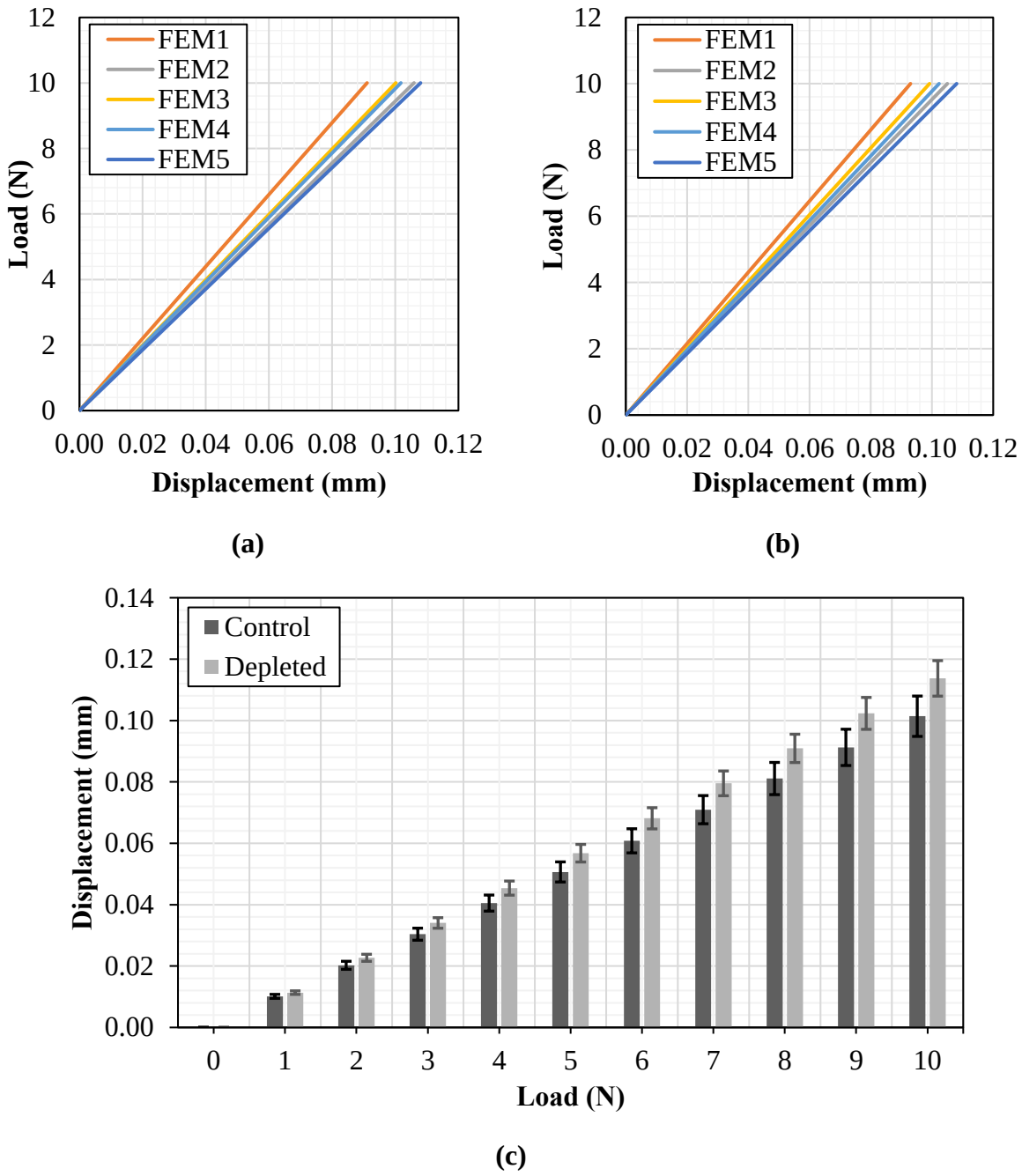

Figure 4.20: Load-displacement curves obtained from the numerical analysis for the control FEMs (a) and the treatment FEMs (b). The load and its corresponding displacement was averaged to compare behaviour of the FEMs with the control (n=5) and the treatment CCLs (n=5) (c). It was noted that cranial drawer displacements due to the applied loads were higher in the treatment compared to the control FEMs. Standard deviations represent sample variations.

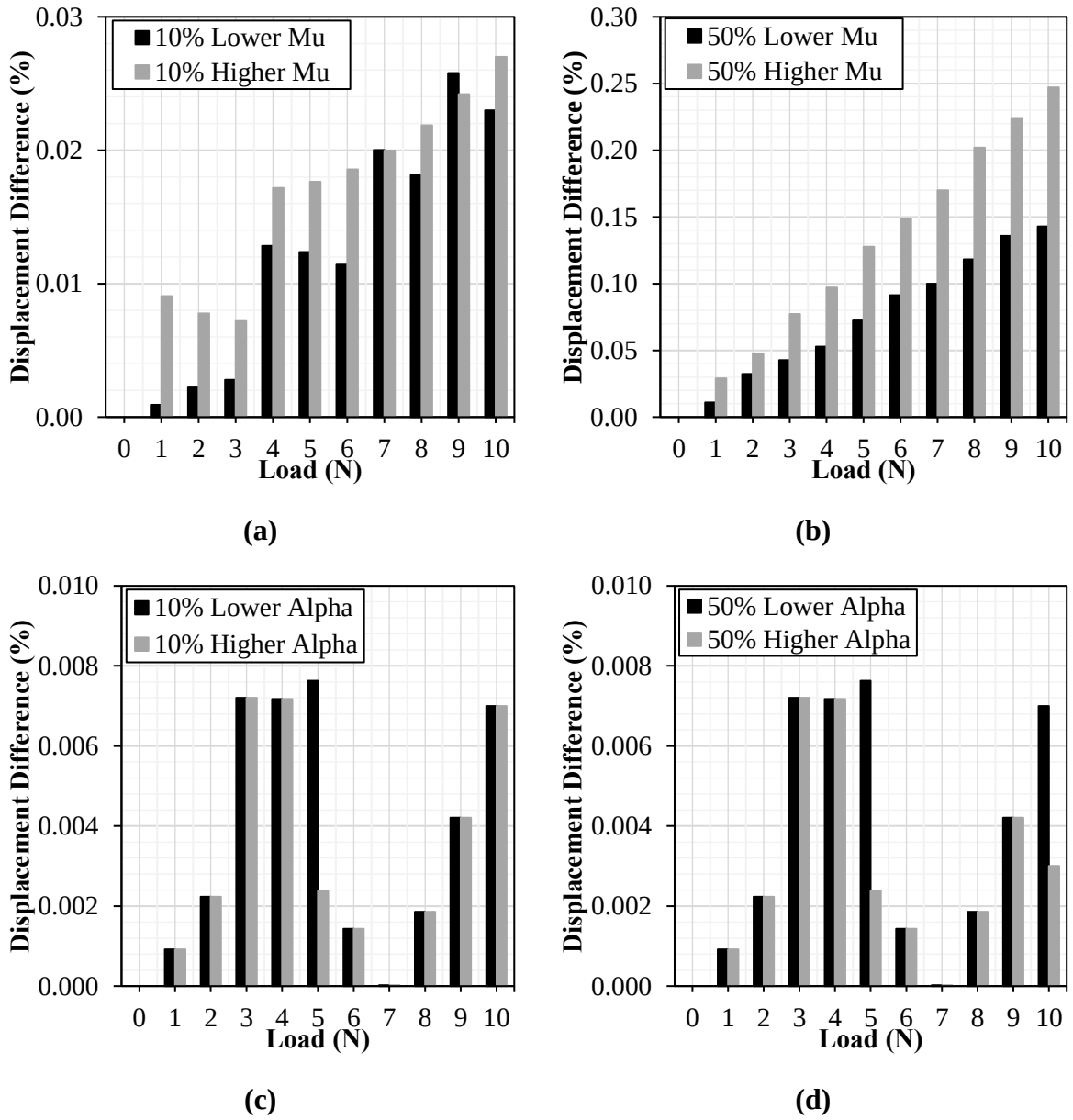

Figure 4.21: Sensitivity analysis results showing variation of percentage differences in cranial drawer displacement with changing mu (μ) by 10% (a) and 50% (b); changing alpha (α) by 10% (c) and 50% (d).

Table 4.5: Results obtained from the statistical analysis for the FEM sensitivity study.

	Changing material parameters by:	**P-value**
Alpha (α)	**10% increase**	4.00×10^{-3}
	10% decrease	1.00×10^{-3}
	50% increase	17.00×10^{-3}
	50% decrease	1.54×10^{-4}
Mu (μ)	**10% increase**	5.00×10^{-8}
	10% decrease	5.07×10^{-6}
	50% increase	2.99×10^{-7}
	50% decrease	6.18×10^{-7}

5. Discussion and Conclusions

5.1. Introduction

In this Chapter, the results presented in Chapter 4 regarding the tensile and viscoelastic behaviour of the canine CCL, the development of CCL-specific FEMs for inverse analysis and the development of a stifle FEM of the whole canine joint are discussed in further detail and with respect to previous findings reported in literature.

5.2. Overall Discussion

The aim of this doctorate research is to gain a greater understanding of a) the biomechanical behaviour of the canine CCLs at the toe-region of the stress-strain curves under slow strain rates, b) the contribution of PGs to the viscoelastic behaviour of the CCLs and c) the effect of PGs in the CCLs on the stability of the whole stifle joint. It is the hypothesis of this study that decreasing PG content in the CCLs would lead to a decrease in water binding molecules, hence less interfibrillar lubrication, thereby increasing interfibrillar friction and resulting in a stiffer behaviour of the ligaments. The findings in this study indicate that the hypothesis can be accepted. Detailed discussion on the experimental and numerical studies carried out to prove the hypothesis are described in the following subsections.

5.2.1. Experimental Study I: Tensile behaviour of CCLs at slow strain rates

Experimental Study I was carried out to investigate the viscoelastic properties of CCLs, such as stress-strain and hysteresis behaviour, from healthy canine stifle joints at slow strain rates (<10%/min) and to identify the best test arrangement for the subsequent experimental tests. The findings in Experimental Study I are the first to report the slow strain rate dependency of

the canine CCL across three orders of magnitude with ascending and descending test arrangements.

Haut and Little (1969) showed that with high strain rates, the toe region of stress-strain curves appears at lower strain levels; therefore, it was the objective of the current study to focus on the stress-strain behaviour at the toe-region (low strain level) and utilise slow strain rates (<10%/min) at different magnitudes such as 0.1, 1, and 10%/min. In the current study, the shape of the stress-strain curves follows a similar pattern to that found previously in biological tissues such as tendons and ligaments (Haut and Little, 1969; Pioletti *et al.*, 1999; Pioletti and Rakotomanana, 2000; Crisco *et al.*, 2002; Bonner *et al.*, 2015). The tensile response of the CCL during ascending and descending tests was found to be significantly different ($p<0.05$), such that during the descending tests the CCL behaved more stiffly and inconsistently at low strain level. This finding of a change in tissue behaviour with altering strain rate orders during tensile tests is not in agreement with the findings previously reported (Pioletti *et al.*, 1999; Pioletti and Rakotomanana, 2000). For example, Pioletti *et al.* (1999) loaded bovine ACLs up to 300N with seven different strain rates (6, 60, 300, 600, 1200, 1800 and 2400 %/min) and then tested for strain rate order by reloading the ACLs at the 6 and 300%/min strain rates. However, they found identical stress-strain behaviour for the initial and reloaded ACLs. It is important to note that these studies applied higher strain rates (6-2400%/min) than those used in the current study and they reloaded the tissue in an ascending strain rate order only (Pioletti *et al.*, 1999; Pioletti and Rakotomanana, 2000). Therefore, it is possible that the effect of the change in strain rate order is more pronounced at slow strain rates (<10%/min) because the unloaded fibrils go through the toe region and show intra-fibrillar gliding (Bonner *et al.*, 2015). However, at fast strain rates (>~300%/min) fibrils go from an unloaded state directly to intra-fibrillar gliding where the matrix bond between the collagen molecules are broken before the removal of collagen crimps (Bonner *et al.*, 2015). Moreover, the strain rate sensitivity of the CCLs was

more pronounced and statistically significant ($p<0.05$) during the ascending than the descending test procedure. Similarly, the increase in transition strain with strain rate, although not statistically significant, was higher in the ascending than the descending tests.

CCL stiffness (tangent modulus) during loading and unloading cycles in the ascending and descending test procedure increased with strain rate (Figure 4.4). Although the tangent modulus-stress curves were different in the ascending and descending tests, this difference was not statistically different (Figure 4.4). In both test procedures, the canine CCL was stiffer during unloading than loading cycles. This resulted in considerable hysteresis (energy dissipation) between the loading and unloading stress-strain curves (Figure 4.5). The stiffer behaviour results in less dissipated energy in the loading and unloading stress-strain curves and hence the magnitude of hysteresis decreased with increasing strain rates. This phenomenon was observed during both ascending and descending tests and the correlation between hysteresis and strain rate was found to be greater during descending tests. Hysteresis was found to be strain rate sensitive during the ascending test in each sample tested which reflects the findings of other authors (Haslach, 2005; Boyce *et al.*, 2007). During descending tests, the CCLs were not strain rate sensitive, and hysteresis was independent from strain rate. Previous studies have shown that if a soft tissue is insensitive to strain rate, the hysteresis is expected to be relatively uniform with respect to strain rates (Woo *et al.*, 1981). The CCL is a history and time dependent biological tissue; therefore, strain history might have caused different CCL behaviour during ascending and descending tests (Thornton *et al.*, 2007). However, recovery procedures reported in previous literature were followed in the current study, allowing adequate recovery time between loading and unloading cycles (Haut and Little, 1969; Lujan *et al.*, 2007; Lujan *et al.*, 2009). It is widely known that a higher strain rate results in the development of a high stress in ligaments (Haut and Little, 1969; Woo *et al.*, 1990c; Bonner *et al.*, 2015), hence a longer time might be needed to allow for the uncrimped collagen fibres to return to the crimped state.

However, a lower strain rate is likely to develop a lower stress in ligaments, hence a shorter time is required to allow for the uncrimped collagen fibres to go back to the normal state (Pioletti *et al.*, 1999). Therefore, it is possible for the CCL to behave in a similar fashion during both ascending and descending tests, given that a longer time is provided for tissue recovery from stresses caused by a higher than a lower strain rate.

Experimental Study I adds knowledge to the existing body of work on the viscoelastic behaviour of the canine CCLs at slow strain rate and laid a foundation for Experimental Study II by identifying the ascending test as an appropriate test arrangement to study viscoelastic behaviour of the canine CCLs.

5.2.2. Experimental Study II: Contribution of PGs to the viscoelastic behaviour of CCLs

Experimental Study II was carried out to investigate the non-linear viscoelastic behaviour of the canine CCLs after treatment with chondroitinase ABC enzyme to deplete PGs in the ligament. A combination of viscoelastic characterisation tests such as hysteresis, tangent modulus and strain rate sensitivity at three strain rates (0.1, 1 and 10%/min) as well as creep and stress relaxation were performed in combination with digital image correlation and inverse analysis.

The biomechanical behaviour of ligaments was closely associated with their macro- and microstructural tissue components (Benjamin and Ralphs, 1997; Lo *et al.*, 2002a; Hayashi *et al.*, 2003a; Hayashi *et al.*, 2003b; Frantz *et al.*, 2010). It was therefore the hypothesis of this study that altering the microstructure of the canine CCLs could lead to a change in the tensile and viscoelastic behaviour of the ligament. This study focused on investigating the contribution of PGs, which is a prominent microstructural component of CCL (approximately <3% of ligament's dry weight), to the viscoelastic behaviour of the CCLs (Hey *et al.*, 1990; Henninger *et al.*, 2010). It is believed that PGs dominate tissue response at the toe region when the collagen

fibres are crimped (Eshel and Lanir, 2001), therefore Experimental Study II tested the effect of PGs with slow strain rates. In Experimental Study II, despite following similar procedure as the preliminary study performed within our research group (Comerford et al., unpublished, 2012), the effect of incubating CCLs in chondroitinase ABC (ChABC) showed 21.11% PG depletion and this depletion was not statistically significant when compared with the control group.

It has been reported that protease-free ChABC product is not guaranteed to be protease-free though the contamination is low (Murienne *et al.*, 2015). A number of authors used non protease-free ChABC and did not find significant effects on the tissue's mechanical behaviour (Al Jamal *et al.*, 2001), compared to studies that used protease-free ChABC with protease inhibitors (Lujan *et al.*, 2009). In the current study, protease-free ChABC with protease inhibitor was used to deplete PGs in the CCLs, therefore the potential impurity in the ChABC did not degrade structural components of the ligaments. The different depletion outcome from Experimental Study II and the preliminary work (Comerford et al., unpublished, 2012) is still not fully understood. However, it is important to note that in the preliminary study femur-CCL-tibia complexes were not used during the PG depletion process, and only the CCLs (excluding the femur and tibia parts) were incubated in the enzyme treatment. Therefore, it is possible that the enzyme concentration adopted for depleting PGs in the femur-CCL-tibia complex might not have been as effective compared to only incubating the ligaments. Hence, this could be an explanation for having different PG depletion results in Experimental Study II and the preliminary study. Further research is required to study the factors affecting sGAGs digestion in canine femur-CCL-tibia complex using ChABC enzyme.

Despite the small amount of PG depletion in the CCLs, the results from Experimental Study II showed that CCLs from the control group had higher stress values than the treatment group

when strain rates increased from 0.1 to 1 and to 10%/min (Section 4.3.3.2.1). However, this difference between the two groups was not statistically significant. Furthermore, strain rate sensitivity, although not statistically significant, was more pronounced in the control than the treatment groups. The stress-strain behaviour reported by the control group (Figure 4.6 (a)) was different to that seen in Experimental Study I which showed that the CCLs were not strain rate sensitive and it may be that the recommended ChABC buffer required to be used with ChABC (20mM Tris pH 7.5, 150mM NaCl, 5mM $CaCl_2$) has resulted in microstructural changes such as tissue permeability. As presented in Figure 3.3, CCLs in the treatment group were incubated in liquid for a longer time compared to the control group, hence the swelling time is not comparable between the two groups. It has been reported that the buffer required to be used with ChABC treatment increases water content in scleral tissue (Murienne *et al.*, 2015). In addition, several authors have observed the reduction in strain rate sensitivity in PG depleted tissues (Elliott *et al.*, 2003; Robinson *et al.*, 2004) which is consistent with the findings in this study.

Transition strain was calculated to investigate the effect of PGs on the non-linearity of the tensile response during loading (Section 3.3.3). CCLs in the control and the treatment groups showed an increase in transition strain during loading (Figure 4.8). The transition strains were found to be higher in the treatment group, but the difference was not statistically significant. The normalised stiffness at 0.3MPa was lower, by 9% and 13% at 1%/min and 10%/min, ($p>0.05$), in the treatment than the control groups. There was an increase in transition strain in the treatment group which indicates an alteration in the tissue's crimp morphology after PGs depletion (Murienne *et al.*, 2015). This alteration also indicates that PGs provide connections between adjacent fibrils (Murienne *et al.*, 2015).

Similar to the hysteresis results in Experimental Study I, dissipated energy between the loading and unloading decreased stress-strain curves was decreasing with increasing strain rate (Section 4.3.3.2.3). However, unlike Experimental Study I, neither CCLs in the control or the treatment groups showed any dependencies between strain rate and hysteresis, nor was there any statistically significant difference in hysteresis between the two groups. In addition, it was found that dissipated energy in the control and the treatment groups was not affected by the number of preconditioning cycles. This phenomenon agrees with previous literature where decorin in human MCL was found to have no effect on the hysteresis of the tissue (Lujan *et al.*, 2007).

CCLs in the control and the treatment groups showed higher strain when exposed to higher load during the creep test (Section 4.3.3.2.4). There were no statistically significant values between creep rate and hold load, however, creep rate was statistically greater at the initial 20s than at the last 500s in both the treatment and the control groups. Creep rate was found to be higher in the control than the treatment groups, however, this behaviour was not statistically significant. Thornton *et al.* (2001) showed an increase in creep rate with increasing water content in rabbit MCLs. This study suggested that when more water is present in the tissue the resistance to creep is decreased because water provides a greater freedom for fibrillar movement (Thornton *et al.*, 2001). However, Murienne *et al.* (2015) associate the slower creep rate with increased interfibrillar friction with sGAG removal. Unlike the current study, they reported an increase in tissue hydration with sGAG removal in scleral tissue. However, they suggested that the increase in water content was in the form of free water rather than that bound to sGAG, and free water molecules could easily move out of the tissue during loading, reducing tissue lubrication between collagen fibrils (Murienne *et al.*, 2015). However, in Experimental Study II, the treatment group showed statistically less water content than the control group.

Hence, the relationship of hydration with creep as explained by Thornton *et al.* (2001) could result in the creep behaviour observed in this study.

Similar to creep in the CCLs, stress relaxation behaviour was statistically different between the initial 20s and the last 500s (Section 4.3.3.2.5). Moreover, the stress relaxation rate was higher in the control than the treatment groups, however not statistically significant. Studies on the effect of PGs on viscoelastic behaviour of the tendon (Elliott *et al.*, 2003) and the effect of GAGs on stress relaxation of tendon fascicles (Legerlotz *et al.*, 2013) showed a greater stress relaxation in decorin-deficient tissues. However, Lujan *et al.* (2009) showed a negligible increase in stress relaxation after depleting PGs in human MCL with ChABC. The role of PGs in ligaments and its effect on stress relaxation behaviour is still being debated. One explanation for the reduction in the stress relaxation value in the treatment group could be that the sGAGs, which are forming cross-links between collagen molecules, and play a part in microstructural organisations, tensile force resistance and transmission between neighbouring fibrils, are altered after the depletion process (Cribb and Scott, 1995). However, unlike creep, there is a lack of collagen fibre realignment during stress relaxation suggesting that uncrimping collagen fibres might not be responsible for this phenomenon (Thornton *et al.*, 2002; Miller *et al.*, 2012). Therefore, it can be suggested that the depletion of PGs in the CCLs leads to a decrease in water content and interfibrillar lubrication, thereby increasing interfibrillar friction and resulting in a lower stress relaxation value (Thornton *et al.*, 2002; Miller *et al.*, 2012).

It is challenging to mechanically characterise the canine CCLs due to its complex geometry and anatomical structure (Arnoczky, 1983). This challenge has been overcome in this study by using the full-field 3D DIC method to capture the whole tissue surface during deformation, and allowing the determination of the material properties of CCLs in the control and the treatment groups. Recently, a study used a similar system to characterise the mechanical properties of the

anterior medial and posterior lateral of ovine ACL (Mallett and Arruda, 2017). Similar to the current study, Mallett and Arruda (2017) used the mid-substance of the tissue to evaluate the characteristics of the tissue because the tensile response of this region was found to be relatively homogenous. These authors used the DIC data and compared them with machine-based results (Mallett and Arruda, 2017). However, no previous studies have utilised full-field 3D DIC in inverse modelling analysis to derive representative material parameters of an articular ligament such as the ACL or canine CCL. The current study used full-field 3D DIC to reconstruct the surfaces of the CCLs, and obtain load-deformation data for CCLs in the control and the treatment groups (Section 4.4 and 4.5). Surface reconstructions of these geometrically challenging ligaments was achieved with high accuracy and the geometries were then used to create ten FEMs of the CCLs (5 CCLs in the control and 5 CCLs in the treatment groups). Subsequently, this information was used to perform inverse analysis (Section 4.6). The results obtained from the inverse analysis were validated by comparing numerical with the experimental findings and the difference between the two was found to be negligible. In addition, the inverse analysis predicted a lower CCL stiffness in the treatment than the control groups.

5.2.3. Experimental Study III: Canine stifle joint finite element model development

In addition to the advances in experimental techniques in studying material behaviour of the canine CCLs, Experimental Study III developed an anatomically representative FEM of a canine stifle joint so that it could be used to investigate joint stability when microstructure of the CCL is altered by the depletion of the PGs (Section 5.4). Collecting detailed MRI scans was central to developing a good geometrical representation of the joint (Li *et al.*, 1999; Weiss *et al.*, 2005; Pena *et al.*, 2006). The accuracy of an FEM is associated with a good geometrical representation of the joint surface, contact points between surfaces, ligaments with their

attachment parts, and consideration of all structurally relevant components with their material properties (Li *et al.*, 1999; Weiss *et al.*, 2005; Pena *et al.*, 2006). All these key factors were considered in developing an anatomically representative FEM of a canine stifle joint in this study. The FEM developed in the current study is incomparable to those reported in the previous literature (Brown *et al.*, 2013; Stylianou *et al.*, 2014). This is because the four major ligaments (CCL, CaCL, LCL and MCL) are generated as complex anatomical structures and their hyperelastic material parameters were defined based on the results obtained from Experimental Study II. However, it is important to note that the current study focused on the material properties of the CCLs; therefore, the material definitions for MCL, LCL and CaCL elements were not experimentally obtained and their elements are defined based on the behaviour of the CCL. The stifle joint used to construct the FEM was not the same stifle joint used to obtain the experimental data, however they were comparable in terms of age and breed (Section 3.2.3). These limitations could be easily overcome since the ligaments and other soft tissues from the left pelvic limb have been collected and stored appropriately for future work.

The material parameters obtained from Experimental Study II (Table 4.4) used to define the CCLs and the rest of the ligaments in the FEM of the stifle. The two groups (control and treatment) of the stifle joint FEM were employed to investigate joint stability by means of the cranial drawer test (Section 3.8). Similar to the experimental results (Section 4.3.3.2), the control FEMs showed greater resistance from the cranial drawer displacement when compared with the treatment FEMs. However, the cranial drawer motions obtained from the two groups were not statistically different. Nevertheless, this finding suggests that when the PG content in the CCL is reduced, the stability in the whole stifle joint is adversely affected. Sensitivity analysis showed that the stifle joint FEM was responsive to altering material characteristics (μ and α) of the CCL, such that when the values of μ and α were changed statistically significant differences were observed in the cranial drawer displacement (Table 4.5).

5.3. Conclusions

The aim and objectives of the current study were achieved using a range of experimental and numerical methods, including uniaxial tensile tests, digital image correlation, inverse FEM analysis and magnetic resonance imaging. The results obtained in this study led to the following conclusions:

- Experimental Study I
    1. The current study is the first to focus on the material behaviour of canine CCLs, including strain rate sensitivity and hysteresis, at low level strain to better understand the tissue behaviour at the toe region to transition strain (physiologically relevant) which is important because at this region ECM components such as PGs dominate tissue response. It is likely that CCLs displayed an initial low stiffness at low strain rates due to uncrimping of collagen fibres and the contribution of other components in the ECM.
    2. Arranging mechanical tests in different orders of strain rates showed different results, such that tensile responses of the CCL during the ascending tests were significantly different from the descending tests. During the ascending tests, the strain rate sensitivity of the CCLs was statistically significant, however it was not statistically significant during descending tests.
    3. The stress-strain behaviour of the CCLs was stiffer during unloading than loading. This resulted in a considerable amount of dissipated energy between loading and unloading stress-strain curves. In addition, the stiffer behaviour during higher strain rates resulted in less hysteresis. Therefore, hysteresis during the ascending tests was found to be dependent on strain rate as it decreased with increasing strain rates. However, this phenomenon was not statistically significant during the descending tests.

4. The different behaviour of the CCLs under tensile tests in the ascending and descending ordering of strain rate may be associated with the strain history of the tissue. Therefore, this study speculates that a longer time may be required for tissue recovery from stresses caused by a higher strain rate. The outcome of this experimental study indicates the need for further investigations on the viscoelastic behaviour of the canine CCLs when loaded with different orders of strain rates (<10%/min).

- Experimental Study II
    1. The depletion process reduced PG content in the CCLs by 21.11%. However, this depletion was not statistically significant. Despite the small amount of PG depletion, water content in the CCLs was reduced significantly.
    2. Loading and unloading behaviour in CCLs from the control and the treatment groups followed similar patterns to each other and to the results found in Experimental Study I.
    3. In both CCL groups, increasing strain rates resulted in stiffer stress-strain behaviour. The strain rate sensitivity was more pronounced in the control than in the treatment groups. Moreover, the transition strain defining the region where the non-linear stress-strain curves change to the linear was higher in the treatment than in the control groups. Although there were no statistically significant values, the results showed that the CCLs from the control group behaved in a stiffer fashion compared to the treatment group. Similarly, the CCLs in the control group showed larger values of hysteresis (dissipated energy) than the CCLs in the treatment group. These findings suggest that depleting PGs in canine CCLs might affect the tissue integrity and its resistance to the applied loads.

4. Creep and stress relaxation rates in the CCLs from the control and the treatment groups were statistically greater at the last 500s than the initial 20s of creep and stress relaxation tests. In studying creep behaviour, no statistically significant difference between the control and the treatment groups were found. At the last 500s of strain-time curves, creep rate was lower in the treatment than the control group ($p>0.05$). At the last 500s of stress-time curves, stress relaxation rate was statistically lower in the treatment than in the control groups ($p<0.05$). These findings suggest that an increase in the constant load (during creep tests) and strain (during stress relaxation tests) could result in an increase in strain and stress respectively, leading to a greater magnitude of creep and stress relaxation rates.
5. In general, CCLs in the treatment group illustrated lower creep and stress relaxation rates. One explanation for the lower creep rate in the treatment group could be associated with the reduction of water content or change in tissue permeability after PG depletion. CCLs in the treatment group consist of less water compared to the control group and less water content could mean greater tissue resistance to creep because water provides a greater freedom for fibrillar movement. Moreover, the lower relaxation rate in the CCLs from the treatment group could be associated with sGAGs which provides cross-links between collagen molecules. Hence, it is possible that an efficient depletion of PGs in canine CCLs could result in significant mechanical changes in the tissue.
6. A novel test procedure, full-field 3D DIC, was developed, which provided strain measurement across the surface of the CCL.
7. CCL-specific FEMs and mid-substance load-deformation behaviour of the CCLs were generated with the aid of full-field 3D DIC.
8. For the first time, the current study used full-field 3D DIC in inverse analysis to derive representative material parameters of the canine CCL.

- Experimental Study III

1. This study developed an FEM of a whole canine joint to characterise an anatomically representative canine stifle joint.
2. The FEM is incomparable with numerical models reported in previous studies because all the major components required for the stability of the joint are included. In addition, non-linear hyperelastic material characteristics, obtained from the inverse analysis, were used to define the material behaviour of the ligaments in the model.
3. The FEM was employed in an intervention study investigating canine stifle stability when PGs in the CCL were depleted. The results reported altering PG content in the CCLs could affect stability of the canine joint. Hence, PG content in the CCL could be one of the ECM components contributing to the mechanical behaviour of the ligament, and affecting the stability in canine stifle joints.
4. The FEM was sensitivity to change in the non-linear hyperelastic material parameters of the CCL, such that statistical significant differences were noted when the values of μ and α were changed.

5.4. Future Work

In this thesis, efforts have been made to provide important information related to various aspects of the material behaviours of the canine CCL, which is the ligament most prone to rupture in stifle joints. There are a number of recommendations for future work which can be provided based on the knowledge acquired through the literature review, experimental work, numerical analysis, and subsequent results obtained from this thesis.

Firstly, the uniaxial tensile test used in this study is not the most desirable method for obtaining the material behaviour of the CCLs, which has a complex anatomical structure (Arnoczky,

1983). This ligament consists of two bands, caudolateral and anteromedial, and they function independently from one another during flexion and extension (Arnoczky, 1983). However, this method was adopted in the study because it requires a straightforward set up and post-test analysis allowed for comparative studies. However, to obtain a regional variation on the material behaviour of the CCL, a non-contact method could be adopted to measure surface deformation (Whitford *et al.*, 2016; Zhou *et al.*, 2016). In this thesis, a novel test procedure using full-field 3D DIC was developed, and this test method could be used to further investigate the biomechanical behaviour of the CCLs in different regions. To address this work, CCL-specific FEMs with their regional load-deformation information could be used in inverse analysis to predict the regional stress-strain behaviour of the ligament. The initial steps to investigate regional variation of the CCLs have been taken, for example FEMs of the CCLs were generated from the DIC method, different regions of the CCLs were identified and load-deformation data for these regions was collected (Figure 5.1). However, currently this research is in its early stages and requires further work.

Secondly, the current study showed changes in the mechanical behaviour of the CCLs after depleting 21.11% of PG. A greater amount of PGs depletion in the ligament might result in significant changes in the tissue mechanics. Hence, experimental study to deplete a greater amount of PG content in canine femur-CCL-tibia complexes and to investigate mechanical properties of the ligament complexes would be of great advantage.

Finally, the current study successfully developed an anatomically representative FEM of a canine stifle joint. The model has been tested, and material parameters of the ligaments have been defined based on the CCLs of a stifle joint from a different canine. However, as described in Chapter 3, the right pelvic limb was collected for the development of the stifle model whereas the left pelvic limb has been retained for future experimental studies. The left pelvic

limb could be used in future experimental investigations to characterise material properties of the ligaments, menisci, articular cartilage, and bones. Subsequently, these experimental data could be coupled with the corresponding stifle model to accurately predict canine stifle response to external loads.

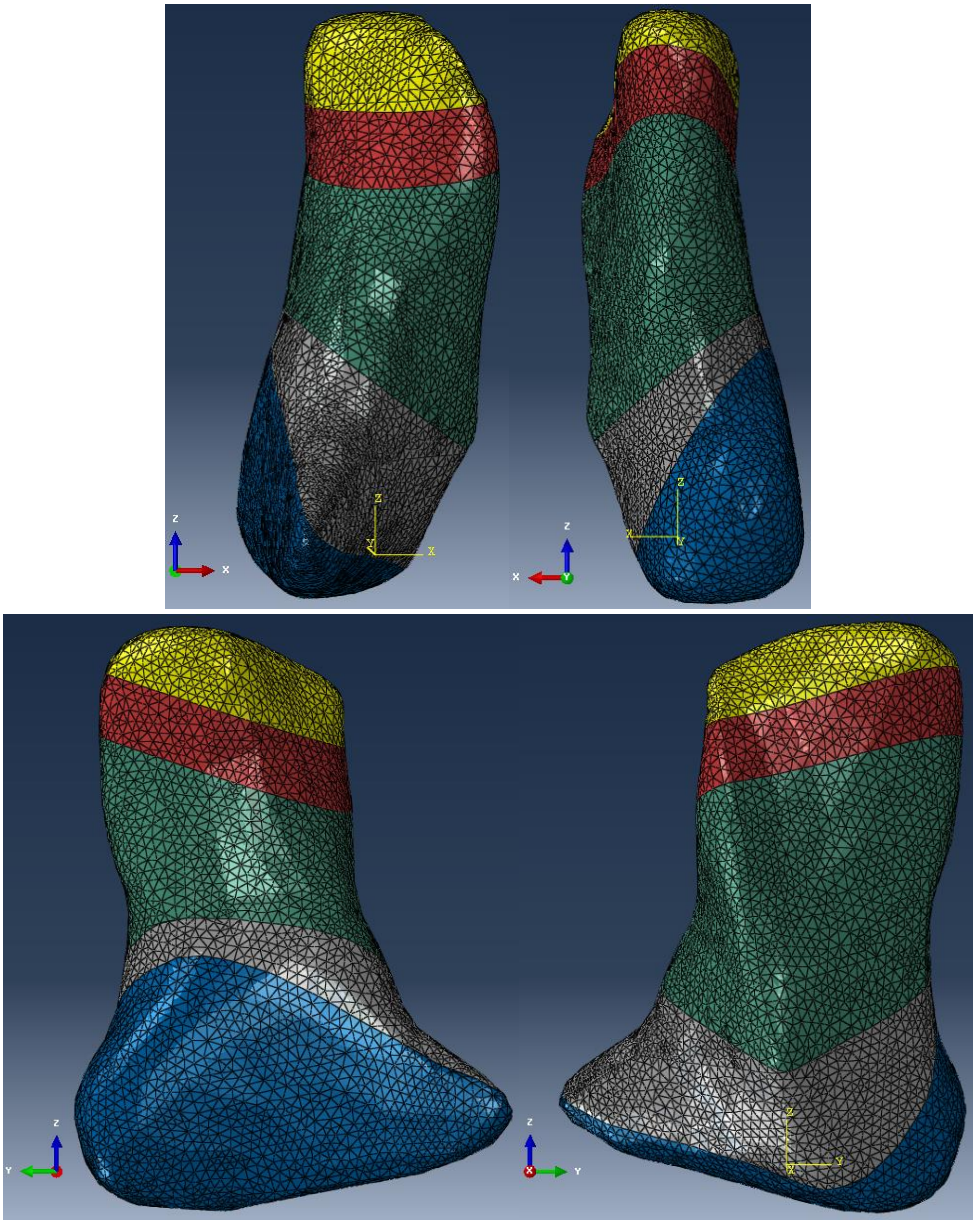

Figure 5.1: A partitioned FEM of a canine CCL from different views. The CCL partitioned into tibia (yellow), tibia insertion (red), middle substance (green), femoral origin (grey) and femur (blue).

References

Adams, D. R. (2004) *Canine anatomy: A systemic study*. Ames, IA: Iowa State Press.

Al Jamal, R., Roughley, P. J. and Ludwig, M. S. (2001) 'Effect of glycosaminoglycan degradation on lung tissue viscoelasticity', *American Journal of Physiology. Lung Cellular and Molecular Physiology*, 280(2), pp. 306-315.

Allaith, S. (2016) *Identifying of key proteoglycans in different anatomical regions of the canine cranial cruciate ligament from dog breeds at an altered risk to ligament disease and rupture*. PhD thesis. The University of Liverpool.

Alm, A. and Stromberg, B. (1974) 'Vascular anatomy of the patellar and cruciate ligaments. A microangiographic and histologic investigation in the dog', *Acta Chirugica Scandinavica*, 445, pp. 25-35.

Amiel, D. (1990) 'Ligament structure, chemistry, and physiology', in O'Connor, J. J., Daniel, D. M. and Akeson, W. H. (eds.) *Knee ligaments: Structure, function, injury and repair*. New York: Raven Press, pp. 77-91.

Amiel, D., Frank, C. B., Harwood, F., Fronek, J. and Akeson, W. (1984) 'Tendons and ligaments: A morphological and biochemical comparison', *Journal of Orthopaedic Research*, 1(3), pp. 257-265.

Amis, A. A. (1998) 'Biomechanics of bone, tendon and ligament', in McCarthy, I. D. and Hughes, S. P. F. (eds.) *Sciences basic to orthopaedics*. London: Saunders, pp. 222-239. 15.

Amis, A. A. and Dawkins, G. P. (1991) 'Functional anatomy of the anterior cruciate ligament. Fibre bundle actions related to ligament replacements and injuries', *The Journal of Bone and Joint Surgery*, 73(2), pp. 260-267.

Arnoczky, S. P. (1983) 'Anatomy of the anterior cruciate ligament', *Clinical Orthopaedics and Related Research*, (172), pp. 19-25.

Arnoczky, S. P. (1985) 'Cruciate ligament rupture and associated injuries', in Nunamaker, D. M. and Newton, C. D. (eds.) *Textbook of small animal orthopaedics*. Philadelphia: Lippincott. 80.

Arnoczky, S. P. and Marshall, J. L. (1977) 'The cruciate ligaments of the canine stifle: An anatomical and functional analysis', *American Journal of Veterinary Research*, 38(11), pp. 1807-1814.

Ascenzi, A. (1993) 'Biomechanics and Galileo Galilei', *Journal of Biomechanics*, 26(2), pp. 95-100.

Baird, A. E., Carter, S. D., Innes, J. F., Ollier, W. E. and Short, A. D. (2014) 'Genetic basis of cranial cruciate ligament rupture (CCLR) in dogs', *Connective Tissue Research*, 55(4), pp. 275-281.

Baird, D. K., Hathcock, J. T., Rumph, P. F., Kincaid, S. A. and Visco, D. M. (1998) 'Low-field magnetic resonance imaging of the canine stifle joint: Normal anatomy', *Veterinary Radiology & Ultrasound*, 39(2), pp. 87-97.

Barranger, Y., Doumalin, P., Dupre, J. C. and Germaneau, A. (2012) 'Strain measurement by digital image correlation: Influence of two types of speckle patterns made from rigid or deformable marks', *Strain*, 48(5), pp. 357-365.

Benjamin, M. and Ralphs, J. R. (1997) 'Tendons and ligaments-an overview', *Histology and Histopathology*, 12(4), pp. 1135-1144.

Benjamin, M. and Ralphs, J. R. (1998) 'Fibrocartilage in tendons and ligaments: An adaptation to compressive load', *Journal of Anatomy*, 193, pp. 481-494.

Bennett, D., Tennant, B., Lewis, D. G., Baughan, J., May, C. and Carter, S. (1988) 'A reappraisal of anterior cruciate ligament disease in the dog', *Journal of Small Animal Practice*, 29(5), pp. 275-297.

Biskup, J. J., Balogh, D. G., Scott, R. M. and Conzemius, M. G. (2017) 'Long-term outcome of an intra-articular allograft technique for treatment of spontaneous cranial cruciate ligament rupture in the dog', *Veterinary Surgery*, 46(5), pp. 691-699.

Boden, B. P., Dean, G. S., Feagin, J. A. and Garrett, W. E. (2000) 'Mechanisms of anterior cruciate ligament injury', *Orthopedics*, 23(6), pp. 573-578.

Bonner, T. J., Newell, N., Karunaratne, A., Pullen, A. D., Amis, A. A., A, M. J. B. and Masouros, S. D. (2015) 'Strain-rate sensitivity of the lateral collateral ligament of the knee', *Journal of the Mechanical Behavior of Biomedical Materials*, 41, pp. 261-270.

Boschiero, L. (2007) 'Giovanni Alfonso Borelli (1608-1679)', in *Experiment and natural philosophy in seventeenth-century Tuscany: The history of the Accademia del Cimento*. Dordrecht: Springer, pp. 59-91.

Boyce, B. L., Jones, R. E., Nguyen, T. D. and Grazier, J. M. (2007) 'Stress-controlled viscoelastic tensile response of bovine cornea', *Journal of Biomechanics*, 40(11), pp. 2367-2376.

Brandt, K. D., Braunstein, E. M., Visco, D. M., O'Connor, B., Heck, D. and Albrecht, M. (1991a) 'Anterior (cranial) cruciate ligament transection in the dog: A bona fide model of osteoarthritis, not merely of cartilage injury and repair', *The Journal of Rheumatology*, 18(3), pp. 436-446.

Brandt, K. D., Myers, S. L., Burr, D. and Albrecht, M. (1991b) 'Osteoarthritic changes in canine articular cartilage, subchondral bone, and synovium fifty-four months after transection of the anterior cruciate ligament', *Arthritis and Rheumatism*, 34(12), pp. 1560-1570.

Braun, G. L. (1941) 'Kinesiology: From Aristotle to the twentieth century', *The Research Quarterly*, 12(2), pp. 163-173.

Bray, R. C., Salo, P. T., Lo, I. K., Ackermann, P., Rattner, J. B. and Hart, D. A. (2005) 'Normal ligament structure, physiology and function', *Sports Medicine and Arthroscopy Review*, 13(3), pp. 127-135.

Bray, R. C., Shrive, N. G., Frank, C. B. and Chimich, D. D. (1992) 'The early effects of joint immobilization on medial collateral ligament healing in an ACL-deficient knee: A gross anatomic and biomechanical investigation in the adult rabbit model', *Journal of Orthopaedic Research*, 10(2), pp. 157-166.

Brown, N. P., Bertocci, G. E. and Marcellin-Little, D. J. (2013) 'Development of a canine stifle computer model to evaluate cranial cruciate ligament deficiency', *Journal of Mechanics in Medicine and Biology*, 13(2), pp. 1350043-1350071.

Budras, K.-D. (2007) *Anatomy of the dog*. 5th edn. Hannover: Schlütersche.

Butler, D. L., Grood, E. S., Noyes, F. R. and Zernicke, R. F. (1978a) 'Biomechanics of ligaments and tendons', *Exercise and Sport Sciences Reviews*, 6, pp. 125-81.

Butler, D. L., Noyes, F. R. and Grood, E. S. (1978b) 'Measurement of the mechanical properties of ligaments', in *CRC handbook of engineering in medicine and biology section B: Instruments and measurements*. West Palm Beach: CRC Press Inc., pp. 279-314.

Carpenter, D. H. and Cooper, R. C. (2000) 'Mini review of canine stifle joint anatomy', *Anatomia, Histologia, Embryologia*, 29(6), pp. 321-329.

Chakrabarti, B. and Park, J. W. (1980) 'Glycosaminoglycans: Structure and interaction', *CRC Critical Review in Biochemistry*, 8(3), pp. 225-313.

Chen, F. X., Chen, X., Xie, X., Feng, X. and Yang, L. X. (2013) 'Full-field 3D measurement using multi-camera digital image correlation system', *Optics and Lasers in Engineering*, 51(9), pp. 1044-1052.

Chen, L., Wu, Y., Yu, J., Jiao, Z., Ao, Y., Yu, C., Wang, J. and Cui, G. (2011) 'Effect of repeated freezing-thawing on the Achilles tendon of rabbits', *Knee Surgery, Sports Traumatology, Arthroscopy*, 19(6), pp. 1028-1034.

Chimich, D., Shrive, N., Frank, C. B., Marchuk, L. and Bray, R. (1992) 'Water content alters viscoelastic behaviour of the normal adolescent rabbit medial collateral ligament', *Journal of Biomechanics*, 25(8), pp. 831-837.

Comerford, E. J., Tarlton, J. F., Avery, N. C., Bailey, A. J. and Innes, J. F. (2006) 'Distal femoral intercondylar notch dimensions and their relationship to composition and metabolism of the canine anterior cruciate ligament', *Osteoarthritis Cartilage*, 14(3), pp. 273-278.

Comerford, E. J., Tarlton, J. F., Innes, J. F., Johnson, K. A., Amis, A. A. and Bailey, A. J. (2005) 'Metabolism and composition of the canine anterior cruciate ligament relate to differences in knee joint mechanics and predisposition to ligament rupture', *Journal of Orthopaedic Research*, 23(1), pp. 61-66.

Conza, N. (2005) 'Part 3: Tissue preconditioning', *Experimental Techniques*, 29(2), pp. 43-46.

Cook, J. L. (2010) 'Cranial cruciate ligament disease in dogs: Biology versus biomechanics', *Veterinary Surgery*, 39(3), pp. 270-277.

Corsini, M., Cignoni, P. and Scopigno, R. (2012) 'Efficient and flexible sampling with blue noise properties of triangular meshes', *IEEE Transactions on Visualization and Computer Graphics*, 18(6), pp. 914-924.

Cribb, A. M. and Scott, J. E. (1995) 'Tendon response to tensile stress: An ultrastructural investigation of collagen: Proteoglycan interactions in stressed tendon', *Journal of Anatomy*, 187, pp. 423-428.

Crisco, J. J., Moore, D. C. and McGovern, R. D. (2002) 'Strain-rate sensitivity of the rabbit MCL diminishes at traumatic loading rates', *Journal of Biomechanics*, 35(10), pp. 1379-1385.

Crowninshield, R. D. and Pope, M. H. (1976) 'The strength and failure characteristics of rat medial collateral ligaments', *The Journal of Trauma*, 16(2), pp. 99-105.

Dale, W. C. and Baer, E. (1974) 'Fiber-buckling in composite systems: A model for ultrastructure of uncalcified collagen tissues', *Journal of Materials Science*, 9(3), pp. 369-382.

Dantec Dynamics (2014) *Istra 4D Software Manual Q-400 System*. Germany: A Nova Instruments Company.

Danto, M. I. and Woo, S. L. Y. (1993) 'The mechanical properties of skeletally mature rabbit anterior cruciate ligament and patellar tendon over a range of strain rates', *Journal of Orthopaedic Research*, 11(1), pp. 58-67.

De Rooster, H., De Bruin, T. and Van Bree, H. (2006) 'Morphologic and functional features of the canine cruciate ligaments', *Veterinary Surgery*, 35(8), pp. 769-780.

De Rooster, H., De Bruin, T. and Van Bree, H. (2010) 'Morphology and function of the cruciate ligaments', in Muir, P. (ed.) *Advances in the canine cranial cruciate ligament*. Iowa: Wiley-Blackwell, pp. xxiii-289. 1.

Dodds, J. A. and Arnoczky, S. P. (1994) 'Anatomy of the anterior cruciate ligament: a blueprint for repair and reconstruction', *Arthroscopy*, 10(2), pp. 132-139.

Donahue, T. L. H., Hull, M. L., Rashid, M. M. and Jacobs, C. R. (2002) 'A finite element model of the human knee joint for the study of tibio-femoral contact', *Journal of Biomechanical Engineering*, 124(3), pp. 273-280.

Donahue, T. L. H., Hull, M. L., Rashid, M. M. and Jacobs, C. R. (2003) 'How the stiffness of meniscal attachments and meniscal material properties affect tibio-femoral contact pressure computed using a validated finite element model of the human knee joint', *Journal of Biomechanics*, 36(1), pp. 19-34.

Dorlot, J. M., Ait Ba Sidi, M., Tremblay, G. M. and Drouin, G. (1980) 'Load elongation behavior of the canine anterior cruciate ligament', *Journal of Biomechanical Engineering*, 102(3), pp. 190-194.

Doschak, M. R. and Zernicke, R. F. (2005) 'Structure, function and adaptation of bone-tendon and bone-ligament complexes', *Journal of Musculoskeletal & Neuronal Interactions*, 5(1), pp. 35-40.

Duval, J. M., Budsberg, S. C., Flo, G. L. and Sammarco, J. L. (1999) 'Breed, sex, and body weight as risk factors for rupture of the cranial cruciate ligament in young dogs', *Journal of the American Veterinary Medical Association*, 215(6), pp. 811-814.

Eckert, C. E., Fan, R., Mikulis, B., Barron, M., Carruthers, C. A., Friebe, V. M., Vyavahare, N. R. and Sacks, M. S. (2013) 'On the biomechanical role of glycosaminoglycans in the aortic heart valve leaflet', *Acta Biomaterialia*, 9(1), pp. 4653-4660.

Elliott, D. M., Robinson, P. S., Gimbel, J. A., Sarver, J. J., Abboud, J. A., Iozzo, R. V. and Soslowsky, L. J. (2003) 'Effect of altered matrix proteins on quasilinear viscoelastic properties in transgenic mouse tail tendons', *Annals of Biomedical Engineering*, 31(5), pp. 599-605.

Elsheikh, A. (2010) 'Finite element modeling of corneal biomechanical behavior', *Journal of Refractive Surgery*, 26(4), pp. 289-300.

Elsheikh, A., Geraghty, B., Alhasso, D., Knappett, J., Campanelli, M. and Rama, P. (2010) 'Regional variation in the biomechanical properties of the human sclera', *Experimental Eye Research*, 90(5), pp. 624-233.

Elsheikh, A., Kassem, W. and Jones, S. W. (2011) 'Strain-rate sensitivity of porcine and ovine corneas', *Acta of Bioengineering and Biomechanics*, 13(2), pp. 25-36.

Elsheikh, A., Wang, D., Rama, P., Campanelli, M. and Garway-Heath, D. (2008) 'Experimental assessment of human corneal hysteresis', *Current Eye Research*, 33(3), pp. 205-213.

Elsheikh, A., Whitford, C., Hamarashid, R., Kassem, W., Joda, A. and Buchler, P. (2013) 'Stress free configuration of the human eye', *Medical Engineering & Physics*, 35(2), pp. 211-216.

Eshel, H. and Lanir, Y. (2001) 'Effects of strain level and proteoglycan depletion on preconditioning and viscoelastic responses of rat dorsal skin', *Annals of Biomedical Engineering*, 29(2), pp. 164-172.

Evans, H. E., DeLahunta, A. and Miller, M. E. (2012) *Miller's anatomy of the dog*. 4th edn. Philadelphia: Saunders.

Farndale, R. W., Buttle, D. J. and Barrett, A. J. (1986) 'Improved quantitation and discrimination of sulphated glycosaminoglycans by use of dimethylmethylene blue', *Biochimica et Biophysica Acta*, 883(2), pp. 173-177.

Frank, C. B. (2004) 'Ligament structure, physiology and function', *Journal of Musculoskeletal & Neuronal Interactions*, 4(2), pp. 199-201.

Frank, C. B., Amiel, D., Woo, S. L. Y. and Akeson, W. (1985) 'Normal ligament properties and ligament healing', *Clinical Orthopaedics and Related Research*, (196), pp. 15-25.

Frank, C. B., Hart, D. A. and Shrive, N. G. (1999) 'Molecular biology and biomechanics of normal and healing ligaments - a review', *Osteoarthritis and Cartilage*, 7(1), pp. 130-140.

Frank, C. B., Woo, S. L. Y., Amiel, D., Harwood, F., Gomez, M. and Akeson, W. (1983) 'Medial collateral ligament healing. A multidisciplinary assessment in rabbits', *American Journal of Sports Medicine*, 11(6), pp. 379-389.

Frantz, C., Stewart, K. M. and Weaver, V. M. (2010) 'The extracellular matrix at a glance', *Journal of Cell Science*, 123(24), pp. 4195-4200.

Fratzl, P., Misof, K., Zizak, I., Rapp, G., Amenitsch, H. and Bernstorff, S. (1998) 'Fibrillar structure and mechanical properties of collagen', *Journal of Structural Biology*, 122(1-2), pp. 119-122.

Freutel, M., Galbusera, F., Ignatius, A. and Durselen, L. (2015) 'Material properties of individual menisci and their attachments obtained through inverse FE-analysis', *Journal of Biomechanics*, 48(8), pp. 1343-1349.

Fung, Y. C. (1967) 'Elasticity of soft tissues in simple elongation', *The American Journal of Physiology*, 213(6), pp. 1532-1544.

Fung, Y. C. (1993) *Biomechanics: Mechanical properties of living tissues*. 2nd edn. New York: Springer.

Gautieri, A., Vesentini, S., Redaelli, A. and Buehler, M. J. (2012) 'Viscoelastic properties of model segments of collagen molecules', *Matrix Biology*, 31(2), pp. 141-149.

Geraghty, B., Jones, S. W., Rama, P., Akhtar, R., Elsheikh, A. (2012) 'Age-related variations in the biomechanical properties of human sclera', *Journal of the Mechanical Behavior of Biomedical Materials*, 16, pp. 181-191.

Giannini, S., Buda, R., Di Caprio, F., Agati, P., Bigi, A., De Pasquale, V. and Ruggeri, A. (2008) 'Effects of freezing on the biomechanical and structural properties of human posterior tibial tendons', *International Orthopaedics*, 32(2), pp. 145-151.

Gianotti, S. M., Marshall, S. W., Hume, P. A. and Bunt, L. (2009) 'Incidence of anterior cruciate ligament injury and other knee ligament injuries: A national population-based study', *Journal of Science and Medicine in Sport*, 12(6), pp. 622-627.

Gillis, C., Sharkey, N., Stover, S. M., Pool, R. R., Meagher, D. M. and Willits, N. (1995) 'Ultrasonography as a method to determine tendon cross-sectional area', *American Journal of Veterinary Research*, 56(10), pp. 1270-1274.

Gold, G. E., Chen, C. A., Koo, S., Hargreaves, B. A. and Bangerter, N. K. (2009) 'Recent Advances in MRI of Articular Cartilage', *American Journal of Roentgenology*, 193(3), pp. 628-638.

Goodship, A. E. and Birch, H. L. (2005) 'Cross sectional area measurement of tendon and ligament in vitro: a simple, rapid, non-destructive technique', *Journal of Biomechanics*, 38(3), pp. 605-608.

Gottlob, C. A., Baker, C. L., Pellissier, J. M. and Colvin, L. (1999) 'Cost effectiveness of anterior cruciate ligament reconstruction in young adults', *Clinical Orthopaedics and Related Research*, (367), pp. 272-282.

Gray, H. (2000) *Anatomy of the human body*. New York: Bartlegy.

Griffin, L. Y., Agel, J., Albohm, M. J., Arendt, E. A., Dick, R. W., Garrett, W. E., Garrick, J. G., Hewett, T. E., Huston, L., Ireland, M. L., Johnson, R. J., Kibler, W. B., Lephart, S., Lewis, J. L., Lindenfeld, T. N., Mandelbaum, B. R., Marchak, P., Teitz, C. C. and Wojtys, E. M. (2000) 'Noncontact anterior cruciate ligament injuries: Risk factors and prevention strategies', *The Journal of the American Academy of Orthopaedic Surgeons*, 8(3), pp. 141-150.

Harasen, G. (2002) 'Diagnosing rupture of the cranial cruciate ligament', *The Canadian Veterinary Journal*, 43(6), pp. 475-476.

Hardingham, T. E. (1981) 'Proteoglycans: Their structure, interactions and molecular organization in cartilage', *Biochemical Society Transactions*, 9(6), pp. 489-497.

Hardingham, T. E. and Bayliss, M. (1990) 'Proteoglycans of articular cartilage: Changes in aging and in joint disease', *Seminars in Arthritis and Rheumatism*, 20(3 Suppl 1), pp. 12-33.

Hardingham, T. E. and Fosang, A. J. (1992) 'Proteoglycans: Many forms and many functions', *Federation of American Societies for Experimental Biology*, 6(3), pp. 861-870.

Hascall, V. C., Riolo, R. L., Hayward, J., Jr. and Reynolds, C. C. (1972) 'Treatment of bovine nasal cartilage proteoglycan with chondroitinases from Flavobacterium heparinum and Proteus vulgaris', *The Journal of Biological Chemistry*, 247(14), pp. 4521-4528.

Hasegawa, A., Nakahara, H., Kinoshita, M., Asahara, H., Koziol, J. and Lotz, M. K. (2013) 'Cellular and extracellular matrix changes in anterior cruciate ligaments during human knee aging and osteoarthritis', *Arthritis Research & Therapy*, 15(1), p. R29.

Haslach, H. W., Jr. (2005) 'Nonlinear viscoelastic, thermodynamically consistent, models for biological soft tissue', *Biomechanics and Modeling in Mechanobiology*, 3(3), pp. 172-189.

Haut, R. C. and Little, R. W. (1969) 'Rheological properties of canine anterior cruciate ligaments', *Journal of Biomechanics*, 2(3), pp. 289-298.

Haut, R. C. and Powlison, A. C. (1990) 'The effects of test environment and cyclic stretching on the failure properties of human patellar tendons', *Journal of Orthopaedic Research*, 8(4), pp. 532-540.

Hayashi, K., Frank, J. D., Dubinsky, C., Zhengling, H., Markel, M. D., Manley, P. A. and Muir, P. (2003a) 'Histologic changes in ruptured canine cranial cruciate ligament', *Veterinary Surgery*, 32(3), pp. 269-277.

Hayashi, K., Frank, J. D., Hao, Z., Schamberger, G. M., Markel, M. D., Manley, P. A. and Muir, P. (2003b) 'Evaluation of ligament fibroblast viability in ruptured cranial cruciate ligament of dogs', *American Journal of Veterinary Research*, 64(8), pp. 1010-1016.

Heffron, L. E. and Campbell, J. R. (1978) 'Morphology, histology and functional anatomy of the canine cranial cruciate ligament', *The Veterinary Record*, 102(13), pp. 280-283.

Helfrick, M. N., Niezrecki, C., Avitabile, P. and Schmidt, T. (2011) '3D digital image correlation methods for full-field vibration measurement', *Mechanical Systems and Signal Processing*, 25(3), pp. 917-927.

Henninger, H. B., Underwood, C. J., Ateshian, G. A. and Weiss, J. A. (2010) 'Effect of sulfated glycosaminoglycan digestion on the transverse permeability of medial collateral ligament', *Journal of Biomechanics*, 43(13), pp. 2567-2573.

Herzog, W., Adams, M. E. and Matyas (1993) 'Hindlimb loading, morphology and biochemistry of articular cartilage in the ACL-deficient cat knee', *Osteoarthritis and Cartilage*, 1(4), pp. 243-251.

Herzog, W., Diet, S., Suter, E., Mayzus, P., Leonard, T. R., Muller, C., Wu, J. Z. and Epstein, M. (1998) 'Material and functional properties of articular cartilage and patellofemoral contact mechanics in an experimental model of osteoarthritis', *Journal of Biomechanics*, 31(12), pp. 1137-1145.

Hewett, T. E., Ford, K. R., Hoogenboom, B. J. and Myer, G. D. (2010) 'Understanding and preventing acl injuries: Current biomechanical and epidemiologic considerations - update 2010', *North American Journal of Sports Physical Therapy*, 5(4), pp. 234-251.

Hey, N. J., Handley, C. J., Ng, C. K. and Oakes, B. W. (1990) 'Characterization and synthesis of macromolecules by adult collateral ligament', *Biochim Biophys Acta*, 1034(1), pp. 73-80.

Hingorani, R. V., Provenzano, P. P., Lakes, R. S., Escarcega, A. and Vanderby, R., Jr. (2004) 'Nonlinear viscoelasticity in rabbit medial collateral ligament', *Annals of Biomedical Engineering*, 32(2), pp. 306-312.

Holden, J. P., Grood, E. S., Korvick, D. L., Cummings, J. F., Butler, D. L. and Bylski-Austrow, D. I. (1994) 'In vivo forces in the anterior cruciate ligament: Direct measurements during walking and trotting in a quadruped', *Journal of Biomechanics*, 27(5), pp. 517-526.

Hu, Z. X., Xie, H. M., Lu, J., Wang, H. X. and Zhu, J. G. (2011) 'Error evaluation technique for three-dimensional digital image correlation', *Applied Optics*, 50(33), pp. 6239-6247.

Hu, Z. X., Xie, H. M., Lu, J. A., Hua, T. and Zhu, J. G. (2010) 'Study of the performance of different subpixel image correlation methods in 3D digital image correlation', *Applied Optics*, 49(21), pp. 4044-4051.

Ichinohe, T., Kanno, N., Harada, Y., Yogo, T., Tagawa, M., Soeta, S., Amasaki, H. and Hara, Y. (2015) 'Degenerative changes of the cranial cruciate ligament harvested from dogs with cranial cruciate ligament rupture', *The Journal of Veterinary Medical Science*, 77(7), pp. 761-770.

Ilic, M. Z., Carter, P., Tyndall, A., Dudhia, J. and Handley, C. J. (2005) 'Proteoglycans and catabolic products of proteoglycans present in ligament', *Biochemical Journal*, 385(2), pp. 381-388.

Kadler, K. E., Baldock, C., Bella, J. and Boot-Handford, R. P. (2007) 'Collagens at a glance', *Journal Of Cell Science*, 120(12), pp. 1955-1958.

Kannus, P. (2000) 'Structure of the tendon connective tissue', *Scandinavian Journal of Medicine & Science Sports*, 10(6), pp. 312-320.

Kastelic, J., Galeski, A. and Baer, E. (1978) 'The multicomposite structure of tendon', *Connective Tissue Research*, 6(1), pp. 11-23.

Kazhdan, M., Bolitho, M. and Hoppe, H. (2006) *Eurographics Symposium on Geometry processing*.

Kharaz, Y. A. (2015) *The molecular and cellular differences between tendons and ligaments*. PhD thesis. The University of Liverpool.

Khatod, M. and Amiel, D. (2003) 'Ligament biochemistry and physiology', in Daniel, D. M., Pedowitz, R. A., O'Connor, J. J. and Akeson, W. H. (eds.) *Daniel's knee injuries: Ligament and cartilage structure, function, injury, and repair*. Philadelphia: Lippincott Williams & Wilkins, pp. 31-42. 3.

Kreis, T. E. and Vale, R. (1993) *Guidebook to the extracellular matrix and adhesion proteins*. Oxford: Oxford University Press.

Legerlotz, K., Riley, G. P. and Screen, H. R. (2013) 'GAG depletion increases the stress-relaxation response of tendon fascicles, but does not influence recovery', *Acta Biomaterialia*, 9(6), pp. 6860-6866.

Levangie, P. K. and Norkin, C. C. (2005) *Joint structure and function: A comprehensive analysis*. 4th edn. Philadelphia: F.A. Davis Co.

Li, G., Gil, J., Kanamori, A. and Woo, S. L. Y. (1999) 'A validated three-dimensional computational model of a human knee joint', *Journal of Biomechical Engineering*, 121(6), pp. 657-662.

Lionello, G., Sirieix, C. and Baleani, M. (2014) 'An effective procedure to create a speckle pattern on biological soft tissue for digital image correlation measurements', *Journal of the Mechanical Behaviour Biomedical Material*, 39, pp. 1-8.

Liu, M. J. J., Chou, S. M., Goh, K. L. and Tan, S. H. (2008) 'Cross-sectional area measurement of soft tissues in vitro: A non-contact laser scan method', *Journal of Mechanics in Medicine and Biology*, 8(3), pp. 353-361.

Lo, I. K., Chi, S., Ivie, T., Frank, C. B. and Rattner, J. B. (2002a) 'The cellular matrix: A feature of tensile bearing dense soft connective tissues', *Histology and Histopathology*, 17(2), pp. 523-537.

Lo, I. K., Ou, Y., Rattner, J. P., Hart, D. A., Marchuk, L. L., Frank, C. B. and Rattner, J. B. (2002b) 'The cellular networks of normal ovine medial collateral and anterior cruciate ligaments are not accurately recapitulated in scar tissue', *Journal of Anatomy*, 200(3), pp. 283-296.

Lujan, T. J., Underwood, C. J., Henninger, H. B., Thompson, B. M. and Weiss, J. A. (2007) 'Effect of dermatan sulfate glycosaminoglycans on the quasi-static material properties

of the human medial collateral ligament', *Journal of Orthopaedic Research*, 25(7), pp. 894-903.
Lujan, T. J., Underwood, C. J., Jacobs, N. T. and Weiss, J. A. (2009) 'Contribution of glycosaminoglycans to viscoelastic tensile behavior of human ligament', *Journal of Applied Physiology*, 106(2), pp. 423-431.
Luyckx, T., Verstraete, M., De Roo, K., De Waele, W., Bellemans, J. and Victor, J. (2014) 'Digital image correlation as a tool for three-dimensional strain analysis in human tendon tissue', *Journal of Experimental Orthopaedics*, 1(1), pp. 1-7.
Luyckx, T., Verstraete, M., Roo, K., Van Der Straeten, C. and Victor, J. (2016) 'High strains near femoral insertion site of the superficial medial collateral ligament of the knee can explain the clinical failure pattern', *Journal of Orthopaedic Research*, 34(11), pp. 2016-2024.
Lydon, C., Crisco, J. J., Panjabi, M. and Galloway, M. (1995) 'Effect of elongation rate on the failure properties of the rabbit anterior cruciate ligament', *Clinical Biomechanics*, 10(8), pp. 428-433.
Mallett, K. F. and Arruda, E. M. (2017) 'Digital image correlation-aided mechanical characterization of the anteromedial and posterolateral bundles of the anterior cruciate ligament', *Acta Biomaterialia*, 56, pp. 44-57.
McNair, P. J., Marshall, R. N. and Matheson, J. A. (1990) 'Important features associated with acute anterior cruciate ligament injury', *The New Zealand Medical Jouranl*, 103(901), pp. 537-539.
Miller, K. S., Edelstein, L., Connizzo, B. K. and Soslowsky, L. J. (2012) 'Effect of preconditioning and stress relaxation on local collagen fiber re-alignment: Inhomogeneous properties of rat supraspinatus tendon', *Journal of Biomechanical Engineering*, 134(3), pp. 31007-31013.
Millis, D. and Mankin, J. (2014) 'Orthopedic and Nurologic Evaluation', in Millis, D. and Levine, D. (eds.) *Canine Rehabilitation and Physical Therapy*. 2nd edn. London: Saunders, pp. 180-200. 10.
Misof, K., Rapp, G. and Fratzl, P. (1997) 'A new molecular model for collagen elasticity based on synchrotron X-ray scattering evidence', *Biophysical Journal*, 72(3), pp. 1376-1381.
Moffat, K. L., Sun, W. H., Pena, P. E., Chahine, N. O., Doty, S. B., Ateshian, G. A., Hung, C. T. and Lu, H. H. (2008) 'Characterization of the structure-function relationship at the ligament-to-bone interface', *Proceedings of the National Academy of Sciences of the United States of America*, 105(23), pp. 7947-7952.
Moon, D. K., Woo, S. L. Y., Takakura, Y., Gabriel, M. T. and Abramowitch, S. D. (2006) 'The effects of refreezing on the viscoelastic and tensile properties of ligaments', *Journal of Biomechanics*, 39(6), pp. 1153-1157.
Murienne, B. J., Jefferys, J. L., Quigley, H. A. and Nguyen, T. D. (2015) 'The effects of glycosaminoglycan degradation on the mechanical behavior of the posterior porcine sclera', *Acta Biomaterialia*, 12, pp. 195-206.
Nagelli, C. V., Cook, J. L., Kuroki, K., Bozynski, C., Ma, R. and Hewett, T. E. (2017) 'Does anterior cruciate ligament innervation matter for joint function and development of osteoarthritis?', *The Journal of Knee Surgery*, 30(4), pp. 364-371.
Naraghi, A. and White, L. M. (2012) 'Three-dimensional MRI of the musculoskeletal system', *American Journal of Roentgenology*, 199(3), pp. 283-293.
Noguchi, M., Kitaura, T., Ikoma, K. and Kusaka, Y. (2002) 'A method of in-vitro measurement of the cross-sectional area of soft tissues, using ultrasonography', *Journal of Orthopaedic Science*, 7(2), pp. 247-251.

Novak, P. J., Bach, B. R., BushJoseph, C. A. and Badrinath, S. (1996) 'Cost containment: A charge comparison of anterior cruciate ligament reconstruction', *Arthroscopy*, 12(2), pp. 160-164.

Noyes, F. R. and Grood, E. S. (1976) 'The strength of the anterior cruciate ligament in humans and Rhesus monkeys', *The Journal of Bone and Joint Surgery*, 58(8), pp. 1074-1082.

Ogden, R. W. (1984) *Non-linear elastic deformations*. Chichester: Ellis Horwood.

Oshkour, A. A., Abu Osman, N. A., Davoodi, M. M., Bayat, M., Yau, Y. H. and Abas, W. A. B. W. (2011) *Kuala Lumpur International Conference on Biomedical Engineering*. Kuala Lumpur, MALAYSIA.

Pankov, R. and Yamada, K. M. (2002) 'Fibronectin at a glance', *Journal of Cell Science*, 115(20), pp. 3861-3863.

Pena, E., Calvo, B., Martinez, M. A. and Doblare, M. (2006) 'A three-dimensional finite element analysis of the combined behavior of ligaments and menisci in the healthy human knee joint', *Journal of Biomechanics*, 39(9), pp. 1686-1701.

Peng, X. Q., Liu, G. and Guo, Z. Y. (2010) 'Finite element contact analysis of a human sagittal knee joint', *Journal of Mechanics in Medicine and Biology*, 10(2), pp. 225-236.

Peters, W. H. and Ranson, W. F. (1982) 'Digital imaging techniques in experimental stress-analysis', *Optical Engineering*, 21(3), pp. 427-431.

Pioletti, D. P. and Rakotomanana, L. R. (2000) 'Non-linear viscoelastic laws for soft biological tissues', *European Journal of Mechanics - A/Solids*, 19(5), pp. 749-759.

Pioletti, D. P., Rakotomanana, L. R. and Leyvraz, P. F. (1999) 'Strain rate effect on the mechanical behavior of the anterior cruciate ligament-bone complex', *Medical Engineering & Physics*, 21(2), pp. 95-100.

Pope, M. H. (2005) 'Giovanni Alfonso Borelli - The father of biomechanics', *Spine*, 30(20), pp. 2350-2355.

Provenzano, P. P., Heisey, D., Hayashi, K., Lakes, R. and Vanderby, R., Jr. (2002) 'Subfailure damage in ligament: A structural and cellular evaluation', *Journal of Applied Physiology*, 92(1), pp. 362-371.

Quapp, K. M. and Weiss, J. A. (1998) 'Material characterization of human medial collateral ligament', *Journal of Biomechanical Engineering*, 120(6), pp. 757-763.

Quinn, K. P. and Winkelstein, B. A. (2011) 'Preconditioning is correlated with altered collagen fiber alignment in ligament', *Journal of Biomechanical Engineering*, 133(6), pp. 64506-64510.

Race, A. and Amis, A. A. (1996) 'Cross-sectional area measurement of soft tissue. A new casting method', *Journal of Biomechanics*, 29(9), pp. 1207-1212.

Ragetly, C. A., Evans, R., Mostafa, A. A. and Griffon, D. J. (2011) 'Multivariate analysis of morphometric characteristics to evaluate risk factors for cranial cruciate ligament deficiency in Labrador retrievers', *Veterinary Surgery*, 40(3), pp. 327-333.

Reilly, D. T. and Burstein, A. H. (1975) 'The elastic and ultimate properties of compact bone tissue', *Journal of Biomechanics*, 8(6), pp. 393-405.

Reilly, D. T., Burstein, A. H. and Frankel, V. H. (1974) 'The elastic modulus for bone', *Journal of Biomechanics*, 7(3), pp. 271-275.

Rigozzi, S., Muller, R. and Snedeker, J. G. (2009) 'Local strain measurement reveals a varied regional dependence of tensile tendon mechanics on glycosaminoglycan content', *Journal of Biomechanics*, 42(10), pp. 1547-1552.

Robinson, P. S., Lin, T. W., Reynolds, P. R., Derwin, K. A., Iozzo, R. V. and Soslowsky, L. J. (2004) 'Strain-rate sensitive mechanical properties of tendon fascicles from mice with genetically engineered alterations in collagen and decorin', *Journal of Biomechanical Engineering*, 126(2), pp. 252-257.

Rumian, A. P., Wallace, A. L. and Birch, H. L. (2007) 'Tendons and ligaments are anatomically distinct but overlap in molecular and morphological features - a comparative study in an ovine model', *Journal of Orthopaedic Research*, 25(4), pp. 458-464.

Ruoslahti, E. (1988) 'Structure and biology of proteoglycans', *Annual Review Cell Biology*, 4, pp. 229-255.

Saunders, J. B. (1933) 'The knee joint-its functional anatomy and the mechanism of certain injuries', *California and Western Medicine*, 39(2), pp. 83-85.

Savelberg, H. H. C. M., Kooloos, J. G. M., Huiskes, R. and Kauer, J. M. G. (1993) 'An Indirect Method to Assess Wrist Ligament Forces with Particular Regard to the Effect of Preconditioning', *Journal of Biomechanics*, 26(11), pp. 1347-1351.

Schagemann, J. C., Chung, H.-W., Mrosek, E. H., O'Drisocll, S. W. and Reinholz, G. G. (2004) 'Glycosaminoglycans and proteoglycans', in Wnek, G. E. and Bowlin, G. L. (eds.) *Encyclopedia of biomaterials and biomedical engineering*. 2nd edn. New York: Marcel Dekker, pp. 1195-1209.

Schatzmann, L., Brunner, P. and Staubli, H. U. (1998) 'Effect of cyclic preconditioning on the tensile properties of human quadriceps tendons and patellar ligaments', *Knee Surgery, Sports Traumatology, Arthroscopy*, 6, pp. 56-61.

Shahar, R. and Banks-Sills, L. (2004) 'A quasi-static three-dimensional, mathematical, three-body segment model of the canine knee', *Journal of Biomechanics*, 37(12), pp. 1849-1859.

Smith, H. C., Vacek, P., Johnson, R. J., Slauterbeck, J. R., Hashemi, J., Shultz, S. and Beynnon, B. D. (2012a) 'Risk factors for anterior cruciate ligament injury: A review of the literature - part 1: Neuromuscular and anatomic risk', *Sports Health*, 4(1), pp. 69-78.

Smith, H. C., Vacek, P., Johnson, R. J., Slauterbeck, J. R., Hashemi, J., Shultz, S. and Beynnon, B. D. (2012b) 'Risk factors for anterior cruciate ligament injury: A review of the literature - part 2: Hormonal, genetic, cognitive function, previous injury, and extrinsic risk factors', *Sports Health*, 4(2), pp. 155-161.

Smith, K. D., Clegg, P. D., Innes, J. F. and Comerford, E. J. (2014) 'Elastin content is high in the canine cruciate ligament and is associated with degeneration', *Veterinary Journal*, 199(1), pp. 169-174.

Smith, K. D., Vaughan-Thomas, A., Spiller, D. G., Clegg, P. D., Innes, J. F. and Comerford, E. J. (2012c) 'Variations in cell morphology in the canine cruciate ligament complex', *Veterinary Journal*, 193(2), pp. 561-566.

Solomonow, M. (2004) 'Ligaments: A source of work-related musculoskeletal disorders', *Journal of Electromyography and Kinesiology*, 14(1), pp. 49-60.

Stylianou, A. P., Guess, T. M. and Cook, J. L. (2014) 'Development and validation of a multi-body model of the canine stifle joint', *Computer Methods in Biomechanics and Biomedical Engineering*, 17(4), pp. 370-377.

Sutton, M. A., Orteu, J. and Schreier, H. W. (2009) *Image correlation for shape, motion and deformation measurements: Basic concepts, theory and applications*. New York: Springer.

Swartz, M. A. and Fleury, M. E. (2007) 'Interstitial flow and its effects in soft tissues', *Annual Review of Biomedical Engineering*, 9, pp. 229-256.

Thornton, G. M., Frank, C. B. and Shrive, N. (2007) 'Ligament', in Nigg, B. M. and Herzog, W. (eds.) *Biomechanics of the musculo-skeletal system*. 3rd edn. Chichester, West Sussex, England: John Wiley & Sons, pp. 123-145. 2.

Thornton, G. M., Shrive, N. G. and Frank, C. B. (2001) 'Altering ligament water content affects ligament pre-stress and creep behaviour', *Journal of Orthopaedic Research*, 19(5), pp. 845-851.

Thornton, G. M., Shrive, N. G. and Frank, C. B. (2002) 'Ligament creep recruits fibres at low stresses and can lead to modulus-reducing fibre damage at higher creep stresses: a study in rabbit medial collateral ligament model', *Journal of Orthopaedic Research*, 20(5), pp. 967-974.

Tozer, S. and Duprez, D. (2005) 'Tendon and ligament: Development, repair and disease', *Birth Defects Research. Part C: Embryo Today*, 75(3), pp. 226-236.

Vasseur, P. B. (2002) 'Stifle joint', in Slatter, D. H. (ed.) *Textbook of small animal surgery*. 3rd edn. Philadelphia: Saunders, pp. 2090-2133. 147.

Vasseur, P. B. and Arnoczky, S. P. (1981) 'Collateral ligaments of the canine stifle joint: Anatomic and functional analysis', *American Journal of Veterinary Research*, 42(7), pp. 1133-1137.

Vasseur, P. B., Pool, R. R., Arnoczky, S. P. and Lau, R. E. (1985) 'Correlative biomechanical and histologic study of the cranial cruciate ligament in dogs', *American Journal of Veterinary Research*, 46(9), pp. 1842-1854.

Vasseur, P. B., Stevenson, S., Gregory, C. R., Rodrigo, J. J., Pauli, S., Heitter, D. and Sharkey, N. (1991) 'Anterior cruciate ligament allograft transplantation in dogs', *Clinical Orthopaedics and Related Research*, (269), pp. 295-304.

Vergari, C., Pourcelot, P., Holden, L., Ravary-Plumioen, B., Laugier, P., Mitton, D. and Crevier-Denoix, N. (2010) 'A linear laser scanner to measure cross-sectional shape and area of biological specimens during mechanical testing', *Journal of Biomechanical Engineering*, 132(10), pp. 105001-105008.

Viidik, A. (1968) 'Elasticity and tensile strength of anterior cruciate ligament in rabbits as influenced by training', *Acta Physiologica Scandinavica*, 74(3), pp. 372-380.

Vogel, K. (1994) 'Glycosaminoglycans and Proteoglycans', in Yurchenco, P. D., Birk, D. E. and Mecham, R. P. (eds.) *Extracellular matrix assembly and structure*. San Diego: Academic Press, pp. 243-273. 8.

Wang, J., Elsheikh, A., Davey, P. G., Wang, W., Bao, F. and Mottershead, J. E. (2014) 'Corneal topography matching by iterative registration', *Proceedings of the Institution of Mechanical Engineers. Part H: Journal of Engineering in Medicine*, 228(11), pp. 1154-1167.

Wang, J. Y. and Roehrl, M. H. (2002) 'Glycosaminoglycans are a potential cause of rheumatoid arthritis', *Proceedings of the National Academy of Sciences of the United States of America*, 99(22), pp. 14362-14367.

Warzee, C. C., Dejardin, L. M., Arnoczky, S. P. and Perry, R. L. (2001) 'Effect of tibial plateau leveling on cranial and caudal tibial thrusts in canine cranial cruciate-deficient stifles: An in vitro experimental study', *Veterinary Surgery*, 30(3), pp. 278-286.

Weiss, J. A., Gardiner, J. C. and Bonifasi-Lista, C. (2002) 'Ligament material behavior is nonlinear, viscoelastic and rate-independent under shear loading', *Journal of Biomechanics*, 35(7), pp. 943-950.

Weiss, J. A., Gardiner, J. C., Ellis, B. J., Lujan, T. J. and Phatak, N. S. (2005) 'Three-dimensional finite element modeling of ligaments: Technical aspects', *Medical Engineering & Physics*, 27(10), pp. 845-861.

Whitford, C., Joda, A., Jones, S., Bao, F., Rama, P. and Elsheikh, A. (2016) 'Ex vivo testing of intact eye globes under inflation conditions to determine regional variation of mechanical stiffness', *Eye and Vision*, 10, pp. 3-21.

Wilke, V. L., Kinghorn, B. P., Conzemius, M. G. and Rothschild, M. F. (2004) 'Prediction of inheritance for cranial cruciate ligament disease in the Newfoundland dog', *Journal of Animal Science*, 82, pp. 36-36.

Wilke, V. L., Robinson, D. A., Evans, R. B., Rothschild, M. F. and Conzemius, M. G. (2005) 'Estimate of the annual economic impact of treatment of cranial cruciate ligament injury

in dogs in the United States', *Journal of the American Veterinary Medical Association*, 227(10), pp. 1604-1607.
Wingfield, C., Amis, A. A., Stead, A. C. and Law, H. T. (2000) 'Comparison of the biomechanical properties of rottweiler and racing greyhound cranial cruciate ligaments', *Journal of Small Animal Practice*, 41(7), pp. 303-307.
Wise, S. G. and Weiss, A. S. (2009) 'Tropoelastin', *The International Journal of Biochemistry & Cell Biology*, 41(3), pp. 494-497.
Wismans, J., Veldpaus, F., Janssen, J., Huson, A. and Struben, P. (1980) 'A three-dimensional mathematical model of the knee-joint', *Journal of Biomechanics*, 13(8), pp. 677-685.
Woo, S. L. Y., Orlando, C. A., Camp, J. F. and Akeson, W. H. (1986) 'Effects of postmortem storage by freezing on ligament tensile behavior', *Journal of Biomechanics*, 19(5), pp. 399-404.
Woo, S. L. Y. (1982) 'Mechanical properties of tendons and ligaments. I. Quasi-static and nonlinear viscoelastic properties', *Biorheology*, 19(3), pp. 385-396.
Woo, S. L. Y., Danto, M. I., Ohland, K. J., Lee, T. Q. and Newton, P. O. (1990a) 'The use of a laser micrometer system to determine the cross-sectional shape and area of ligaments: A comparative study with two existing methods', *Journal of Biomechanical Engineering*, 112(4), pp. 426-431.
Woo, S. L. Y., Debski, R. E., Withrow, J. D. and Janaushek, M. A. (1999) 'Biomechanics of knee ligaments', *The American Journal of Sports Medicine*, 27(4), pp. 533-543.
Woo, S. L. Y., Gomez, M. A. and Akeson, W. H. (1981) 'The time and history-dependent viscoelastic properties of the canine medical collateral ligament', *Journal of Biomechanical Engineering*, 103(4), pp. 293-298.
Woo, S. L. Y., Hollis, J. M., Adams, D. J., Lyon, R. M. and Takai, S. (1991) 'Tensile properties of the human femur-anterior cruciate ligament-tibia complex. The effects of specimen age and orientation', *The American Journal of Sports Medicine*, 19(3), pp. 217-225.
Woo, S. L. Y., Hollis, J. M., Roux, R. D., Gomez, M. A., Inoue, M., Kleiner, J. B. and Akeson, W. H. (1987) 'Effects of knee flexion on the structural properties of the rabbit femur-anterior cruciate ligament-tibia complex (FATC)', *Journal of Biomechanics*, 20(6), pp. 557-563.
Woo, S. L. Y., Newton, P. O., MacKenna, D. A. and Lyon, R. M. (1992) 'A comparative evaluation of the mechanical properties of the rabbit medial collateral and anterior cruciate ligaments', *Journal of Biomechanics*, 25(4), pp. 377-386.
Woo, S. L. Y., Ohland, K. J. and Weiss, J. A. (1990b) 'Aging and sex-related changes in the biomechanical properties of the rabbit medial collateral ligament', *Mechanisms of Ageing and Development*, 56(2), pp. 129-142.
Woo, S. L. Y., Peterson, R. H., Ohland, K. J., Sites, T. J. and Danto, M. I. (1990c) 'The effects of strain rate on the properties of the medial collateral ligament in skeletally immature and mature rabbits: a biomechanical and histological study', *Journal of Orthopaedic Research*, 8(5), pp. 712-721.
Yahia, L. H. and Drouin, G. (1989) 'Microscopical investigation of canine anterior cruciate ligament and patellar tendon: Collagen fascicle morphology and architecture', *Journal of Orthopaedic Research*, 7(2), pp. 243-251.
Yahia, L. H. and Drouin, G. (1990) 'Study of the hysteresis phenomenon in canine anterior cruciate ligaments', *Journal of Biomedical Engineering*, 12(1), pp. 57-62.
Yamada, K. M., Akiyama, S. K., Hasegawa, T., Hasegawa, E., Humphries, M. J., Kennedy, D. W., Nagata, K., Urushihara, H., Olden, K. and Chen, W. T. (1985) 'Recent advances in research on fibronectin and other cell attachment proteins', *Journal of Cellular Biochemistry*, 28(2), pp. 79-97.

Yamaguchi, I. (1981) 'A laser-speckle strain-gauge', *Journal of Physics. E: Scientific Instruments*, 14(11), pp. 1270-1273.

Yang, L., Tsai, C. M., Hsieh, A. H., Lin, V. S., Akeson, W. H. and Sung, K. L. (1999) 'Adhesion strength differential of human ligament fibroblasts to collagen types I and III', *Journal of Orthopaedic Research*, 17(5), pp. 755-762.

Yang, P. J. and Temenoff, J. S. (2009) 'Engineering orthopedic tissue interfaces', *Tissue Engineering*, 15(2), pp. 127-141.

Zhou, B., Ravindran, S., Ferdous, J., Kidane, A., Sutton, M. A. and Shazly, T. (2016) 'Using digital image correlation to characterize local strains on vascular tissue specimens', *Journal of Visualized Experiments*, (107).

Appendix (1): Preliminary study on PGs depletion (Comerford et al., unpublished, 2012).

Table 1: This Table shows wet and dry weight (mg) of canine CCLs used to calculate water content (%) for the Time-course by Comerford *et al.* (unpublished, 2012). The Table also shows sGAG content relative to dry weight of the CCLs.

CCL groups	Wet weight (mg)	Dry weight (mg)	% Water content	Microgram of sGAG/mg dry weight	Microgram sGAG/mg dry weight (%)
Control 1 - time 0 hr	19.21	5.59	70.90	26.19	2.62
Control 2 - time 0 hr	8.93	2.69	69.88	17.30	1.73
Control 1 - time 3 hr	14.27	3.35	76.52	4.55	0.46
Control 2 - time 3 hr	10.03	2.42	75.87	33.81	3.38
Control 1 - time 6 hr	23.25	5.18	77.72	22.60	2.26
Control 2 - time 6 hr	11.62	3.16	72.81	26.15	2.62
Control 1 - time 12 hr	12.75	3.62	71.61	8.92	0.89
Control 2 - time 12 hr	28.29	6.41	77.34	9.33	0.93
Control 1 - time 24 hr	32.46	7.77	76.06	11.03	1.10
Control 2 - time 24 hr	9.61	2.24	76.69	9.16	0.92
1IU 1 - time 0 hr	12.23	3.84	68.60	34.30	3.43
1IU 2 - time 0 hr	15.08	4.57	69.69	31.68	3.17
1IU 1 - time 3 hr	21.57	6.33	70.65	6.37	0.64
1IU 2 - time 3 hr	9.80	2.75	71.94	1.68	0.17
1IU 1 - time 6 hr	24.69	6.57	73.39	2.15	0.21
1IU 2 - time 6 hr	15.65	3.97	74.63	11.38	1.14
1IU 1 - time 12 hr	23.95	6.48	72.94	2.70	0.27
1IU 2 - time 12 hr	21.97	5.70	74.06	3.49	0.35
1IU 1 - time 24 hr	32.32	7.27	77.51	1.62	0.16
1IU 2 - time 24 hr	24.94	6.15	75.34	2.31	0.23
0.5IU 1 - time 0 hr	19.10	5.67	70.31	16.45	1.64
0.5IU 2 - time 0 hr	18.53	4.43	76.09	8.15	0.82
0.5IU 1 - time 3 hr	42.42	5.30	87.51	1.30	0.13
0.5IU 2 - time 3 hr	20.15	4.34	78.46	0.75	0.08
0.5IU 1 -time 6 hr	39.54	9.57	75.80	3.26	0.33
0.5IU 2 - time 6 hr	27.18	4.52	83.37	1.75	0.17
0.5IU 1 -time12 hr	21.10	5.27	75.02	2.63	0.26
0.5IU 2 - time12 hr	14.74	2.40	83.72	2.11	0.21
0.5IU 1 -time24 hr	27.74	6.02	78.30	1.45	0.14
0.5IU 2 - time24 hr	33.52	5.38	83.95	4.37	0.44
0.25IU 1 - time 0 hr	14.58	4.88	66.53	17.35	1.73
0.25IU 2 - time 0 hr	23.26	6.61	71.58	21.36	2.14
0.25IU 1 - time 3 hr	17.55	4.77	76.64	3.50	0.35

0.25IU 2 - time 3 hr	15.69	3.76	74.89	3.32	0.33
0.25IU 1 -time 6 hr	20.28	4.10	76.48	1.91	0.19
0.25IU 2 - time 6 hr	14.26	3.94	73.63	2.63	0.26
0.25IU 1 -time12 hr	18.35	3.53	80.76	1.11	0.11
0.25IU 2 - time12 hr	15.73	3.36	78.64	0.94	0.09
0.25IU 1 -time24 hr	30.30	4.40	85.48	0.95	0.10
0.25IU 2 - time24 hr	20.13	4.06	79.83	0.69	0.07

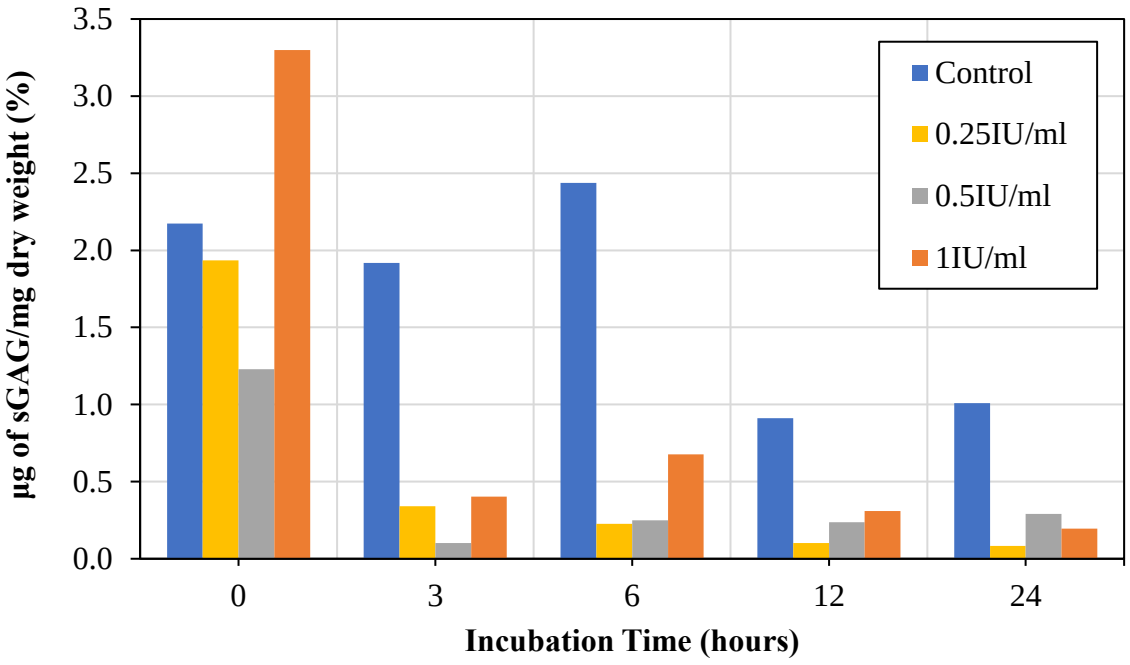

Figure 1: This Figure is based on the data presented in Appendix (1): Table 1. The Figure showing change in sGAG content (%) in canine CCLs with incubation time for different ChABC concentrations. The Figure confirms that after three hours of the CCL incubation in 0.25IU/ml ChABC, approximately 82.3% of sGAG is depleted.

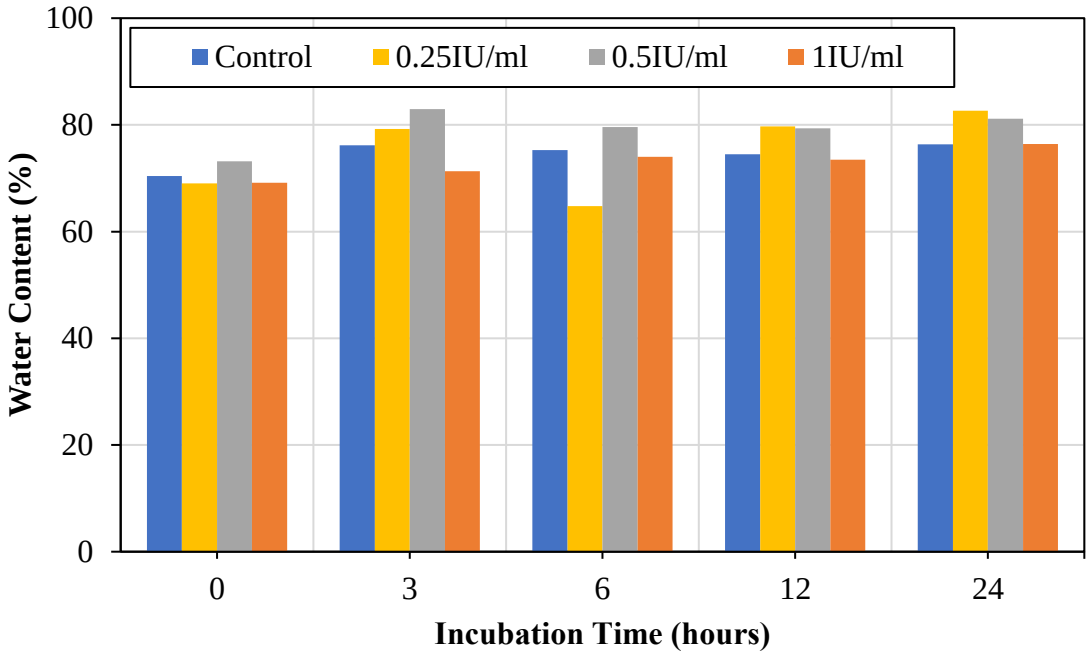

Figure 2: This Figure is based on the data presented in the Table above in Appendix (1): Table 1. The Figure showing change in water content (%) in canine CCLs with incubation time for different ChABC concentrations.

Appendix (2): Computer screen-captures of the steps taken to calibrate two adjacent cameras (i.e. camera 1 and camera 2) using Dantec target plate and Istra4D software.

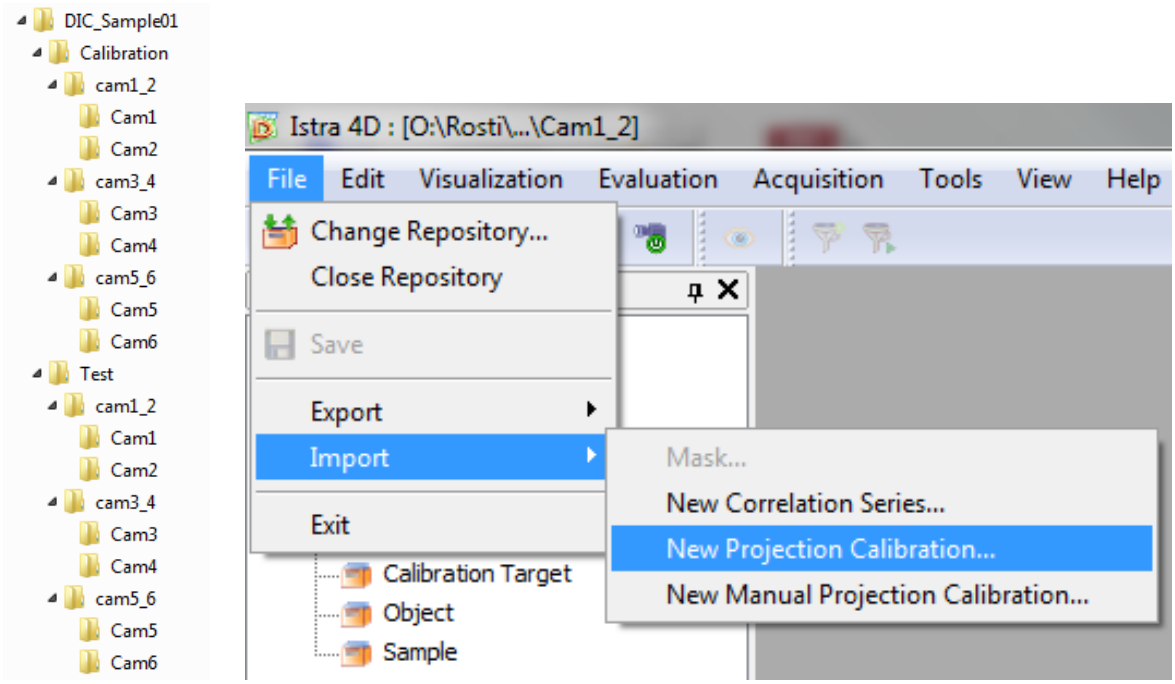

(a) **(b)**

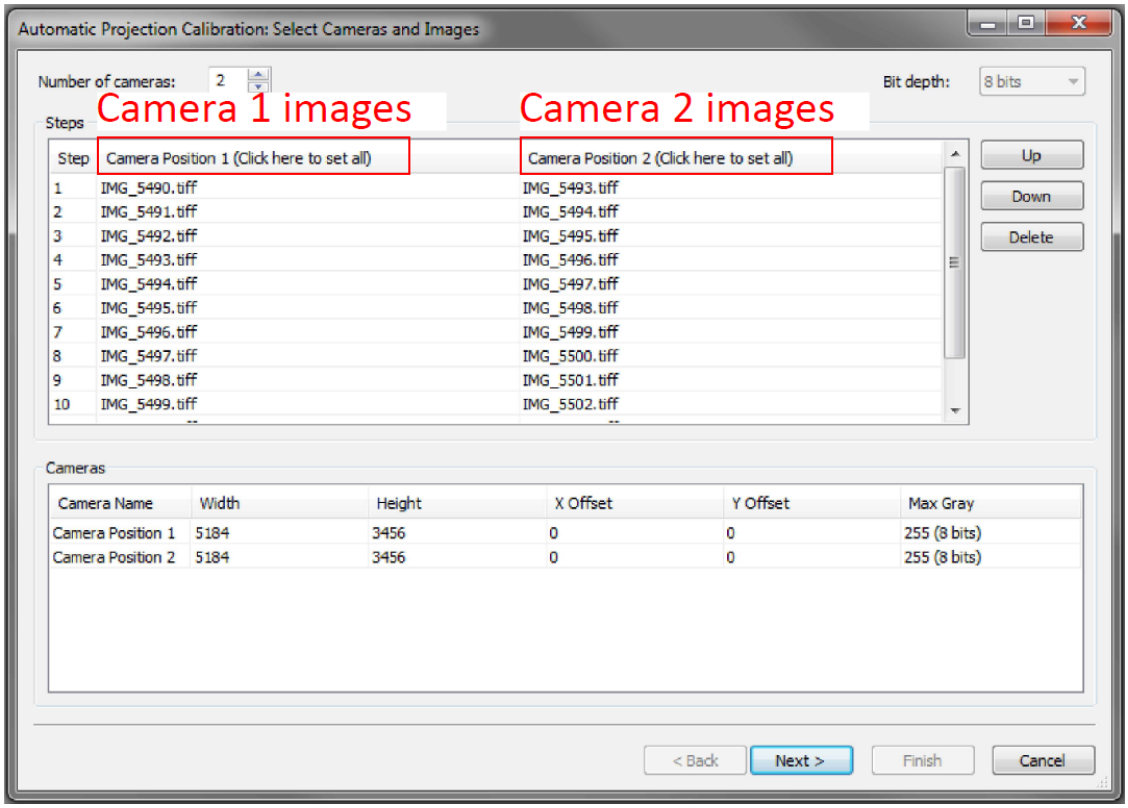

(c)

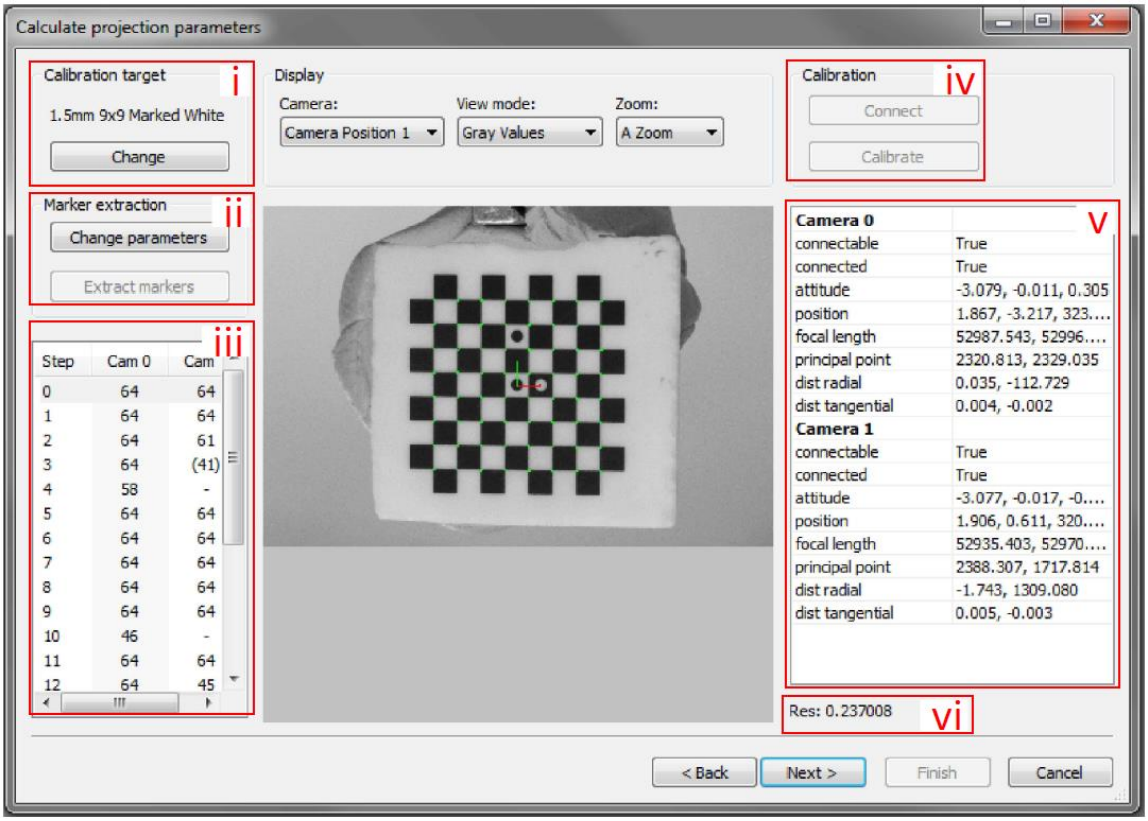
Calculate projection parameters
Calibration target
i
1.5mm 9x9 Marked White
Change
Display
Camera:
Camera Position 1
View mode:
Gray Values
Zoom:
A Zoom
Calibration
iv
Connect
Calibrate
Marker extraction
ii
Change parameters
Extract markers
iii
Step
Cam 0
Cam
0 64 64
1 64 64
2 64 61
3 64 (41)
4 58 -
5 64 64
6 64 64
7 64 64
8 64 64
9 64 64
10 46 -
11 64 64
12 64 45
v
Camera 0
connectable True
connected True
attitude -3.079, -0.011, 0.305
position 1.867, -3.217, 323....
focal length 52987.543, 52996....
principal point 2320.813, 2329.035
dist radial 0.035, -112.729
dist tangential 0.004, -0.002
Camera 1
connectable True
connected True
attitude -3.077, -0.017, -0....
position 1.906, 0.611, 320....
focal length 52935.403, 52970....
principal point 2388.307, 1717.814
dist radial -1.743, 1309.080
dist tangential 0.005, -0.003
Res: 0.237008
vi
< Back
Next >
Finish
Cancel

(d)

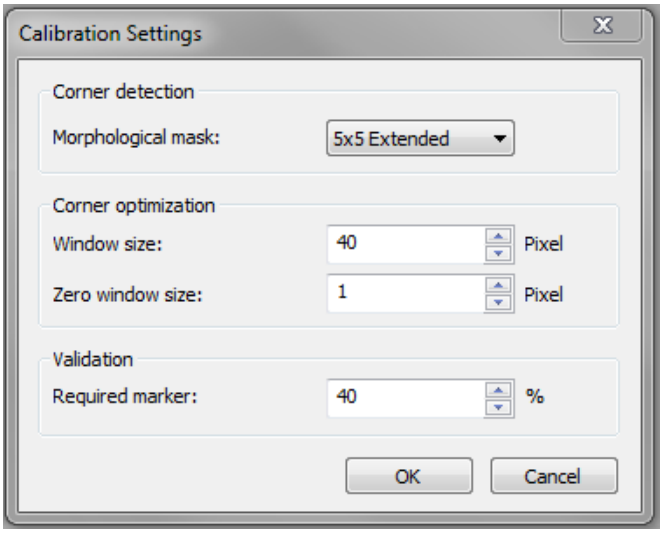
Calibration Settings
Corner detection
Morphological mask:
5x5 Extended
Corner optimization
Window size:
40
Pixel
Zero window size:
1
Pixel
Validation
Required marker:
40
%
OK
Cancel

(e)

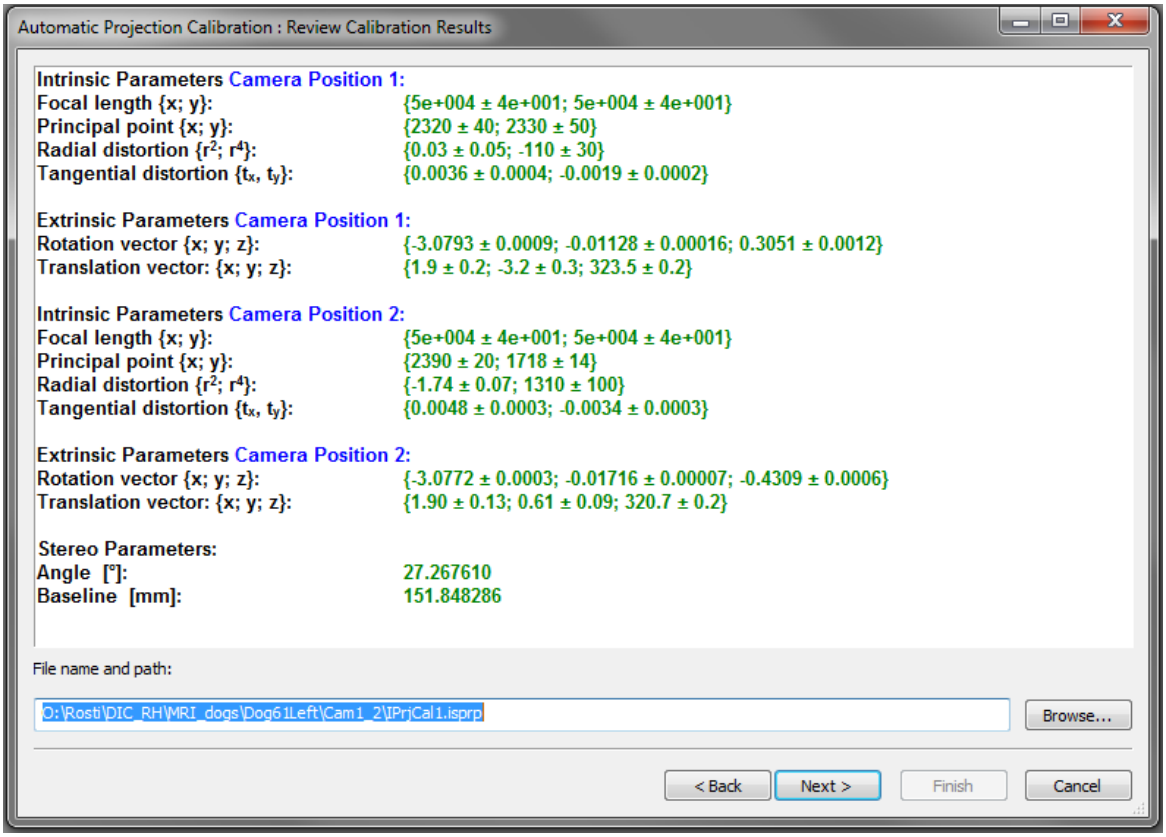

(f)

Figure 1: Computer screen-captures of the steps taken to calibrate two adjacent cameras (i.e. camera 1 and camera 2) using Dantec target plate and Istra4D software.

Appendix (3): Illustration, using computer screen-captures, of the steps taken to analyse images of the calibration object from two adjacent cameras (i.e. camera 1 and camera 2) using Istra4D software.

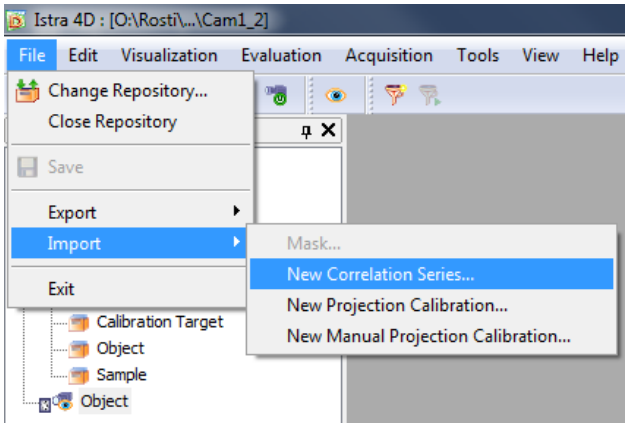

(a)

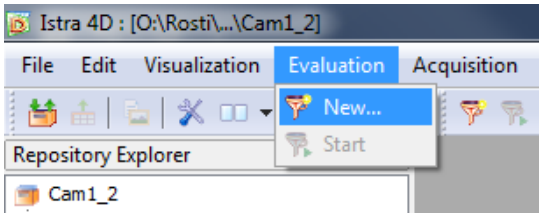

(b)

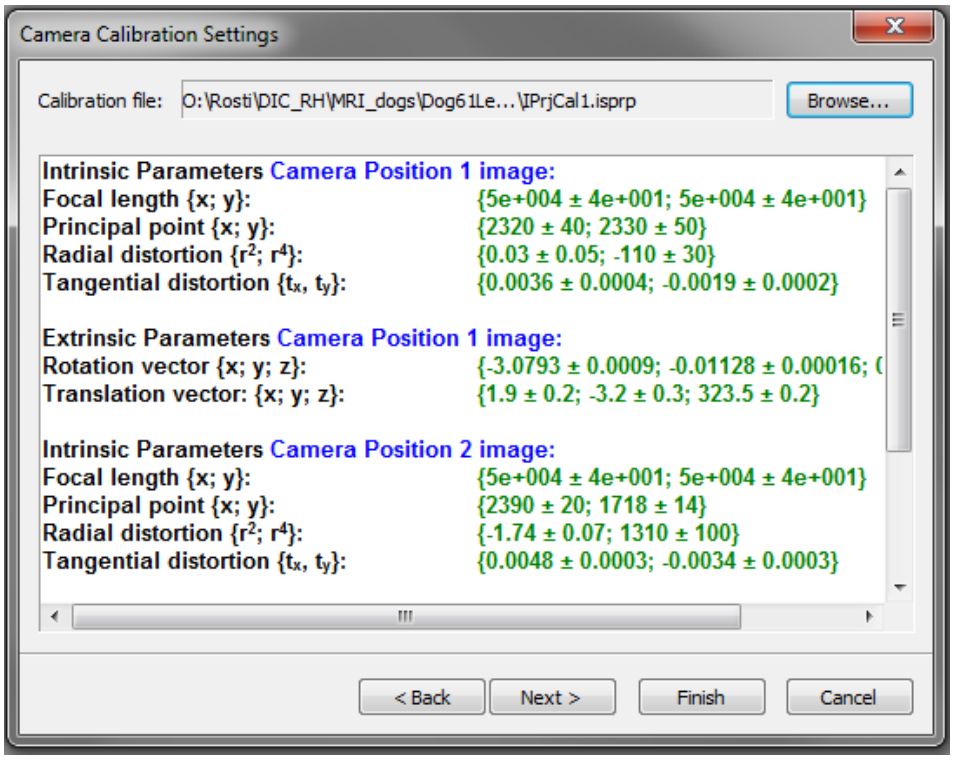

(c)

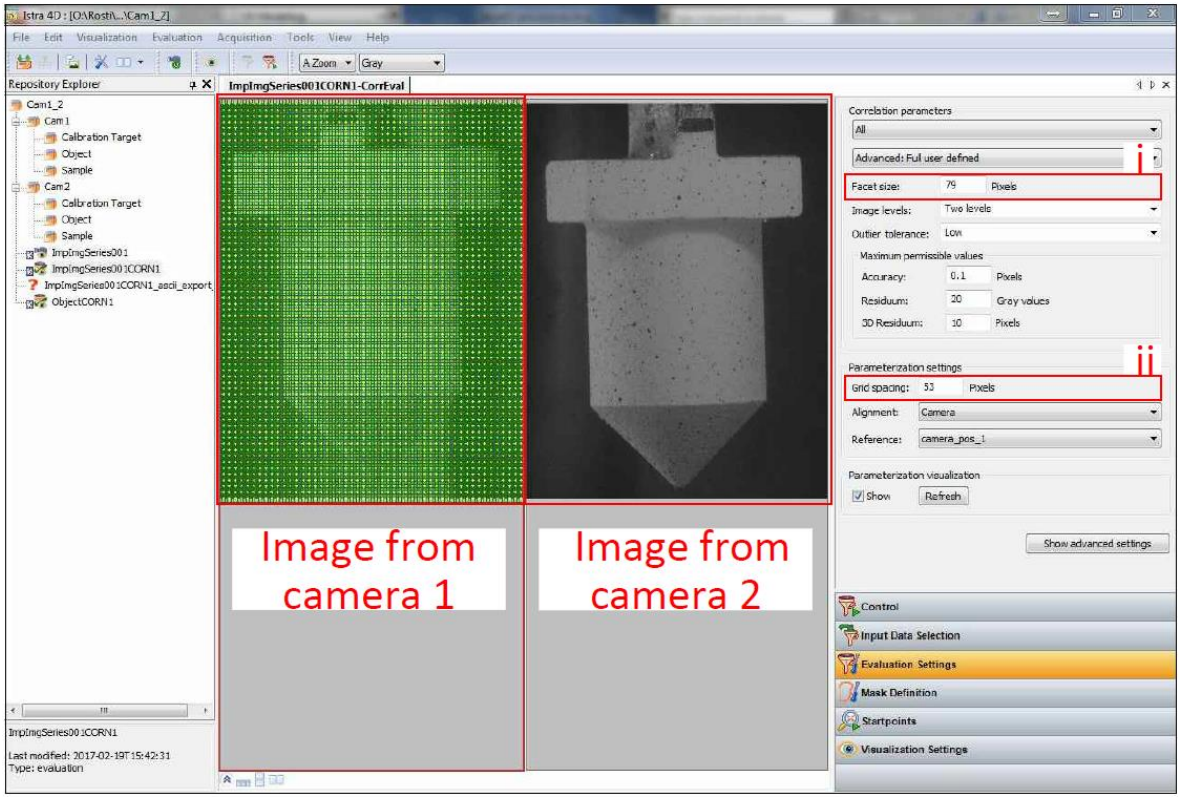
Repository Explorer
ImpImgSeries001CORN1-CorrEval
Image from camera 1
Image from camera 2
Correlation parameters
Facet size:
Image levels:
Outlier tolerance:
Maximum permissible values
Accuracy:
Residuum:
3D Residuum:
Parameterization settings
Grid spacing:
Alignment:
Reference:
Parameterization visualization
Show advanced settings
Control
Input Data Selection
Evaluation Settings
Mask Definition
Startpoints
Visualization Settings

(d)

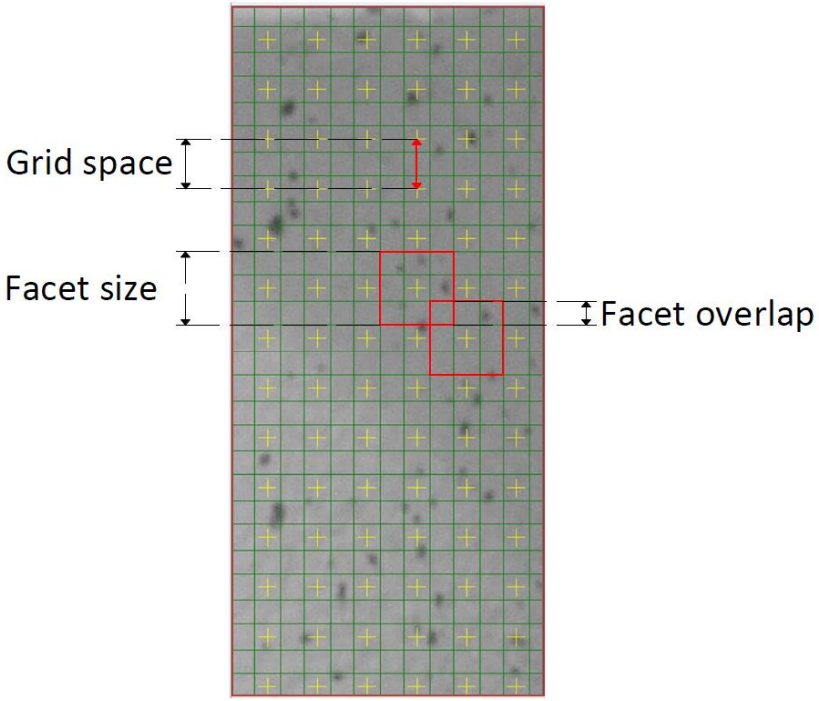
Grid space
Facet size
Facet overlap

(e)

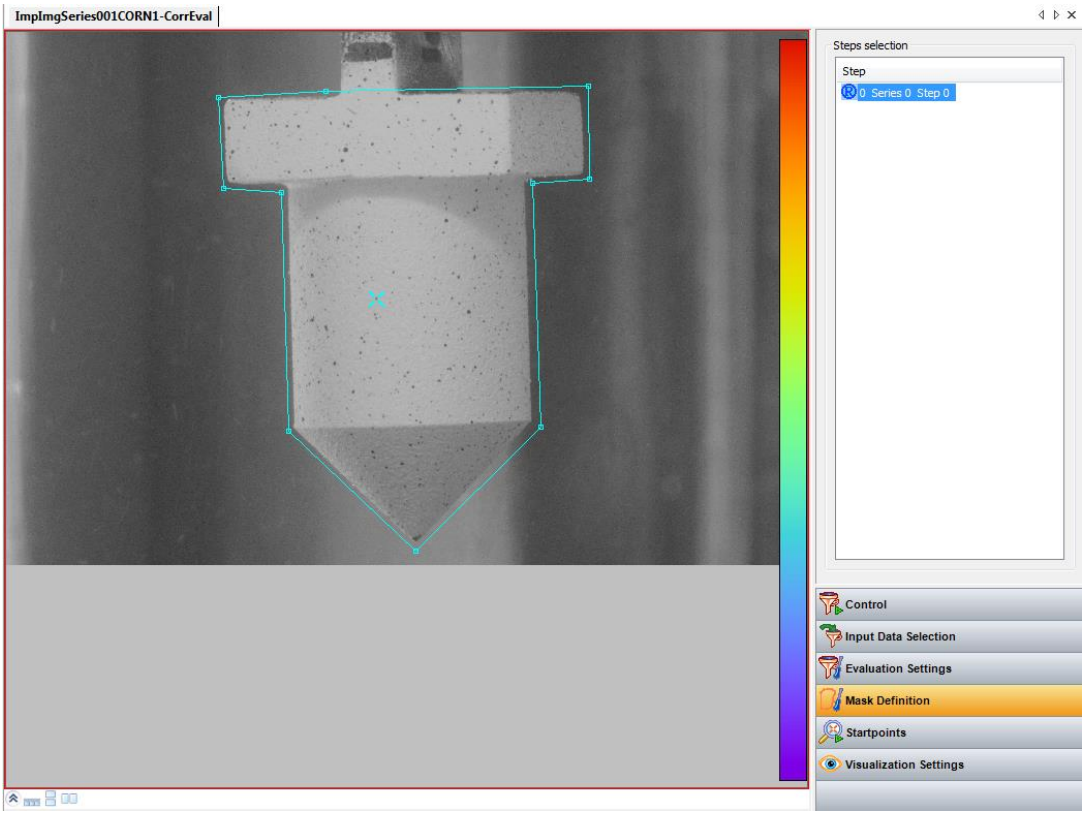
ImpImgSeries001CORN1-CorrEval
Steps selection
Step
0 Series 0 Step 0
Control
Input Data Selection
Evaluation Settings
Mask Definition
Startpoints
Visualization Settings

(f)

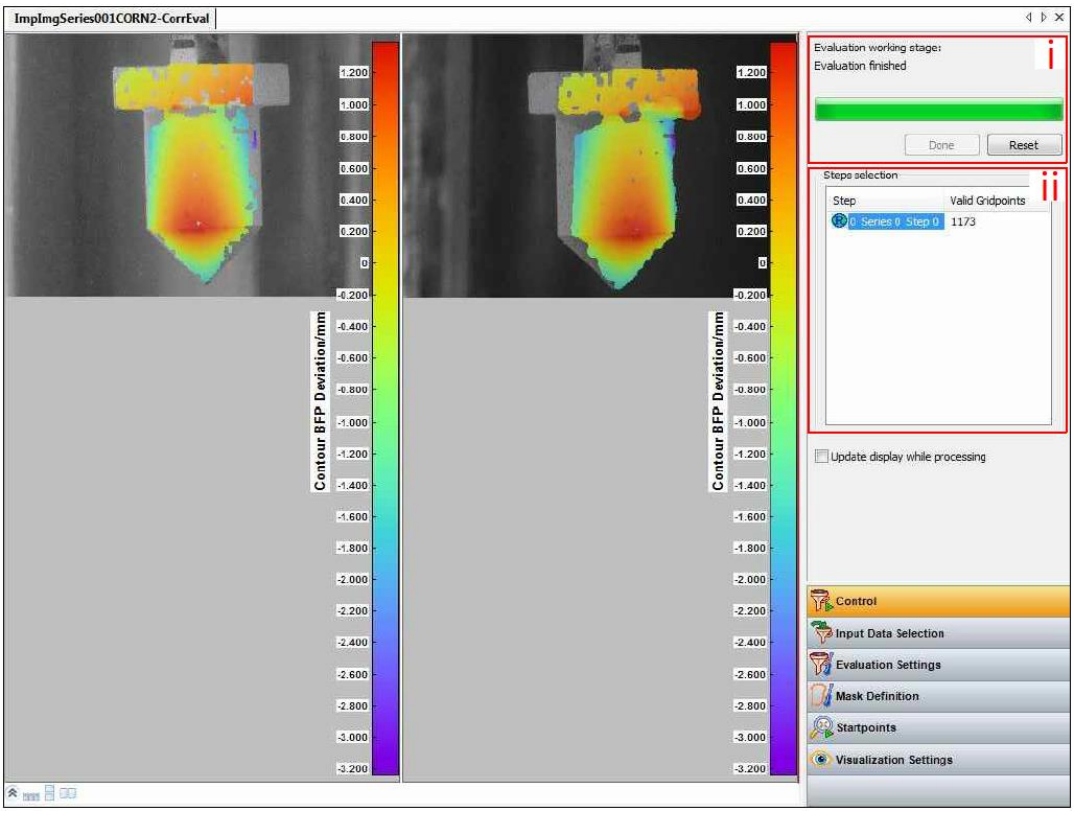
ImpImgSeries001CORN2-CorrEval
Contour BFP Deviation/mm
1.200
1.000
0.800
0.600
0.400
0.200
0
-0.200
-0.400
-0.600
-0.800
-1.000
-1.200
-1.400
-1.600
-1.800
-2.000
-2.200
-2.400
-2.600
-2.800
-3.000
-3.200
Evaluation working stage:
Evaluation finished
Done
Reset
Steps selection
Step
Valid Gridpoints
0 Series 0 Step 0
1173
Update display while processing
Control
Input Data Selection
Evaluation Settings
Mask Definition
Startpoints
Visualization Settings

(g)

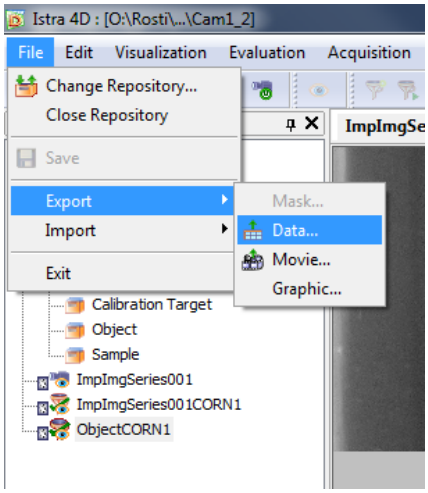

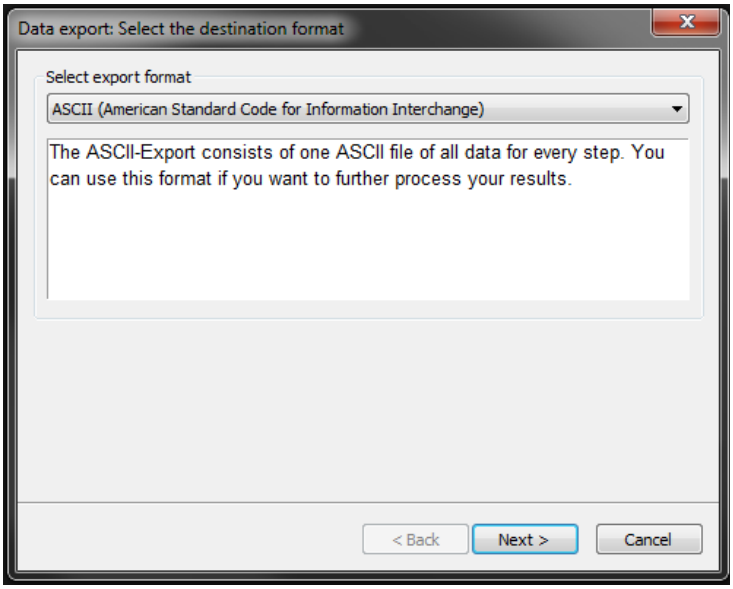

(h) **(i)**

Figure 1: Illustration, using computer screen-captures, of the steps taken to analyse images of the calibration object from two adjacent cameras (i.e. camera 1 and camera 2) using Istra4D software.

Appendix (4): Image of a CCL from a reference camera with a mask at the mid-substance of the ligament (a). Views of a CCL from the first (b), second (c) and third (d) camera pairs. The right-hand side of screen-capture panes show solved images (images with valid grid points) which were taken during loading.

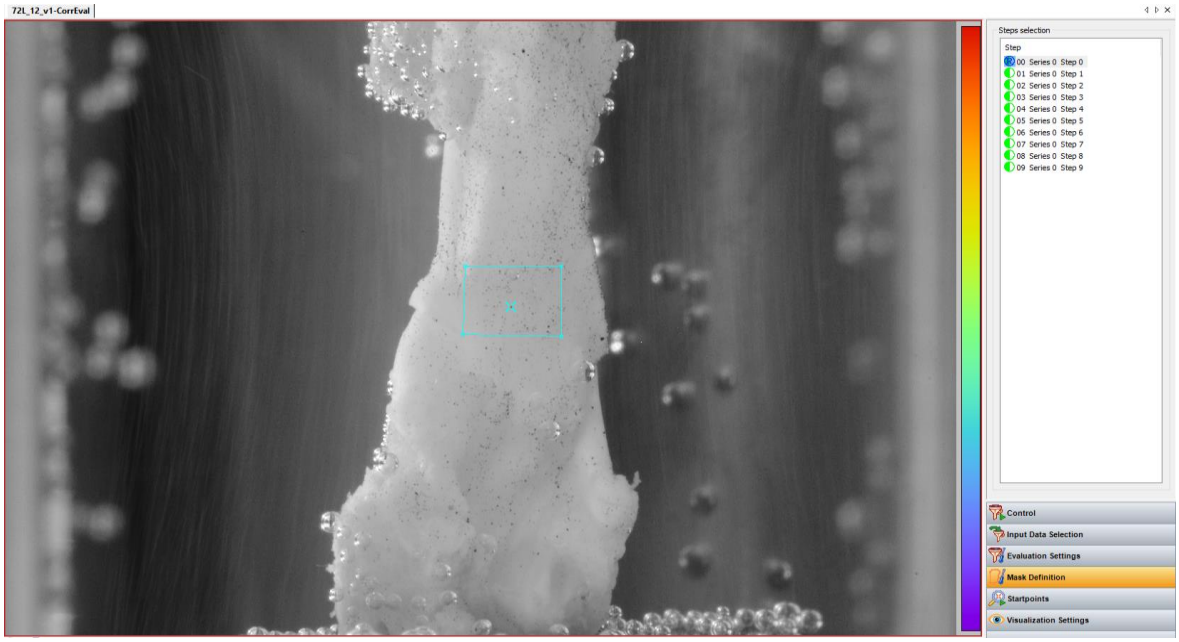

(a)

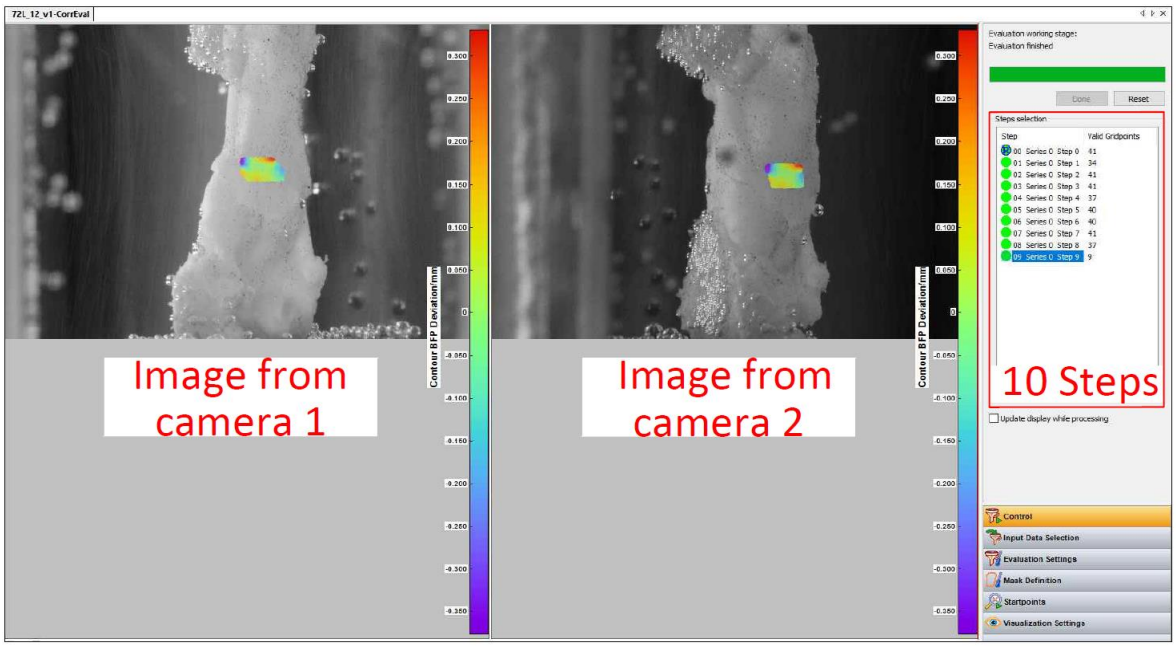

(b)

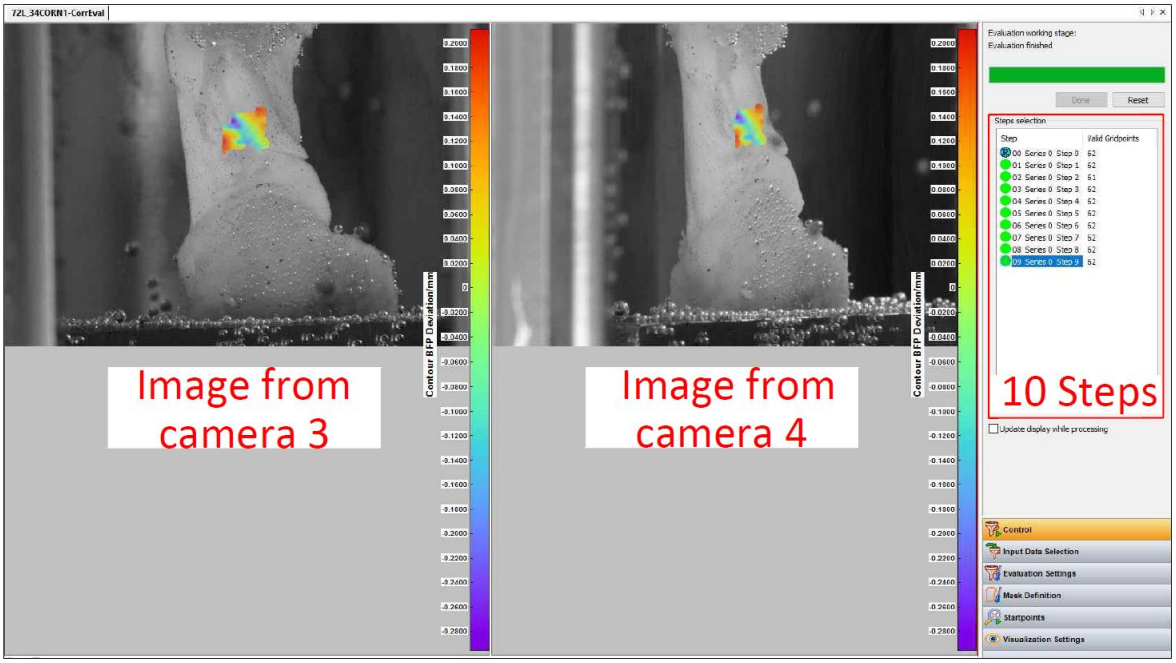

(c)

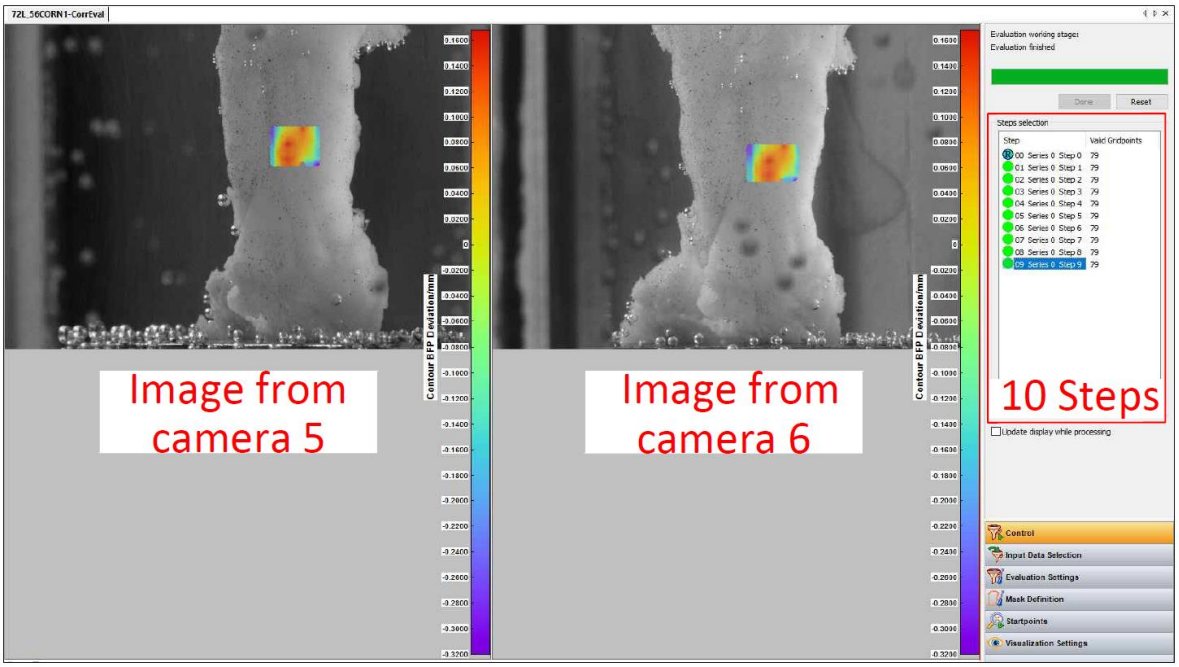

(d)

Figure 1: Image of a CCL from a reference camera with a mask at the mid-substance of the ligament (a). Views of a CCL from the first (b), second (c) and third (d) camera pairs. The right-hand side of screen-capture panes show solved images (images with valid grid points) which were taken during loading.

Appendix (5): Optimisation code used in MATLAB for defining the geometry of the calibration object and performing the iterative closest point algorithm.

```
%% Optimisation of three surfaces using ICP
%% %%%%%%%%%%%%%%%%Generating the cylinder shape%%%%%%%%%%%%%%%%%%%%%
%Generating the cylinder
p0 = [0,0,3];
r = 4;                % r is the radius of the cylinder
n = 360;              % Plot a full cylinder (360 degrees)
a=1;
hold on
for v = 1:0.2:9;     % v is steps along cylinders axis
for u = 1:360;        % u draws a circle at each v axis step
theta = ( 2.0 * pi * ( u - 1 ) ) / n;
x(a) = p0(1) + r * cos(theta);
y(a) = p0(2) + r * sin(theta);
z(a) = p0(3) + v;
a=a+1;
end
end
%plot3(x,y,z);
%hold all
cylinder = [x; y; z];
%% %%%%%%%%%%%%%%%%%%Generating the cone shape%%%%%%%%%%%%%%%%%%%%%%%
%Generating the cone shape
m = 360;
b=1;
k=4/4;                    % the hegiht divided by radius of the cone.
for u1 = 1:0.5:360;
for r1=0:0.5:4;
A= ( 2.0 * pi * ( u1 - 1 ) ) / m;
x2(b) = r1* cos(A);
y2(b) = r1* sin(A);
```

```
z2(b) = k*r1;
b=b+1;
end
end
%plot3(x2,y2,z2);
cone = [x2; y2; z2];
%% %%%%%%%%%%%%%%%%%%Generating the cubic shape%%%%%%%%%%%%%%%%%%%%%%%
%Generating the cubic shape
%Bottom
[Xp1,Yp1,Zp1]=meshgrid(-5:1:5, 5, 12);
[Xp2,Yp2,Zp2]=meshgrid(5,-5:1:5,12);
[Xp3,Yp3,Zp3]=meshgrid(-5:1:5,-5,12);
[Xp4,Yp4,Zp4]=meshgrid(-5,-5:1:5,12);
Xbottom= [Xp1(:); Xp3(:); Xp2; Xp4];
Ybottom= [Yp1(:); Yp3(:); Yp2; Yp4];
Zbottom= [Zp1(:); Zp3(:); Zp2; Zp4];
[xb, yb, zb] = meshgrid(Xbottom, Ybottom, Zbottom);
%Top
[Xp5,Yp5,Zp5]=meshgrid(-5:1:5, 5, 15);
[Xp6,Yp6,Zp6]=meshgrid(5,-5:1:5,15);
[Xp7,Yp7,Zp7]=meshgrid(-5:1:5,-5,15);
[Xp8,Yp8,Zp8]=meshgrid(-5,-5:1:5,15);
Xtop= [Xp5(:); Xp7(:); Xp6; Xp8];
Ytop= [Yp5(:); Yp7(:); Yp6; Yp8];
Ztop= [Zp5(:); Zp7(:); Zp6; Zp8];
[xt, yt, zt] = meshgrid(Xtop, Ytop, Ztop);
%side1
[Xps01,Yps01,Zps01]=meshgrid(-5:1:5, 5, 12);
[Xps11,Yps11,Zps11]=meshgrid(5, 5, 12:1:15);
[Xps21,Yps21,Zps21]=meshgrid(-5:1:5, 5, 15);
[Xps32,Yps32,Zps32]=meshgrid(-5, 5, 12:1:15);
Xside1= [Xps01(:); Xps11(:); Xps21(:); Xps32(:)];
Yside1= [Yps01(:); Yps11(:); Yps21(:); Yps32(:)];
Zside1= [Zps01(:); Zps11(:); Zps21(:); Zps32(:)];
```

```
[xs1, ys1, zs1] = meshgrid(Xside1, Yside1, Zside1);
%side2
[Xps02,Yps02,Zps02]=meshgrid(5,-5:1:5,12);
[Xps12,Yps12,Zps12]=meshgrid(5, -5, 12:1:15);
[Xps22,Yps22,Zps22]=meshgrid(5, -5:1:5,15);
[Xps32,Yps32,Zps32]=meshgrid(5, 5, 12:1:15);
Xside2= [Xps02(:); Xps12(:); Xps22(:); Xps32(:)];
Yside2= [Yps02(:); Yps12(:); Yps22(:); Yps32(:)];
Zside2= [Zps02(:); Zps12(:); Zps22(:); Zps32(:)];
[xs2, ys2, zs2] = meshgrid(Xside2, Yside2, Zside2);
%side3
[Xps03,Yps03,Zps03]=meshgrid(-5:1:5,-5,12);
[Xps13,Yps13,Zps13]=meshgrid(-5, -5, 12:1:15);
[Xps23,Yps23,Zps23]=meshgrid(-5:1:5,-5,15);
[Xps33,Yps33,Zps33]=meshgrid(5, -5, 12:1:15);
Xside3= [Xps03(:); Xps13(:); Xps23(:); Xps33(:)];
Yside3= [Yps03(:); Yps13(:); Yps23(:); Yps33(:)];
Zside3= [Zps03(:); Zps13(:); Zps23(:); Zps33(:)];
[xs3, ys3, zs3] = meshgrid(Xside3, Yside3, Zside3);
%side4
[Xps04,Yps04,Zps04]=meshgrid(-5, -5:1:5, 12);
[Xps14,Yps14,Zps14]=meshgrid(-5,-5:1:5,12);
[Xps24,Yps24,Zps24]=meshgrid(-5,-5:1:5,15);
[Xps34,Yps34,Zps34]=meshgrid(-5, 5, 12:1:15);
Xside4= [Xps04(:); Xps14(:); Xps24(:); Xps34(:)];
Yside4= [Yps04(:); Yps14(:); Yps24(:); Yps34(:)];
Zside4= [Zps04(:); Zps14(:); Zps24(:); Zps34(:)];
[xs4, ys4, zs4] = meshgrid(Xside4, Yside4, Zside4);
Xall = [xb(:); xt(:); xs1(:); xs2(:); xs3(:); xs4(:)];
Yall = [yb(:); yt(:); ys1(:); ys2(:); ys3(:); ys4(:)];
Zall = [zb(:); zt(:); zs1(:); zs2(:); zs3(:); zs4(:)];
cubic = [Xall Yall Zall];
%plot3(Xall,Yall,Zall);
AllShape=[cylinder, cone, cubic.'];
```

```
nAllShape= length (AllShape);
%% %%%%%%%%%%%%%%%%%%%%%Load surface data%%%%%%%%%%%%%%%%%%%%%%%%%%%%
vect012=vect012';   %loading the data for surface 1
vect034=vect034';   %loading the data for surface 2
vect056=vect056';   %loading the data for surface 3
n12 = length (vect012);
n34 = length (vect034);
n56 = length (vect056);
%% %%%%%%%%%%%%%%%%%%%%%%%Translation%%%%%%%%%%%%%%%%%%%%%%%%%%%%%%%%%%
%Surface 1 translation (if needed)
Tx1 = -0.1; %Translation value in x
Ty1 = -0.5; %Translation value in y
Tz1 = 8.7; %Translation value in z
T1 = [Tx1; Ty1; Tz1];
%************************************************************
%Surface 2 translation (if needed)
Tx2 = 0.5; %Translation value in x
Ty2 = 0.1; %Translation value in y
Tz2 = 7; %Translation value in z
T2 = [Tx2; Ty2; Tz2];
%************************************************************
%Surface 3 translation (if needed)
Tx3 = 1; %Translation value in x
Ty3 = 1.3; %Translation value in y
Tz3 = 9; %Translation value in z
T3 = [Tx3; Ty3; Tz3];
%% %%%%%%%%%%%%%%%%%%%%%%%Rotation%%%%%%%%%%%%%%%%%%%%%%%%%%%%%%%%%%%%
rx1 = 0.508*pi;        %Rotation value (rad) in x for surface 1
ry1 = 0.025;       %Rotation value (rad) in y for surface 1
rz1 = 2*pi;        %Rotation value (rad) in z for surface 1
rx2 = 0.465*pi;      %Rotation value (rad) in x for surface 2
ry2 = 10.04;        %Rotation value (rad) in y for surface 2
rz2 =1.95*pi;    %Rotation value (rad) in z for surface 2
rx3 = 0.45*pi;      %Rotation value (rad) in x for surface 3
```

```
ry3 = 0.73*pi;          %Rotation value (rad) in y for surface 3
rz3 = 2.03*pi;    %Rotation value (rad) in z for surface 3
%Surface 1 rotation
Rx1 = [1 0 0;
    0 cos(rx1) -sin(rx1);
    0 sin(rx1) cos(rx1)];
Ry1 = [cos(ry1) 0 sin(ry1);
      0 1 0;
      -sin(ry1) 0 cos(ry1)];
Rz1 = [cos(rz1) -sin(rz1) 0;
      sin(rz1) cos(rz1) 0;
      0 0 1];
R1 = Rx1*Ry1*Rz1;                    %Rotation matrix
M1 = R1*vect012+repmat (T1,1,n12);   %Apply rotation & translation
x_rot12=M1(1,:);
y_rot12=M1(2,:);
z_rot12=M1(3,:);
nM1 = length (M1);
%************************************************************
%Surface 2 rotation
Rx2 = [1 0 0;
    0 cos(rx2) -sin(rx2);
    0 sin(rx2) cos(rx2)];
Ry2 = [cos(ry2) 0 sin(ry2);
      0 1 0;
      -sin(ry2) 0 cos(ry2)];
Rz2 = [cos(rz2) -sin(rz2) 0;
      sin(rz2) cos(rz2) 0;
      0 0 1];
R2 = Rx2*Ry2*Rz2;                    %Rotation matrix
M2 = R2*vect034+repmat (T2,1,n34);   %Apply rotation & translation;
x_rot34=M2(1,:);
y_rot34=M2(2,:);
z_rot34=M2(3,:);
```

```
nM2 = length (M2);
%************************************************************
%Surface 3 rotation
Rx3 = [1 0 0;
    0 cos(rx3) -sin(rx3);
    0 sin(rx3) cos(rx3)];
Ry3 = [cos(ry3) 0 sin(ry3);
      0 1 0;
      -sin(ry3) 0 cos(ry3)];
Rz3 = [cos(rz3) -sin(rz3) 0;
      sin(rz3) cos(rz3) 0;
      0 0 1];
R3 = Rx3*Ry3*Rz3;                    %Rotation matrix
M3 = R3*vect056 +repmat (T3,1,n56);  %Apply rotation & translation;
x_rot56=M3(1,:);
y_rot56=M3(2,:);
z_rot56=M3(3,:);
nM3 = length (M3);
%% %%%%%%%%%%%%%%RUN ITERATIVE CLOSEST POINTS (ICP)%%%%%%%%%%%%%%%%%%
% Run ICP (fast kDtree matching and extrapolation)
%ICP on surface 1
[Ricp1 Ticp1 ER1 t1] = icp(AllShape, M1,60, 'Matching', 'kDtree',
'Extrapolation', true);
%ICP on surface 2
[Ricp2 Ticp2 ER2 t2] = icp(AllShape, M2, 60, 'Matching', 'kDtree',
'Extrapolation', true);
%ICP on surface 3
[Ricp3 Ticp3 ER3 t3] = icp(AllShape, M3, 60, 'Matching', 'kDtree',
'Extrapolation', true);
% Transform data-matrix using ICP result
Dicp1 = Ricp1 * M1 + repmat(Ticp1, 1, nM1); %surface 1
Dicp2 = Ricp2 * M2 + repmat(Ticp2, 1, nM2); %surface 2
Dicp3 = Ricp3 * M3 + repmat(Ticp3, 1, nM3); %surface 3
%%%%%%%%%%%%%%%%%%%%%%%%%Plot the results%%%%%%%%%%%%%%%%%%%%%%%%%%%%
plot3(Dicp1(1,:),Dicp1(2,:),Dicp1(3,:),'m.');
plot3(Dicp2(1,:),Dicp2(2,:),Dicp2(3,:),'g.');
```

```
plot3(Dicp3(1,:),Dicp3(2,:),Dicp3(3,:),'r.');
% figure
% hold all
% axis equal;
% xlabel('x'); ylabel('y'); zlabel('z');
% title('ICP result');
% figure
% % Plot RMS curve - surface 1
% subplot(2,2,[3 4]);
% plot(0:60,ER1,'--x');
% xlabel('iteration#');
% ylabel('d_(Stylianou et al.)');
% legend('kDtree matching and extrapolation');
% title(['Total elapsed time: ' num2str(t1(end),2) ' s']);
% figure
% % Plot RMS curve - surface 2
% subplot(2,2,1);
% plot(0:60,ER2,'--x');
% xlabel('iteration#');
% ylabel('d_(Stylianou et al.)');
% legend('kDtree matching and extrapolation');
% title(['Total elapsed time: ' num2str(t2(end),2) ' s']);
% figure
% % Plot RMS curve - surface 3
% subplot(2,2,2);
% plot(0:60,ER3,'--x');
% xlabel('iteration#');
% ylabel('d_(Stylianou et al.)');
% legend('kDtree matching and extrapolation');
% title(['Total elapsed time: ' num2str(t3(end),2) ' s']);
%% %%%%%%%%%%%%%%Apply Corrections to CCL Surfaces%%%%%%%%%%%%%%%%%%
%Correcting samples
sample12_corr0 = R1*(sample12')+repmat(T1,1,length(sample12));
sample34_corr0 = R2*(sample34')+repmat(T2,1,length(sample34));
```

```
sample56_corr0 = R3*(sample56')+repmat(T3,1,length(sample56));

sample12_corr1              =             Ricp1*sample12_corr0             +
repmat(Ticp1,1,length(sample12_corr0));

sample34_corr1              =             Ricp2*sample34_corr0             +
repmat(Ticp2,1,length(sample34_corr0));

sample56_corr1              =             Ricp3*sample56_corr0             +
repmat(Ticp3,1,length(sample56_corr0));

hold all

plot3 (sample12_corr1(1,:), sample12_corr1(2,:), sample12_corr1(3,:),'r.');

plot3 (sample34_corr1(1,:), sample34_corr1(2,:), sample34_corr1(3,:),'b.');

plot3 (sample56_corr1(1,:), sample56_corr1(2,:), sample56_corr1(3,:),'g.');
```

Appendix (6): Statistical analysis for length measurements and CSA measurements for the CCLs used in the experimental studies.

Table 1: Results obtained from the statistical analysis in Experimental Study I and II.

	Cranial and Caudal Planes	**Cranial and Medial Planes**	**Cranial and Lateral Planes**	**Caudal and Medial Planes**	**Caudal and Lateral Planes**	**Medial and Lateral Planes**
Experimental Study I	$p = 1.59 \times 10^{-6}$	$p = 1.11 \times 10^{-3}$	$p = 8.21 \times 10^{-4}$	$p = 5.57 \times 10^{-5}$	$p = 8.86 \times 10^{-5}$	$p = 0.92$
Experimental Study II	$p = 3.78 \times 10^{-11}$	$p = 3.96 \times 10^{-8}$	$p = 1.50 \times 10^{-7}$	$p = 2.77 \times 10^{-5}$	$p = 2.36 \times 10^{-6}$	$p = 0.32$

Table 2: CSA of CCLs in mm^2 for Experimental Study I.

CCL Number	**Non-hanged**		**Hanged**	
	Right	**Left**	**Right**	**Left**
1	12.58	14.99	12.25	21.30
2	14.39	14.41	17.05	18.37
3	15.48	13.98	11.52	15.95
4	12.91	15.69	19.29	20.61
5	14.93	23.62	8.77	22.40
Mean ± SD	**16.09 ± 5.10**		**18.88 ± 6.55**	

Table 3: CSA of CCLs in mm^2 for Experimental Study II.

CCL Number	**Non-hanged**	
	Right (Control)	**Left (Treatment)**
1	20.14	29.21
2	25.80	31.57
3	24.05	20.81
4	20.43	28.92
5	17.98	16.07
Mean ± SD	**21.68 ± 3.17**	**25.32 ± 6.58**

Appendix (7): Data collected about the biochemical assays on Experimental Study II.

Table 1: This Table shows wet and dry weight (mg) of canine CCLs used to calculate water content (%) for Experimental Study II. The Table also shows sGAG content relative to dry weight of the CCLs (n=5 pairs).

CCLs	Wet weight (mg)	Dry weight (mg)	% Water content	Microgram of sGAG/mg dry weight	Microgram of sGAG/mg dry weight (%)
Control 1	53.56	12.10	77.41	38.11	3.81
Control 2	71.51	18.43	74.23	65.79	6.58
Control 3	86.19	23.10	73.20	21.47	2.15
Control 4	63.26	17.80	71.86	21.61	2.16
Control 5	33.25	9.13	72.54	38.68	3.87
0.25IU 1	88.18	25.31	71.30	27.17	2.72
0.25IU 2	87.66	25.14	71.32	47.00	4.70
0.25IU 3	31.96	10.05	68.55	17.12	1.71
0.25IU 4	96.33	25.75	73.27	21.99	2.20
0.25IU 5	35.25	12.08	65.73	35.19	3.52

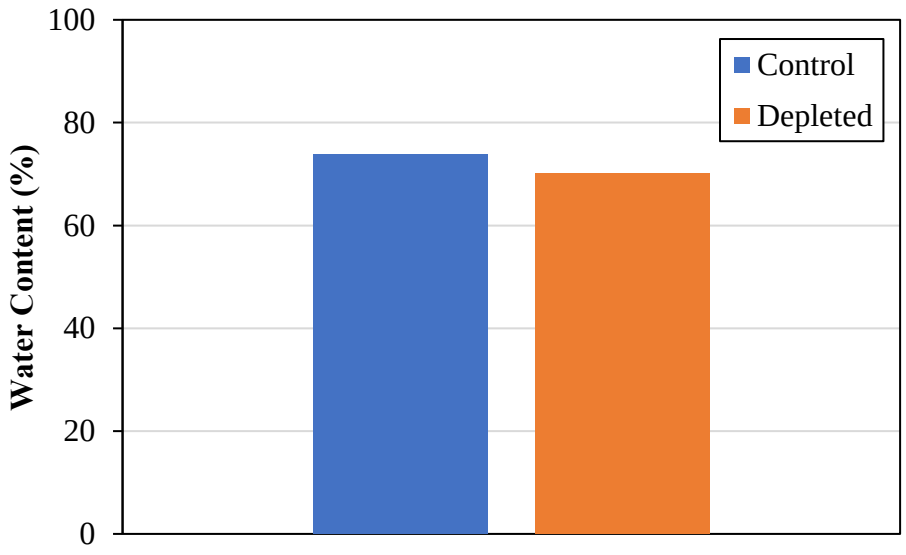

Figure 1: This Figure is based on the data presented in Appendix (4): Table 1. The Figure showing average water content (%) for the CCLs (n=5 pairs) in the control and treatment groups.

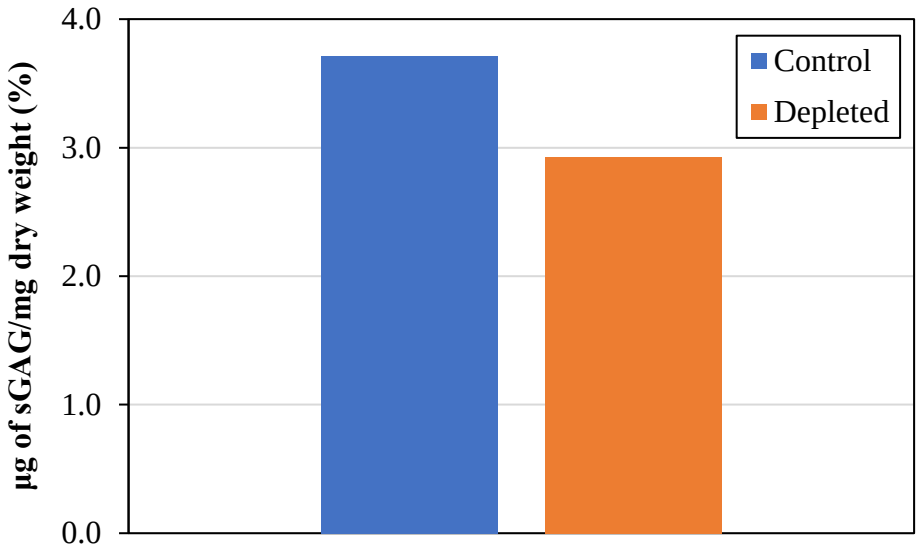

Figure 2: This Figure is based on the data presented in Appendix (4): Table 1. The Figure showing average sGAG content (%) for the CCLs (n=5 pairs) in the control and treatment groups.

Appendix (8): Load-displacement behaviour of individual ligaments tested during Experimental Study I.

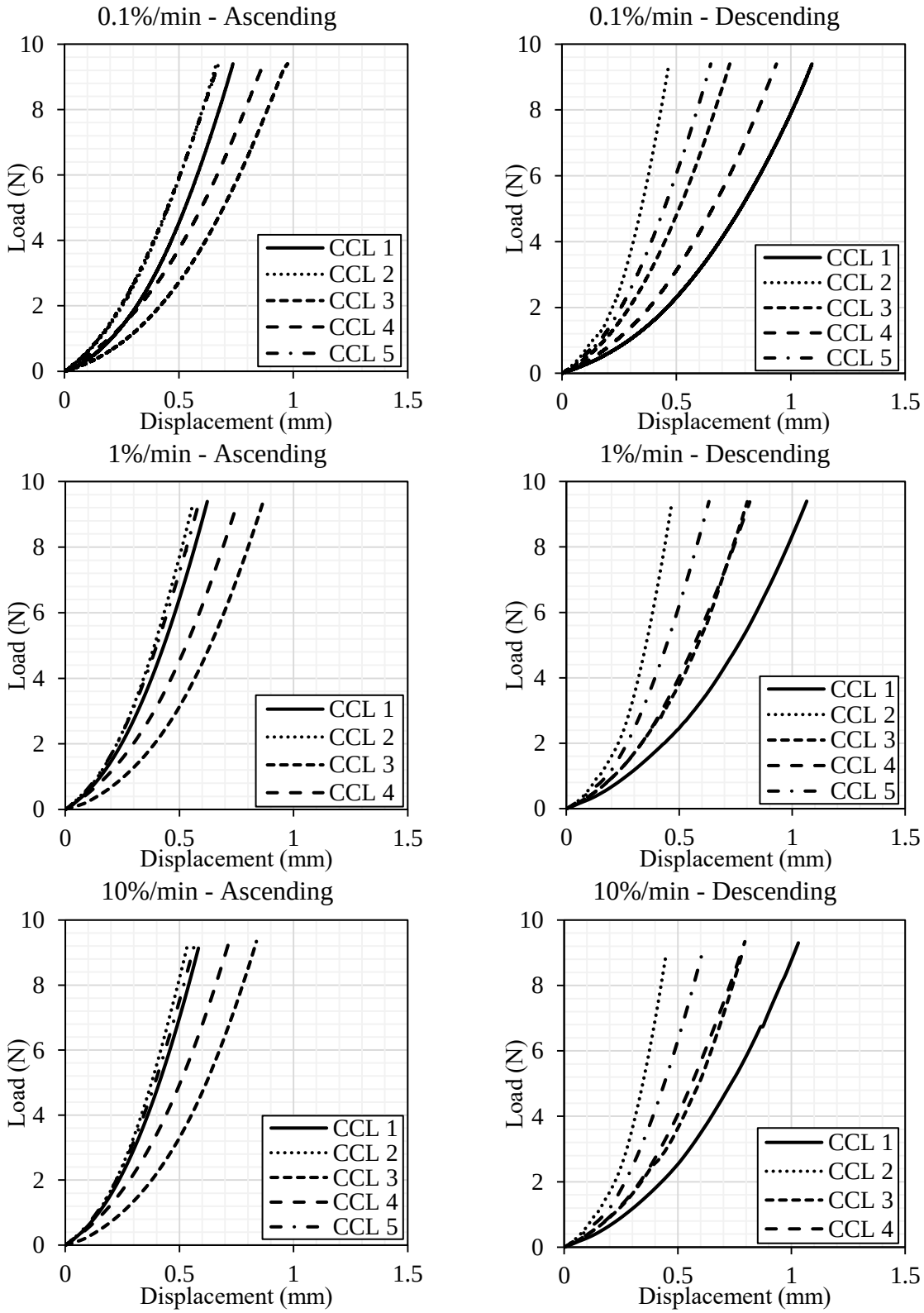

Figure 1: Shows load-displacement behaviour of ligaments (n=5) during loading at different strain rates.

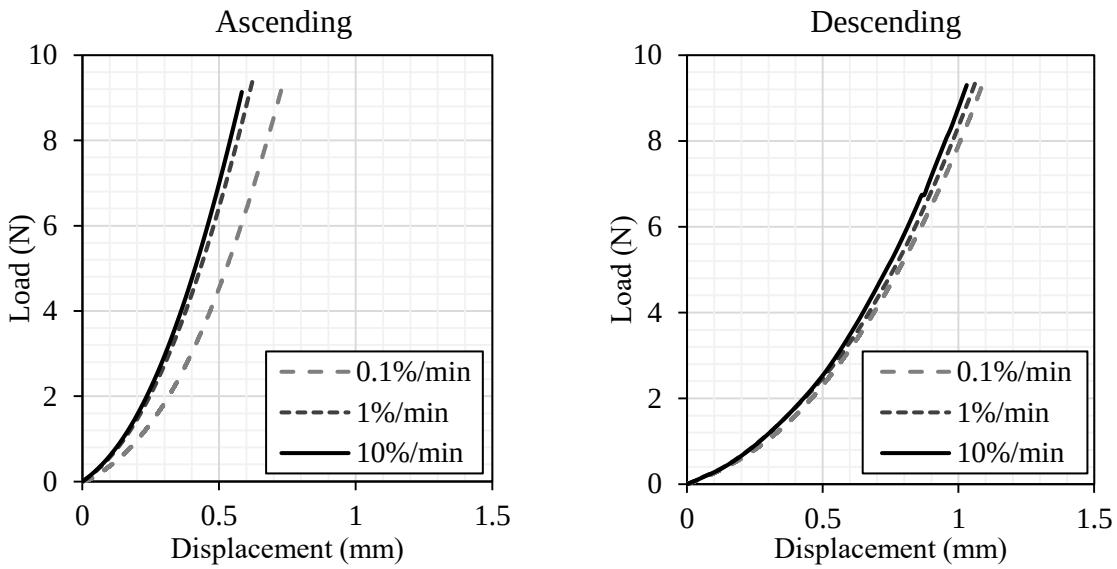

Figure 2: Shows average load-displacement behaviour of ligaments (n=5) during loading at different strain rates.

Appendix (9): Unloaded CCL - Specific FEMs.

CCL 1 (Depleted)	CCL 1 (Control)
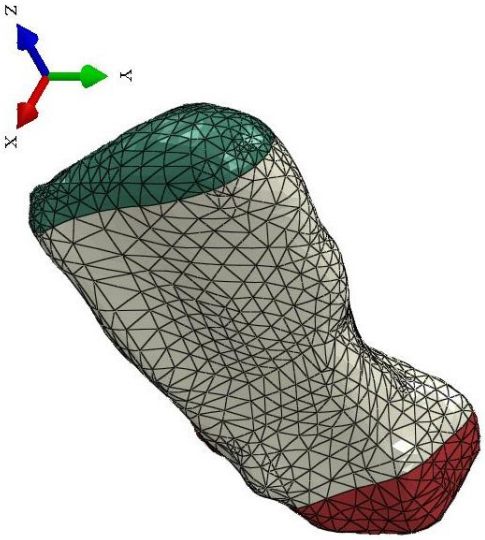	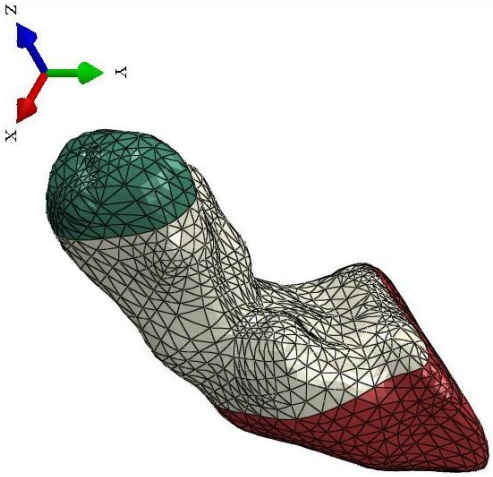
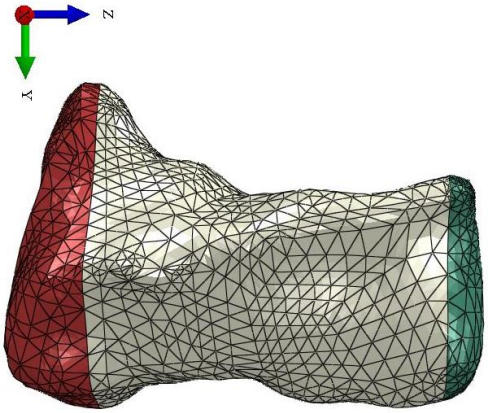	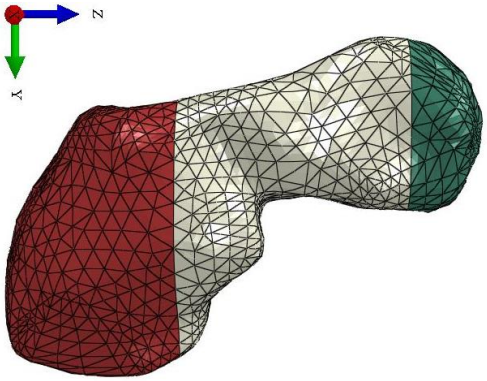
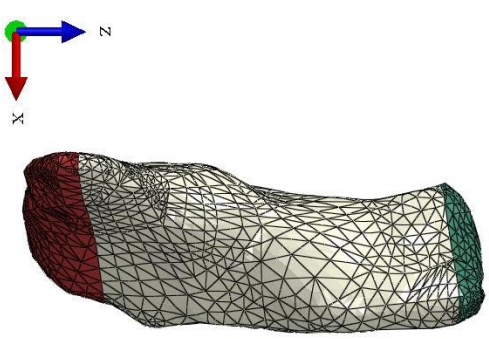	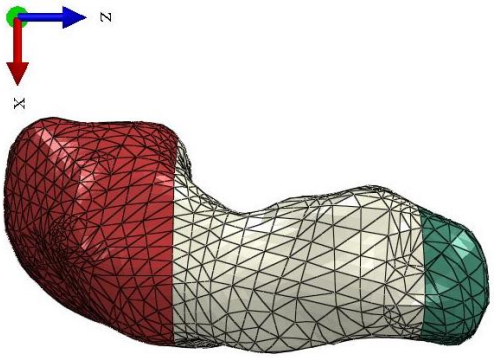

CCL 2 (Depleted)	CCL 2 (Control)
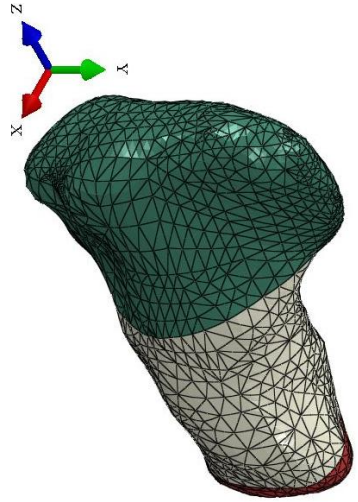	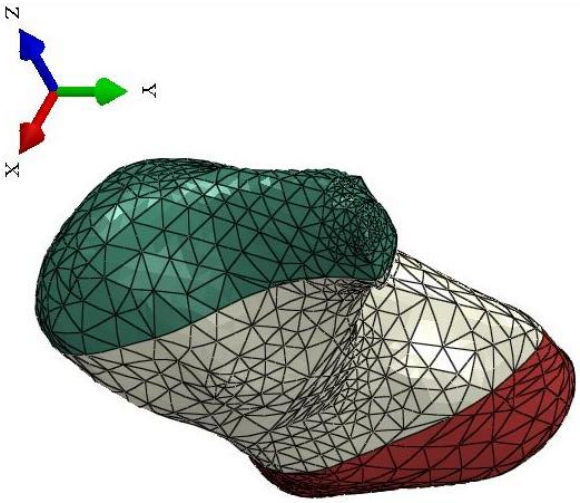
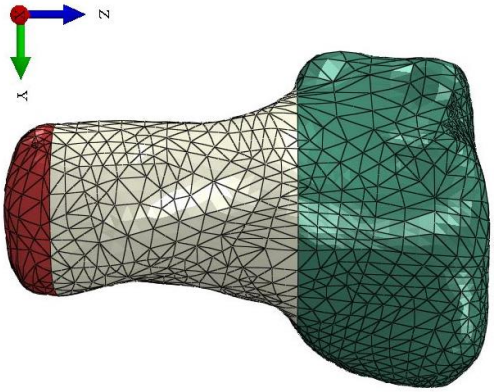	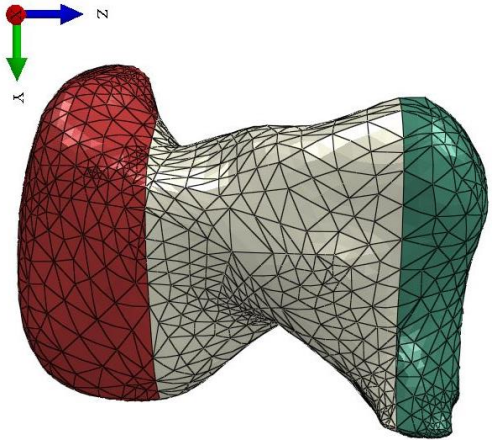
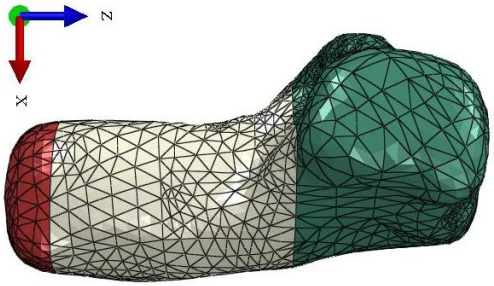	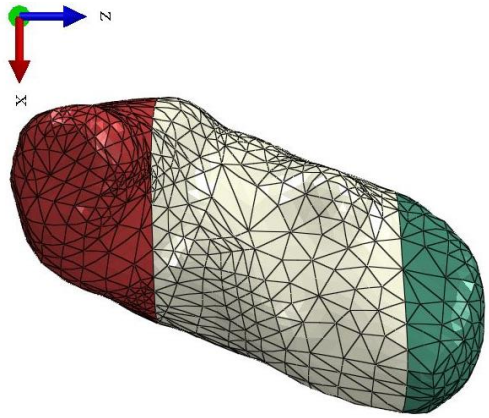

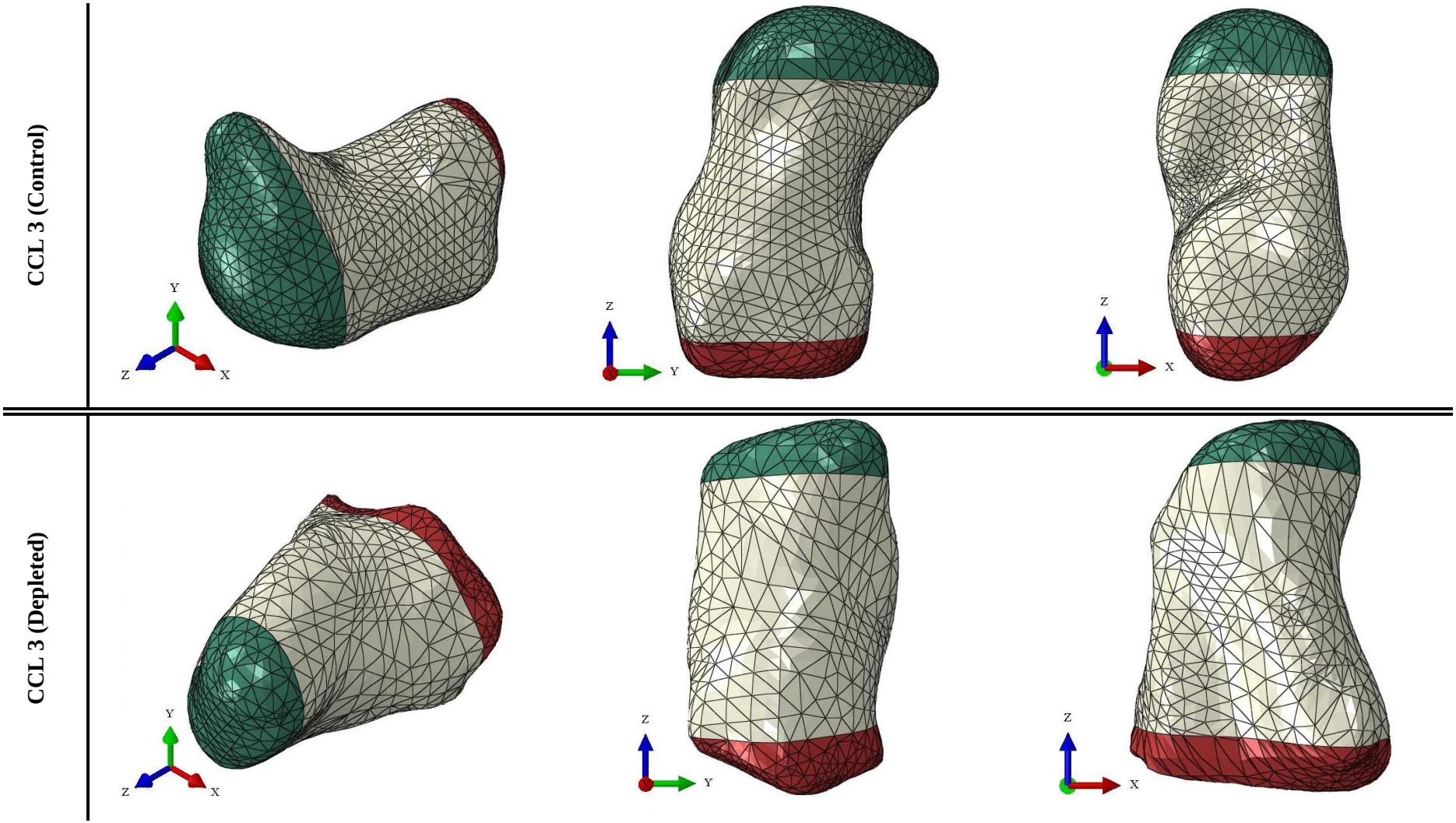
CCL 3 (Control)
CCL 3 (Depleted)
Y
Z
X
Z
Y
Z
X
Y
Z
X
Z
Y
Z
X

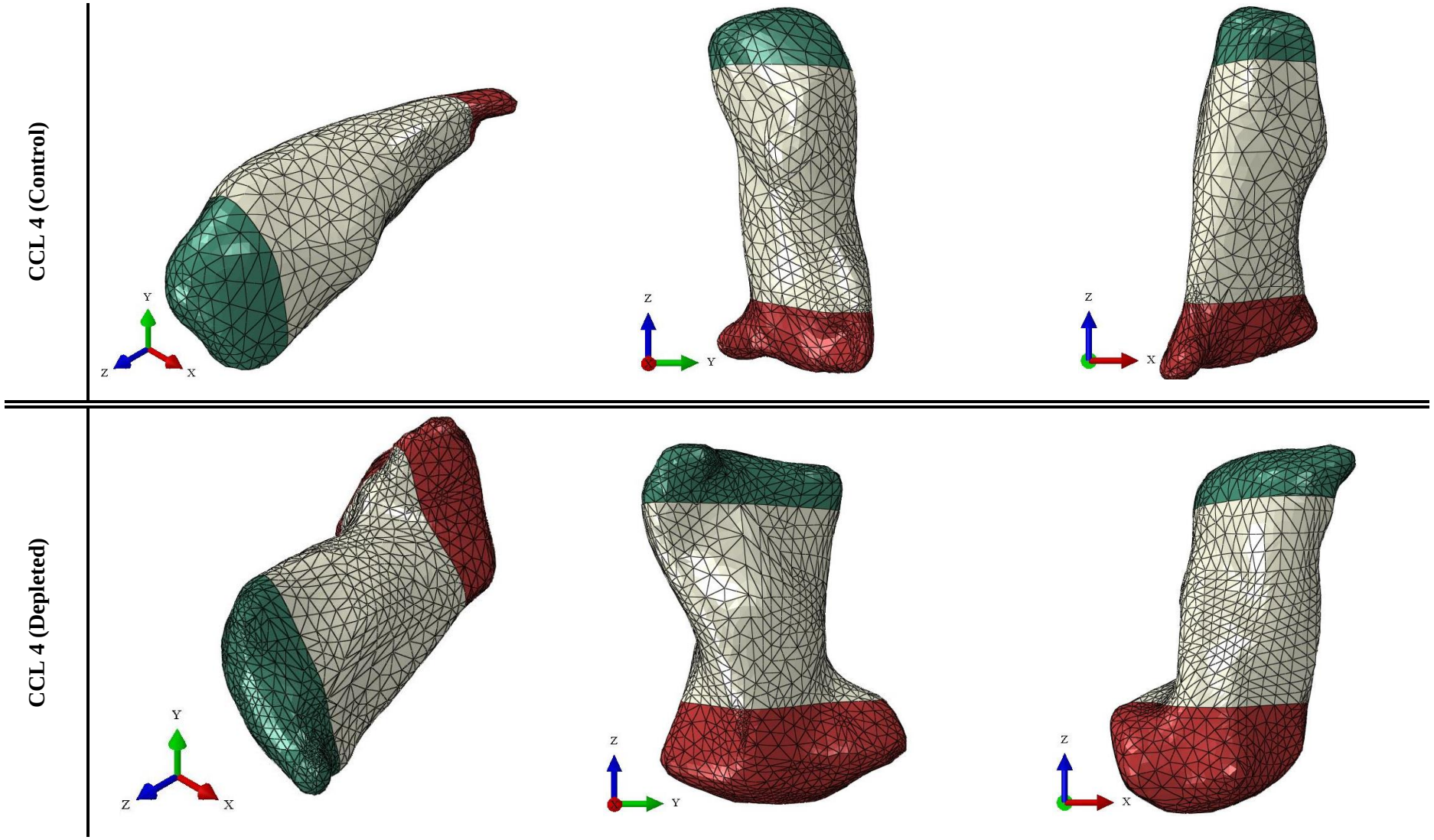
CCL 4 (Control)
CCL 4 (Depleted)
Y
Z
X
Z
Y
Z
X
Y
Z
X
Z
Y
Z
X

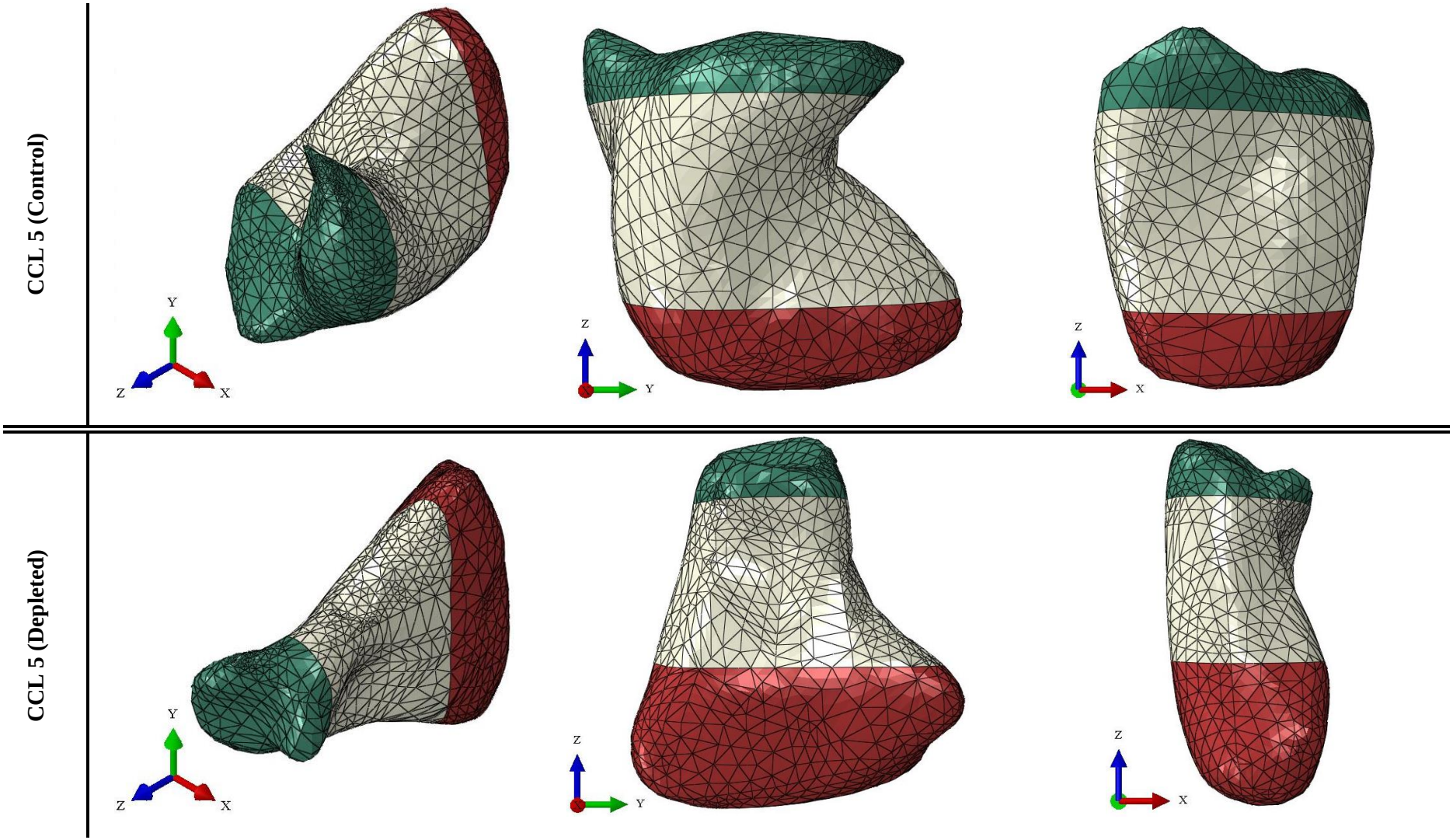

Figure 1: CCL-specific FEMs (Five CCLs in the control and five CCLs in the treatment groups) generated in Abaqus software and presented with different views which are isometric, front and back showing the femur (green) and tibia (red) bones, and the CCL mid-substance (grey).

Appendix (10): CCL-specific FEMs under loading.

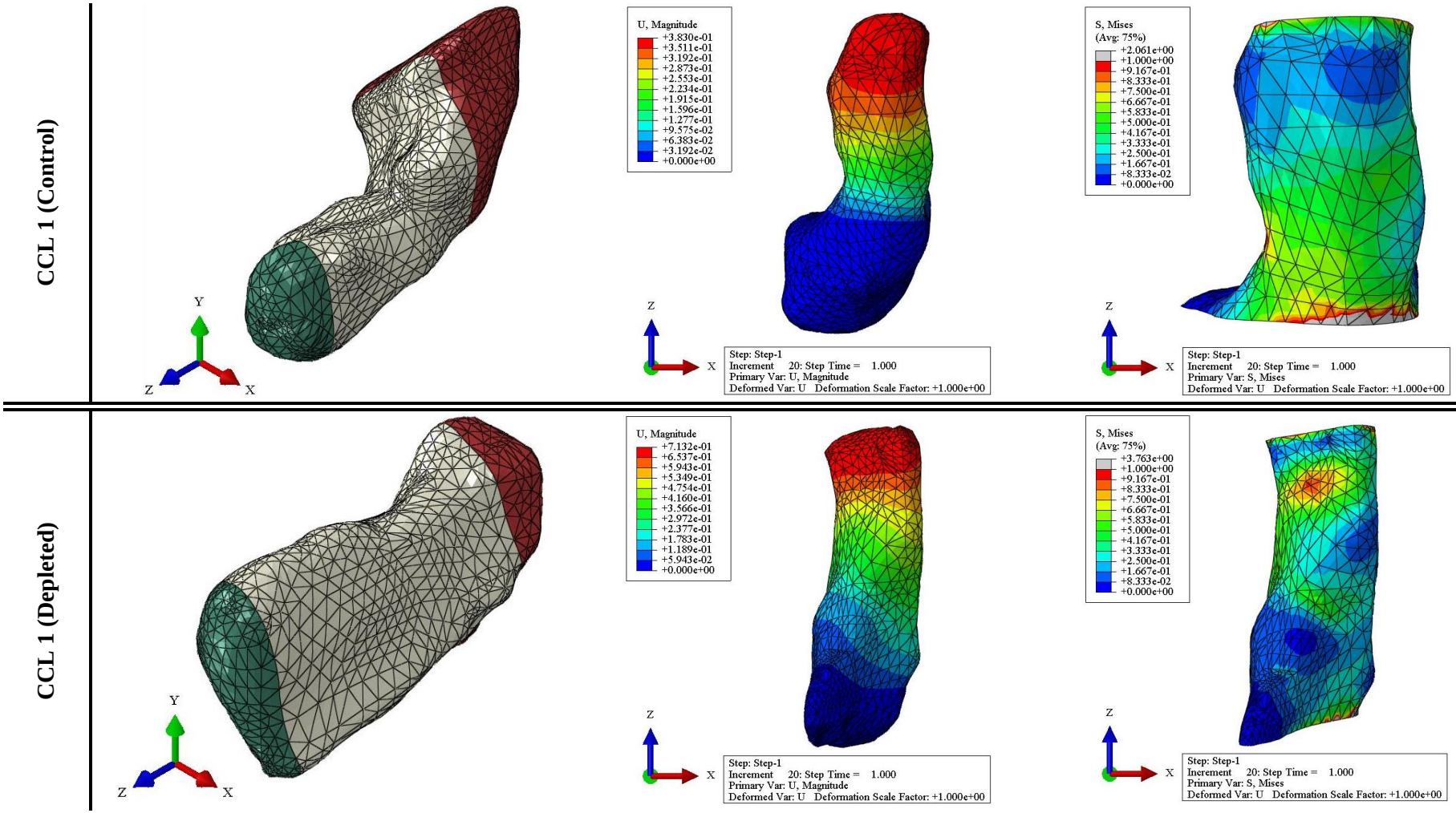
CCL 1 (Control)
U, Magnitude
+3.830e-01
+3.511e-01
+3.192e-01
+2.873e-01
+2.553e-01
+2.234e-01
+1.915e-01
+1.596e-01
+1.277e-01
+9.575e-02
+6.383e-02
+3.192e-02
+0.000e+00
S, Mises
(Avg: 75%)
+2.061e+00
+1.000e+00
+9.167e-01
+8.333e-01
+7.500e-01
+6.667e-01
+5.833e-01
+5.000e-01
+4.167e-01
+3.333e-01
+2.500e-01
+1.667e-01
+8.333e-02
+0.000e+00
Step: Step-1
Increment 20: Step Time = 1.000
Primary Var: U, Magnitude
Deformed Var: U Deformation Scale Factor: +1.000e+00
Step: Step-1
Increment 20: Step Time = 1.000
Primary Var: S, Mises
Deformed Var: U Deformation Scale Factor: +1.000e+00
CCL 1 (Depleted)
U, Magnitude
+7.132e-01
+6.537e-01
+5.943e-01
+5.349e-01
+4.754e-01
+4.160e-01
+3.566e-01
+2.972e-01
+2.377e-01
+1.783e-01
+1.189e-01
+5.943e-02
+0.000e+00
S, Mises
(Avg: 75%)
+3.763e+00
+1.000e+00
+9.167e-01
+8.333e-01
+7.500e-01
+6.667e-01
+5.833e-01
+5.000e-01
+4.167e-01
+3.333e-01
+2.500e-01
+1.667e-01
+8.333e-02
+0.000e+00
Step: Step-1
Increment 20: Step Time = 1.000
Primary Var: U, Magnitude
Deformed Var: U Deformation Scale Factor: +1.000e+00
Step: Step-1
Increment 20: Step Time = 1.000
Primary Var: S, Mises
Deformed Var: U Deformation Scale Factor: +1.000e+00

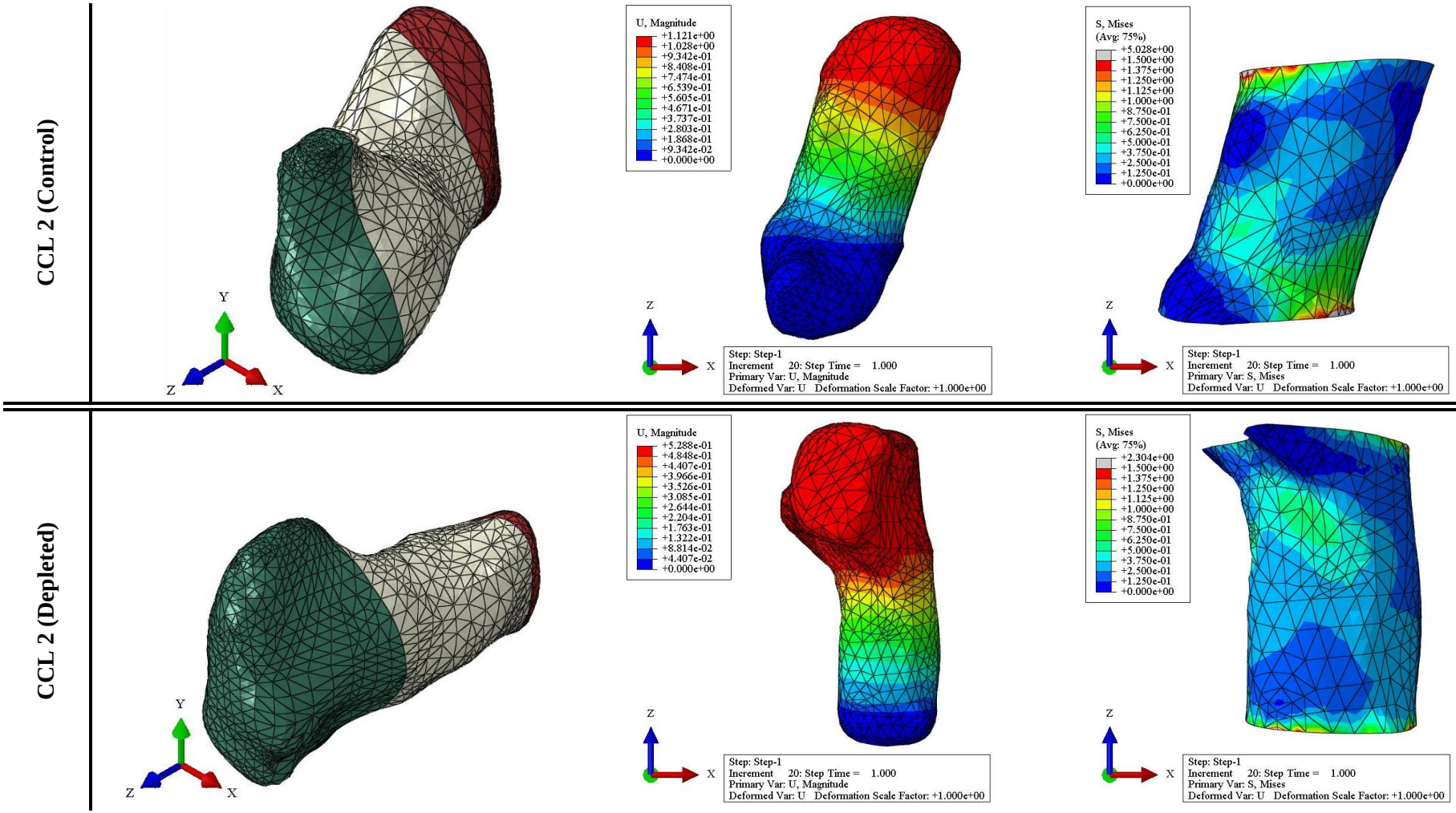
CCL 2 (Control)
CCL 2 (Depleted)
U, Magnitude
+1.121e+00
+1.028e+00
+9.342e-01
+8.408e-01
+7.474e-01
+6.539e-01
+5.605e-01
+4.671e-01
+3.737e-01
+2.803e-01
+1.868e-01
+9.342e-02
+0.000e+00
S, Mises
(Avg: 75%)
+5.028e+00
+1.500e+00
+1.375e+00
+1.250e+00
+1.125e+00
+1.000e+00
+8.750e-01
+7.500e-01
+6.250e-01
+5.000e-01
+3.750e-01
+2.500e-01
+1.250e-01
+0.000e+00
U, Magnitude
+5.288e-01
+4.848e-01
+4.407e-01
+3.966e-01
+3.526e-01
+3.085e-01
+2.644e-01
+2.204e-01
+1.763e-01
+1.322e-01
+8.814e-02
+4.407e-02
+0.000e+00
S, Mises
(Avg: 75%)
+2.304e+00
+1.500e+00
+1.375e+00
+1.250e+00
+1.125e+00
+1.000e+00
+8.750e-01
+7.500e-01
+6.250e-01
+5.000e-01
+3.750e-01
+2.500e-01
+1.250e-01
+0.000e+00
Step: Step-1
Increment 20: Step Time = 1.000
Primary Var: U, Magnitude
Deformed Var: U Deformation Scale Factor: +1.000e+00
Step: Step-1
Increment 20: Step Time = 1.000
Primary Var: S, Mises
Deformed Var: U Deformation Scale Factor: +1.000e+00
Step: Step-1
Increment 20: Step Time = 1.000
Primary Var: U, Magnitude
Deformed Var: U Deformation Scale Factor: +1.000e+00
Step: Step-1
Increment 20: Step Time = 1.000
Primary Var: S, Mises
Deformed Var: U Deformation Scale Factor: +1.000e+00
Y
Z
X

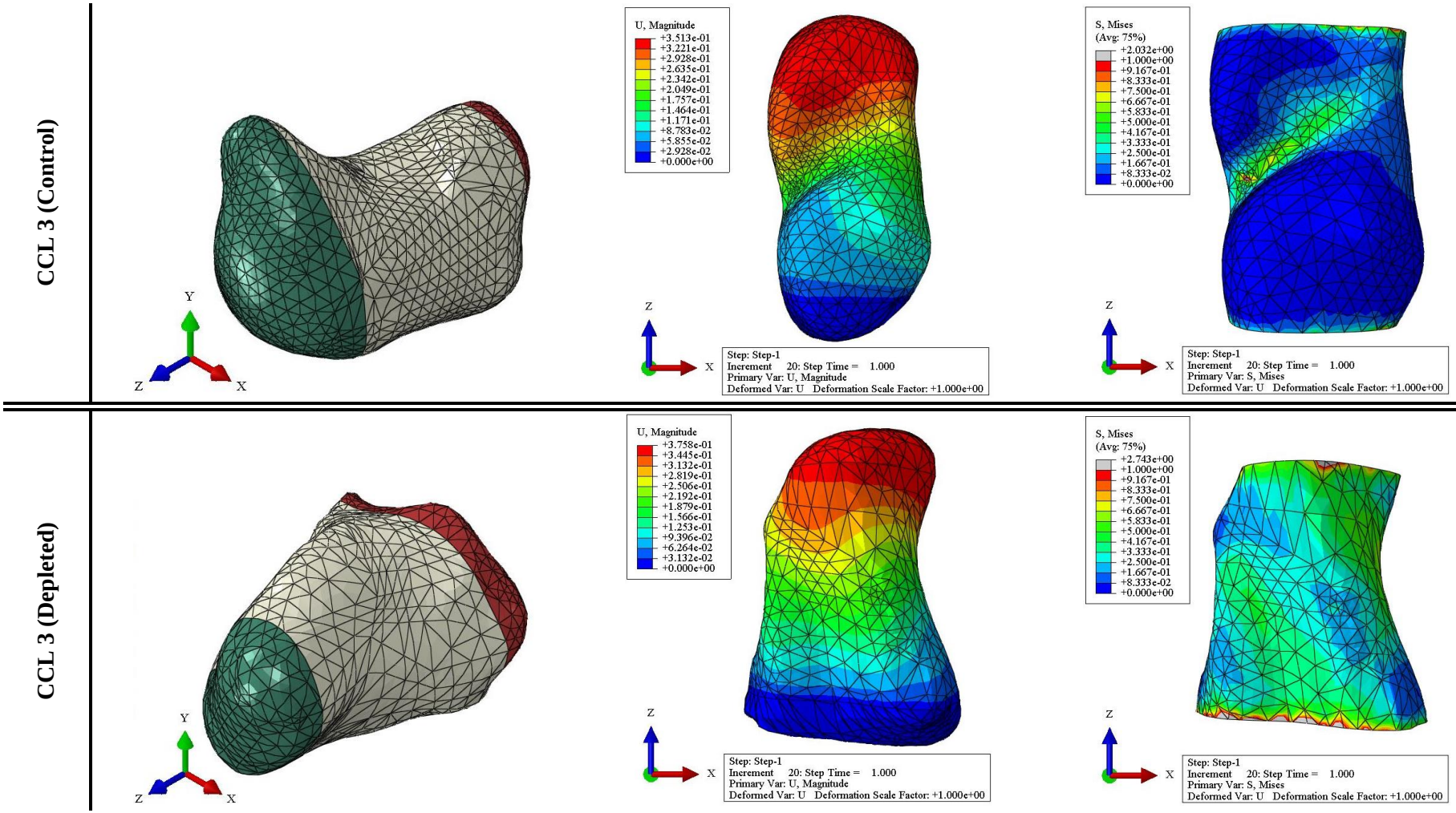
CCL 3 (Control)
U, Magnitude
+3.513e-01
+3.221e-01
+2.928e-01
+2.635e-01
+2.342e-01
+2.049e-01
+1.757e-01
+1.464e-01
+1.171e-01
+8.783e-02
+5.855e-02
+2.928e-02
+0.000e+00
S, Mises
(Avg: 75%)
+2.032e+00
+1.000e+00
+9.167e-01
+8.333e-01
+7.500e-01
+6.667e-01
+5.833e-01
+5.000e-01
+4.167e-01
+3.333e-01
+2.500e-01
+1.667e-01
+8.333e-02
+0.000e+00
Step: Step-1
Increment 20: Step Time = 1.000
Primary Var: U, Magnitude
Deformed Var: U Deformation Scale Factor: +1.000e+00
Step: Step-1
Increment 20: Step Time = 1.000
Primary Var: S, Mises
Deformed Var: U Deformation Scale Factor: +1.000e+00
CCL 3 (Depleted)
U, Magnitude
+3.758e-01
+3.445e-01
+3.132e-01
+2.819e-01
+2.506e-01
+2.192e-01
+1.879e-01
+1.566e-01
+1.253e-01
+9.396e-02
+6.264e-02
+3.132e-02
+0.000e+00
S, Mises
(Avg: 75%)
+2.743e+00
+1.000e+00
+9.167e-01
+8.333e-01
+7.500e-01
+6.667e-01
+5.833e-01
+5.000e-01
+4.167e-01
+3.333e-01
+2.500e-01
+1.667e-01
+8.333e-02
+0.000e+00
Step: Step-1
Increment 20: Step Time = 1.000
Primary Var: U, Magnitude
Deformed Var: U Deformation Scale Factor: +1.000e+00
Step: Step-1
Increment 20: Step Time = 1.000
Primary Var: S, Mises
Deformed Var: U Deformation Scale Factor: +1.000e+00

CCL 4 (Control)

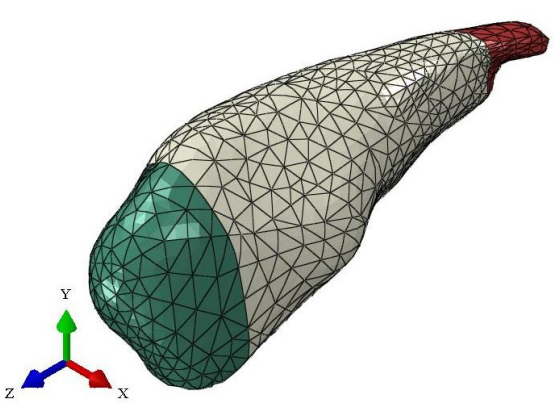

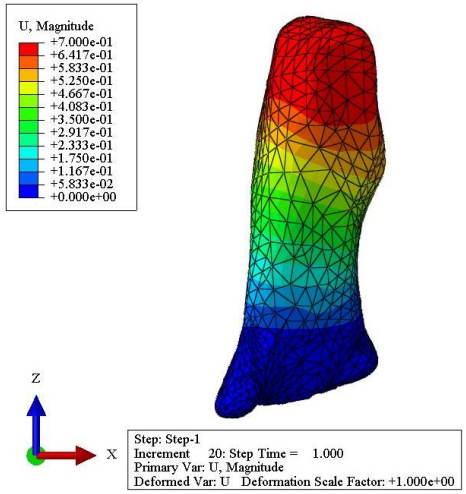

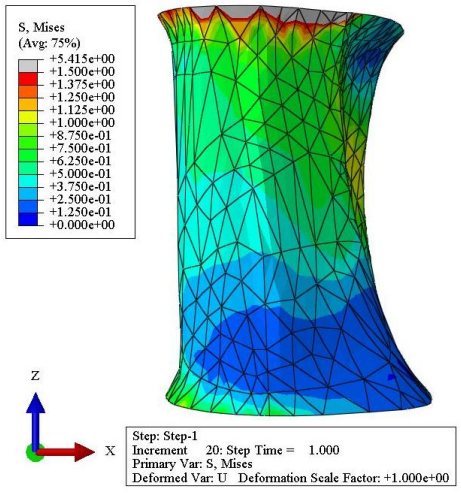

CCL 4 (Depleted)

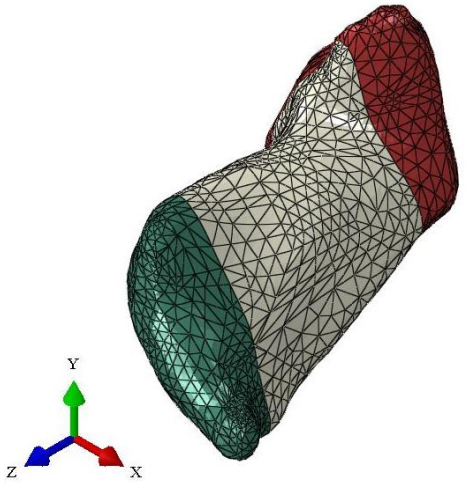

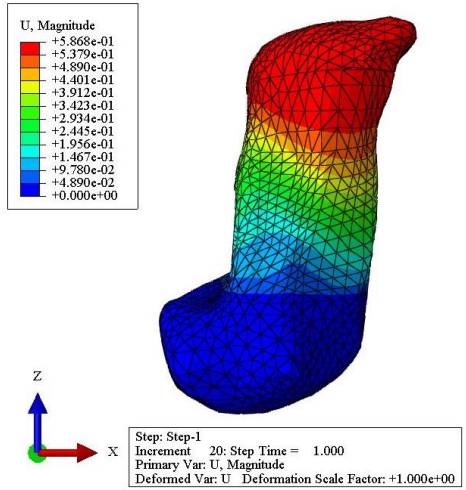

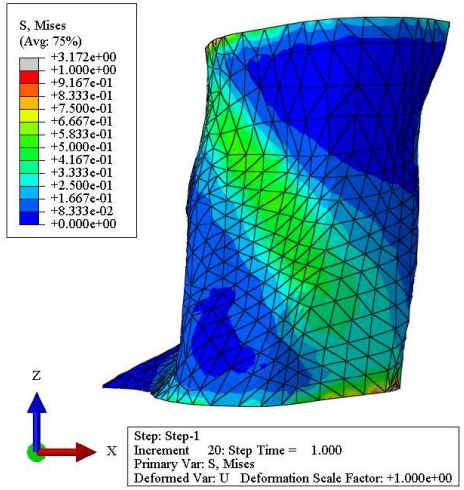

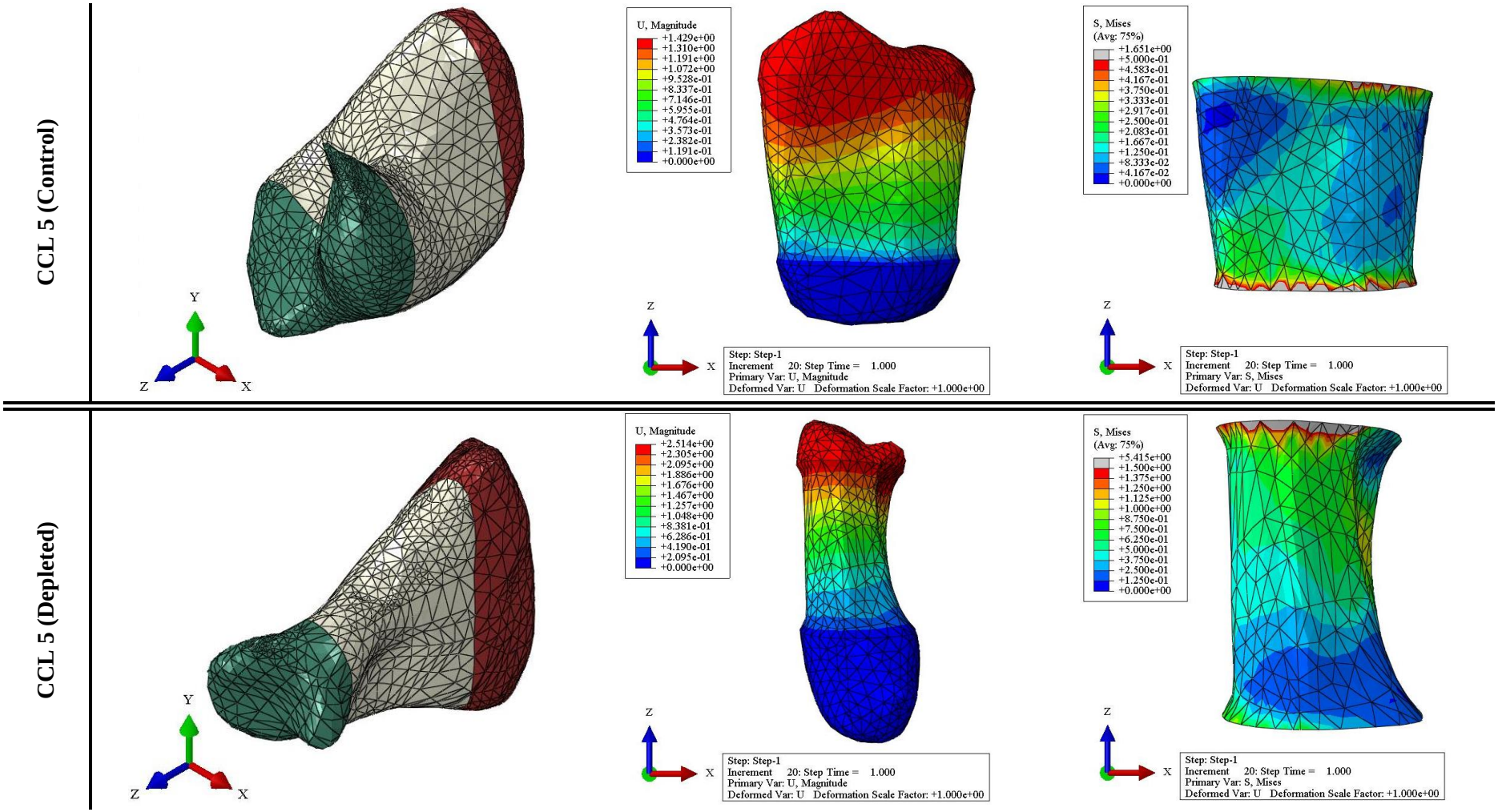

Figure 1: Simulations of the CCL-specific FEMs (n=5 pairs) in the control and the treatment groups. The FEMs at zero (left) and the maximum (centre) applied load (10N) are illustrated to show maximum deformation on the surface of the ligament along with their corresponding colour map of von Mises stress concentration (right) at mid-substance of the CCLs.